THE JOURNAL
OF
CHEMICAL PHYSICS

VOLUME 17, NUMBER 9 SEPTEMBER, 1949

# Compressibility of Gases at High Temperatures. II. The Second Virial Coefficient of Helium in the Temperature Range 0°C to 600°C

W. G. SCHNEIDER AND J. A. H. DUFFIE
*Division of Chemistry, National Research Laboratories, Ottawa, Canada*
(Received January 3, 1949)

The second virial coefficient of helium was measured in the temperature range 0° to 600°C by an expansion procedure previously described. Within our limits of error, estimated to be approximately 0.5 percent at 0° and approximately 1 percent at 600°, the results (expressed in Amagat units of volume) are given by: $10^3B_T=0.5485-0.1315\times10^{-3}T+(3.754/T)$ where $T$ is in °K. A comparison with existing data is given.

## INTRODUCTION

IN a recent paper[1] methods for measuring the compressibility of gases at high temperatures were described. These were based on an expansion method due to Burnett[2] and eliminate the necessity of making volume measurements directly. The pressure of the gas in a pipet maintained at constant temperature is measured, the gas is then expanded into a second pipet at the same temperature, and the pressure is remeasured. If $P_m$ and $P_{m+1}$ are the respective pressures before and after expansion, it can easily be shown that:

$$P_m/P_{m+1}=N+(N-1)(B_T/A_T)P_m, \qquad (1)$$

where $N$ is the ratio of the sum of the two gas-pipet volumes to the volume of the first pipet, and $A_T$ and $B_T$ are the first and second virial coefficients, respectively, at temperature $T$.

Equation (1) supposes that the isotherm can be expressed by the simple linear relation:

$$PV/n=A_T+B_TP, \qquad (2)$$

where $n$ is the mole number. The helium isotherms are accurately represented by Eq. (2) at temperatures above 0°C and at pressures at least up to 100 atmospheres. In the present work, expansion measurements were made for helium at pressures from approximately 75 or 80 atmos. down to about 6 atmos. Several such series of expansions were carried out at 100-degree intervals in the range from 0°C to 600°C. At each temperature a least-squares plot was made of the pressure ratios $P_m/P_{m+1}$ against $P_m$, the pressures before expansion. From the slope and intercept of this plot, the second virial coefficient was evaluated in accordance with Eq. (1). Typical plots of this kind for a series of expansions at 0°C and at 600°C are reproduced in reference 1 (hereafter referred to as *I*).

The first virial coefficients are given by:

$$A_T=A_0T/T_0, \qquad (3)$$

where $A_0$ is the corresponding coefficient at 0°C. The latter was evaluated from a pressure ratio-pressure plot at 0°C and the additional relation

$$A_0+B_0=1, \qquad (4)$$

which follows from the definition of Amagat units.

For the measurements at 600°C a few runs were also carried through, with the first pipet at 600°C and the second pipet at 0°C, in order to test the feasibility of applying this method at even higher temperatures where the first pipet could be heated in a furnace. In this case, in place of Eq. (1) we obtain

$$P_m/P_{m+1}+(B_0/A_0)(P_m-P_{m+1})-(M-1)(B_T/A_T)^2P_mP_{m+1}=M+(M-1)(B_T/A_T)(P_m+P_{m+1}), \qquad (5)$$

where $(M-1)=(A_TV_0/A_0V_T)=(T/T_0)(N-1)$ and $N=(V_T+V_0/V_T)$, $V_T$ being the volume of the first pipet which is at temperature $T$, and $V_0$ the volume of the second pipet held at 0°. The third term on the left is small and can be evaluated by an iteration process.

[1] W. G. Schneider, Can. J. Research **27**, 339–353 (1949).
[2] E. S. Burnett, J. App. Mech. **3**, A137–A140 (1936).

## RESULTS

The results of the measurements are summarized in Table I, where values of the first and second virial coefficients are shown at each temperature, both in terms of Amagat units of volume and in terms of cm³/mole. For the case of 600° the mean value of the second virial coefficient measured with both pipets at 600°, and that obtained with one pipet at 600°, and the second at 0°, are shown separately and are in excellent agreement. In the sixth column of Table I are shown, for each temperature, the number of runs which were averaged to give the final result shown, each run consisting of about six expansions.

A number of measurements of the second virial coefficient of helium have been reported. These measurements have recently been summarized by Keesom.[3] Two sets of data cover a fairly wide temperature range, the measurements of Keesom and co-workers at Leiden extending from −259° to 100° C, and those of Holborn and Otto[4] from −258° to 400°C. The discrepancy between these two sets of data, amounting at 0°C to approximately 5 percent, is considerably larger than the estimated limits of error in the measurements. Table II shows a comparison of the two sets of data with the present measurements. Included also are some measurements by Wiebe, Gaddy, and Heins[5] and by Michels and Wouters.[6] Figure 1 is a graphical comparison. At 0°C and 100°C all the measurements are in fair agreement except those of the Leiden workers. It is difficult to account for this discrepancy. However, it is interesting to note that the Leiden measurements were carried out with a multiple mercury column as the pressure-measuring instrument, whereas in all the other measurements a free piston gauge was employed.

The present measurements agree with those of Holborn and Otto to about 0.2 percent at 0°, 100°, and 200°. At 300° and 400° our values are approximately 3 percent higher.

A smooth curve drawn through our values from 0° to 600° can be fitted within our limits of error by the equation:

$$10^3 B_T = 0.5485 - 0.1315 \times 10^{-3} T + (3.754/T). \quad (6)$$

From 200° to 600° the second virial coefficient appears to fall off linearly with temperature.

TABLE I. Summary of coefficients in the series equation, $PV = A_T + B_T P$, for helium.

| Temperature °C | Volume expressed in terms of: Amagat units $A_T$ | Amagat units $B_T \times 10^3$ | cm³/mole* $A_T$ | cm³/mole* $B_T$ | No. of runs |
|---|---|---|---|---|---|
| 0 | 0.999475 | 0.525 | 22415.2 | 11.77 | 8 |
| 100 | 1.365369 | 0.509 | 30621.1 | 11.42 | 6 |
| 200 | 1.731262 | 0.494 | 38827.0 | 11.08 | 6 |
| 300 | 2.097156 | 0.480 | 47032.9 | 10.76 | 6 |
| 400 | 2.463050 | 0.466 | 55238.8 | 10.45 | 6 |
| 500 | 2.828943 | 0.452 | 63444.7 | 10.14 | 8 |
| 600 | 3.194837 | 0.438 | 71650.6 | 9.82 | 10 |
| 600 (second pipet at 0°C) | | 0.438 | | | 5 |

* The value of the normal volume used to convert to units of cm³/mole was 22427.0 cm³, where the molecular weight of helium was taken as 4.00248 g and the normal density as $0.178467 \times 10^{-3}$ g/cm³ (see reference 3).

## TREATMENT OF DATA

Before a pressure ratio-pressure plot is made, a number of corrections have to be applied to the pressures measured by the free piston gauge. These include corrections for:

(*a*) variation in barometric pressure;
(*b*) air buoyancy of the weights and the scale pan of the piston gauge;
(*c*) variation in the temperature of the piston;
(*d*) a small hydrostatic pressure due to the oil in the line connecting the piston gauge to the mercury U-tube serving as a null indicator.
(*e*) lack of uniformity of temperature due to a small dead space or unheated space in the capillaries connecting the gas pipets to the expansion valve and mercury U-tube, the latter being outside the thermostat.

The barometric reading is corrected in the usual manner to give the atmospheric pressure.

The steel weights used with the piston gauge were calibrated (to "vacuum" weight) by the Metrology Section of the National Research Council of Canada, as were also the scale pan of the gauge and the piston itself. The sum of these three weights constitutes (apart from the barometric pressure) the total loading on the piston. The scale pan is constructed partly of aluminum and partly of steel. To apply an air buoyancy correction, the steel and aluminum components are weighed separately. Then the buoyant force to be subtracted from the total vacuum weight can be represented as $m_b \rho_a / \rho_w$ where $m_b$ includes the total vacuum weight, the weight of the aluminum component of the scale pan having been expressed as an equivalent vacuum weight of steel, and $\rho_a/\rho_w$ = density of air/density of steel $= (1/\rho_w)(M_p/RT) =$ constant $\times p/T$. Here $M$ is the molecular weight of air of mean relative humidity, $R$ the gas constant, $p$ the corrected baro-

TABLE II. Comparison of second virial coefficient data for helium by various authors

| Temperature °C | $B_T \times 10^3$ (Amagat units) Michels and Wouters | Wiebe, Gaddy, and Heins | Keesom *et al.* | Holborn and Otto | Present measurements |
|---|---|---|---|---|---|
| 0 | 0.529 | 0.522 | 0.501 | 0.524 | 0.525 |
| 100 | 0.506 | 0.504 | 0.480 | 0.508 | 0.509 |
| 200 | | 0.478 | | 0.494 | 0.494 |
| 300 | | | | 0.468 | 0.480 |
| 400 | | | | 0.452 | 0.466 |
| 500 | | | | | 0.452 |
| 600 | | | | | 0.438 |

[3] W. H. Keesom, *Helium* (Elsevier Press, Amsterdam, 1942), Chapter II.
[4] L. Holborn and J. Otto, Zeits. f. Physik **33**, 1–11 (1925); see also, J. Otto, Zeits. f. Instrumentenk. **48**, No. 6, 257–8 (1928).
[5] R. Wiebe, V. L. Gaddy, and C. Heins, J. Am. Chem. Soc. **53**, 1721–5 (1931).
[6] A. Michels and H. Wouters, Physica **8**, 923 (1941).

metric pressure, and $T$ (°K) the temperature of the room. Actually it is found sufficiently accurate for a large number of measurements to take a mean value of $p$ and $T$ and use a corresponding constant mean value for $\rho_a$, the air density.

In order to correct the piston gauge constant $C$ for variation in piston temperature, the relation $C_t = C_{30}[1-2.2\times10^{-5}(t-30)]$ is employed, where $C_t$ and $C_{30}$ are the gauge constants at $t$°C and 30°C, and the coefficient of linear expansion of steel (of the piston) is taken to be $1.1\times10^{-5}$/deg. This value was verified by measuring the gauge constant $C_t$ by balancing the piston gauge against the vapor pressure of carbon dioxide at 0°C and varying the temperature of the piston from 18° to 38°C. These measurements yielded $1.09\times10^{-5}$/deg. for the linear expansion coefficient of the piston.

The correction to the pressure due to the hydrostatic head in the oil line, which transmitted the pressure from the gauge to the mercury U-tube, amounted to about 17 mm Hg and was computed from the measured height of the oil and its measured density at room temperature.

The dead-space volume of the pipet assembly amounted to approximately 0.5 percent of the total volume and was slightly different when the gas was contained in the first pipet only from what it was when the gas was contained in both pipets. In order to apply a correction, the dead space in each case is subdivided into regions of uniform temperature. The volume and mean temperature of each region are measured separately. The procedures used in computing the dead-space correction factors are given in I. Although the total unheated volume is relatively small, it was found that in order to achieve an accuracy within one percent in the second virial coefficient, the correction had to be made with considerable accuracy, particularly at the higher temperatures; specifically, it was found necessary in making these corrections to use Eq. (2) instead of the perfect gas law. These difficulties could, however, be quite considerably reduced by using larger gas pipets. For the present measurements the pipet volumes were approximately 58 cc and 28 cc for the first and second pipets respectively. This ratio of volumes gives a convenient spacing of points on the pressure ratio-pressure plot.

The final corrected pressure in each case is obtained in international millimeters of mercury and converted to normal atmospheres (76 cm Hg, density 13.5951 g/cm³, g=980.665 cm/sec.²).

The pressure ratios are computed from the final corrected pressures and are plotted against the initial pressures (the pressures before expansion). The values of the slope and intercept, from which the second virial coefficient is computed, are obtained for each run from a least-squares fit. In doing this it is desirable to weight the ratios corresponding to higher pressures more heavily than those corresponding to lower pressures,

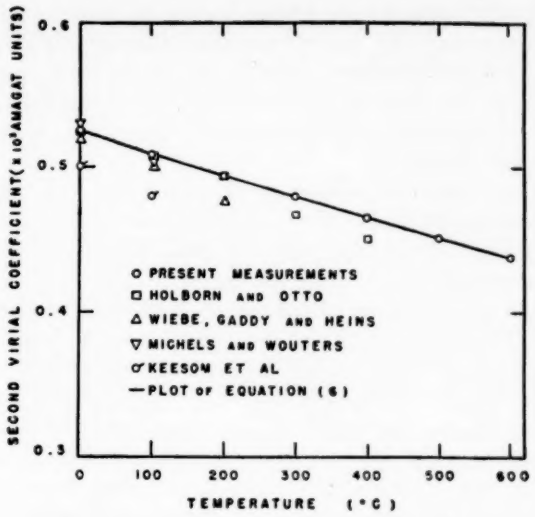


FIG. 1. Plot of second virial coefficient data.

since the relative precision with which the higher pressures can be measured with the piston gauge is greater. Accordingly each point is weighted in direct proportion to the pressure shown on the abscissa. The values of the second virial coefficients shown in Table I represent the mean of a number of plots at each temperature.

For the runs at 600°C with one pipet at 0°C, the procedure is identical except that a preliminary plot is first made of Eq. (5), omitting the last term on the left hand side. The slope and intercept obtained from this plot are then used as a first approximation in an iteration procedure to evaluate this term. After weighting each point as before, the final slope and intercept and thus the second virial coefficient are obtained from a least-squares fit.

## ESTIMATE OF ERRORS

The error associated with measurement of the temperature, estimated to be ±0.01°C, is negligible, particularly since for helium in the temperature range from 0°C to 600°C the second virial coefficient varies but slowly with temperature. It is therefore necessary to consider only errors associated with the pressure measurements.

The piston gauge was calibrated against the vapor pressure of pure carbon dioxide at 0°C. Bridgeman[7] gives the precision of the vapor pressure at this temperature as 1/26,000. A number of calibrations carried out during the course of the present measurements were reproducible to about 1/10,000. These two factors combined may give rise to a maximum error in $B$ of the order of 0.1 percent.

The sensitivity of the piston gauge was approximately 0.3 g, or (for the piston used) about 0.25 mm Hg. This gives rise to a slight scatter of the points on the straight line pressure ratio-pressure plot. In a typical

[7] O. C. Bridgeman, J. Am. Chem. Soc. 49, 1174–1183 (1927).

plot of a single run the probable error in $B$, obtained by a least-squares fit, was 0.3 percent. (Part of this scatter may be attributable to small variations in the temperature of the dead space.) Averaging over several runs should reduce the error due to this cause to at least as low as 0.2 percent.

The source of greatest error, at least at the higher temperatures, is the dead-space volume. This is a consequence of the difficulty of measuring very small volumes accurately and the fact that the dead space is not at a uniform temperature. The latter difficulty can, to a large extent, be overcome by subdividing the dead space into smaller regions and measuring the temperature of each region. This subdivision must, however, not be carried too far, since then the error in measuring the volume of each region becomes large. Moreover, it introduces some uncertainty to assume that at the boundary of each region the temperature changes in a discontinuous manner, while throughout the particular region it remains uniform. Assuming a possible error in the dead-space temperature of 1° and a possible error in the dead-space volume of 20 percent, leads to a possible error in $B$ at 600°C, due to the uncertainty in the dead-space correction, of approximately 0.5 percent. At 0°C the corresponding error in $B$ is less than 0.1 percent.

In calculating the dead-space correction factor, Eq. (2) was employed rather than the perfect gas law. With the experimental arrangement employed, use of the perfect gas law would have led to an error in $B$ at 600°C of 3 percent. In applying Eq. (2) to calculate the dead-space correction factor (see I), a rather cumbersome expression is obtained. It was found possible to replace this by the relation

$$F=F_0(1-\alpha P), \tag{6}$$

where $F$ is the dead-space correction factor, $F_0$ is the equivalent dead-space correction factor calculated from the ideal gas law, and $\alpha$ is a parameter evaluated empirically. The error introduced by the approximation (Eq. (6)) amounts only to about 0.1 percent in $B$ at 600°.

Taking all errors into account the over-all possible error in the mean value of $B$ amounts at 600°C to about 1 percent, while at 0°C it is well within ½ percent.

## EXPERIMENTAL

### Purification of Helium

The helium used for the present measurements was obtained from the Amarillo Helium Plant of the U. S. Bureau of Mines. It was stated to contain several percent of nitrogen and possibly a trace of hydrocarbon. It was found to contain, in addition, approximately 1.8 percent of hydrogen. To purify the helium it was passed first through a combustion tube at 450°C filled with copper and copper oxide turnings to remove hydrogen (and oxygen), then through a liquid air trap, and finally through two liquid air traps packed with granular charcoal. The latter were found to remove nitrogen (but not hydrogen) very effectively from the helium gas. Several batches of gas which had been twice passed slowly through the purification train were each analysed by a mass spectrometer for nitrogen and hydrogen content.[8] The purified gas was found to contain in each case less than 0.02 percent nitrogen and 0.06 percent hydrogen.

### Apparatus and Procedure

The apparatus used for the pressure and temperature measurements, and the procedure employed, are described in I. For the measurements at each temperature, the thermostat was adjusted exactly to the desired temperature to within 0.01°. In this manner a temperature correction of the final data to the even temperatures shown in Table I was avoided. Exact adjustment of the thermostat temperature was easily accomplished by adjusting the Wheatstone bridge used in the temperature control circuit.

## ACKNOWLEDGMENTS

We wish to thank Mr. Y. Lupien for assistance in the measurements, and Mr. K. Milliken for assistance in the computations.

[8] We are greatly indebted to Mr. M. H. Thomas and co-workers at the Chalk River Laboratories for carrying out these analyses.

# The Heats of Vaporization of Uranium Hexafluoride*

JOSEPH F. MASI
*National Bureau of Standards, Washington, D. C.*
(Received September 27, 1948)

Vaporizations of uranium hexafluoride were carried out in a heavy-wall, nickel-plated calorimeter. Measurements of the heat of vaporization of the solid were made at seven temperatures and of the liquid at four temperatures, covering the range from 4° to 90°C. The apparatus was tested before beginning the measurements by obtaining the heats of vaporization of water at three temperatures.

The scattering of the data on $UF_6$ is about one percent. The measured heats of vaporization have been used to obtain a consistent correlation of the vapor pressures, heat of fusion, and triple point given in the literature. The results are expressed as vapor pressure equations and an equation of state for the saturated vapor. From these equations and the National Bureau of Standards values for the thermodynamic properties of the solid and liquid, the entropies of the ideal gas are calculated and compared with those given in the literature from spectroscopic data and molecular structure.

## INTRODUCTION

URANIUM hexafluoride has been extensively investigated. The heat capacities of the solid and liquid from 15° to 370°K were measured at the National Bureau of Standards by Brickwedde, Hoge, and Scott;[1] the vapor pressures of the solid and liquid from 0° to 85°C were measured by Weinstock and Crist;[2] and the calculation of thermodynamic properties of the ideal gas from structural and spectroscopic data have been reported by Bigeleisen, Mayer, Stevenson, and Turkevich.[3] The heats of vaporization of the solid and liquid from 4° to 90°C have now been measured, thereby providing the data required for a consistent correlation of the other thermal data and a critical analysis of the thermodynamic properties of $UF_6$.

## APPARATUS

The apparatus used for measuring the heats of vaporization is shown in Fig. 1. The vaporization chamber was made of copper $\frac{1}{8}$ inch thick, nickel-plated on all interior surfaces. The lower part, containing the solid or liquid material, had vanes of nickel-plated copper for conducting heat to the sample. The copper block in the upper portion of the chamber forced the vapor to take a long path near the heated wall of the container, bringing it up to temperature after the cooling effect of vaporization. The throttling valve for controlling the flow of vapor was made of brass with a nickel stem. The numbers indicate location of the elements of a multi-junction Chromel-Constatan thermocouple. Copper leads were located at the points numbered 1, 3, 4, and 5, and four readings of the temperature difference between the calorimeter and the jacket could be obtained by using the pairs of leads 1–3, 3–4, 4–5, and 1–5. A nickel thermometer on the copper-nickel tube ($N$) was used to observe changes in temperature of the emergent vapor during a vaporization experiment. A brass vacuum-jacket ($J$), with a ring ($R$) on which leads were wound for tempering, surrounded the vaporization chamber. The whole apparatus was suspended in a stirred bath, which was maintained at a constant temperature within 0.002°C by use of a copper resistance thermometer. The temperature of the bath was measured with a platinum resistance thermometer.

The receiving cans ($C$) were chilled to about −25°C. The copper-nickel tube leading to the cans was wound with a heater, and the tube and valves were kept hotter than the bath to avoid condensation. The connection

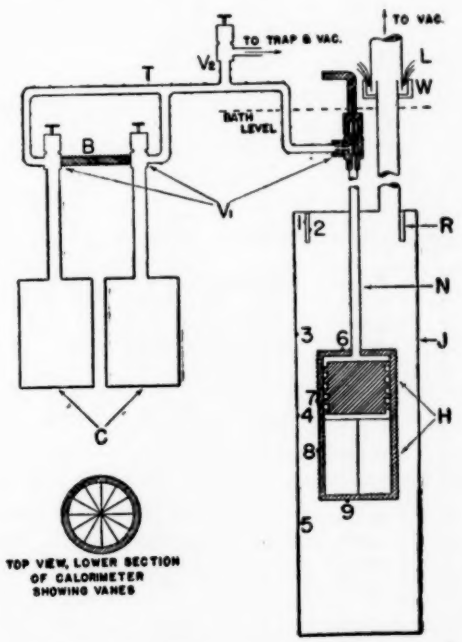


FIG. 1. Apparatus for heat of vaporization of $UF_6$.

| | |
|---|---|
| $B$ Heated support | $R$ Ring |
| $C$ Receiving cans | $T$ Heated tube |
| $H$ Heaters | $V_1$ Valves, nickel stems |
| $J$ Brass jacket | $V_2$ Valve, steel stem |
| $L$ Leads | $W$ Wax seal |

Numbers give location of thermocouple junctions

* This work was supported in part by the Manhattan District, U. S. Army Corps of Engineers, and in part by the AEC.

[1] Brickwedde, Hoge, and Scott, J. Chem. Phys. **16**, 429 (1948).
[2] B. Weinstock and R. H. Crist, J. Chem. Phys. **16**, 436 (1948).
[3] Bigeleisen, Mayer, Stevenson, and Turkevich, J. Chem. Phys. **16** 442 (1948).

to the vacuum system was through a U-shaped trap, kept in liquid air.

The circuits for controlling and measuring the electrical energy supplied to the heater ($H$), and for measuring the resistances of the platinum and nickel thermometers, have been previously described.[4] The galvanometer used for the thermocouple indications was sensitive enough to give deflections of 1 to 4 millimeters per millidegree, depending on the number of junctions being used. A synchronous electric timer operated by a controlled 60-cycle signal measured the heating intervals with an accuracy of 0.01 or 0.02 second.

TABLE I. Experimental and calculated values of $\gamma$ for $UF_6$. The fourth column gives the sum of corrections for heat leak, drift, and difference between initial and final temperature. The calculated values ($\gamma_{calc.}$) are obtained from Eqs. (4) and (6).

| Temp. °C | Sample No. | $\gamma_{obs.}$ cal mole$^{-1}$ | $\Sigma_{corr.}$ cal mole$^{-1}$ | $\gamma_{corr.}$ cal mole$^{-1}$ | $\gamma_{calc.}$ cal mole$^{-1}$ | $\gamma_{corr.} - \gamma_{calc.}$ cal mole$^{-1}$ |
|---|---|---|---|---|---|---|
| | | | **Solid** | | | |
| 4.32 | 6 | 12,085 | −27 | 12,058 | 12,002 | 56 |
| | 6 | 12,120 | 7 | 12,127 | | 125 |
| | 6 | 12,038 | − 5 | 12,033 | | 31 |
| | 6 | 12.012 | 29 | 12,041 | | 39 |
| 14.71 | 6 | 12,159 | −77 | 12,082 | 11,945 | 137 |
| 24.38 | 6 | 11,988 | 3 | 11,991 | 11,882 | 109 |
| | 6 | 11,860 | 22 | 11,882 | | 0 |
| | 6 | 11,881 | 2 | 11,883 | | 1 |
| 41.72 | 1 | 11,907 | 11 | 11,918 | 11,736 | 182 |
| | 2 | 11,688 | 37 | 11,725 | | − 11 |
| | 2 | 11,683 | 43 | 11,726 | | − 10 |
| | 2 | 11,748 | 103 | 11,851 | | 115 |
| | 2 | 11,666 | 38 | 11,704 | | − 32 |
| 47.42 | 2 | 11,724 | 18 | 11,742 | 11,678 | 64 |
| | 2 | 11,581 | 175 | 11,756 | | 78 |
| 48.18 | 2 | 11,463 | 94 | 11,557 | 11,670 | −113 |
| | 2 | 11,451 | 85 | 11,536 | | −134 |
| 54.80 | 2 | 11,427 | 125 | 11,552 | 11,593 | − 41 |
| | 2 | 11,400 | 105 | 11,505 | | − 88 |
| | 2 | 11,490 | 31 | 11,521 | | − 72 |
| | 2 | 11,503 | 17 | 11,520 | | − 73 |
| | | | | | Mean | ± 72 |
| | | | **Liquid** | | | |
| 65.19 | 3 | 6,972 | −75 | 6,897 | 6,880 | 17 |
| | 3 | 6,982 | 76 | 7,058 | | 178 |
| | 5 | 6,900 | −85 | 6,815 | | − 65 |
| | 5 | 6,884 | −40 | 6,844 | | − 36 |
| 70.14 | 3 | 6,838 | −60 | 6,778 | 6,811 | − 33 |
| | 4 | 6,923 | −45 | 6,878 | | 67 |
| | 4 | 6,860 | 5 | 6,865 | | 54 |
| | 4 | 6,775 | −28 | 6,747 | | − 64 |
| | 4 | 6,854 | −38 | 6,816 | | 5 |
| 80.28 | 4 | 6,718 | 6 | 6,724 | 6,679 | 45 |
| | 4 | 6,714 | −22 | 6,692 | | 13 |
| | 5 | 6,866 | −40 | 6,826 | | 147 |
| | 5 | 6,662 | 2 | 6,664 | | − 15 |
| | 5 | 6,667 | 12 | 6,679 | | 0 |
| | 5 | 6,629 | 40 | 6,669 | | − 10 |
| | 6 | 6,669 | 23 | 6,692 | | 13 |
| | 6 | 6,668 | −11 | 6,657 | | − 22 |
| | 6 | 6,623 | 27 | 6,650 | | − 29 |
| 90.26 | 6 | 6,541 | 24 | 6,565 | 6,559 | 6 |
| | 6 | 6,568 | −14 | 6,554 | | − 5 |
| | | | | | Mean | ± 41 |

[4] Scott, Meyers, Rands, Brickwedde, and Bekkedahl, J. Research Nat. Bur. Stand. **35**, 39 (1945) RP1661.

TABLE II. Heats of vaporization of $UF_6$ and entropies of the ideal gas.

| Temp. °K | $L$ cal mole$^{-1}$ | $L/T$ cal mole$^{-1}$ deg$^{-1}$ | $S°$ cal mole$^{-1}$ deg$^{-1}$ | $S°_{spect}$ cal mole$^{-1}$ deg$^{-1}$ |
|---|---|---|---|---|
| | | **Solid** | | |
| 273.16 | 12,023 | 44.02 | 87.56 | 87.65 |
| 280 | 11,988 | 42.81 | 88.39 | 88.30 |
| 290 | 11,929 | 41.13 | 89.57 | 89.48 |
| 298.16 | 11,872 | 39.82 | 90.50 | 90.34 |
| 300 | 11,858 | 39.53 | 90.70 | 90.50 |
| 310 | 11,772 | 37.97 | 91.80 | 91.56 |
| 320 | 11,666 | 36.46 | 92.86 | 92.58 |
| 330 | 11,537 | 34.96 | 93.87 | 93.54 |
| 337.21 | 11,429 | 33.89 | 94.59 | 94.20 |
| | | **Liquid** | | |
| 337.21 | 6859 | 20.34 | 94.59 | 94.20 |
| 340 | 6817 | 20.05 | 94.88 | 94.47 |
| 350 | 6671 | 19.06 | 95.90 | 95.40 |
| 360 | 6533 | 18.15 | 96.91 | 96.30 |
| 370 | 6404 | 17.31 | 97.95 | 97.20 |

## EXPERIMENTAL

Samples of $UF_6$ were prepared for the calorimeter by three successive sublimations and condensations. The purification train consisted of Pyrex traps, connected in series, which were carefully outgassed by heating and evacuating before the $UF_6$ was introduced. Six fillings of the calorimeter were made.

Analyses of the samples as introduced into the calorimeter indicated an average of about one percent impurity. Most of this could be attributed to non-volatile material, such as $UO_2F_2$, which would have a negligible effect on the heat of vaporization. Possible volatile impurities are HF and $SiF_4$.

Each sample was introduced into the vaporization chamber by melting and allowing it to flow in under the vapor pressure of the liquid.

In preparation for a heat of vaporization experiment, the evacuated and weighed receiving cans were put in place and chilled, the vapor line was evacuated, and usually the sample in the calorimeter required some pumping to remove gas. The calorimeter was warmed to the temperature of the bath and allowed to come to thermal equilibrium as evidenced by the constancy of the indications of the four thermo-element combinations and the resistance thermometers. A determination was begun by turning on the timer and heater current simultaneously and opening the throttle valve very gradually. The valve was adjusted as necessary during the run to keep the temperature of the calorimeter slightly lower than that of the surrounding jacket,

to prevent condensation in the tube. Data taken continuously during a determination were the readings of nickel thermometer resistance, heater current and potential, and deflections of thermocouples 1–3, 3–4, 4–5, 1–5. The time required to vaporize a 10g portion of the sample was 15 to 40 minutes, depending on rate of heating. At the end of an experiment the temperature of the calorimeter was adjusted to reproduce the starting conditions as closely as possible. This was done by supplying energy to the calorimeter for a short measured period. After two successive vaporizations, the receiving cans were removed and weighed.

The accuracy of the calorimeter was tested, and the best method of operation was found, by a series of experiments on the heat of vaporization of water. By the procedure described above, there were 12 determinations at 60°C, one at 70°C, and three at 95°C. The average deviations from the means of the determinations at 60° and 95°C were 0.12 and 0.20 percent, respectively. The mean values at 60° and 95°C were 0.05 percent smaller and 0.07 percent smaller, respectively, than the values at those temperatures given by Osborne, Stimson, and Ginnings.[5] Thus, the consistent error was not large.

## RESULTS AND CALCULATIONS

The quantity measured in heat of vaporization experiments is $\gamma$ in the equation

$$L=\gamma[1-(V_c/V_g)] \qquad (1)$$

where $L$ is the latent heat of vaporization and $V_c$ and $V_g$ are the molar volumes of the condensed phase and vapor, respectively. Forty-one acceptable values of $\gamma$ for $UF_6$ were obtained; these are listed in the second column of Table I. The sum of the calculated corrections for heat leaks, drifts, and differences in beginning and ending temperature is given in the third column. The corrected values of $\gamma$ are given in the fourth column of Table I and plotted in Fig. 2. All results are expressed in the defined calorie, equivalent to 4.1840 absolute joules.

The only previously available heats of vaporization of $UF_6$ are those calculated from the vapor pressure data of Weinstock and Crist.[2] These calculated results are represented in Fig. 2 by curve $B$, which assumes the ideal gas law for the vapor, and by curve $C$, which assumes the Berthelot equation and the critical constants given by Kirschenbaum.[6] The vapor pressure data have about the same precision as the measured heats of vaporization. The two sets of data can be reconciled, as can be seen in Fig. 2, by using an equation of state somewhat less drastic than the Berthelot. Consequently, an equation of state of the form $PV=RT+BP$ was assumed, and the virial coefficient $B$ was investigated both as functions of $T^{-1}$ and $T^{-2}$. It was found that the function

$$B(\text{cm}^3)=1082-(1.81\times10^6)T^{-2} \qquad (2)$$

produced the best agreement between the measured heats of vaporization and the vapor pressure data of Weinstock and Crist.

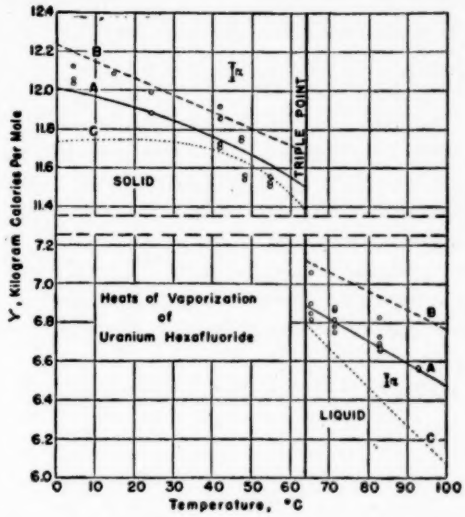


FIG. 2. Heats of vaporization of $UF_6$. The circles are the experimental values ($\gamma_{corr}$) given in the fifth column of Table I. Curve $A$ is calculated from Eqs. (4) and (6). Curves $B$ and $C$ are calculated from the vapor pressure data of Weinstock and Crist assuming ($B$) the ideal gas law and ($C$) the Berthelot equation.

Curve $A$ of Fig. 2 was obtained from the following set of equations:

Solid:

$$\log_{10}P_{mm}=-(2858.2/T)+16.3619-1.9116\log_{10}T \qquad (3)$$

$$\gamma=RZ(6581.2-1.9116T) \qquad (4)$$

Liquid:

$$\log_{10}P_{mm}=-(2466.0/T)+26.1868-6.2582\log_{10}T \qquad (5)$$

$$\gamma=RZ(5678.2-6.2582T) \qquad (6)$$

where

$$Z=1+(BP/RT)$$

and $B$ is obtained from Eq. (2). Equations (4) and (6) are obtained directly from Eqs. (3) and (5), respectively, by the Clausius-Clapeyron equation.

These equations are made to reproduce the heats of fusion (4588 cal mole$^{-1}$) found by Brickwedde, Hoge, and Scott within their experimental error of about 0.5 percent. The vapor pressure data of Weinstock and Crist are represented by these equations as closely as by their own. The heats of vaporization are reproduced satisfactorily within the experimental accuracy.

Calculated values of the heat of vaporization were obtained by substituting the values of $\gamma$ obtained from Eqs. (4) and (6) in Eq. (1), and are tabulated at ten-degree intervals in the second column of Table II.

[5] N. S. Osborne, H. F. Stimson, and D. C. Ginnings, J. Research Nat. Bur. Stand. **23**, 256 (1939).
[6] I. Kirschenbaum, Columbia Report A753.

The corresponding entropies of vaporization are given in the third column.

The molar volume of the solid was assumed constant at 70.42 cc. Its variation would be expected to be small, and would have a negligible effect in calculating $L$. The volumes of the liquid were obtained from the density measurements of Hoge and Wechsler.[7]

The entropies of the ideal gas at one atmosphere were obtained by the usual third-law addition of entropies,

$$S^\circ = S_{sat} + (L/T) + \Delta S(\text{ideal-real}) + R \ln(P_{mm}/760) \quad (7)$$

and are tabulated in the fourth column of Table III. The required values of $S_{sat}$ are taken from Brickwedde, Hoge, and Scott,[1] except that those for the liquid have been lowered by 0.05 cal mole$^{-1}$ deg$^{-1}$ corresponding to a change in the heat of fusion from 4588 to 4570 cal mole$^{-1}$. In the last column of Table III are tabulated for comparison the values of $S^\circ$ obtained by interpolating in the table calculated by Bigeleisen, Mayer, Stevenson, and Turkevich[3] from the spectroscopic data.

The steadily increasing difference between the third-law and spectroscopic entropies, and the extremely low Boyle point calculated from Eq. (2), seem to indicate that there is a consistent temperature-dependent error in the experimental measurements. The tests with water indicate that this is not due to the vaporization calorimeter. The determination of the accuracy of the equations presented here may have to await measurements of the $P$-$V$-$T$ relationships of $UF_6$ gas. From a consideration of the estimated errors of the present measurements and the consistency of the correlation of these results with other thermal data, it appears reasonable to assign a probable error of about one percent to the tabulated values of latent heat of vaporization. This accuracy is an order of magnitude worse than is usually obtained in this laboratory, but it seems to be comparable with that obtained in measuring other properties of $UF_6$; and, in view of the refractory nature of this compound, an error of one percent is not excessive.

[7] H. J. Hoge and M. T. Wechsler, J. Chem. Phys. (in press).

THE JOURNAL OF CHEMICAL PHYSICS VOLUME 17, NUMBER 9 SEPTEMBER, 1949

# Catalysis on Non-Uniform Surfaces

G. D. HALSEY, JR.*
*Department of Chemistry, Harvard University, Cambridge, Massachusetts*
(Received October 12, 1948)

Using the ammonia decomposition as an example, the kinetics of a heterogeneous reaction are discussed. On a continuously non-uniform surface, no single reaction step is the limiting one; on the optimum sites two reaction steps are equally slow. The expression for over-all velocity is developed, and solved exactly for the case of an exponential distribution of activation energies. It appears that if the distribution is broad, its exact shape is unimportant, but that a factor $r$, connected with the amount of adsorption energy available for catalytic work, is important. It is shown that for a broad distribution, the pressure dependence of the over-all rate is the same as the pressure dependence on the optimum sites. Because the position of the optimum depends on pressure, one cannot assume that the surface is "effectively uniform." The simplest of ammonia kinetics is discussed, but it appears that on a non-uniform surface, much more extensive experiments than have been available are necessary to elucidate properly the kinetics of a reaction.

## I. INTRODUCTION

IT is generally recognized that from the standpoint of gas adsorption studies, the surface of a catalyst is often quite non-uniform. That is, heats of adsorption and energies of activation for adsorption and desorption vary widely over the surface.[1]

When catalytic reactions are studied, it is equally well known that the same surface often is treated as if it were uniform; from this apparent contradiction, it emerges that often only a small fraction of the surface available for gas adsorption is effective in bringing about a reaction. This contention is supported by the investigation of catalytic poisoning, when it is found that a small fraction of the amount of poison necessary to saturate the surface will stop reaction. A consideration of these phenomena leads to the "Theory of Active Centers" (H. S. Taylor).

Constable[2] attempted to reconcile the dualism between the data of adsorption and catalysis. He postulated an exponential distribution of the values of the activation energy over the surface, and assumed that there existed a "lowest value" for this energy, below which reaction would not proceed. He was thus able to show that the effective value of the activation energy for reaction was little different from the minimum value. His treatment is essentially incomplete in that it leaves unexplained the factors that determine the "minimum activation energy." The factors will now be considered.

* Junior Fellow, Harvard Society of Fellows, 1948– .
[1] G. M. Schwab, H. S. Taylor, and R. Spence, *Catalysis* (D. Van Nostrand Company, New York, 1937).
[2] F. H. Constable, Proc. Roy. Soc. A108, 355 (1925).

## II. NATURE OF HETEROGENEOUS CATALYSIS

When a reaction takes place on a uniform surface, it is quite reasonable to say that a certain process is the rate determining step. Usually this process will be either adsorption, reaction, or desorption. However, it appears that the statement that one of these processes is the limiting one is no longer possible, if the reaction takes place on a non-uniform surface, with a complete range of activation energies available. It is apparent that on one part of the surface one process will limit the reaction, while on another, a different process will be rate determining. That is, on a totally indifferent part of the surface, the decomposition of ammonia will be limited by the activation energy for decomposition in the bulk phase, although the desorption of the resulting nitrogen might take place very easily. On the other hand, on a part of the surface with a very great attraction for nitrogen, the ammonia would be torn apart, but the nitrogen would not be desorbed and the site would become effectively poisoned by the reaction product.

The essential nature of heterogeneous catalysts is that the adsorption energy of the activated complex reduces the activation energy for reaction. The stronger the adsorption, the lower the activation energy for reaction, but the higher the activation energy for the desorption of products.

On a certain part of the surface, the two activation energies have their optimum values. On examining a less efficient site, with a lower than optimum value of one activation energy, one will find a higher than optimum value of the other energy. For example, in the rearrangement of an organic molecule, the energy of adsorption of the activated complex on the optimum site will be large enough to make rearrangement possible, but not so large as to make desorption of the product too slow. When one considers another site that is more rapid in rearranging the molecule, it will be found to be too slow in desorbing the product. A slight decrease in one of the activation energies, say $F_A$, causes an increase in the other, $F_B$. A unit change in $F_A$ will define a change of $r$ units in $F_B$. Thus, on a continuously non-uniform catalyst one can write a general relationship between the two activation energies, in the vicinity of optimum conditions:

$$dF_B=-rdF_A. \tag{1}$$

For convenience, the activations for the two reactions are expressed in free energy, so that partition functions for the initial and activated states will not have to be explicitly carried. Throughout the presentation the methods of the Eyring theory of reaction rates will be employed.[3]

Now $r$ is not necessarily a constant, but in view of the small change in energy that will almost suppress reaction, it will be treated as a constant over the small fraction of the surface catalytically active. Thus

$$rF_A+F_B=F_0 \tag{2}$$

where $F_0$ is a constant.

[3] H. Eyring, J. Chem. Phys. **3**, 107 (1935).

The simplest example of a catalyzed reaction will be formulated as an example. A molecule of gaseous reactant will be assumed to go through three processes: adsorption, rearrangement, and desorption. Each of the processes will be assumed to be unimolecular, and all backward reactions will be neglected.

On a given part of the surface, a fraction $\theta_A$ of the surface will be covered with adsorbed reactant, while a fraction $\theta_B$ will be covered with the rearranged reactant prior to desorption. The rest will be bare. It is assumed that the coverage $\theta_A$ assumes its equilibrium value, given by the Langmuir expression

$$\theta_A/1-\theta_A-\theta_B=k_Ap_A$$
$$\theta_A=(k_Ap_A/1+k_Ap_A)(1-\theta_B)\equiv L_A(1-\theta_B).$$

The theory of absolute reaction rates shows that the rate of a surface reaction is

$$(kT/h)\theta_R(f^\ddagger/f_R)\exp\{-\Delta H^\ddagger/RT\}=(kT/h)\theta_R\exp\{-\Delta F^\ddagger/RT\},$$

when $kT/h$ is the usual frequency factor, $\theta_R$ the concentration of the reactant molecules, and $f$ and $f_R$ the partition functions of activated complex and reactant, respectively, $\Delta H$ is the heat of activation, into which the logarithm of the partition function ratio $f^\ddagger/f_R$ is adsorbed for convenience, to constitute $F^\ddagger$ the free energy of activation. Thus, the steady state value of $\theta_B$ is determined by the expression

$$d\theta_B/dt=(kT/h)[\theta_A\exp\{-F_A/RT\}-\theta_B\exp\{-F_B/RT\}]=0. \tag{3}$$

Thus,

$$\theta_B=L_A\exp\{-F_A/RT\}/(L_A\exp\{-F_A/RT\}+\exp\{-F_B/RT\}.$$

The velocity per site on the particular part of the surface in question is

$$v=\frac{kT}{h}\theta_B\exp\{-F_B/RT\}.$$

Assuming, for simplicity, $r=1$, one can write $F_A+F_B=F_0$, and $v$ becomes

$$kT/hL_A\exp\{-F_0/RT\}/(L_A\exp\{-F_0/RT+F_B/RT\}+\exp F_B/RT.$$

If one writes

$$\varphi\equiv\exp\{-F_B/RT\}/L_A^{\frac{1}{2}}\exp\{-F_0/RT\}$$
$$v=\text{const}\times L_A^{\frac{1}{2}}\exp\{-F_0/2RT\}/(\varphi^{-1}+\varphi).$$

The over-all rate, $w=\int NvdF_B$ where $N$ is the distribution function of sites with activation energy of rearrangement $F_B$. If $N$ has the exponential form $N=c\times\exp\{-F_B/F_m\}$, where $F_m$ is a constant modulus, the value of $w$ can be found exactly. Inserting the value of $F_B$ in terms of $\varphi$, $N=c\times(\varphi L_A^{\frac{1}{2}}\exp\{-F_0/RT\})^{RT/F_m}$ and $dF_B=-(1/RT)d\ln\varphi$, whence

$$w=\text{const}\times[L_A^{\frac{1}{2}}\exp\{F_0/2RT\}(L_A^{\frac{1}{2}}\exp\{F_0/RT\})^{RT/F_m}]\times\left[-1/RT\int_\infty^0\frac{\varphi^{RT/F_m}}{\varphi^{-1}+\varphi}d\ln\varphi\right].$$

The value of this definite integral is independent of $\varphi$, and thus $L_A$, so collecting powers of $L_A$,

$$w = \text{const} \times L_A^{\frac{1}{2}+RT/F_m}.$$

When, as Constable assumed, $F_m/RT$ is large, $w$ is proportional to $L_A^{\frac{1}{2}}$. Under these conditions, the majority of the reaction is taking place on the sites where $F_B$ is near its optimum value. Now $v_{\max}$ can be found by setting $dv/dF_B=0$, or since $dF_B=-(1/RT)d\ln\varphi$ by setting $dv/d\varphi=0$:

$$dv/d\varphi = \text{const} \times L_A^{\frac{1}{2}} \times \exp\{-F_0/RT\}(1-\varphi^{-2})/(\varphi^{-1}+\varphi)^2=0,$$

whence $v_{\max}=\text{const}\times L_A^{\frac{1}{2}}$, in agreement with the result above.

It is interesting to compare this result with the results that would be obtained assuming a uniform surface. If the rearrangement were the limiting process the rate would obviously become proportional to the first power of $L_A$. On the other hand, by hypothesis, the rearranged product is much more strongly adsorbed than the reactant, and so, if desorption is the rate determining step, then reaction becomes proportional to the zeroth power of $L_A$, that is, independent of the pressure of the reactants.

It emerges, then, that on a continuously non-uniform surface, the behavior is roughly halfway in between these two cases. If the modulus $F_m$ is large, it is tantamount to saying that the distribution in the neighborhood of optimum condition is so broad that it can be approximated by a straight line, that is the sites of different kinds are equally numerous. In this case the Langmuir pressure function is raised to the half power, and the behavior of the reaction is exactly halfway in between the two extremes.

It is thus apparent that a very non-uniform surface may appear uniform for a reaction occurring under a given set of conditions, but that the pressure dependence of the reaction, calculated on the basis of a uniform surface, will be in error. Therefore, one cannot assume that the surface is "effectively" uniform, and calculate the proper pressure dependence of a reaction. Although the exponential distribution has been used here it appears that the exact functional form of a distribution is not important, if the distribution is a broad one.

## III. GENERAL EXPRESSION FOR OPTIMUM SITES

Although the example given above serves as a general indication of the picture of catalysis proposed here, it is too simple to be applied to actual cases, and so a more general expression will be derived.

For a given kind of site, assume that a fraction $\theta_A$ is covered with reactants in state $A$, a fraction $\theta_B$ with reacted matter in state $B$, and a fraction $\sum\theta_i$ with other material. The Langmuir expression applies to the concentration $\theta_A$;

$$\theta_A/1-\theta_A-\theta_B-\sum\theta_i=k_Ap_A{}^a,$$

where $p_A$ is the pressure of reactant, $k_A$ is a constant, and the exponent $a$ allows for association or dissociation upon adsorption.

Similarly,

$$\sum\theta_i/1-\theta_A-\theta_B-\sum\theta_i=\sum_i k_ip_i{}^{a_i}.$$

Combining,

$$\theta_A=\Lambda_A(1-\theta_B),$$

where

$$\Lambda_A=\frac{k_Ap_A{}^a/(1+k_Ap_A{}^a)}{1+\sum_i k_ip_i{}^{a_i}+k_Ap_A{}^a/(1+k_Ap_A{}^a)}.$$

The equation governing $d\theta_B/dt$ is

$$d\theta_B/dt=(kT/h)A\Lambda_A(1-\theta_B)\exp\{-F_A/RT\} - (kT/h)(B\theta_B)^n\exp\{-F_B/RT\}. \quad (4)$$

The factors $A$ and $B$ allow equilibrium loss or gain of constituents of the reacting molecule preceeding reaction and desorption, respectively.

In the simple example treated previously no particles were gained or lost, and the derivation therefore applied only to a simple rearrangement. Now the catalytic scheme is generalized to include (1) equilibrium adsorption of reactants, (2) equilibrium loss or gain of particles up to first difficult (slow) step, (3) first difficult step, (4) further equilibrium loss or gain of particles, and finally (5) last difficult step.

$A$ and $B$, then, contain the various equilibrium constant factors that determine the actual reactant concentration, just prior to the two assumed difficult steps. Their construction will become clear when the specific example of the ammonia decomposition is treated in the next section.

The exponent $n$ in Eq. (4) gives the relative order of the two limiting reactions, being two for the decomposition of ammonia when it is assumed that the evolution of nitrogen is bimolecular. The constant $r$ will no longer be assumed to be unity.

In order to calculate $w$, the over-all rate, Eq. (4) will be put in another form. Substituting $v=(kT/h)(B\theta_B)^n \times\exp\{-F_B/RT\}$ and $rF_A+F_B=F_0$ yields

$$0=(kT/h)A\Lambda_A\{1-(1/B)(h/kT)^{1/n} \times\exp\{F_B/nRT\}v^{1/n}\}\exp\{(F_B-F_0)/rRT\}-v. \quad (5)$$

This equation can be put in the form

$$1-ivz-jv^{1/n}z^{-r/n}=0, \quad (6)$$

where

$$i=1/(kTh)A\Lambda_A\exp\{-F_0/RT\}, \quad (7)$$

$$j=(1/B)(h/kT)^{1/n}, \quad (8)$$

and

$$z=\exp\{-F_B/rRT\}. \quad (9)$$

Equivalent to (6) is the expression

$$1-(pv)(qz)-(pv)^{1/n}(qz)^{-r/n}=0, \quad (10)$$

where

$$p=i^{r/1+r}j^{n/1+r}, \quad (11)$$

and

$$q=i^{1/1+r}/j^{n/1+r}. \tag{12}$$

Writing

$$y=qz, \tag{13}$$

one can solve (10) to give

$$v=(1/p)f(y), \tag{14}$$

where $f(y)$ is the functional solution of the fractional order algebraic equation.

Now, assuming an exponential distribution,

$$w=c\int_{-\infty}^{\infty}\exp\{F_B/F_m\}vdF_B,$$

and substituting

$$F_B=-rRT\ \ln y-rRT\ \ln q \tag{15}$$

yields

$$w=-[(crRT)/(pq^{rRT/F_m})]\int_{+\infty}^{0}y^{-rRT/F_m}f(y)d\ \ln y.$$

Recalling that the definite integral is independent of $y$, and therefore independent of the pressures, one can collect the pressure terms outside of the integral, using (11) and (12) to find

$$w=\text{const}\times(A\Lambda_A)^{r/1+r}B^{n/1+r}\times[(A\Lambda_A)^{r/1+r}B^{nr/1+r}]^{RT/F_m}. \tag{16}$$

At large values of $F_m/RT$, this expression becomes

$$w=\text{const}\times(A\Lambda_A)^{r/1+r}B^{n/1+r}. \tag{17}$$

Again, this result is in agreement with the pressure dependence at $v_{\max}$. To find $v_{\max}$ (6) is differentiated with respect to $z$, and thus $F_B$:

$$-iv+(r/n)jv^{1/n}z^{-(r/n)+1}=0$$
$$z=(rj/niv^{1-1/n})^{n/r+n}. \tag{18}$$

Substituting (18) in (6) one finds

$$v_{\max}=\text{const}\times j^{-n/r+1}i^{-r/r+1}$$
$$=\text{const}\times(A\Lambda_A)^{r/r+1}B^{n/r+1},$$

equivalent to (17).

The complexity of the result (16) is apparent and the approximate form (17) will be used to discuss the ammonia decomposition.

## IV. THE DECOMPOSITION OF AMMONIA

Love and Emmett[4] investigated the decomposition of ammonia over a number of iron synthetic ammonia catalysts. The simplest results were obtained over a doubly promoted (Fe, $K_2O$, $Al_2O_3$) catalyst 931. Velocity of reaction was found to be proportional to $p_{NH_3}{}^{0.56-0.80}/p_{H_2}{}^{0.78-0.85}$.

[4] K. S. Love and P. H. Emmett, J. Am. Chem. Soc. **63**, 3297 (1941).

Assuming that (a) ammonia is not near saturation and (b) hydrogen adsorption is not competing with ammonia, then $\Lambda_A\sim p_{NH_3}$. Thus, the exponent of $\Lambda_A$, $r/1+r=0.56$–$0.80$, and $r$ is about 2.

It appears that the final slow process in the decomposition of ammonia is the evolution of nitrogen as $N_2$; therefore, $n=2$. However, the first slow process could be the loss of any of the three hydrogen atoms, whichever is held most tightly. If it is the last, $A=kp_{H_2}{}^{-1}/1+kp_{H_2}{}^{-1}$, the fraction of NH present in the nitrogen hydrides on the surface. $B=1$, because, the last hydrogen being lost, no further particles are lost before the evolution of nitrogen. If the first hydrogen is the most tightly held, $A=1$, because the adsorbed $NH_3$ need lose no particles to be ready to take part in the first slow reaction. However, in this case $B=kp_{H_2}{}^{-1}/1+kp_{H_2}{}^{-1}$ because two more hydrogens must be lost before $N_2$ can be evolved. Similarly, if the second hydrogen is the tightest, $A=B=kp_{H_2}{}^{-\frac{1}{2}}/1+kp_{H_2}{}^{-\frac{1}{2}}$. It is not possible to decide between these alternatives on the basis of the experimental evidence, because for $r=n=2$, they give similar dependence on $p_{H_2}$. The marked influence of hydrogen shows that $1>kp_{H_2}{}^{-1}$, and for each case the exponent of the hydrogen in the velocity expression comes out somewhat too low, at $\frac{2}{3}$. By assuming that the hydrogen is near saturation on independent sites of its own and that a vacant site of this kind is needed to receive the tightest hydrogen, this discrepancy can be removed, but there is no reason to believe that this is so, or that the alternative explanation that $RT/F_m$ is not negligible is incorrect. Similarly, the other, more complicated, results on other catalysts can be explained in a variety of ways.

## V. EFFECTIVELY UNIFORM SURFACES

It is by no means true that if adsorption studies with the appropriate gases have shown evidence for nonuniform surface, that the treatment given above is necessarily correct for catalysts occurring on that surface. If the distribution of activation energies is not sufficiently broad or continuous, or if the optimum sites are not present in appreciable numbers, then one process may be definitely rate determining, and the surface will behave kinetically like a uniform one, when appropriate averages are used.

In general, evidence for an effectively uniform surface is found when rate *versus* pressure obeys a Langmuir plot, although adsorption may not. On the other hand, when rate *versus* pressure plots extend in an approximation at a straight line over many cycles of log–log plot, it is evidence for the type of catalysis discussed above.

Therefore, adsorption data as such have no direct connection with catalysis, and rate theories based on gross over-all coverages are likely to be wrong, because sites that contribute negligible amounts to adsorption isotherm or rate data are often of paramount importance for catalysis.

# Statistical Mechanics of Adsorption. VI. Localized Unimolecular Adsorption on a Heterogeneous Surface

TERRELL L. HILL
*Department of Chemistry, University of Rochester, Rochester, New York*
(Received October 12, 1948)

The Langmuir isotherm for localized unimolecular adsorption is generalized (using statistical methods) in order to discuss adsorption on a heterogeneous surface, with and without interactions between adsorbed molecules. The configurational entropy, and the nature of the phase changes on a random heterogeneous surface are discussed. In particular, on this type of surface, the theory predicts, at least for one special case, that condensation will occur in two steps (instead of the customary one step) at low enough temperatures.

## I. INTRODUCTION

ANY general theory of adsorption must recognize the heterogeneity (in energy of adsorption) of actual surfaces due to impurities, cracks, edges and corners, lattice imperfections, different crystal faces, etc. We restrict ourselves in this paper to a study of *localized unimolecular* adsorption on a heterogeneous surface (one component systems). In particular, our purpose is to extend the type of treatment given by Fowler and Guggenheim[1] for localized unimolecular adsorption on a uniform surface to the heterogeneous case. Actual physical systems to which this treatment might apply are those involving physical adsorption at low enough temperatures (for localization[2–6]) or chemisorption. Recent discussions of other aspects of heterogeneous surfaces have been given by Sips,[7] Halsey and Taylor,[8] and Miller.[9]

In Section II we consider adsorption in the absence of interactions between adsorbate molecules, and direct particular attention to the configurational entropy. In Section III interactions are taken into account. It is found that condensation can occur in two steps as well as in the more usual single step (uniform surface).

## II. ADSORPTION IN THE ABSENCE OF INTERACTIONS

### A. General Equations

We make the same assumptions as Fowler and Guggenheim[1] except that the energy of adsorption (the ground state energy of an adsorbed molecule referred to infinite separation of gas molecules as zero) differs for different sites. We assume that of the total $B$ sites, $B_i$ have an energy $-\epsilon_i$, where $B_i$ (for all $i$) as well as $B$ is a large number. We assume further that a molecule on any of these $B_i$ sites has the same partition function $j_i(T)$ for the three vibrational degrees of freedom of the center of mass and the usual internal degrees of freedom.

If $N$ molecules are adsorbed on the $B$ sites, we let $N_i \leqslant B_i$ be the number on sites of energy $-\epsilon_i$. The $N_i$ are also assumed to be large numbers. For a given $N$, any distribution $N_i$ among the $B_i$ contributes a term $Q_{N_i}$ to the partition function $Q(N, B, T)$, where $Q_{N_i}$ is given by

$$Q_{N_i}=\prod_i \frac{B_i!}{N_i!(B_i-N_i)!} j_i^{N_i} \exp(N_i\epsilon_i/kT). \quad (1)$$

We make the usual excellent approximation of replacing $\ln Q$ by the logarithm of the largest $Q_{N_i}$. We therefore proceed to find the distribution $N_i$ which gives the largest term in $Q$. This is done by the standard method of undetermined multipliers: $\ln Q_{N_i}$ is maximized with respect to the $N_i$, keeping $N=\sum_i N_i$ fixed. One finds as the equilibrium (maximum term) distribution

$$N_i=\frac{B_i}{(1/j_i)\exp[\alpha-(\epsilon_i/kT)]+1}, \quad (2)$$

where $\alpha$ is the undetermined multiplier. The treatment of this section bears an obvious close relationship to Fermi-Dirac statistics[10] and the perfect Fermi-Dirac gas. On substituting Eq. (2) into Eq. (1) we find

$$\ln Q=\sum_i B_i\left\{-\ln\left[\frac{(1/j_i)\exp[\alpha-(\epsilon_i/kT)]}{(1/j_i)\exp[\alpha-(\epsilon_i/kT)]+1}\right]+\frac{\alpha}{(1/j_i)\exp[\alpha-(\epsilon_i/kT)]+1}\right\}. \quad (3)$$

Equation (2) with $N=\sum N_i$ gives $\alpha=\alpha(N, B, T)$. We now take the partial derivative with respect to $N$ of both sides of $N=\sum N_i$ and use this in $(\partial \ln Q/\partial N)_{B,T}$, from Eq. (3), and find

$$-\frac{\mu}{kT}=\left[\frac{\partial\left(-\frac{A}{kT}\right)}{\partial N}\right]_{B,T}=\left(\frac{\partial \ln Q}{\partial N}\right)_{B,T}=\alpha, \quad (4)$$

[1] R. H. Fowler and E. A. Guggenheim, *Statistical Thermodynamics* (Cambridge University Press, London, 1939), pp. 426–444.
[2] T. L. Hill, J. Chem. Phys. **14**, 441 (1946).
[3] T. L. Hill, J. Chem. Phys. **14**, 263 (1946).
[4] T. L. Hill, J. Chem. Phys. **15**, 767 (1947).
[5] T. L. Hill, J. Chem. Phys. **16**, 181 (1948).
[6] T. L. Hill, J. Chem. Phys. **17**, 520 (1949).
[7] R. Sips, J. Chem. Phys. **16**, 490 (1948).
[8] G. Halsey and H. S. Taylor, J. Chem. Phys. **15**, 624 (1947).
[9] A. R. Miller, J. Chem. Phys. **16**, 841 (1948).
[10] J. E. Mayer and M. G. Mayer, *Statistical Mechanics* (John Wiley and Sons, Inc., New York, 1940), Chapters 5 and 16.

as in Fermi-Dirac statistics.[10] $A$ is the Helmholtz free energy and $\mu$ is the chemical potential ($\mu=F/N$, where $F$ is the Gibbs free energy). The relation $\alpha=-\mu/kT$ can be found alternatively using $\varphi=-(\partial A/\partial \mathfrak{A})_{N,T}$ and[6] $N\mu=A+\varphi\mathfrak{A}$, where $\varphi$ is the two-dimensional spreading pressure and $\mathfrak{A}$ is the surface area (proportional to $B$). We may therefore substitute $-\mu/kT$ for $\alpha$ in Eqs. (2) and (3).

The adsorption isotherm is obtained from Eq. (2):

$$N=\sum_i \frac{B_i}{(1/j_i)\exp[-(\mu+\epsilon_i)/kT]+1}. \tag{5}$$

This gives, essentially, $N=N(p, T, B)$, where $p$ is the pressure of gas in equilibrium with adsorbate since, at equilibrium, $\mu=\mu_{\text{gas}}$ and, for a perfect gas,

$$\frac{\mu_{\text{gas}}}{kT}=\ln p+\ln\left[\left(\frac{h^2}{2\pi mkT}\right)^{\frac{3}{2}}\frac{1}{kTj_G(T)}\right]. \tag{6}$$

In Eq. (6) $j_G$ is the internal partition function of a gas molecule. Equation (5), with $(1/j_i)\exp(-\mu/kT)$ replaced by $a_i(T)/p$, is of course well-known[7,8,11] as the Langmuir isotherm for a heterogeneous surface. The statistical significance of $a_i$ is provided by the present treatment. It might be remarked here that Sips makes the rather serious assumption that $a_i$ is the same for all $i$.

Throughout this paper, if the molecular species is different in the adsorbed state than in the gaseous state (e.g., $H_2$), the only property of the adsorbate in our equations that is changed is the relation between $\mu$ and $p$ (see reference 1, p. 428).

For a given distribution $B_i$, Eq. (5) allows us to calculate $\theta=N/B$ as a function of $\mu$ (and therefore of $p$) and $T$. Equation (3) similarly gives $A=A(\mu, T)$ since $A=-kT\ln Q$. $\varphi\mathfrak{A}$ can then be found from $\varphi\mathfrak{A}=N\mu-A$. The remaining thermodynamic functions[6] $E$, $S=E/T-A/T$ and $H=E+\varphi\mathfrak{A}$ can be obtained as functions of $\mu$ and $T$ if $E$ is known. But

$$E=kT^2(\partial \ln Q/\partial T)_{N,B}$$

$$=\sum_i \frac{B_i}{(1/j_i)\exp[-(\mu+\epsilon_i)/kT]+1}\times\left(kT^2\frac{\partial \ln j_i}{\partial T}-\epsilon_i\right). \tag{7}$$

Now $\theta=\theta(\mu, T)$ from Eq. (5) also gives $\mu=\mu(\theta, T)$ and hence all the thermodynamic functions can be found as functions of $\theta$ and $T$.

If the distribution $B_i$ is such that we can replace summation over the $B_i$ by integration,[7,8,11] we let $Bf(\epsilon)d\epsilon$ be the number of sites with values of $\epsilon_i$ between $\epsilon$ and $\epsilon+d\epsilon$. Then

$$\int f(\epsilon)d\epsilon=1, \tag{8}$$

$$\theta=\int\frac{f(\epsilon)d\epsilon}{[1/j(\epsilon, T)]\exp[-(\mu+\epsilon)/kT]+1}, \tag{9}$$

$$-\frac{A}{B}=\int\left\{kT\ln\frac{[1/j(\epsilon, T)]\exp[-(\mu+\epsilon)/kT]+1}{[1/j(\epsilon, T)]\exp[-(\mu+\epsilon)/kT]}-\frac{\mu}{[1/j(\epsilon, T)]\exp[-(\mu+\epsilon)/kT]+1}\right\}f(\epsilon)d\epsilon, \tag{10}$$

$$\frac{E}{B}=\int\left[kT^2\frac{\partial \ln j(\epsilon, T)}{\partial T}-\epsilon\right]\times\frac{f(\epsilon)d\epsilon}{[1/j(\epsilon, T)]\exp[-(\mu+\epsilon)/kT]+1}. \tag{11}$$

Sips[7] and Halsey and Taylor[8] have used $-\infty$ and $+\infty$ as limits of integration in their isotherm equations equivalent to Eq. (9). However, negative values of $\epsilon$ seem rather unrealistic in ordinary cases so $f(\epsilon)=0$ for $\epsilon<0$ usually. In fact in most cases $f(\epsilon)$ must be essentially zero except in a range $\epsilon_1<\epsilon<\epsilon_2$ where $\epsilon_1>0$ and $\epsilon_2<+\infty$. Using the range $-\infty\leqslant\epsilon\leqslant+\infty$, Sips[7] gives a very elegant procedure to find the unique $f(\epsilon)$ which is responsible for a given $\theta(p)$ *assuming* localized adsorption with $j$ independent of $\epsilon$ and $w=0$ (see below). Almost certainly when this method is applied to experimental data and it is found that the unique $f(\epsilon)>0$ (appreciably) for $\epsilon<0$, it must mean that these assumptions are quite unjustified (as they presumably are in most cases).

In the electron theory of metals a single $f(\epsilon)$ is of interest and it is definitely worth while to obtain series expansions for the integrals giving the thermodynamic functions (for both low and high temperature cases). Here, however, $f(\epsilon)$ varies from case to case and furthermore the presence of $j(\epsilon, T)$ in the equations complicates matters considerably. Hence no such expansions are attempted.

We use integrals instead of summations henceforth in this section as a matter of convenience. The entropy is given by Eqs. (10) and (11). It is interesting to divide the entropy into a configurational entropy $S_c$ and a nonconfigurational entropy $S_{nc}=S-S_c$. $S_c$ is associated with the possible configurational arrangements of the molecules among the sites while $S_{nc}$ is the entropy associated with the internal degrees of freedom and the three vibrational degrees of freedom of the center of mass. In the absence of interactions (as is assumed in

[11] S. Brunauer, *Adsorption of Gases and Vapors* (Princeton University Press, Princeton, 1943), pp. 82–83.

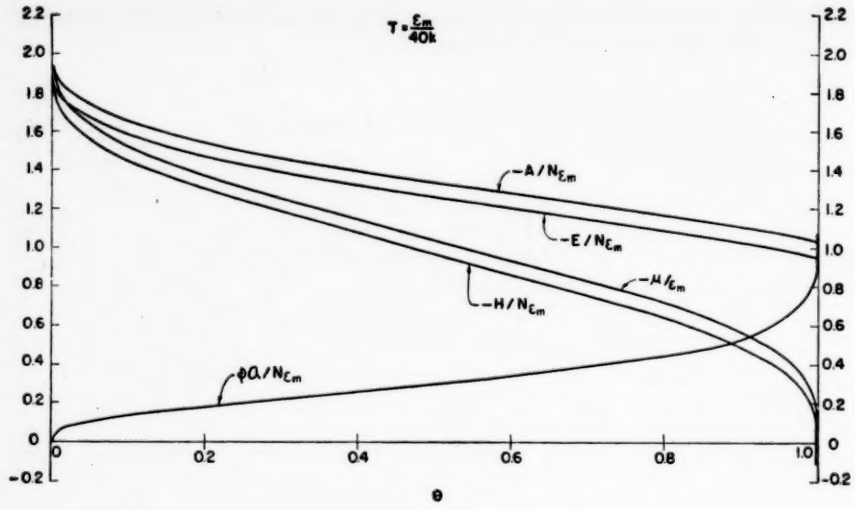


FIG. 1. Thermodynamic functions of adsorbed molecules in the absence of interactions.

this section),

$$S_c = k \ln \prod_i \frac{B_i!}{N_i!(B_i-N_i)!} \tag{12}$$

$$= kB \int \left\{ \ln \frac{(1/j)\exp[-(\mu+\epsilon)/kT]+1}{(1/j)\exp[-(\mu+\epsilon)/kT]} + \frac{\ln(1/j)\exp[-(\mu+\epsilon)/kT]}{(1/j)\exp[-(\mu+\epsilon)/kT]+1} \right\} f d\epsilon \tag{13}$$

and

$$S_{nc} = kB \int \frac{\left( T\frac{\partial \ln j}{\partial T} + \ln j \right) f d\epsilon}{(1/j)\exp[-(\mu+\epsilon)/kT]+1}. \tag{14}$$

In the presence of interactions the division into configurational and non-configurational entropy (see Eqs. (33), for example) becomes rather arbitrary.

Finally, we discuss here the dependence of $j$ on $\epsilon$. The electronic and internal vibrational degrees of freedom should be independent of $\epsilon$ to a first order of approximation (in physical adsorption). However, rotation and the vibration of the center of mass ought to be considerably affected[5] by the value of $\epsilon$. In general, rotation should be more restricted the larger $\epsilon$, but the dependence is complicated.[5] We therefore confine ourselves for simplicity to a monatomic molecule where rotation can be ignored. Taking the weight of the ground electronic state as unity, we have approximately, in this simple case

$$j = [1-\exp(h\nu_h/kT)]^{-2}[1-\exp(-h\nu_v/kT)]^{-1}, \tag{15}$$

where the vibrational motion is assumed simple harmonic and the two horizontal (motion in the plane of the surface) frequencies $\nu_h$ are assumed equal.

For physical adsorption, it can be deduced from Eqs. (9) and (3) of reference 5 that $\nu_v \alpha \epsilon^{\frac{1}{2}}$ is approximately the correct dependence of $\nu_v$ on $\epsilon$ (for $\epsilon \gtrsim 0$ of course). For chemisorption information from ordinary diatomic molecules should be fairly valid. For thirteen molecules,[12] using the Morse curve

$$U = D\{1-\exp[-a'(r-r_e)]\}^2,$$

for which

$$\nu = a' D^{\frac{1}{2}}/2^{\frac{1}{2}}\pi\mu^{\frac{1}{2}} \tag{16}$$

($\mu$ is the reduced mass here), $a'$ varies only from about 1.9 to 3.1 $A^{-1}$ while $D$ varies from about 1.5 to 9.6 electron volts. From Eq. (16), we therefore again deduce that $\nu_v \alpha \epsilon^{\frac{1}{2}}$ is a good approximation. With regard to $\nu_h$, in physical adsorption this frequency is proportional to the square root of the potential barrier (Eq. (15) of reference 2) but the potential barrier is probably approximately directly proportional to $\epsilon$ (i.e., if the whole scale of the potential energy surface is expanded uniformly both $\nu_v$ and $\nu_h$ vary as $\epsilon^{\frac{1}{2}}$). In chemisorption if, for example, a light adsorbate atom is bonded to a heavy adsorbent atom to form a diatomic molecule, the three translational degrees of freedom of the adsorbate atom become the one vibrational ($\nu_v$) and two rotational degrees of freedom of the diatomic molecule. However, the two rotational degrees of freedom will ordinarily be highly restricted and thus will be essentially horizontal vibrations to which the preceding discussion of $\nu_h$ in physical adsorption ought to apply approximately.

On the basis of the above very rough argument, the conclusion is that if any simple and general approximations are to be made, $\nu_v \alpha \epsilon^{\frac{1}{2}}$ and $\nu_h \alpha \epsilon^{\frac{1}{2}}$ appear to be the correct choice. It might be noted that at high enough temperatures Eq. (15) becomes $j = (kT/h\nu_h)^2(kT/h\nu_v)$, or $j \alpha \epsilon^{-\frac{3}{2}}$.

### B. A Numerical Example and the Configurational Entropy

In order to illustrate the equations of Section IIA we have made calculations, using numerical integrations, for a hypothetical case which resembles rather closely what is known about the adsorption of argon on KCl,

[12] $H_2$, CH, NH, OH, HCl, NO, $O_2$, $N_2$, CO, $C_2$, $Cl_2$, $Br_2$, $I_2$.

except that a quite arbitrary $f(\epsilon)$ was chosen (but the maximum in $f(\epsilon)$ was designed to fall approximately at the observed heat of adsorption, 2000 cal./mole). Actually KCl should present a relatively uniform surface.

We take as a convenient function of reasonable form

$$f(\epsilon)=\sin^2(\pi\epsilon/2\epsilon_m), \quad 0\leqslant\epsilon\leqslant 2\epsilon_m, \qquad (17)$$
$$=0, \quad \epsilon<0, \quad \epsilon>2\epsilon_m.$$

Equation (15) was used with

$$\nu_v=\nu_h=(\epsilon_m^{\frac{1}{2}}/40h)\epsilon^{\frac{1}{2}} \qquad (18)$$

(which gives $\nu(\epsilon_m)=5.24\times10^{11}$ sec.$^{-1}$ with $\epsilon_m=2000$ cal./mole). Two temperatures were employed: $T=\epsilon_m/40k$ and $T=\epsilon_m/10k$ (corresponding to about 25°K and 100°K for argon on KCl). The calculations also apply to chemisorption (larger $\epsilon_m$) at correspondingly higher temperatures. In this case the frequencies given by Eq. (18) are still reasonable.

The results are shown in Figs. 1 and 2. In Fig. 1, thermodynamic functions per molecule are plotted against $\theta$ for the lower temperature, $T=\epsilon_m/40k$. The curve for $\mu$ is essentially the adsorption isotherm. The general tendency of $A/N$, $E/N$, $F/N$ and $H/N$ to decrease as $\theta$ decreases is of course due to the preferential filling of the low energy sites (high $\epsilon$) at low $\theta$. The difference between $A$ and $E$ and between $F$ and $H$ is due to $TS$. The entropy is thus seen to be small compared to the other functions, except for $\theta$ very small. In Fig. 2 we plot $S$, $S_c$ and $S_{nc}$ for the two temperatures, in units of calories degree$^{-1}$ mole$^{-1}$. At both temperatures: (1) $S_{nc}$ is rather large compared to $S_c$ over most of the range in $\theta$; (2) $S$ stays fairly constant except at small $\theta$; and (3) $S_{nc}$ decreases with decreasing $\theta$ due to the higher vibrational frequencies associated with low energy (high $\epsilon$) sites. $S_c$ is small (except for low $\theta$) at the lower temperature but, at the higher temperature, is about half of the maximum possible configurational entropy $S_m$ ($T$ infinite). $S_m$ is given by

$$S_m=k\ln\frac{B!}{N!(B-N)!}, \qquad (19)$$

and is independent of $f(\epsilon)$: $S_m$ is also the configurational entropy on a uniform surface.

As in Fermi-Dirac statistics, in general, for a given $\theta$ and $T$, the lowest energy sites are practically completely filled and the highest energy sites are practically completely empty. There is a transition range in $\epsilon$ in which there are appreciable numbers of both filled and empty sites. It is easy to show that it is only this transition range in $\epsilon$ which contributes appreciably to $S_c$. This is to be expected, of course, since if sites of a given energy are completely filled or completely empty, the contribution to the total entropy is zero in either case. For a given $\theta$, the transition range in $\epsilon$ is larger at higher temperatures and hence $S_c$ increases with $T$. At $T=0$, the transition range vanishes, so that usually (see below) $S_c=0$ and $S=0$ (assuming no electronic ground state degeneracy). But $S_c=0$ at $T=0$ necessarily only for a "smooth" $f(\epsilon)$. If, on the other hand, $f(\epsilon)$ has any extremely high and sharp peaks (corresponding, for example, to nearly perfect crystals presenting a very large number of sites with essentially the same energy), then there will be an appreciable zero-point configurational entropy for those values of $\theta$ such that the sites belonging to any peak (only one peak can be involved for a given $\theta$) are incompletely filled at $T=0$ (all sites of lower energy than that of the peak are filled; all sites of higher energy are empty). Presumably this type of $f(\epsilon)$ should not be uncommon. If it eventually proves possible to obtain the zero-point configurational entropy of a system as a function of $\theta$, using entropies from heat capacity data and/or entropies from equilibrium isotherm data,[6] then this configurational entropy will furnish a "spectrum" of the *peaks* in $f(\epsilon)$, with their values of $B_i$.

## III. ADSORPTION WITH INTERACTIONS

### A. General Equations

We assume that: (1) only interactions between adsorbed molecules on nearest neighbor sites need be taken into account; (2) that the potential energy of interaction for any nearest neighbor pair is $-w$; (3) that the total interaction energy is $-\mathfrak{N}w$ where $\mathfrak{N}$ is the number of nearest neighbor pairs; and (4) that each site has $z$ nearest neighbor sites. These are the same as-

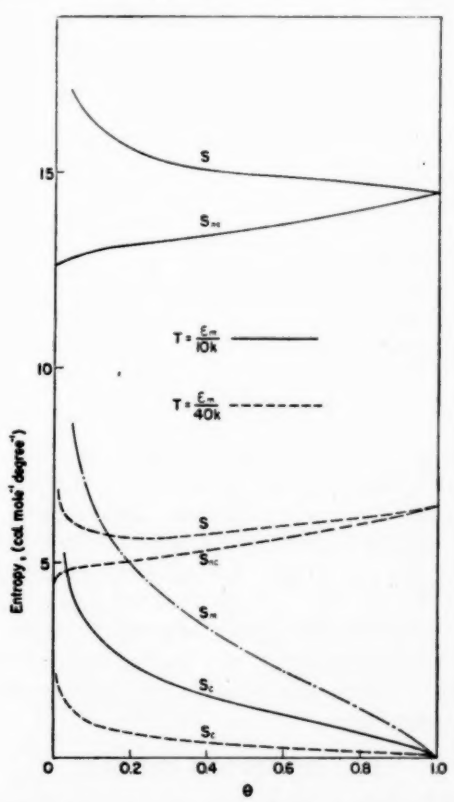


FIG. 2. Entropy of adsorbed molecules in the absence of interactions.

sumptions made by Fowler and Guggenheim[1] for a uniform surface. They are clearly less accurate for a heterogeneous surface. No assumption is made in this section about the manner in which sites of varying energies of adsorption are scattered over the surface.

We first find the equation analogous to Eq. (1). For the given distribution $N_i$ among the $B_i$ there are a total of

$$\prod_i \frac{B_i!}{N_i!(B_i-N_i)!}=\Omega_{N_i}$$

different configurations. Each of these configurations has a certain number of nearest neighbor pairs $\mathfrak{N}$. We arrange the $\Omega_{N_i}$ configurations according to the value of $\mathfrak{N}$. Suppose that out of the total $\Omega_{N_i}$ there are $g(\mathfrak{N})$ configurations with $\mathfrak{N}$ nearest neighbor pairs:

$$\sum_{\mathfrak{N}} g(\mathfrak{N})=\Omega_{N_i}.$$

Then

$$Q_{N_i}=\sum_{\mathfrak{N}} \{g(\mathfrak{N})[\prod_i j_i^{N_i}\exp(N_i\epsilon_i/kT)] \times\exp(\mathfrak{N}w/kT)\}, \quad (20)$$

$$=[\prod_i j_i^{N_i}\exp(N_i\epsilon_i/kT)] \times\sum_{\mathfrak{N}} g(\mathfrak{N})\exp(\mathfrak{N}w/kT). \quad (21)$$

In the usual way[1,4] we define $\mathfrak{N}'$ by

$$\exp(\mathfrak{N}'w/kT)=\frac{\sum g(\mathfrak{N})\exp(\mathfrak{N}w/kT)}{\sum g(\mathfrak{N})} \quad (22)$$

and $\bar{\mathfrak{N}}$ by

$$\bar{\mathfrak{N}}=\frac{\sum \mathfrak{N}g(\mathfrak{N})\exp(\mathfrak{N}w/kT)}{\sum g(\mathfrak{N})\exp(\mathfrak{N}w/kT)}. \quad (23)$$

Thus

$$Q_{N_i}=\left[\prod_i \frac{B_i!}{N_i!(B_i-N_i)!}j_i^{N_i}\exp(N_i\epsilon_i/kT)\right] \times\exp(\mathfrak{N}'w/kT) \quad (24)$$

is our desired result. $\bar{\mathfrak{N}}$ and $\mathfrak{N}'$ are related by

$$\bar{\mathfrak{N}}=-T^2[\partial(\mathfrak{N}'/T)/\partial T]. \quad (25)$$

$Q_{N_i}$ is merely one term in the complete partition function $Q$. The next step is to find, for a given $N$, the distribution $N_i$ (the equilibrium distribution) which gives the largest term $Q_{N_i}$ in $Q$. However, in order to do this, the way in which sites of different energy are distributed over the surface must be known, as this distribution of sites determines the way in which $\mathfrak{N}'$ depends on the distribution $N_i$. In the next section we make one of the simplest possible assumptions about the distribution of sites.

### B. The Random Surface

We assume here that sites of different energy are scattered *completely at random* over the surface. This should be a fairly reasonable assumption in some cases but not in others.

The number $\Omega_{N_i}$ is a fraction of the total number of ways, $\Omega$, of putting $N$ molecules on $B$ sites:

$$\Omega=[B!/N!(B-N)!].$$

Since the sites of different energy are distributed randomly, the $\Omega_{N_i}$ configurations comprise a random sampling from the total $\Omega$. Now suppose we arrange the $\Omega$ configurations according to the value of $\mathfrak{N}$: there are, say, $G(\mathfrak{N})$ configurations with $\mathfrak{N}$ nearest neighbor pairs and $\sum G(\mathfrak{N})=\Omega$. Now, by virtue of the fact that the $\Omega_{N_i}$ configurations are a random sampling from $\Omega$, we have

$$G(\mathfrak{N})/g(\mathfrak{N})=\Omega/\Omega_{N_i} \quad (26)$$

for all $\mathfrak{N}$. Defining

$$\bar{\mathfrak{N}}_G=\frac{\sum \mathfrak{N}G(\mathfrak{N})\exp(\mathfrak{N}w/kT)}{\sum G(\mathfrak{N})\exp(\mathfrak{N}w/kT)} \quad (27)$$

we find from Eqs. (23), (26) and (27) that $\mathfrak{N}=\bar{\mathfrak{N}}_G$. That is, for a random surface, $\bar{\mathfrak{N}}$ is the same as for a uniform surface ($\bar{\mathfrak{N}}_G$): $\bar{\mathfrak{N}}$ depends on $N$, $B$ and $T$ but not on the way $N$ is divided up into the $N_i$. These same remarks hold for $\mathfrak{N}'$, in view of Eq. (25). Thus, for a random surface, $\ln Q_{N_i}$ (Eq. (24)) can be maximized with respect to the $N_i$ for a fixed $N$ and we obtain, in fact, just Eq. (2) again. However $\alpha$ has a different meaning here as we shall see below.

From Eqs. (2) and (24) we have

$$\ln Q=\sum_i B_i\left\{-\ln\left[\frac{(1/j_i)\exp[\alpha-(\epsilon_i/kT)]}{(1/j_i)\exp[\alpha-(\epsilon_i/kT)]+1}\right] +\frac{\alpha}{(1/j_i)\exp[\alpha-(\epsilon_i/kT)]+1}\right\}+\mathfrak{N}'w/kT. \quad (28)$$

Following the procedure used to obtain Eq. (4) we find

$$\alpha=-[1/kT][\mu+w(\partial\mathfrak{N}'/\partial N)_{B,T}]. \quad (29)$$

The thermodynamic properties are then given by (in integral form)

$$\theta=\int\frac{f(\epsilon)d\epsilon}{(1/j)\exp[\alpha-(\epsilon/kT)]+1}, \quad (30)$$

$$-A=BkT\int\left\{\ln\frac{(1/j)\exp[\alpha-(\epsilon/kT)]+1}{(1/j)\exp[\alpha-(\epsilon/kT)]} +\frac{\alpha}{(1/j)\exp[\alpha-(\epsilon/kT)]+1}\right\}f(\epsilon)d\epsilon+\mathfrak{N}'w, \quad (31)$$

$$E=B\int\left[kT^2\frac{\partial\ln j}{\partial T}-\epsilon\right] \times\frac{f(\epsilon)d\epsilon}{(1/j)\exp[\alpha-(\epsilon/kT)]+1}-\bar{\mathfrak{N}}w. \quad (32)$$

having used Eq. (25) to obtain Eq. (32). Equation (30) gives $\alpha=\alpha(\theta, T)$, the same function as in the absence of interactions ($w=0$). The adsorption isotherm is found by putting $\alpha(\theta, T)$ in Eq. (29) to get $\mu=\mu(\theta, T)$ or $\theta=\theta(\mu, T)$.

Since $\alpha(\theta, T)$ is the same for any $w$ including $w=0$, if we substitute $\alpha(\theta, T)$ into Eqs. (31) and (32) we find, for any given $\theta$,

$$\begin{aligned}
&\mu=\mu_{w=0}-w(\partial\Re'/\partial N),\\
&A=A_{w=0}-\Re' w,\\
&E=E_{w=0}-\bar{\Re}w,\\
&S=S_{w=0}+(w/T)(\Re'-\bar{\Re}),\\
&\varphi\mathfrak{A}=(\varphi\mathfrak{A})_{w=0}+w[\Re'-N(\partial\Re'/\partial N)].
\end{aligned} \tag{33}$$

The values of the functions with subscript $w=0$ are those which would be found from the equations of Section IIA for the same $\theta$ and $T$. Numerical calculations based on Section IIA can therefore be used here to considerable advantage.

We now summarize for convenience explicit formulas for $\bar{\Re}$, $\Re'$ and $\partial\Re'/\partial N$ based on two approximations discussed in Fowler and Guggenheim.[1] The equations of Fowler and Guggenheim are applicable here since $\bar{\Re}$ and $\Re'$ are the same for a random surface as for a uniform surface, as pointed out above.

(1) Crude approximation (molecules distributed as if $w=0$ and then nearest neighbors counted):

$$\bar{\Re}=\Re'=\tfrac{1}{2}zB\theta^2, \tag{34}$$

$$(\partial\Re'/\partial N)_{B,T}=z\theta. \tag{35}$$

(2) Quasi-chemical approximation:

$$\bar{\Re}=\frac{zB}{2}\left[\theta-\frac{2\theta(1-\theta)}{\beta+1}\right], \tag{36}$$

$$\Re'=\frac{zB}{2}\left\{\theta-\frac{kT}{w}\left[\theta\ln\frac{(\beta-1+2\theta)(1-\theta)}{(\beta+1-2\theta)\theta}+\ln\frac{(\beta+1-2\theta)}{(\beta+1)(1-\theta)}\right]\right\}, \tag{37}$$

$$\frac{\partial\Re'}{\partial N}=\frac{z}{2}\left[1-\frac{kT}{w}\ln\frac{(\beta-1+2\theta)(1-\theta)}{(\beta+1-2\theta)\theta}\right], \tag{38}$$

$$\beta=\{1-4\theta(1-\theta)[1-\exp(w/kT)]\}^{\frac{1}{2}}. \tag{39}$$

### C. The Random Surface—An Example

In order to study the condensation properties of an adsorbate with interactions on a random heterogeneous surface, we investigate a very simple case. We take

$$\begin{aligned}
f(\epsilon)&=\frac{1}{2\epsilon_0}, \quad \epsilon_m-\epsilon_0\leqslant\epsilon\leqslant\epsilon_m+\epsilon_0, \quad \epsilon_0\geqslant 0,\\
&=0, \quad \epsilon<\epsilon_m-\epsilon_0, \quad \epsilon>\epsilon_m+\epsilon_0
\end{aligned} \tag{40}$$

and $j$ independent of $\epsilon$ in the range $\epsilon_m-\epsilon_0\leqslant\epsilon\leqslant\epsilon_m+\epsilon_0$. This simple case has the advantage of giving fairly tractable expressions, and should exhibit condensation properties of some general qualitative significance. Halsey and Taylor[8] and Sips[7] discussed this $f(\epsilon)$, obtaining the isotherm in the $w=0$ case.

We use the quasi-chemical approximation. From Eqs. (29), (30), (38) and (40), we find for the adsorption isotherm

$$P(\theta)\equiv\frac{j\lambda\exp(zw/2kT)\exp(\epsilon_m/kT)}{s}=\frac{x(y-1)}{1-ys^2} \tag{41}$$

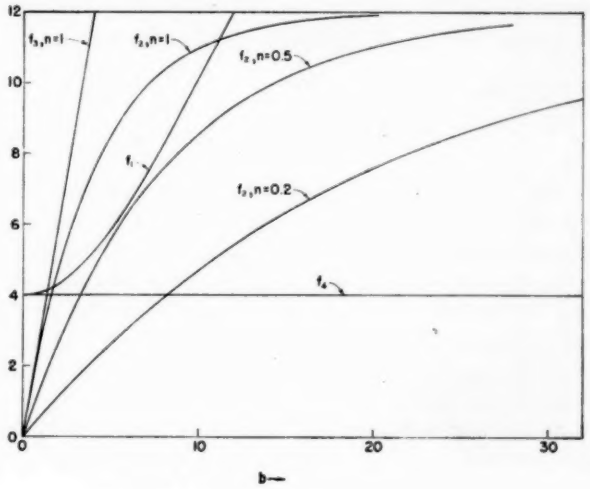


FIG. 3.

where

$$\lambda=\exp(\mu/kT), \qquad s=\exp(-b/2),$$

$$x=\left[\frac{(\beta-1+2\theta)(1-\theta)}{(\beta+1-2\theta)\theta}\right]^{z/2}, \quad b=2\epsilon_0/kT,$$

$$y=\exp(b\theta).$$

$P$ is not the equilibrium gas pressure but is directly proportional to it (Eq. (6)). For $\epsilon_0=0$ (uniform surface), Eq. (41) reduces to Eq. (1012,7) of Fowler and Guggenheim. It is easy to see that

$$P(1-\theta)P(\theta)=\exp(b)=[P(\tfrac{1}{2})]^2$$

and hence that $\ln[P(\theta)/P(\frac{1}{2})]$ is an odd function of $\theta-\frac{1}{2}$.

After lengthy algebra one can show that

$$\frac{\partial\ln P}{\partial\theta}=\frac{z}{2}\frac{(1-\beta)}{\beta\theta(1-\theta)}-\frac{by(s^2-1)}{(1-y)(ys^2-1)}, \tag{42}$$

and

$$\frac{\partial^2\ln P}{\partial\theta^2}=\frac{z}{4}\frac{(1-2\theta)(2\beta^3-3\beta^2+1)}{\beta^3\theta^2(1-\theta)^2}-\frac{b^2y(s^2-1)(s^2y^2-1)}{(1-y)^2(ys^2-1)^2}. \tag{43}$$

We note that $\theta=\frac{1}{2}$ is always a root of $\partial^2 \ln P/\partial\theta^2=0$ so that $\ln P$ has an inflection point at $\theta=\frac{1}{2}$. We now substitute $\theta=\frac{1}{2}$ into Eq. (42) to find the slope of $\ln P$ at this inflection point. We obtain

$$\left(\frac{\partial \ln P}{\partial\theta}\right)_{\theta=1/2}=b\coth\frac{b}{4}-2z[1-\exp(-w/2kT)]. \quad (44)$$

To study the effect of a temperature change on the condensation properties at constant $\epsilon_0$ and $w$, we set $w=n\epsilon_0$ ($n$ is thus a measure of the ratio of the interaction energy to the "spread" in the energy of adsorption) and let $b$ vary ($b=2\epsilon_0/kT$) keeping $n$ and $\epsilon_0$ constant:

$$(\partial \ln P/\partial\theta)_{\theta=1/2}=b\coth(b/4) -2z[1-\exp(-nb/4)]. \quad (45)$$

In Fig. 3 we plot the functions $f_1=b\coth(b/4)$ and $f_2=2z[1-\exp(-nb/4)]$ against $b(b\geqslant 0)$ for $z=6$ and several values of $n$. We see that for a sufficiently large value of $n$ ($n=1$ for example when $z=6$) the slope at $\theta=\frac{1}{2}$ is positive ($f_1>f_2$) at the highest temperatures ($b$ small), is zero at a critical temperature ($f_1=f_2$) and becomes negative at temperatures lower than the critical temperature, thus indicating a phase change. However, at still lower temperatures the slope again becomes positive and in fact approaches $+\infty$ as $b\to\infty$ ($T\to 0$). This indicates a relatively complicated behavior which we shall discuss below.

We digress briefly to examine the crude approximation (Eqs. (34) and (35)) in connection with Fig. 3. This approximation amounts to using only the first two terms in the expansion of $\exp(-nb/4)$ in Eq. (45). We get

$$(\partial \ln P/\partial\theta)_{\theta=1/2}=b\coth(b/4)-(nbz/2). \quad (46)$$

The function $f_3=nbz/2$ is a straight line with the same slope at the origin as $f_2$. For $n>2/z$ there is only one temperature (one value of $b$) at which $f_1=f_3$ and $(\partial \ln P/\partial\theta)_{\theta=\frac{1}{2}}$ is negative for all temperatures below this critical temperature. This is the same type of critical behavior as for a uniform surface (for a uniform surface, $f_1=b\coth(b/4)$ becomes $(\epsilon_0\to 0)f_4=4$). From Eq. (46) the critical temperature is

$$kT_c=\frac{\epsilon_0}{2\coth^{-1}(nz/2)}. \quad (47)$$

The adsorption isotherm in this crude approximation turns out to be

$$P=\frac{j\lambda\exp(\epsilon_m/kT)}{s}\,\frac{v(y-1)}{1-ys^2}, \quad (48)$$

where $v=\exp(-zw\theta/kT)$. For $n<2/z$, one can show

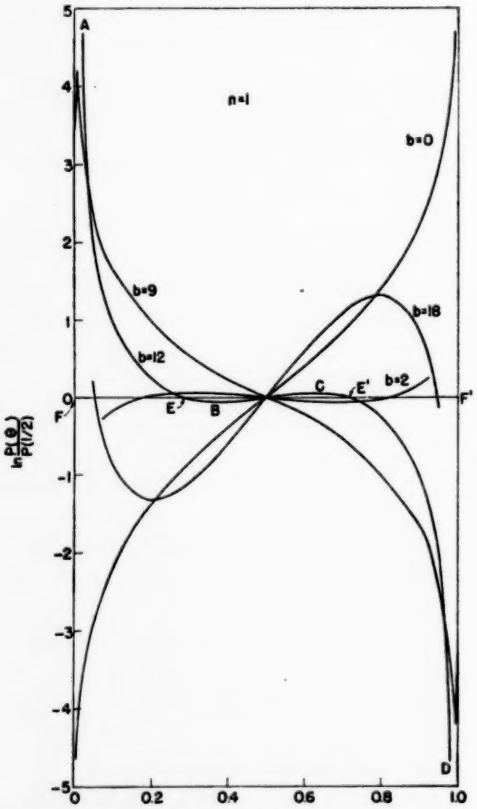


FIG. 4. Critical isotherm properties, $n=1$.

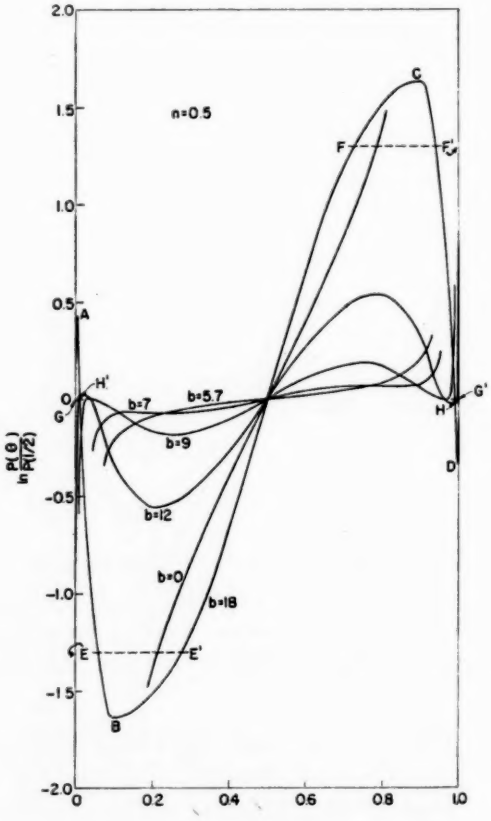


FIG. 5. Critical isotherm properties, $n=0.5$.

from Eq. (48) that $\partial \ln P/\partial\theta > 0$ for all $0 \leqslant \theta \leqslant 1$ and $b \geqslant 0$ and hence that there is no phase change no matter how low the temperature. For $n=2/z$, $T_c=0$. The above properties are interesting but should not be taken seriously in as much as the more accurate quasi-chemical approximation leads to qualitatively different behavior. Incidentally, as is well known, for a *uniform* surface the crude ($f_3$ and $f_4$) and quasi-chemical ($f_2$ and $f_4$) approximations have the *same* essential qualitative features.

We now return to the quasi-chemical approximation and discuss Figs. 4–6 in which isotherms in the form $\ln[P(\theta)/P(\frac{1}{2})]$ *versus* $\theta$ are plotted for $z=6$. A complete explicit analytical discussion of the critical properties of Eq. (41) turns out to be difficult. Reference to isotherms is therefore especially helpful. In Fig. 4, isotherms for the case $n=1$ are given. As $b$ increases from $b=0$ to $b=2$ the critical value of $b\cong 1.75$ (Fig. 3) is passed and therefore the $b=2$ isotherm shows a slight loop, and a phase change. As $b$ increases further the slope at $\theta=\frac{1}{2}$ becomes more negative up to about $b=6$ (Fig. 3) and then less negative until the slope at $\theta=\frac{1}{2}$ is again zero at $b\cong 11.2$ (Fig. 3). The isotherm for $b=9$ is given and illustrates further the behavior in the range $1.75<b<11.2$. There is a single loop and phase change of the usual type in this region. For $b>11.2$, for example at $b=12$ and $b=18$ (Fig. 4), the slope at $\theta=\frac{1}{2}$ is again positive (Fig. 3). There are now two loops between $\theta=0$ and $\theta=1$. The behavior of the $b=12$ and $b=18$ isotherms for very small $\theta$ resembles the $b=9$ curve, but these isotherms go off the graph with this scale. Although there are two loops at $b=12$ it is clear from the areas involved[13] that there is just one phase change between $\theta=0$ and $\theta=1$ (at $P(\theta)=P(\frac{1}{2})$). However a *rough* estimate of the areas indicates that for $b=18$ there are two phase changes, the first going from $\theta\cong 0$ to $\theta\cong 0.46$ and the second from $\theta\cong 0.54$ to $\theta\cong 1$. For $n=1$, there is thus a critical value of $b$, probably between $b=12$ and $b=18$, at which the transition takes place from two loops and one phase change to two loops and two phase changes. As is clearer in Figs. 5 and 6 (see also Eqs. (52)–(55)), as $b$ gets still larger the two jumps in $\theta$ (phase changes) remain but go from $\theta\cong 0$ to $\theta=a$ and $\theta=1-a$ to $\theta\cong 1$, where $a\to 0$ as $b\to\infty$ ($T\to 0$). Thus, although the loops themselves get more extreme as $T\to 0$, their physical manifestation (the jumps in $\theta$) actually tends to disappear. The above qualitative behavior for $n=1$ is presumably general for any $n>0.53$ (for $z=6$, $f_2$ is tangent to $f_1$ at $n\cong 0.53$ and $b\cong 5.7$; for $z=4$, $n\cong 1.05$ and $b\cong 4.55$).

It might be pointed out here that the above discussion of phase changes in terms of areas can be translated into a consideration of $\varphi$ *versus* $\ln[P(\theta)/P(\frac{1}{2})]$ curves ($\ln[P/P(\frac{1}{2})]$ is proportional to $\mu$ so this is essentially $\varphi$ *versus* $\mu$). We show *schematically* (the detailed calculation has not been made) in Fig. 7 the $\varphi$ *versus* $\mu$ curve for $b=12$, $n=1$ (see Fig. 4). This curve is analogous to

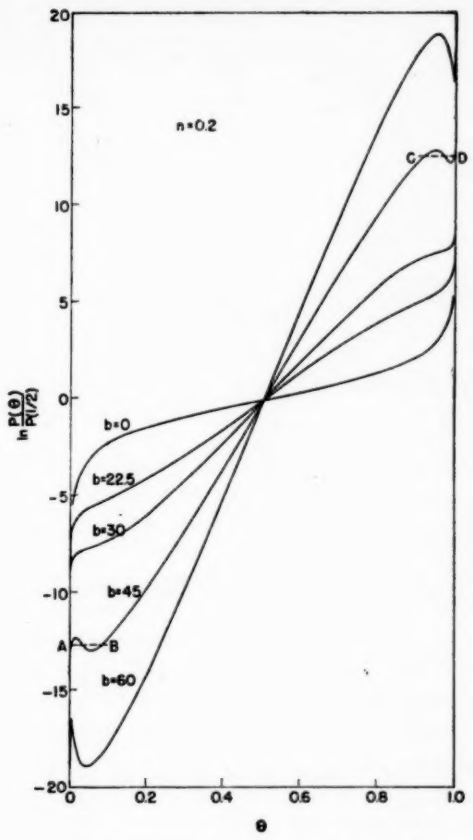


FIG. 6. Critical isotherm properties, $n=0.2$.

Fig. XII-4 as given by Slater[14] for a three-dimensional system ($p$ *versus* $\mu$). The stable equilibrium path is $a$, $FF'$, $b$ (see also Fig. 4). On adsorption, the only accessible metastable path is $FA$; on desorption, $F'D$. $BC$ is metastable but inaccessible. Figure 8 gives the corresponding curve for a case with two phase changes. It represents *schematically* $b=18$ in Fig. 5 ($b=18$ in Fig. 4 would be similar). The stable equilibrium path is $a$, $EE'$, $FF'$, $b$. On adsorption the metastable paths $EA$, $G'F'$ and $FC$ are accessible, on desorption $F'D$, $GE$ and $E'B$. The phase change can take place in one jump using the metastable path $E$, $GG'$, $F'$. Curves of this type are also helpful in investigations of capillary condensation and hysteresis.[4]

Figures 3 and 5 show that for $n=0.5$, $(\partial \ln P/\partial\theta)_{\theta=\frac{1}{2}}$ decreases from a positive value at $b=0$ to very nearly zero at $b\cong 5.7$ and then increases again with increasing $b$. There is no critical point (first and second derivatives of $\ln P$ equal to zero) at $\theta=\frac{1}{2}$ for any value of $b$ when $n<0.53$ ($z=6$). However, for $n=0.5$, a critical point does appear at $b\cong 7$ and $\theta=0.2$, 0.8. For $n<0.53$, only the double phase change behavior is observed. Again the actual magnitude of the jumps decreases as $b\to\infty$. Figure 6 with $n=0.2$ shows essentially similar behavior, which is presumably typical for any $0<n<0.53$. One

[13] See p. 433 of reference 1 and pp. 775–776 of reference 4.

[14] J. C. Slater, *Introduction to Chemical Physics* (McGraw-Hill Book Company, Inc., New York, 1939), p. 188.

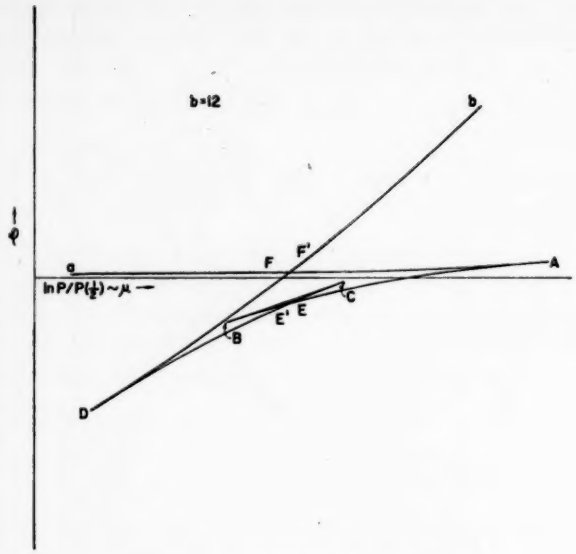


FIG. 7. $\varphi$ *versus* $\mu$-curve for $b=12$, $n=1$ (see Fig. 4).

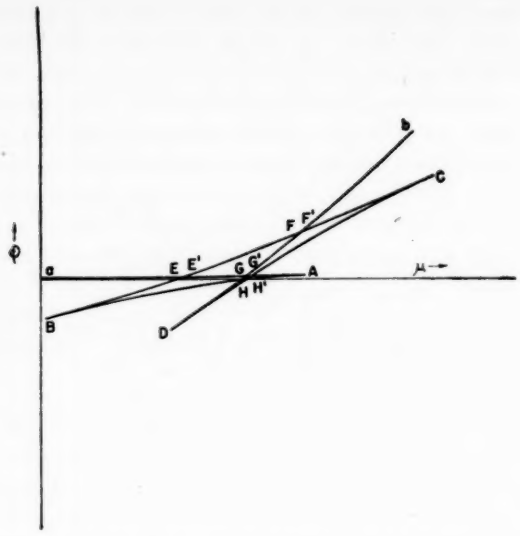


FIG. 8. $\varphi$ *versus* $\mu$-curve for $b=18$, $n=0.5$ (see Fig. 5).

can prove from Eq. (42) that $\partial \ln P/\partial\theta>0$ for all $\theta$ when[15] $n\leqslant 0$; there is no phase change when $n\leqslant 0$.

More detailed information about the nature of the phase changes described above can be obtained by investigating the integrand of Eq. (30) using Eq. (29). For the particular example being studied in the present section, the contribution $d\theta$ to $\theta$ from sites with $\epsilon$ between $\epsilon$ and $\epsilon+d\epsilon$ is

$$d\theta=\frac{1}{2\epsilon_0}\frac{d\epsilon}{(1/j)\exp[\alpha-(\epsilon/kT)]+1} \qquad \epsilon_m-\epsilon_0\leqslant\epsilon\leqslant\epsilon_m+\epsilon_0, \tag{49}$$

$$=0. \quad \epsilon<\epsilon_m-\epsilon_0, \quad \epsilon>\epsilon_m+\epsilon_0.$$

If we define as a convenient energy parameter $\eta=(\epsilon-\epsilon_m)/\epsilon_0$, one finds, using Eqs. (49), (29), (38) and (41),

$$g(\eta,\theta)\equiv 2\frac{d\theta}{d\eta}=\left\{\frac{1-ys^2}{y-1}\exp\left[\frac{b}{2}(1-\eta)\right]+1\right\}^{-1} \qquad -1\leqslant\eta\leqslant+1 \tag{50}$$

$$=0. \quad \eta<-1, \quad \eta>+1,$$

$$\tfrac{1}{2}\int_{-1}^{+1} g(\eta,\theta)d\eta=\theta.$$

In Fig. 9 we give as an example $g(\eta)$ just before and just after each of the two phase changes in the case $n=0.2$, $b=45$ (Fig. 6). The jumps in $\theta$ are approximately (1) $\theta=0.001\rightarrow 0.08$ and (2) $\theta=0.92\rightarrow 0.999$. The $g(\eta)$ curves labelled $A$, $B$, $C$, $D$ represent the different distributions in energy of occupied sites for the above four values of $\theta$, respectively (see also Fig. 6). At low temperatures (large $b$) the tendency (because of $w/kT$) for the molecules to form a condensed phase filling most of the sites in one jump is opposed by the tendency to fill only low energy sites. A compromise is reached in which a partial condensation takes place ($A\rightarrow B$) involving sites of fairly low energy only. The eventual second phase change ($C\rightarrow D$) fills in suddenly most of the remaining high energy sites. The symmetry evident in the curves of Fig. 9 follow from Eq. (50):

$$g(\eta,\theta)+g(-\eta,1-\theta)=1, \qquad g(\eta_0+\xi,\theta)+g(\eta_0-\xi,\theta)=1 \tag{51}$$

where

$$g(\eta_0,\theta)=\tfrac{1}{2}.$$

The first condensed phase probably resembles a loose net-work of filled sites. Conversely, just before the second phase change, there exists an equivalent network of empty sites. As $T\rightarrow 0$, fewer sites are filled in the first jump because only the very lowest energy sites remain acceptable.

For fairly small $b$ (high $T$) but large enough $n$ ($n>0.53$ at least) so that condensation still occurs, the special role played by the very low and high energy sites tends to disappear (as $T\rightarrow\infty$, the surface becomes *effectively* more uniform) and the behavior resembles that of a uniform surface: only one phase change occurs between $\theta=0$ and $\theta=1$.

The behavior under the *crude* assumption (Eq. (48)) is qualitatively different from the above because, for a given $\theta$, no tendency to increase the number of nearest neighbors (which would lead to the first phase change at low temperatures) is present in the equations (see (1) above Eq. (34)). Only one phase change occurs.

[15] It might be remarked that the distance between nearest neighbor sites in KCl is 3.15A, which distance corresponds to $w<0$ using the unperturbed van der Waals potential energy curve for argon. $w>0$ for next nearest neighbor sites. This is presumably a fairly common situation.

For large enough values of $b$ it is possible to get asymtotic expressions locating the first two zeros in $\partial \ln P/\partial\theta$. The first zero (e.g., point $A$ in Fig. 5) occurs approximately at

$$\ln P/P(\tfrac{1}{2}) = -\frac{z}{2}\ln(z-1) - \frac{b}{2} + \ln b - \left(\frac{z}{2}-1\right)\ln\theta, \quad (52)$$

with

$$\theta = (z-1)/((z-2)^2[\exp(nb/2)-1]) \quad (53)$$

provided that $1/(z-2) \gg 2\theta$, $b \gg 1$ and $b\theta \ll 1$. The second zero (e.g., point $B$ in Fig. 5) is given approximately by

$$P = (1-\theta/\theta)^{z/2}[\exp(b\theta)-1] \quad (54)$$

and

$$-\frac{z}{2}\frac{1}{\theta(1-\theta)} + \frac{b\exp(b\theta)}{\exp(b\theta)-1} = 0 \quad (55)$$

provided that $\beta \gg 1$ and $b \gg 1$. As $b \to \infty$, Eq. (55) becomes, for $z=6$, $\theta = 2.821/b$.

One can show that for any $n > 0$, no matter how small, a phase change occurs at large enough $b$. We have to prove that $\partial \ln P/\partial\theta$ is negative for some $\theta$. One can always find, for a given $n$, a $b$ and a $\theta$ such that $\theta \ll 1$, $b\theta = \delta \ll 1$ and $4\theta\exp(nb/2) = C \gg 1$. Then Eq. (42) becomes

$$\partial \ln P/\partial\theta \cong -(z/2)(1/\theta) + (1/\theta) < 0,$$

for physically important values of $z$. We have

$$n = (2/b)\ln(Cb/4\delta),$$

which shows that $b \to \infty$ as $n \to 0$.

Although the equations of this section apply to a particular $f(\epsilon)$, the qualitative conclusions should be rather generally applicable to *random* heterogeneous surfaces, especially if $f(\epsilon)$ is "smooth." The most important single feature is that, unlike a uniform surface, at low temperatures condensation does not take place over the whole surface in one jump, but, because of the tendency to avoid higher energy sites, there is first a partial condensation on low energy sites eventually followed by a second condensation.

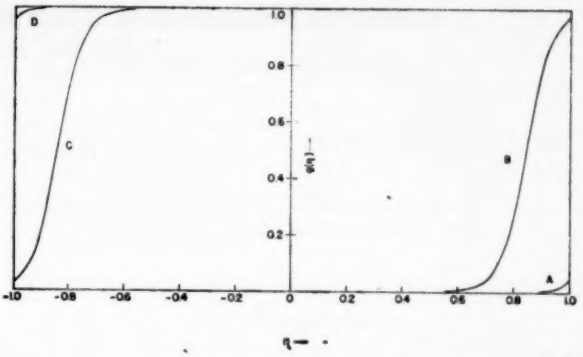


FIG. 9. Distributions in energy of occupied sites before and after phase changes.

As far as the author is aware, phase changes involving *localized* adsorption have not yet been studied experimentally.

## ACKNOWLEDGMENTS

I had the privilege of reading a manuscript by Doctors R. A. Beebe and G. L. Kington which provided the stimulus for the work in Section II. In this manuscript Beebe and Kington suggested the use of $\nu\alpha\epsilon^{\frac{1}{2}}$ as an approximation and discussed the consequent decrease in the vibrational entropy with decreasing $\theta$. I am indebted to Dr. J. A. Morrison for pointing out to me the interest in zero point configurational entropy in connection with heat capacity measurements.

# Statistical Mechanics of Adsorption. VII. Thermodynamic Functions for the B.E.T. Theory*

TERRELL L. HILL
*Department of Chemistry, University of Rochester, Rochester, New York*
(Received October 13, 1948)

As an application of the thermodynamic methods discussed in an earlier paper, thermodynamic functions are calculated from the B.E.T. statistical model.

## I. INTRODUCTION

THE thermodynamic methods given in an earlier paper[1] can be used to calculate thermodynamic functions from experimental isotherm data. In particular, the free energy of the adsorbate, assuming an inert adsorbent,[1] can be broken down into the entropy and heat content of the adsorbate. When an appreciable number of suitable experimental systems have been treated in this way, the results should be very useful in testing theories of adsorption. In anticipation of this, we summarize here for future reference the thermodynamic functions calculated from the statistical B.E.T. theory.[2,3] The B.E.T. theory is the only real theory of physical adsorption in tractable form at the present time. It is well known that the theory fails in general, on comparing theoretical and experimental isotherms, outside the range $0.05<p/p_0<0.35$. Since the adsorption isotherm gives, essentially, the Gibbs free energy of the adsorbate, it follows that thermodynamic functions calculated from the B.E.T. theory outside the above range will generally disagree with experimental functions. Inside the range, in view of the crudeness of the B.E.T. model, it is rather to be expected that, although the Gibbs free energy may be correct, the division of the free energy into heat content and entropy terms will be predicted incorrectly by the theory. This remains to be seen.

In general, only statistical mechanical theories are useful in the above connection, as kinetic (e.g., the original B.E.T. theory[2]) or thermodynamic theories do not give the dependence of crucial parameters on temperature and on detailed molecular properties. Ultimately, the adsorbate will have to be treated as essentially a liquid perturbed by the surface.

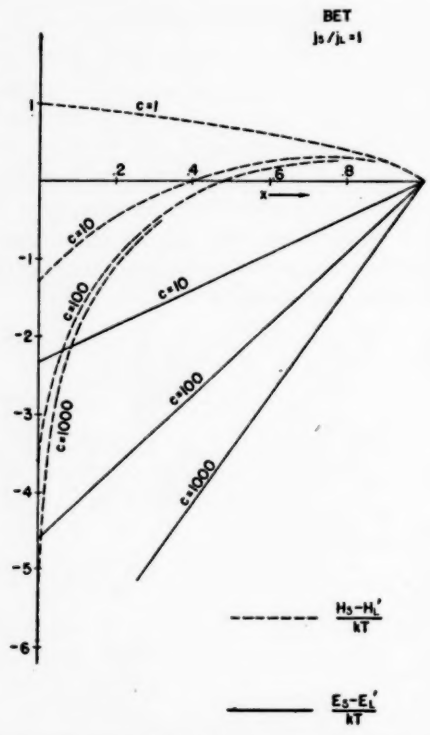


FIG. 1. Heat content and internal energy per molecule of adsorbate relative to the liquid state ($L'$) as zero.

## II. THE B.E.T. MODEL

We follow reference 3 closely (and therefore omit details), except for a few obvious changes in notation. The adsorption isotherm is, writing $x=p/p_0$,

$$\theta=N_S/B=cx/(1-x)(1-x+cx)=N_S/\alpha\mathfrak{A}=\Gamma/\alpha, \quad (1)$$

where $\mathfrak{A}$ is the surface area, $\Gamma$ the surface concentration, and

$$c=(j_S/j_L)\exp[(\epsilon_1-\epsilon_L)/kT]. \quad (2)$$

The quantities $j_L$ and $\epsilon_L$ refer to the liquid state[4] ($L'$) in which liquid is in equilibrium with gas at vapor pressure $p_0$.

We restrict the generality of the following treatment in this way: We assume $\epsilon_1$, $\epsilon_L$, and $\alpha$ are independent of temperature.

From standard statistical formulas relating $E_s$ and $A_s$ to the partition function $Q_s$, we find

$$E_S=[1-x][-\epsilon_1+kT^2(\partial \ln j_S/\partial T)] +x[-\epsilon_L+kT^2(\partial \ln j_L/\partial T)], \quad (3)$$

* Presented at an A.A.A.S. Gordon Research Conference, New London, New Hampshire, June 23, 1948.

[1] Terrell L. Hill, J. Chem. Phys. **17**, 520 (1949).

[2] S. Brunauer, P. H. Emmett, and E. Teller, J. Am. Chem. Soc. **60**, 309 (1938).

[3] T. L. Hill, J. Chem. Phys. **14**, 263 (1946).

[4] T. L. Hill, J. Chem. Phys. **15**, 767 (1947), Eq. (21). We might point out here that in writing Eq. (13) of reference 3 the approximation was made (but not mentioned) of writing $\mu_L=A_L/N_L$ (i.e., the term $PV_L/N_L$ was ignored). Of course, this is ordinarily an excellent approximation. An equivalent assumption was made in obtaining Eq. (10) from Eq. (9) of that paper. The same approximation has also been used elsewhere in this series.

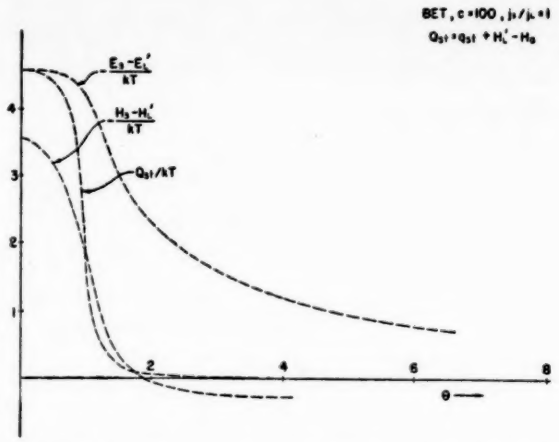


FIG. 2. Heat content, internal energy, and isosteric heat per molecule of adsorbate relative to the liquid state ($L'$) as zero.

where $E_S=E_S/N_S$ (we use small capital letters throughout to represent extensive properties per molecule—see reference 1), and for the spreading pressure $\varphi$,

$$\varphi/\alpha kT=\ln[B/(B-X)]=\ln[(1-x+cx)/(1-x)], \quad (4)$$

which is a well-known result ($X$ is the equilibrium number of molecules in the first layer). Then[5]

$$H_S=E_S+(\varphi/\Gamma)=E_S+[(1-x)(1-x+cx)/cx]kT \times\ln[(1-x+cx)/(1-x)]. \quad (5)$$

For the liquid in the state $L'$,

$$E_L'=kT^2(\partial\ln j_L/\partial T)-\epsilon_L\cong H_L'. \quad (6)$$

Then

$$E_S-E_L'=(1-x)[(-\epsilon_1+kT^2(\partial\ln j_S/\partial T)) -(-\epsilon_L+kT^2(\partial\ln j_L/\partial T))], \quad (7)$$

$$H_S-H_L'=E_S-E_L'+[(1-x)(1-x+cx)/cx]kT \times\ln[(1-x+cx)/(1-x)]. \quad (8)$$

We assume the gas phase is a perfect gas. Then

$$E_G=(3/2)kT+kT^2(\partial\ln j_G/\partial T), \quad (9)$$
$$H_G=E_G+kT, \quad (10)$$

where $j_G$ is the internal partition function. The (equilibrium) values for $\Delta E$, $\Delta H$, and $\Delta S$ of adsorption are then easily found. For example,

$$H_S-H_G=T[S_S-S_G(p)] \quad (11)$$
$$=E_S+(\varphi/\Gamma)-(5/2)kT-kT^2(\partial\ln j_G/\partial T). \quad (12)$$

From the definition[1] of the differential heat of adsorption,

$$q_d=E_G-E_S-N_S(\partial E_S/\partial N_S)_{\mathcal{A},T} =E_G-E_S-N_S(\partial E_S/\partial x)_T(\partial x/\partial N_S)_{\mathcal{A},T} \quad (13)$$

$$=E_G-E_S+[-\epsilon_1+\epsilon_L+kT^2(\partial\ln j_S/j_L/\partial T)] \times[x(1-x)(1-x+cx)/(1+x^2(c-1))]. \quad (14)$$

The isosteric heat $q_{st}$ is given by[1] $q_{st}=q_d+kT=H_G-\bar{H}_S$, where $\bar{H}_S=(\partial H/\partial N_s)_{P,T,\mathcal{A}}$ and $H=E+PV$ refers to the complete two-component phase adsorbent-adsorbate as in solution thermodynamics.

The above relations have been used to check thermodynamic equations such as[1]

$$H_G-\bar{H}_S=q_{st}=H_G-H_S+(T/\Gamma)(\partial\varphi/\partial T)_\Gamma, \quad (15)$$

$$(\partial\ln p/\partial T)_\varphi=(H_G-H_S)/kT^2, \text{ etc.} \quad (16)$$

## Special Case

In order to make numerical calculations, specific choices must be made for $j_S$, $j_L$, and $j_G$. We consider the following simple special case:[3]

$$j_L=(kT/h\nu_L)^3e, \quad (17)$$

$$j_S=(kT/h\nu_S)^3, \quad (18)$$

$$(\partial\ln j_G/\partial T)=0, \quad (19)$$

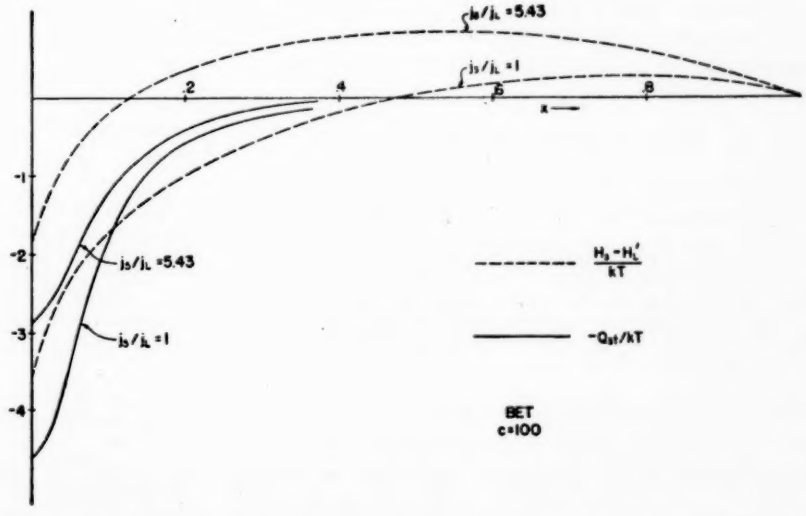


FIG. 3. Effect of $j_S/j_L$ value on heat of adsorption for $c=100$.

[5] In $H_s=E_s+\varphi\mathcal{A}+PV_s$[1] and similar equations, the (negligible) term $PV_s$ is not provided by the B.E.T. model in its usual form. See references 3 and 4.

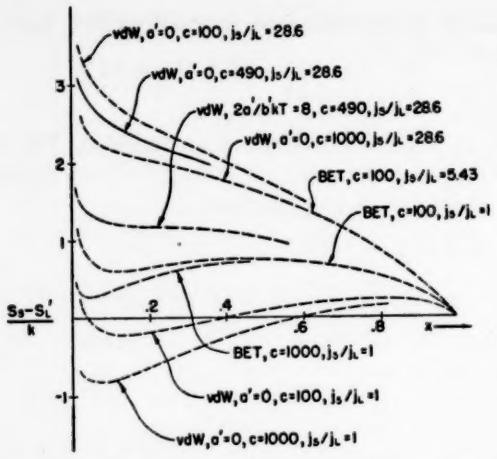


FIG. 4. Entropy per molecule of adsorbate relative to the liquid state ($L'$) as zero. *vdW* refers to a van der Waals first layer. The curves labeled (1) *vdW*, $a'=0$, $c=1000$, $j_S/j_L=28.6$, and (2) B.E.T., $c=100$, $j_S/j_L=5.43$ happen virtually to coincide. We have used the equation $T(S_S-S_L')=H_S-H_L'-kT\ln x$ in calculating these curves.

where $\nu_S$ and $\nu_L$ are independent of $T$. We then find, for example,

$$(E_S-E_L')/kT=-((\epsilon_1-\epsilon_L)/kT)(1-x), \tag{20}$$

$$(H_S-H_L')/kT=-[(\epsilon_1-\epsilon_L)/kT][1-x]+[(1-x)(1-x+cx)/cx]\times\ln[(1-x+cx)/(1-x)], \tag{21}$$

$$H_G-\bar{H}_S=q_{st}=(1-x)\epsilon_1+x\epsilon_L-\tfrac{1}{2}kT-[(\epsilon_1-\epsilon_L)x(1-x)(1-x+cx)/(1+x^2(c-1))]. \tag{22}$$

It is convenient to define** an "isosteric" equivalent of $H_L'-H_S$, $Q_{st}$:

$$Q_{st}\equiv q_{st}-(H_G-H_L')=H'_L-\bar{H}_S \tag{23}$$

$$=[(\epsilon_1-\epsilon_L)/kT][(1-x)^2/(1+x^2(c-1))]. \tag{24}$$

It will be noticed that $Q_{st}\geqslant 0$ for all $x$ if $\epsilon_1>\epsilon_L$.

One can show, incidentally, that for $j_S/j_L=1$ the minimum in the entropy curve (Fig. 4) occurs at $\theta\to 1$ and $x\to 1/c^{\frac{1}{2}}$ as $c\to\infty$.

## III. MOBILE FIRST ADSORBED LAYER

For comparison, we give here equations for the special case equivalent to Eqs. (17)–(19) when the first layer obeys a two-dimensional van der Waals equation[6] (put $jj_n=kT/h\nu_n$ in Part III of reference 6). One finds by the same methods as above, using Eqs. (17) and (19),

$$\varphi/\alpha kT=[\theta(1-x)/(1-\theta(1-x))]-(\beta/2)\theta^2(1-x)^2=\ln[Cx(1-\theta+\theta x)/\theta(1-x)^2], \tag{25}$$

$$(E_S-E_L')/kT=-(1-x)[[(\epsilon_1-\epsilon_L)/kT]+1+(\beta/2)\theta(1-x)], \tag{26}$$

$$(H_S-H_L')/kT=-(1-x)[[(\epsilon_1-\epsilon_L)/kT]+\beta\theta(1-x)-[\theta(1-x)/(1-\theta(1-x))]], \tag{27}$$

where $\alpha=1/b'$ and $\beta=2a'/b'kT$.

## IV. DISCUSSION

Curves calculated for the above special cases are given in Figs. 1–4. Figure 1 gives $H_S$ and $E_S$ for the B.E.T. model and $j_S/j_L=1$. The abscissa is also the $c=1$ curve for $E_S$. Figure 2 gives more details for $c=100$. The functions given are plotted against $\theta$ instead of $x$ in this figure. The expected effect on the heat content and isosteric heat of changing $j_S/j_L$ (keeping $c$ constant; see Eq. (2)) is shown in Fig. 3. The significance of the value $j_S/j_L=5.43$ is discussed below.

Figure 4 gives the entropy of the adsorbate for a number of cases. The lowest pair of curves may be considered as reference curves for a van der Waals first layer; the next lowest pair serve as references for the B.E.T. (localized) model. The relative position (localized *versus* mobile) of these two pairs of curves can be analyzed but has little physical significance because the choice $j_S/j_L=1$ for both is unrealistic. Using the methods of an earlier paper[7] we have estimated, as an example, that for argon on potassium chloride at 90°K $j_S/j_L$ (mobile)$=28.6$ and $j_S/j_L$ (localized)$=5.43$. The effect on the reference curves of changing $j_S/j_L=1$ to these values can be observed in Fig. 4. The entropy increases with increasing $j_S/j_L$.[8] The mobile model now has a higher entropy than the localized model. The van der Waals curve for $a'=0$, $C=490$, and $j_S/j_L=28.6$ has not been calculated but must fall between the two neighboring curves in Fig. 4. The anticipated effect of attraction between the molecules may be seen by comparing this curve with the curve labeled $2a'/b'kT=8$.

** In a recent paper which had not come to the author's attention when the present paper was submitted, Gregg and Jacobs [Trans. Faraday Soc. **44**, 574 (1948)] obtain an equation equivalent to Eq. (24). Also, Davis and De Witt [J. Am. Chem. Soc. **70**, 1139 (1948)] give an expression for a quantity $\Delta E_R$ $(=Q_{st})$ which a little algebra shows is also equivalent to Eq. (24). Incidentally, there is a typographical error in their Eq. (6). The denominator is supposed to read $[(1-\theta)^2+(4\theta/c)]^{\frac{1}{2}}$.

[6] Terrell L. Hill, J. Chem. Phys. **14**, 441 (1946).

[7] Terrell L. Hill, J. Chem. Phys. **16**, 181 (1948).

[8] However, $j_S/j_L$ is not a pure entropy factor. In general it contributes to both energy (Eq. (7)) and entropy.

THE JOURNAL OF CHEMICAL PHYSICS VOLUME 17, NUMBER 9 SEPTEMBER, 1949

# Statistical Mechanics of Adsorption. VIII. The Statistical Analogue of the B.E.T. Constant $a_1b_2/b_1a_2$ for Simulated Benzene and Hydrogen Iodide Molecules on Graphite

J. W. Drenan and Terrell L. Hill
*Department of Chemistry, The University of Rochester, Rochester, New York*
(Received October 25, 1948)

The approximate study of the restricted rotation of molecules near a surface is extended to an unsymmetrical diatomic molecule, hydrogen iodide, and a ring molecule, benzene, for a graphite surface in each case. Calculations of the factor $R$ in the BET constant $C=R\exp(\epsilon_1-\Lambda)/kT$ are carried out for these cases. $R$ is found to be of the same order of magnitude (2–20) as for the symmetrical diatomic molecule.

## I. INTRODUCTION

In a theoretical treatment of the statistical mechanics of adsorption, it is of interest to consider the effect which the surface has upon the adsorbed molecule. At low pressures, the general adsorption equation $v/v_m=Cx$ is valid, where $v$ is the volume of gas adsorbed, $v_m$ is the volume of gas which can be adsorbed in a complete monomolecular layer, and $x=p/p_0$, the ratio of the gas pressure to the vapor pressure for the temperature existing in the system. $C$, the fundamental parameter, is given by

$$C=R\exp(\epsilon_1-\Lambda)/kT$$

with $\Lambda$ the heat of vaporization of the liquid and $-\epsilon_1$ the energy of an isolated molecule in its ground state relative to infinite separation from the surface as the zero of energy. Since $R$ depends upon the partition functions of the molecule as a gas and as an adsorbate, the effect of the adsorbing surface upon the molecule adsorbed is worthy of study.

This problem has been treated by Hill[1] for the case of a symmetrical diatomic molecule. The purpose of this paper is to make a similar study for two other cases: $A$ an unsymmetrical diatomic molecule, and $B$ a molecule representable by a ring. In order to make the results more tangible, calculations have been carried out for two molecules which have been studied experimentally to some extent: hydrogen iodide[2,3] and benzene.[4–7] A smooth, non-polar surface which does not react chemically with the gas to be adsorbed is postulated; for this graphite has been chosen as the model.

The general method and the assumptions are the same as those in Hill's paper. Thus, a van der Waals interaction equation of the form

$$u=u_0\left(\frac{r_0}{r}\right)^{12}-2u_0\left(\frac{r_0}{r}\right)^{6} \qquad (1)$$

is assumed to represent the interaction between each atom of the molecule to be adsorbed and a single molecule of the adsorbent. Here $u$ is the energy of interaction, $r$ is the distance between the atom of gas and the surface molecule, $r_0$ is the equilibrium distance between the two, and $u_0$ is the interaction energy corresponding to the distance $r_0$. The van der Waals interaction of the gas molecule with a single adsorbent molecule is assumed to be the sum of the atomic interactions of this type. To calculate the interaction of the gas molecule with the entire adsorbent, integration in the manner of London[8] is employed, instead of the more refined and more laborious procedure of summation. The partition function for internal vibrations of the molecule to be adsorbed is assumed to be identical in the gas and adsorbate phases; i.e., the perturbation on these particular degrees of freedom resulting from the surface is ignored. The surface is considered uniform in that no periodic variation of the energy of adsorption over the surface is postulated. Free migration over the surface (mobile adsorption) is also assumed. The use of Eq. (1) predicates that there are no electrostatic effects to be considered; terms to take these into account could be introduced, but, in view of the hypothetical nature of the problem resulting from the above assumptions, the extra labor involved seems unwarranted.

Hydrogen iodide has been chosen as an example of case $A$ because it is very unsymmetrical, yet has only a small dipole moment[9] ($0.38\times10^{-18}$ e.s.u.) and thus little ionic character. Benzene is certainly the most obvious example for case $B$.

## II. CASE A: SIMULATED HYDROGEN IODIDE

Let the diatomic molecule have atoms, with masses $m_1$ and $m_2$, separated by a constant dis-

[1] Terrell L. Hill, J. Chem. Phys. 16, 181 (1948).
[2] M. Dubinin, Zeits. f. physik. Chemie 123, 86 (1926).
[3] L. H. Reyerson and C. Bemmels, J. Phys. Chem. 46, 35 (1942).
[4] A. S. Coolidge, J. Am. Chem. Soc. 46, 596 (1924).
[5] B. Lambert and A. M. Clark, Proc. Roy. Soc. A122, 497 (1929).
[6] W. G. Palmer, Proc. Roy. Soc. A168, 190 (1938).
[7] C. Kemball and E. K. Rideal, Proc. Roy. Soc. A187, 53 (1946); *ibid.* A190, 117 (1947).
[8] F. London, Zeits. f. physik. Chemie B11, 222 (1930).
[9] L. Pauling, *The Nature of the Chemical Bond* (Cornell University Press, Ithaca, New York, 1945).

tance $d$. Let the perpendicular distance from the center of gravity of the molecule to the surface be $z=\rho$. Let $\theta$ be the angle between $z$ and the line connecting the centers of the atoms. Let the surface of the adsorbent be the $xy$ plane, with $z$ negative in the adsorbent. Let $\phi$ be the angle between the plane containing the nuclei and the $z$ axis, and the $xz$ plane; a change in $\phi$ then represents a rotation of the molecule about the $z$ axis. It is obvious that a change of $\phi$ does not affect the distance of either atom from the surface, so that for a uniform

TABLE I. Atomic interactions.

| | | N(C) | H | I |
|---|---|---|---|---|
| $T_c$ (°K) | | 126.0 | — | 826.1 |
| $u_0$ (molecule) | $\times 10^{15}$ ergs | 13.61 | 4.25 | 89.22 |
| $u_0$ (atom) | $\times 10^{15}$ ergs | 6.60 | 2.06 | 43.26 |
| $u_0$ (atom to carbon) | $\times 10^{15}$ ergs | 6.60 | 3.687 | 16.90 |

surface a rotation of this type has no effect upon the van der Waals interaction energy. Let $r_{01}$ and $r_{02}$ be the equilibrium van der Waals distances of the two atoms from a surface molecule; i.e., $r_{01}$ is the sum of the van der Waals radii of atom 1 and of a surface molecule. Let $\rho_1$ and $\rho_2$ be the perpendicular distances of these atoms from the surface. Let $N_0$ be the number of adsorbent molecules per cc.

In (1), $r$ is a function of the coordinates $x$, $y$, and $z$ of the adsorbent molecule; $r=(x^2+y^2+[z-\rho]^2)^{\frac{1}{2}}$. If we integrate (1) over all values of $x$ and $y$, and over those values of $z$ such that $z\leqslant 0$, we will have approximated the interaction of one atom of the diatomic molecule with the entire adsorbent. Such integration gives

$$u_s=\frac{u_0 r_0^{12}\pi N_0}{45\rho^9}-\frac{u_0 r_0^6\pi N_0}{3\rho^3}.$$

The interaction of the entire molecule with the adsorbent will be the sum of two such terms:

$$U=\frac{u_{01}r_{01}^{12}\pi N_0}{45\rho_1^9}-\frac{u_{01}r_{01}^6\pi N_0}{3\rho_1^3}+\frac{u_{02}r_{02}^{12}\pi N_0}{45\rho_2^9}-\frac{u_{02}r_{02}^6\pi N_0}{3\rho_2^3}.$$

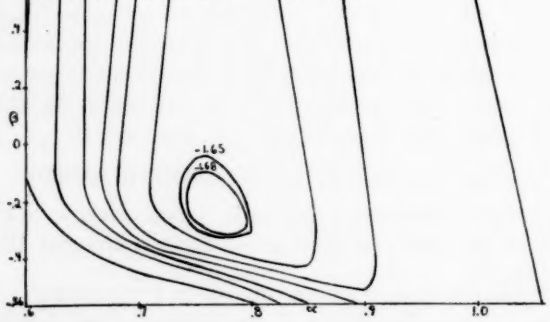


FIG. 1.

It is apparent that

$$\rho_1=z+\frac{m_2 d\cos\theta}{m_1+m_2} \quad \text{and} \quad \rho_2=z+\frac{m_1 d\cos\theta}{m_1+m_2}.$$

Making this substitution and letting

$$a_1=u_{01}r_{01}^3\pi N_0/3,\quad a_2=u_{02}r_{02}^3\pi N_0/3,\quad \alpha_1=z/r_{01},$$

$$\alpha_2=z/r_{02},\quad \beta_1=\frac{m_2 d\cos\theta}{r_{01}(m_1+m_2)},\quad \text{and}\quad \beta_2=\frac{m_1 d\cos\theta}{r_{02}(m_1+m_2)},$$

we find

$$U=a_1\left(\frac{1}{15(\alpha_1-\beta_1)^9}-\frac{1}{(\alpha_1-\beta_1)^3}\right)+a_2\left(\frac{1}{15(\alpha_2+\beta_2)^9}-\frac{1}{(\alpha_2+\beta_2)^3}\right). \tag{2}$$

For the particular case of hydrogen iodide, $m_2/(m_1+m_2)=0.0079$. For $\alpha$ of the order of 1, we may then approximate $\alpha_1-\beta_1$ by $\alpha_1$. This is equivalent to saying that the iodine atom is essentially the center of mass of the hydrogen iodide molecule.

Pauling[9] and Stuart[10] give the van der Waals radii of hydrogen as 1.2, carbon as 1.67, and iodine as 2.07A. Then $r_{0\,CI}=1.67+2.07=3.74$A, and $r_{0\,CH}=1.67+1.2=2.87$A. Then

$$\frac{\alpha_2}{\alpha_1}=\frac{z/2.87}{z/3.74}=1.303.$$

Let us replace $\alpha_1$ by $\alpha$ and $\alpha_2$ by $1.303\alpha$. The interatomic distance, $d$, for hydrogen iodide[9] is 1.62A. Then Eq. (2) becomes

$$U=a_1\left(\frac{1}{15\alpha^9}-\frac{1}{\alpha^3}\right)+a_2\left(\frac{1}{15(1.303\alpha+0.560\cos\theta)^9}-\frac{1}{(1.303\alpha+0.560\cos\theta)^3}\right).$$

Let us next find the position of minimum energy; this involves taking derivatives of $U(\alpha,\theta)$ with respect to $\alpha$ and to $\theta$, and setting each to 0. The results are $\alpha=(\frac{1}{5})^{1/6}=0.7647$, and $\theta=114°34'$. The molecule is then in the most stable position when the iodine atom is at a distance from the surface equal to 0.7647 times the sum of the van der Waals radii of carbon and iodine; it may readily be shown that, with $\theta=114°34'$, the hydrogen atom is also a distance 0.7647 times the sum of the van der Waals radii of carbon and hydrogen from the surface. This value of 0.7647 $r_0$ is the same result found for

[10] H. A. Stuart, *Molekülstruktur* (Verlag Julius Springer, Berlin, 1934).

TABLE II. Integration for HI at 81.33°K.

| $\beta$ | $f(\beta)$ | $\int f(\beta)d\beta$ |
|---|---|---|
| 0.56 | $1.390\times10^{5}$ | |
| 0.53 | 1.415 | |
| 0.50 | 1.433 | 8483 |
| 0.4 | 1.555 | |
| 0.3 | 1.720 | |
| 0.2 | 1.913 | |
| 0.1 | 2.180 | |
| 0.0 | 2.540 | |
| −0.1 | 3.214 | 121595 |
| −0.15 | 3.635 | |
| −0.20 | 3.882 | |
| −0.25 | 3.990 | |
| −0.30 | 3.336 | |
| −0.35 | 1.710 | |
| −0.40 | 0.844 | |
| −0.45 | 0.460 | |
| −0.50 | 0.177 | 91159 |
| −0.53 | 0.080 | |
| −0.56 | 0.000 | 497 |
| | | $Q(T)=2.217\times10^{5}$ |

TABLE III. Integration for HI at 244°K.

| $\beta$ | $f(\beta)$ | $\int f(\beta)d\beta$ |
|---|---|---|
| 0.56 | 23.95 | |
| 0.53 | 24.28 | |
| 0.5 | 24.63 | 1.46 |
| 0.4 | 25.92 | |
| 0.3 | 27.22 | |
| 0.2 | 28.64 | |
| 0.1 | 30.02 | |
| 0.0 | 31.82 | |
| −0.1 | 33.79 | |
| −0.2 | 35.36 | |
| −0.3 | 33.69 | |
| −0.4 | 23.96 | |
| −0.5 | 15.69 | 29.08 |
| −0.53 | 14.15 | |
| −0.56 | 12.88 | 0.85 |
| | | $Q(T)=31.39$ |

the symmetrical diatomic molecule and for the monatomic case, as expected.

$a_1$ and $a_2$ should next be evaluated. $a_1 = u_{0\,CI} r^3_{0\,CI} N_0/3$, and for graphite $N_0 = 1.128\times10^{23}$ atoms per cc. To find $u_0$, the following method may be adopted. Values of the critical temperatures of $I_2$ and of $N_2$ are selected. ($N_2$ is used as the best substitute for $C_2$ for which no data are available.) Then the assumption $u_0 = 0.1080 T_c \times 10^{-15}$ ergs, for symmetrical non-polar molecules, is made on the basis of Hill's calculations.[11] The contribution of each *atom* to $u_0$ is taken to be 16/33 of the total for a symmetrical diatomic molecule.[11] Then the interaction energy is assumed to be the geometric mean of the atomic values thus obtained: $u^2_{0\,CI} = u_{0C} u_{0I}$. The values used are shown in Table I. The value given for $u_0$ for hydrogen is taken from Hill's paper. This procedure is admittedly a very rough approximation, but it is employed in the absence of a better available method. Use of these values leads to $a_1 = 1.044\times10^{-13}$ and $a_2 = 1.030\times10^{-14}$ erg per molecule.

Equation (3) may now be used to calculate a potential energy surface for the hydrogen iodide molecule near the graphite surface. The results are shown graphically in Fig. 1. $U_0$, the potential energy at the position of minimum energy ($\alpha_0 = 0.7647$; $\theta_0 = 114°34'$), is $-1.710\times10^{-13}$ erg per molecule (2460 calories per mole). The potential energy surface is of course not symmetrical. However, crudely we may say that as the hydrogen atom revolves away from the surface, the system tries to remain in the potential energy valley by having the iodine atom move slightly nearer the surface at first. For a complete rotation (in $\theta$) of the molecule about its center of gravity, an energy barrier of about 520 calories per mole must be overcome if the system remains in the potential valley; a similar rotation by any other path will naturally involve a higher barrier.

The next problem is to find the partition function for the molecule, treated as a rigid rotator, near the adsorbing surface. The Hamiltonian $H$ is given by

$$H = \frac{p_x^2 + p_y^2 + p_z^2}{2M} + \frac{p_\theta^2}{2I} + \frac{p_\phi^2}{2I\sin^2\theta} + U(z,\theta),$$

where $U(z,\theta)$ is given by (3) or by Fig. 1. Since the exact quantum mechanical determination of the energy levels for a molecule with this Hamiltonian is out of the question, at least for the present, Hill's suggestion of the use of the Pitzer-Gwinn approximation[12] is resorted to:

$$f = f_{\text{classical}} \frac{f_{\text{HO quantal}}}{f_{\text{HO classical}}},$$

where

$$f_{\text{class}} = \frac{1}{h^5}\int\cdots \times \int e^{-H/kT} dx dy dz d\theta d\phi dp_x dp_y dp_z dp_\theta dp_\phi,$$

and the harmonic oscillator partition functions are calculated from the shape of the potential energy surface near the minimum.

In order to calculate the harmonic oscillator expressions the normal coordinates for the oscillations must be found. $U(\alpha, \theta)$ may be expanded in a Taylor series about $\theta_0$ and $\alpha_0$:

$$U = U_0 + [9.203(\theta-\theta_0)^2 - 47.05(\theta-\theta_0)(\alpha-\alpha_0) + 419.3(\alpha-\alpha_0^2)]\times10^{-14}\text{ erg.} \quad (5)$$

This represents the potential energy of the system

[11] Terrell L. Hill, J. Chem. Phys. 16, 399 (1948).

[12] K. S. Pitzer and W. D. Gwinn, J. Chem. Phys. 10, 428 (1942).

near $U_0$, where it behaves like a harmonic oscillator. The kinetic energy for these two coordinates is given by $T=\frac{1}{2}M\dot{z}^2+\frac{1}{2}I\dot{\theta}^2$. It may readily be shown that normal coordinates $w_1$ and $w_2$ exist such that Eq. (5) is transformed into

$$U=2565w_1^2+4165800w_2^2, \tag{6}$$

where

$$w_1+w_2=z-z_0,\quad 10^8(-0.725w_1+67.28w_2)=\theta-\theta_0.$$

We are now in a position to find the harmonic oscillator partition functions. Substitution of (6) into (4) gives

$$f_{\text{HO class}}=\frac{1}{h^5}\int\cdots\int\exp-\Big[U_0+2565w_1^2+4165800w_2^2+\frac{p_{w_1}^2}{2\mu_1}+\frac{p_{w_2}^2}{2\mu_2}+\frac{p_x^2+p_y^2}{2M}+\frac{p_\phi^2}{2I\sin^2\theta}\Big]\Big/kT \times dxdydw_1dw_2d\phi dp_xdp_ydp_{w_1}dp_{w_2}dp_\phi,$$

where $\mu$ is the appropriate reduced mass. Integration leads to

$$f_{\text{HO class}}=\frac{2\pi MkT}{h^2}\mathfrak{A}\frac{2\pi(2\pi IkT)^{\frac{1}{2}}}{h}\times\frac{kT}{h\nu_{w_1}}\frac{kT}{h\nu_{w_2}}\exp(-U_0/kT), \tag{7}$$

where $\nu_{w_1}=7.781\times10^{11}$/sec. and $\nu_{w_2}=3.288\times10^{12}$/sec. and $\mathfrak{A}$ is the surface area of the adsorbent. Since the variables have been separated, we may write

$$f_{\text{HO QM}}=\frac{2\pi MkT}{h^2}\mathfrak{A}\frac{2\pi(2\pi IkT)^{\frac{1}{2}}}{h}\times[1-\exp(-h\nu_{w_1}/kT)]^{-1}[1-\exp(-h\nu_{w_2}/kT)]^{-1}\times\exp(-U_0/kT).$$

The problem is then to find $f_{\text{class}}$. Following the method of Hill[1] we arrive at

$$f_{\text{class}}=\Big(\frac{2\pi MkT}{h^2}\Big)^{\frac{3}{2}}\mathfrak{A}\frac{8\pi^2IkT}{h^2}\frac{r_{0\,\text{CH}}r_{0\,\text{CI}}}{0.992d}\times\int\int\exp(-U/kT)\text{erf}(-U/kT)^{\frac{1}{2}}d\alpha d\beta,$$

$$-0.560\cos\theta\leqslant\beta\leqslant+0.560\cos\theta,\ U\leqslant0. \tag{8}$$

Because of the nature of $U$, which is given by (3), this integration must be carried out numerically. $\beta$ is held constant while $\alpha$ is integrated, by means of Simpson's rule, from the value of $\alpha$ such that $U=0$ to a sufficiently large value of $\alpha$; beyond here the integral is evaluated analytically, using asymptotic expressions, to $\alpha=\infty$. These results are then integrated from $\beta=-0.560\cos\theta$ to $\beta=0.560\cos\theta$. Calculations for two temperatures (81.33°K and 244°K) have been carried out. The results are given in Tables II and III. Let $Q(T)$ be the result of the second integration for temperature $T$.

The final results for $f_{\text{class}}$ are

$$f_{\text{class}}=\Big(\frac{2\pi MkT}{h^2}\Big)^{\frac{3}{2}}\mathfrak{A}\frac{8\pi^2IkT}{h^2}\frac{r_{0\,\text{CH}}r_{0\,\text{CI}}}{0.992d}Q(T).$$

When substituted into (4), these lead to

$$f=\rho_1\rho_2j_{\text{el}}j_{\text{vib}}\mathfrak{A}\Big(\frac{2\pi MkT}{h^2}\Big)^{\frac{3}{2}}\frac{8\pi^2IkT}{h^2}\frac{r_{0\,\text{CH}}r_{0\,\text{CI}}}{0.992d}Q(T)\times\frac{h\nu_{w_1}}{kT}\frac{h\nu_{w_2}}{kT}[1-\exp(-h\nu_{w_1}/kT)]^{-1}\times[1-\exp(-h\nu_{w_2}/kT)]^{-1}. \tag{9}$$

Here $\rho_i$ is the nuclear spin of atom $i$ of the adsorbed molecule, and $j_{\text{el}}$ and $j_{\text{vib}}$ are the electronic and internal vibrational partition functions, respectively, for such a molecule. Inserting the proper numerical values, we find that

$$f=\rho_1\rho_2j_{\text{el}}j_{\text{vib}}\Big(\frac{2\pi MkT}{h^2}\Big)^{\frac{3}{2}}\mathfrak{A}\frac{8\pi^2IkT}{h^2}\times(4.181\cdot10^{-2})\quad T=81.33,$$

$$f=\rho_1\rho_2j_{\text{el}}j_{\text{vib}}\Big(\frac{2\pi MkT}{h^2}\Big)^{\frac{3}{2}}\mathfrak{A}\frac{8\pi^2IkT}{h^2}\times(3.070\cdot10^{-6})\quad T=244. \tag{10}$$

The BET constant $C$ may be written in the form $C=R\exp(\epsilon_1-\Lambda)/kT$. If we consider adsorption at very low pressures, so that the adsorbed molecules do not interact with each other to any appreciable extent, we can arrive[1] at the expression

$$C=\frac{f}{N^0}\frac{p_0}{kT}\Big(\frac{h^2}{2\pi MkT}\Big)^{\frac{3}{2}}\Big(\frac{h^2}{8\pi^2IkT}\Big)\frac{1}{\rho_1\rho_2j_{\text{el}}j_{\text{vib}}},$$

where $N^0$ is the maximum number of molecules that can be adsorbed in the first layer, and $p_0$ is the vapor pressure, at the temperature $T$, of the gas being adsorbed. Since $p_0$ may be written[1] as $\delta\exp(-NkT)$, and since we have already found $1.710\times10^{-13}$ erg per molecule for $\epsilon_1$,

$$R=1.027\times10^{-8}(\mathfrak{A}/N^0)(\delta/kT)\quad T=81.33,$$
$$R=1.919\times10^{-8}(\mathfrak{A}/N^0)(\delta/kT)\quad T=244. \tag{11}$$

Use of the values $\Lambda = 4332$ calories per mole and $p_0 = 713.1$ mm of mercury for hydrogen iodide at 236.1°K leads to the result $\delta = 9.784 \times 10^9$. $\mathfrak{a}/N^0$, the area occupied per molecule adsorbed in a completed first layer, may be calculated[1] from

$$\mathfrak{a}/N^0 = 6.354(T_c/P_c)^{\frac{1}{2}},$$

where $T_c$ and $P_c$ are the critical temperature and pressure, respectively. If $T_c$ is taken as 424.2°K and $P_c$ as 82 atmospheres, $\mathfrak{a}/N^0 = 19.00$ sq. A.

Substitution of these values into (11) leads to $R = 10.58$ at 244°K and to $R = 16.99$ at 81.33°K. These $R$ values are of the same order of magnitude as those found by Hill for the symmetrical diatomic molecule. It is of interest to note that in this case $R$ is roughly proportional to $T^{-\frac{1}{2}}$.

Actually, of course, at 81.33°K there is a good possibility of localized adsorption, so the value of $R_{\text{loc}}$ (localized) should also be found. We employ Eqs. (35) and (36) in reference 1. Assuming that for graphite the potential barriers lie at the centers of hexagons, we get for $s$, the barrier spacing, 2.46A. If $V_0$, the height of the barrier, is then taken as 1000 calories per mole, which is probably a rather high value, the frequency of vibration parallel to the surface is $3.68 \times 10^{11}$ per second, and $R_{\text{loc}}$ becomes $0.127R = 2.16$.

### III. CASE B: SIMULATED BENZENE

Another type of molecule for which calculations of this sort may be of interest is the ring molecule. Benzene is probably the most important example of this type, and it is with this molecule we deal specifically, but a similar treatment should be applicable to certain other organic molecules.

Since benzene contains twelve atoms, calculations of the energy of adsorption by summing the interaction energies of each atom with the surface would be extremely laborious, at best. The molecule to be adsorbed is therefore temporarily taken to be in the form of two coplanar, concentric, circular rings, one of carbon and one of hydrogen. In each ring, the mass is assumed to be continuous and uniformly distributed around the circumference, with the total mass of the ring equal to the sum of the corresponding atomic masses. The molecule is regarded as rigid, so that the radius and mass distribution of each ring remains constant.

Let us consider a single circular ring or loop whose center is at a distance $z_0$ from a uniform surface which is represented by the $xy$ plane; let the $z$ axis pass through the center of the loop. Let the radius of the ring be $d$. Let a line be drawn through the center of the loop and perpendicular to its plane; this line makes an angle $\theta$ with the $z$ axis, corresponding to the $\theta$ in case $A$.

The interaction of a mass point on this ring with

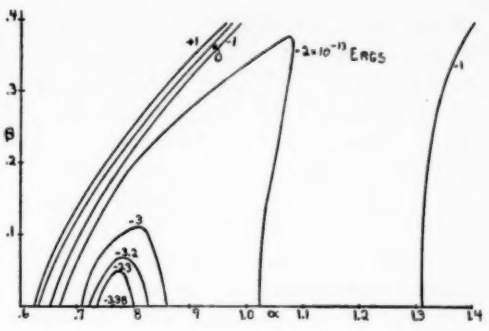


FIG. 2.

the surface will be again represented by

$$u_s = \frac{u_0 r_0^{12} \pi N_0}{45\rho^9} - \frac{u_0 r_0^6 \pi N_0}{3\rho^3}.$$

The interaction of the entire loop with the surface will be found by integration of this equation around the loop. For a ring of $n$ atoms, we find

$$U = -\frac{n}{\pi}\left\{\frac{\pi u_0 r_0^{12} N_0}{45}\,\frac{\pi}{128} \times\left[\frac{128a^8+1792a^6b^2+3360a^4b^4+1120a^2b^6+35b^8}{(a^2-b^2)^{17/2}}\right] - \frac{\pi u_0 r_0^6 N_0}{3}\left[\frac{2a^2+b^2}{(a^2-b^2)^{5/2}}\right]\right\}$$

where $a = z_0$ and $b = d\sin\theta$.

The benzene might now be approximated by a ring of six carbon atoms. It would also be possible to use (12) for the carbon and hydrogen rings separately, and add the results. However, the most practical course seems to be to postulate a hypothetical ring of six "C—H" atoms such that the interaction of each member of the ring with the graphite surface is given by

$$u_{\text{HC-C}} = u_{0\ \text{HC-C}}\left(\frac{r_{0\ \text{HC-C}}}{r}\right)^{12} - 2u_{0\ \text{HC-C}}\left(\frac{r_{0\ \text{HC-C}}}{r}\right)^{6}. \quad (1A)$$

The values for $r_{0\ \text{HC-C}}$ and $u_{0\ \text{HC-C}}$ are approximated as follows. In the more complete interaction equation

$$u_{0\ \text{HC-C}} = u_{0\ \text{HC}}\left(\frac{r_{0\ \text{HC}}}{r}\right)^{12} - 2u_{0\ \text{HC}}\left(\frac{r_{0\ \text{HC}}}{r}\right)^{6} + u_{0\ \text{CC}}\left(\frac{r_{0\ \text{CC}}}{r}\right)^{12} - 2u_{0\ \text{CC}}\left(\frac{r_{0\ \text{CC}}}{r}\right)^{6} \quad (1B)$$

the values $u_{0\,CC}=6.60\times10^{-15}$ erg, $u_{0\,HC}=3.687\times10^{-15}$ erg, $r_{0\,HC}=2.87$A, and $r_{0\,CC}=3.34$A are substituted; these values are those obtained from Table I. Equation (1B) is differentiated with respect to $r$. Then, setting $du/dr=0$, a condition which holds at the position of minimum $u$, we solve for $r$ and find that $r=3.281$A. This value is taken to be $r_{0\,HC-C}$; it is now substituted for $r$ in Eq. (1B), and the resulting $u=9.078\times10^{-15}$ erg is considered to be $u_{0\,HC-C}$.

The radius of the carbon "ring" in benzene is 1.39A; the radius of the surrounding hydrogen loop[9] is 2.47A. In selecting a value for $d$, the radius of the hypothetical C—H ring, it seems desirable to weight these radii in accordance with their interaction energies with graphite. For this reason, $d$ is taken to be

$$1.39+\frac{u_{0\,HC}}{u_{0\,HC}+u_{0\,CC}}(2.47-1.39)=1.78\text{A}.$$

(For convenience, $r_{0\,HC-C}$ will henceforth be denoted by $r_0$ and $u_{0\,HC-C}$ by $u_0$.)

Using $n=6$, Eq. (12) becomes

$$U=\frac{A}{960}\left[\frac{128\alpha^8+1792\alpha^6\beta^2+3360\alpha^4\beta^4+1120\alpha^2\beta^6+35\beta^8}{(\alpha^2-\beta^2)^{17/2}}\right]-A\left[\frac{2\alpha^2+\beta^2}{(\alpha^2-\beta^2)^{5/2}}\right], \quad (13)$$

where $\alpha=a/r_0$, $\beta=b/r_0$, and $A=\pi r_0^3u_0N_0=1.136\times10^{-13}$ erg per molecule.

Equation (13) is now used to find $U(\alpha,\beta)$. The results are shown graphically in Fig. 2. The plot, as expected, is symmetrical about the line $\beta=0$. The position of minimum energy is determined, as before, by the conditions $\partial U/\partial\alpha=0$ and $\partial U/\partial\beta=0$; it occurs at $\beta=0$, $\alpha=0.7647r_0$ in analogy with the monatomic case. The potential energy of the system at this point, $U_0$, is $-3.388\times10^{-13}$ erg per molecule (4875 calories per mole). As $\beta$ increases, and the molecule tilts relative to the surface, the center of mass of the molecule is found to move away from the surface in order to be in the position of least potential energy. This motion results naturally from the fact that, as $r$ decreases, the repulsive term increases more rapidly than the attractive one. For the molecule to flip over, it must overcome a potential barrier of approximately 3400 calories per mole, if it follows the path of least resistance.

TABLE IV. Integration for $C_6H_6$ at 273°K.

| $\beta$ | $f(\beta)$ | $\frac{\beta}{[(d/r_0)^2-\beta^2]^{\frac{1}{2}}}$ | $\frac{f(\beta)\beta}{[(d/r_0)^2-\beta^2]^{\frac{1}{2}}}$ | $\int\frac{f(\beta)\beta d\beta}{[(d/r_0)^2-\beta^2]^{\frac{1}{2}}}$ |
|---|---|---|---|---|
| 0.0 | 1108.43 | 0 | 0 | |
| 0.05 | 836.56 | 0.172 | 143.80 | |
| 0.1 | 483.56 | 0.353 | 170.70 | 12.43 |
| 0.2 | 153.38 | 0.790 | 123.48 | |
| 0.3 | 65.71 | 1.476 | 96.97 | |
| 0.4 | 36.30 | 3.000 | 108.90 | |
| 0.5 | 24.03 | 15.473 | 371.82 | 55.53 |
| 0.54 | 21.76 | | | 4.68 |
| 0.6 | 18.35 | | | — |
| | | | | $Q=72.64$ |

To find the partition function for this molecule considered as a rigid rotator, we write its Hamiltonian

$$H=\frac{p_x^2+p_y^2+p_{z_0}^2}{2M}+\frac{p_\theta^2}{2A}+\frac{(p_\phi-\cos\theta p_\psi)^2}{2A\sin^2\theta}+\frac{p_\psi^2}{2C}+U(z,\theta), \quad (14)$$

where $A$ is the moment of inertia of the molecule about a diameter; $C$ is the moment about an axis perpendicular to the loop and through its center; $U(z,\theta)$ is given by (13); and $\phi$, $\theta$, and $\psi$ are the normal Eulerian angles.[13]

Since the quantum mechanical problem for a rotator with this Hamiltonian is unsolved, the Pitzer-Gwinn approximation is again resorted to. Near the point $(\alpha=\alpha_0,\ \beta=\beta_0)$, $U(\alpha,\beta)$ may be expanded in a Taylor's series:

$$U=-3.388\times10^{-13}+3.911\times10^{-12}(\alpha-\alpha_0)^2+7.822\times10^{-12}(\beta-\beta_0)^2. \quad (15)$$

The partition function $f_{HO\ class}$ may then be found by the integration of

$$f_{HO\ class}=\frac{1}{h^6}\int\cdots\int\exp-\Big[U_0+\frac{c_1}{r_0^2}(z_0-z_{00})^2+\frac{c_2}{r_0^2}d^2(\sin\theta-\sin\theta_0)^2+\frac{p_x^2+p_y^2+p_{z_0}^2}{2M}+\frac{p_\theta^2}{2A}+\frac{(p_\phi-\cos\theta p_\psi)^2}{2A\sin^2\theta}+\frac{p_\psi^2}{2C}\Big]\Big/kT$$
$$\times dx\,dy\,dz_0\,d\theta\,d\phi\,d\psi\,dp_x\,dp_y\,dp_{z_0}\,dp_\theta\,dp_\phi\,dp_\psi.$$

Here $c_1$ and $c_2$ are the respective coefficients of the square terms in (15), and $z_{00}(=\alpha_0r_0)$ is the value of $z_0$ for which $U$ is a minimum. The limits of integration are 0 to $\pi$ for $\theta$, 0 to $2\pi$ for $\phi$ and $\psi$, the limits of the surface for $x$ and $y$, and $-\infty$ to $+\infty$ for the other variables. In our case, $\theta_0=0$, so

[13] Equation (14) is equivalent to Eq. (8.9) in Mayer and Mayer's *Statistical Mechanics* (John Wiley & Sons, Inc., New York, 1940).

$\sin\theta_0=0$. Furthermore, since we are interested only in oscillations very near the minimum, we may make the approximation that $\sin\theta=\theta$. If then it is assumed that

$$\int_0^{\pi} e^{-a\theta^2}\theta d\theta=\int_0^{\infty} e^{-a\theta^2}\theta d\theta,$$

the result is

$$f_{\text{HO class}}=4\pi^2\mathfrak{A}\frac{r_0^3kT}{2c_2d^2}\left(\frac{\pi kT}{c_1}\right)^{\frac{1}{2}}\left(\frac{2\pi MkT}{h^2}\right)^{\frac{1}{2}}\times\left(\frac{2\pi AkT}{h^2}\right)\frac{(2\pi CkT)^{\frac{1}{2}}}{h}\exp(-U_0/kT).$$

For a harmonic oscillator subject to (15)

$$\nu_{z_0}=\frac{1}{\pi r_0}\left(\frac{c_1}{2M}\right)^{\frac{1}{2}}=1.69\times10^{12}$$

and $$\nu_\theta=\frac{d}{\pi r_0}\left(\frac{c_2}{2A}\right)^{\frac{1}{2}}=2.38\times10^{12}/\text{sec.}$$

The above may then be written

$$f_{\text{HO class}}=\mathfrak{A}\frac{2\pi MkT}{h^2}2\pi\frac{(2\pi CkT)^{\frac{1}{2}}}{h}\times\frac{kT}{h\nu_{z_0}}\left(\frac{kT}{h\nu_\theta}\right)^2\exp(-U_0/kT). \quad (16)$$

Making the usual assumptions about the definition of an adsorbed molecule, one arrives at the result

$$f_{\text{class}}=4\pi^2\mathfrak{A}\left(\frac{2\pi MkT}{h^2}\right)^{\frac{1}{2}}\left(\frac{2\pi AkT}{h^2}\right)\frac{(2\pi CkT)^{\frac{1}{2}}}{h}\times2\iint\limits_{\substack{0\le\theta\le\pi/2\\U\le0}}\exp(-U/kT)erf(-U/kT)^{\frac{1}{2}}\sin\theta d\theta dz_0.$$

Upon substitution of $d\alpha=dz/r_0$, $\sin\theta=\beta r_0/d$, and $d\theta=r_0d\beta/d\cos\theta$, there results

$$f_{\text{class}}=4\pi^2\mathfrak{A}\left(\frac{2\pi MkT}{h^2}\right)^{\frac{1}{2}}\left(\frac{2\pi AkT}{h^2}\right)\frac{(2\pi CkT)^{\frac{1}{2}}}{h}\times\frac{2r_0^2}{d}\int_0^{d/r_0}\frac{\beta d\beta}{[(d^2/r_0^2)-\beta^2]^{\frac{1}{2}}}\times\int_{U\le0}\exp(-U/kT)erf(-U/kT)^{\frac{1}{2}}d\alpha. \quad (17)$$

The integral in (17) may be evaluated numerically. The integration is first performed over all those values of $\alpha$ such that $U$ is negative (out to some $\alpha$ beyond which the integral may be evaluated analytically by the use of asymptotic expressions), and then over $\beta$. The results are given in Table IV; $Q$, the result of the final integration, $=72.64$, if the temperature is taken to be 273°K.

Use of Eq. (4) yields

$$f=f_{\text{class}}\frac{p^2}{\sigma}j_{\text{el}}j_{\text{vib}}\left(\frac{h\nu_{z_0}}{kT}\right)\left(\frac{h\nu_\theta}{kT}\right)^2\left[1-\exp\left(-\frac{h\nu_{z_0}}{kT}\right)\right]^{-1}\left[1-\exp\left(-\frac{h\nu_\theta}{kT}\right)\right]^{-2}, \quad (18)$$

where $\sigma$ is the symmetry number of the adsorbed molecule. Following the method used in case $A$, we find

$$R=Q\frac{\mathfrak{A}}{N^0}\frac{r_0^2}{d}\frac{\delta}{kT}\exp(-U_0/kT)\nu^{**},$$

where $\nu^{**}$ is the product of the frequency factors in (18). $\mathfrak{A}/N^0$, the area occupied per molecule adsorbed in a completed first layer, is calculated by $\mathfrak{A}/N_0=6.354(T_c/P_c)^{\frac{1}{2}}$; using $T_c=561.7$°K and $P_c=47.7$ atmospheres, gives 32.89 sq. A. If the latent heat of vaporization of benzene is taken to be 447.8 joules per gram at 273°K, and the corresponding vapor pressure is 26.54 mm of mercury, use of the equation $p_0=\delta\exp(-\Lambda/kT)$ gives the result that $\delta$ for benzene is $1.717\times10^{11}$.

Employing these values, we find that $R$ for mobile adsorption is 14.27. This is of the same order of magnitude as the results found for previous cases. The classical result, which is found by employing $f_{\text{class}}$ instead of $f$, differs only by the product of the frequency factors. Since this is 1.731, we find $R_{\text{class}}=R/1.731=8.245$.

# Determination of Electronic Structure of Molecules from Nuclear Quadrupole Effects

C. H. TOWNES
*Department of Physics,*

AND

B. P. DAILEY
*Department of Chemistry, Columbia University, New York, New York*

(Received November 1, 1948)

Nuclear quadrupole coupling constants in molecules depend on the nuclear quadrupole moments and the variation in electrostatic field at the nucleus. It is shown that this variation of electric field is usually simply related to the molecular electronic structure, being primarily dependent on the way in which valence electrons fill the lowest-energy $p$-type orbits. Structural information which can consequently be obtained from known quadrupole coupling constants is discussed. Hybridization of the normal covalent bonds of N, Cl, and As with at least 15 percent $s$ character is clearly shown. The alkali halides appear to be almost purely ionic; the quadrupole coupling data allow no more than 3 percent covalent character. In addition to molecular structure, some nuclear quadrupole moments are approximately evaluated by use of the theory developed here.

MOLECULAR constants called nuclear quadrupole coupling constants have already been measured by means of radio spectroscopy for about fifteen nuclei in twice as many molecules, and future measurements will probably provide many more cases. This coupling constant depends on the quadrupole moment of the nucleus and the second derivatives of the electrostatic potential at the nucleus due to all molecular charges outside the nucleus. The quadrupole moment $Q$ is a characteristic of the particular nucleus and is a measure of the departure of the nuclear charge distribution from spherical shape. Thus an "elongated" nucleus has a positive $Q$ and a "flattened" nucleus a negative $Q$. If the molecular electric field acting on the nuclear charges changes rapidly with angle from some molecular axis, then various orientations of a non-spherical nucleus with respect to this axis give various energies. The quadrupole coupling constant is a measure of this variation of electrostatic energy with orientation of the nucleus. In a linear or symmetric top molecule, the quadrupole coupling may be specified by one constant, which may be written $eQ(\partial^2V/\partial z^2)$, where $e$ is the protonic charge, $Q$ the nuclear quadrupole moment, $V$ the electrostatic potential, and $z$ the coordinate along the molecular axis.[1,2] Complete description of quadrupole effects in asymmetric molecules requires two constants instead of one, but in many cases a similar single constant is expected to be adequate.[3]

In order to calculate $\partial^2V/\partial z^2$ (hereinafter often abbreviated to $q$), the distribution of charges in the molecule must be known, which entails primarily a determination of wave functions for the electrons. A straightforward theoretical determination of these quantities is usually very complex, and only for the hydrogen molecule[4] has a value of $q$ been obtained by determination of an accurate wave function and subsequent calculation of $\partial^2V/\partial z^2$. A method of approximating $q$ has been previously suggested,[5] and will be developed more fully below.

Approximate wave functions are frequently used to explain, in at least a qualitative way, various molecular properties. Thus when the chemist writes down a structural formula for a molecule, he is making a guess at the distribution of charges in the molecule, or specifying an approximation to the molecular wave function. Such a structural formula, or the wave function in terms of which it may be expressed, allows approximate calculation of such quantities as dipole moment, internuclear distances, bond angles, and binding energy. Useful and, in some cases, fairly accurate information can also be obtained about $q$ from structural considerations because $q$ depends on a few rather simple parameters of bond structure.

The magnitude of $q$ at a nucleus depends almost entirely on the way in which the lowest available $p$-type orbits are occupied by valence electrons surrounding the nucleus. An $s$-type orbit or any closed shell of electrons is spherically symmetric and hence gives no contribution to the variation of energy with nuclear ori-

TABLE I. Quadrupole coupling constants of $Cl^{35}$.

| Molecule | Most important structure | Quadrupole coupling constant $eqQ$ in megacycles/sec. |
|---|---|---|
| Atomic Cl | | $-110.4$ |
| ICl | I—Cl | $-82.5$ |
| ClCN | Cl—C≡N | $-83.2$ |
| $CH_3Cl$ | $H_3C$—Cl | $-75.13$ |
| NaCl | $\overset{+}{Na}\overset{-}{Cl}$ | $< 1$ |

* Work supported by the Signal Corps.

[1] J. M. B. Kellogg, I. I. Rabi, N. F. Ramsey, and H. R. Zacharias, Phys. Rev. **57**, 677 (1940).

[2] J. H. Van Vleck, Phys. Rev. **71**, 468 (1947); D. K. Coles and W. E. Good, Phys. Rev. **70**, 979 (1946); J. Bardeen and C. H. Townes, Phys. Rev. **73**, 97 (1948).

[3] J. K. Bragg, Phys. Rev. **74**, 533 (1948).

[4] A. Nordsieck, Phys. Rev. **58**, 310 (1940).

[5] C. H. Townes, Phys. Rev. **71**, 909 (1947).

entation or to $\partial^2V/\partial z^2$ at the nucleus.** However, a $p$-type orbit gives the necessary variation of charge distribution with angle and because it gives the electron considerable probability of being near the nucleus, the effect of the lowest-energy $p$-type orbit is usually considerably greater than that of any other orbit or of any charges on nearby atoms in the molecule. In addition, distortion of the lowest-energy $p$ orbit by hybridization or combination with other orbits can be shown to produce little effect on its contribution to $q$ except by decreasing the importance of the $p$ orbit as a result of normalization of the wave function.

Consider as an example the chlorine atom. As a neutral atom, it lacks one $p$ electron from completing a closed spherical shell of charge, and hence shows a rather large value of $q$. If chlorine is covalently bonded in a molecule, the simplest idea of its bond would indicate that it lacks one $p$ electron (oriented along the bond axis) from having a spherical shell, and that again $q$ should be large and approximately equal to its value for a free atom. If the chlorine accumulates an extra electron and is ionic either as a free ion or in a molecule, there is no $p$-electron defect from a closed shell, and $q$ might be expected to be very small or zero. That this description gives a good first approximation to $q$ can be readily seen from a comparison in Table I of quadrupole coupling constants $eqQ$ for the chlorine atom and for chlorine covalently or ionicly bonded in various molecules. Table I applies to the nucleus $Cl^{35}$ only; similar results are available for $C^{37}$ which has a slightly smaller value of $Q$ than does $Cl^{35}$.

Chlorine covalently bonded in various molecules shows a fairly constant quadrupole coupling and one which is not far from the value for atomic Cl. The strikingly low value of $eqQ$ for NaCl indicates the very great difference between its bond and those of the other molecules listed, and that NaCl must involve only a very small amount of covalent character. That couplings for covalently bonded Cl are approixmately 25 percent less than the value for atomic Cl will be shown below to be good evidence that the covalent Cl bond is an $s-p$ hybrid. In addition, the small variations in $eqQ$ between various covalent cases are useful information and will be discussed.

Another example is afforded by a comparison of coupling constants of $N^{14}$ given in Table II. For all molecules where $N^{14}$ is triply bonded ($NH_3$, HCN, ClCN, and $CH_3CN$), the coupling constant is about 4 megacycles. For the two known cases where $N^{14}$ is rather surely quadruply bonded ($CH_3NC$ and the central nitrogen in $N_2O$) so that a complete valence shell is filled and the surrounding electrons therefore nearly spherically distributed, the coupling constant is less than 0.5 Mc.

Thus quadrupole coupling constants afford a new source of information about the character of molecular bonds, a source which in some cases appears to give different and more reliable information than is otherwise available. In addition, experimentally measured quadrupole coupling constants can be used to evaluate nuclear quadrupole moments in case the molecular or bond structure is sufficiently well known to allow determination of $\partial^2V/\partial z^2$ by the approach outlined here. Of course, for a measurable coupling constant the nuclear quadrupole moment must not be zero. Since the nuclear quadrupole moment can be shown to be zero for all nuclei of spin less than one, some chemical elements show no quadrupole effects and give no information of the type considered here. But the $N^{14}$ and $S^{33}$ nuclei and all of the halogens excepting F show these effects, as well as a large number of nuclei less commonly encountered.

TABLE II. Quadrupole coupling constants of $N^{14}$.

| Molecule | Most important structures | Quadrupole coupling constant $eqQ$ in megacycles/sec. |
|---|---|---|
| $NH_3$ | 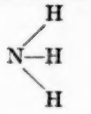 | ±4.10 |
| HCN | H—C≡N | −4.7 |
| $CH_3CN$ | $H_3C{-}C{\equiv}N$ | −4.67 |
| BrCN | Br—C≡N | −3.83 |
| $CH_3NC$ | $H_3C{-}\overset{+}{N}{\equiv}\overset{-}{C}$ | <0.5 |
| $N_2O$ | $N{\equiv}\overset{+}{N}{-}\overset{-}{O}$, $\overset{-}{N}{=}\overset{+}{N}{=}O$ | −0.27 (central N) |

We will attempt below to justify and make more quantitative the procedure for evaluating $q$ which has been suggested, and discuss most of the molecules for which quadrupole coupling constants have been measured with the purpose of testing this procedure and of obtaining information about the structure of the molecular bonds involved.

## QUADRUPOLE COUPLING IN ATOMS

Before discussing in detail the evaluation of quadrupole coupling constants in molecules, we shall consider the simpler atomic case. In this case it can readily be shown that, neglecting spin effects, the value of $\partial^2V/\partial z^2$ at the nucleus due to a single electron of orbital angular momentum $l$ is $-(2le/2l+3)\langle r^{-3}\rangle$, where $e$ is the electronic charge and $\langle r^{-3}\rangle$ is the average of the inverse third power of the distance between the nucleus and electron. In this case $z$ represents some fixed direction in space and the atom is assumed to be in such a state that the projection of $l$ on $z$ has its maximum value ($m=l$). For

** One might object that an $s$-type orbit produces a charge density $\rho$ at the nucleus which from Poisson's equation gives a value $-4\pi\rho/3$ to $\partial^2V/\partial z^2$ at the nucleus. Because of spherical symmetry, however, this contribution produces no energy change with nuclear orientation and is specificially omitted from $\partial^2V/\partial z^2$ which was defined above as the second derivative of the potential produced by all molecular charges outside the nucleus.

a hydrogen-like electronic wave function,

$$\langle r^{-3}\rangle = Z^3/n^3a_0^3l(l+\tfrac{1}{2})(l+1), \quad (1)$$

where $Z$ is the number of protonic charges on the nucleus, $n$ the total quantum number, and $a_0$ the Bohr radius 0.53A.

A closed shell of electrons around a nucleus produces a spherically symmetric charge distribution for which $\partial^2V/\partial z^2$ at the nucleus is zero. If, in addition to closed shells, there is one valence electron, then to take into account screening effects one must use an effective value of $Z$ or of $n$ in expression (1). There are fortunately other spectroscopically determinable quantities which involve $\langle r^{-3}\rangle$, namely, the atomic fine structure due to spin-orbit coupling, and hyperfine structure connected with a nuclear magnetic moment. In many cases $\langle r^{-3}\rangle$, or good values for the effective $Z$ or $n$, may therefore be determined experimentally. Thus, using the fine structure doublet separation $\Delta\nu$, one obtains[6]

$$(\partial\nu/\partial z^2)_{\text{atom}} = -2le\Delta\nu/Z_i R\alpha^2a_0^3(l+\tfrac{1}{2})(2l+3), \quad (2)$$

where $Z_i$ is the effective "unscreened" value of $Z$ defined by Landé and for $p$ electrons may usually be taken as the atomic number of the nucleus less four. $R$ and $\alpha$ are the Rydberg and fine structure constants, respectively. In case the nuclear gyromagnetic ratio and the resulting hyperfine structure are known, one may use the following expression[6] which completely eliminates the uncertainties of "effective" $Z$ and $n$,

$$(\partial^2V/\partial z^2)_{\text{atom}} = -\frac{aeM}{g_I\mu_0{}^2m}\,\frac{J(J+1)}{(l+1)(2l+3)}, \quad (3)$$

where $e$, $m$ = electronic charge and mass, respectively, $\mu_0$ = Bohr magnetron, $M$ = proton mass, $J$ = total angular momentum of the electron ($l$ plus spin), $g_I$ = gyromagnetic ratio of nucleus of spin $I$, and $a$ = hyperfine structure parameter such that energy of magnetic interaction of nucleus and electron is $a(I\cdot J)$.

The case of interactions between the nucleus and more than one electron is somewhat more complex and can be less exactly evaluated. A few of such cases, as well as corrections for relativistic effects, are discussed by Casimir.[7]

## QUADRUPOLE COUPLING IN MOLECULES—GENERAL CONSIDERATIONS

To evaluate $\partial^2V/\partial z^2$ at a particular nucleus in a molecule, we shall discuss separately the contributions of valence electrons which have a high probability of being found near this nucleus, of the inner core of electrons which are definitely associated with the nucleus and whose contribution undergoes relative small changes due to location of the atom in a molecule, and, finally, of the remaining charges in the molecule such as electrons and ions at distances of an atomic radius and more from the nucleus in question. The problem of computing exactly the contributions to $q$ from these different sources is obviously a complex one and requires a rather complete knowledge of the molecular wave function. We shall examine here the character and relative size of the various contributions, and find that in many cases one or two simple terms give the dominating contributions to the quantity to be computed, and hence these cases lend themselves to a rather simple approximate evaluation of $q$.

Consider first an atom with one valence electron outside of a closed shell. The wave function for this electron in a molecule may be expanded in terms of the atomic wave functions $\psi_{nlm}$; thus

$$\psi = \sum_{nlm} a_{nlm}\psi_{nlm}. \quad (4)$$

Of course, the electron wave functions may be expanded in somewhat different functions, such as the $p_x$, $p_y$, and $p_z$ orbitals often used in discussions of molecular bonds, but for convenience we have chosen atomic wave functions designated as usual by $n$, $l$, and $m$—the total quantum number, azimuthal, and magnetic quantum numbers, respectively. The lowest energy atomic orbits not occupied by electrons forming closed shells may be expected to be present most importantly in the molecular wave function of the valence electron. Thus usually $a_{nlm}$ will be largest for the lowest allowed values of $n$ and $l$. Of course, expression (4) must provide some probability of the electron's being found in an approximately atomic orbit of an adjacent atom to which it forms a bond. This results in the presence of a number of atomic wave functions of rather large $n$ and $l$, each, however, with rather small coefficients $a_{nlm}$ by comparison with the lowest atomic energy states of the particular atom on which our attention is centered.

TABLE III. Relative values of electronic quadrupole field $q_{nl0}\equiv(\partial^2V/\partial z^2)_{n,l,m=0}$ for various atomic states. The very large effect of screening is shown by comparison of the third and fourth columns.

| Electronic state | Atomic example for which fine structure is known | Values of $q_{nl0}$ from fine structure | Relative values of $q_{nl0}$ assuming hydrogen wave functions and no screening (Eq. (7)) |
|---|---|---|---|
| | | | Relative to $5p$ |
| $5p$ | I | $45\times10^{15}$ e.s.u. | 1.00 |
| $5d$ | Cs | $0.31\times10^{15}$ | 0.14 |
| $5f$ | Cs | | 0.048 |
| $6p$ | Cs | $3.4\times10^{15}$ | 0.58 |
| $6d$ | Cs | $0.16\times10^{15}$ | 0.08 |
| $6f$ | Cs | | 0.028 |
| $7p$ | Cs | $1.1\times10^{15}$ | 0.36 |
| $7d$ | Cs | $0.09\times10^{15}$ | 0.05 |
| | | | Relative to $2p$ |
| $2p$ | F | $21\times10^{15}$ | 1.00 |
| $3p$ | Na | $0.7\times10^{15}$ | 0.30 |
| $4p$ | Na | $0.2\times10^{15}$ | 0.12 |

[6] Cf. H. A. Bethe and R. F. Bacher, Rev. Mod. Phys. 8, 209 226 (1936).

[7] H. B. G. Casimir, *On the Interaction between Atomic Nuclei and Electrons* (Teyler's Tweede Genootschap, E. F. Bohn, Haarlem, 1936).

We choose the axis of the molecular bond as a reference direction for the magnetic quantum numbers $m$, and evaluate the contribution of this valence electron to $\partial^2V/\partial z^2$ at the nucleus. Since $\partial^2/\partial z^2(e/r)=(3\cos^2\theta-1)e/r^3$, where $\theta$ is the azimuthal angle with respect to the bond axis,

$$\partial^2V/\partial z^2=e\int\psi^*[(3\cos^2\theta-1)/r^3]\psi d\tau.$$

Using the series expansion of $\psi$ given in (4),

$$\frac{\partial^2V}{\partial z^2}=\sum_{nlm}|a_{nlm}|^2q_{nlm,\,nlm}+\sum_{nlm,\,n'l'm}a_{nlm}a_{n'l'm}{}^*q_{nlm,\,n'l'm}, \quad (5)$$

where

$$q_{nlm,\,n'l'm'}=\int\psi_{nlm}[(3\cos^2\theta-1)/r^3]\psi_{n'l'm'}{}^*d\tau$$

and the second sum is over all non-identical $nl$ and $n'l'$, since all terms for which $n=n'$ and $l=l'$ are collected in the first sum. For a non-zero value of $q_{nlm,\,n'l'm'}$, $m$ must equal $m'$, and either $l=l'\neq0$ or $l=l'\pm2$. This conveniently eliminates a large number of terms from the second sum of (5). To obtain a rough approximation to the magnitude of other terms of this part of (5), one may use hydrogen-like wave functions for the $\psi_{nlm}$.

The quantities $q_{nlm,\,nlm}$ of (5) are simply the values of $\partial^2V/\partial z^2$ or $q$ for each of the atomic states, and are multiplied by $|a_{nlm}|^2$, the fractional importance of the respective atomic states in the molecular wave function. It is quite significant that $q_{nlm,\,nlm}$ (which we hereby shorten to $q_{nlm}$) is a rapidly decreasing function of $n$ and $l$ except that for an $s$ state $q_{n0m}=0$. Hence the dominating term in the first sum of (5) will usually be the state of lowest allowed $n$ because not only will energy considerations make the amplitude $a_{nlm}$ of this wave function large but, in addition, the $q_{nlm}$ for this state is considerably larger than for the higher energy states. We shall demonstrate this in more detail for the cases where $m=0$.

The value of $q$ for the atomic state with $m$, or the projection of $l$ on the $z$ axis, equal to zero differs from that for the case of $m=l$ discussed above by the factor $-(l+1)/(2l-1)$, so that

$$(\partial^2V/\partial z^2)_{l,\,m=0}=[2l(l+1)/(2l-1)(2l+3)]\langle r^{-3}\rangle. \quad (6)$$

For hydrogenic wave functions, from Eq. (1)

$$q_{nl0}=4Z^3/n^3a_0{}^3(2l-1)(2l+1)(2l+3). \quad (7)$$

If the effects of screening around a heavy nucleus are allowed for, $q_{nl0}$ decreases still more rapidly with $n$ and $l$ than indicated by expression (7). Table III shows the relative magnitudes for various states $nl$ and compares the relative values computed for the hydrogenic case (Eq. (7)) with those obtained from the fine structure splitting (expression (2) modified by the factor $-(l+1)/(2l-1)$). Due to dependence on $n$ and to screening effects, the element $q_{nl0}$ for the $5p$ state of iodine is fourteen times larger than that for the $6p$ state of caesium, and similarly the value for the $6p$ state of Cs is considerably larger than that for any other state of Cs, the most marked differences occurring with the change of $l$ which produces a correspondingly large change in screening. Although fine structure measurements are less complete in F and Na, Table III shows that even in these light nuclei where screening effects are less important, $q$ decreases very rapidly with increasing $n$ or $l$.

We now examine in more detail the magnitudes of terms in the second sum of Eq. (5), remembering that only two types of terms exist, those for which $l=l'\neq0$ and for which $l=l'\pm2$. An estimate of their size may be obtained by using hydrogenic wave functions with rough corrections for screening as indicated by Table III. Calculation with this type of wave function shows that $q_{nlm,\,n'l'm}$ is slightly less than $(q_{nlm}q_{n'l'm})^{\frac{1}{2}}$ except for the cases $l=l'\pm2$ and $n=n'$ ($q_{nlm,\,nl'm}$ is then identically zero), or when $l$ or $l'$ equals zero.

If a $p$-type wave function is the largest component of the molecular wave function, cross-product terms involving its amplitude $a_{nlm}$ might be expected to be the largest. The only terms of this type involve mixing of this $p$ state with other $p$ and $f$ states. Consider the cross-product terms of the $p$ state with an $f$ state. If the two states have the same $n$, then the term $q_{n1m,\,n3m}$ is zero for the hydrogenic case. Allowing for screening effects, $q_{n1m,\,n3m}$ may not be exactly zero, but in any case it would be $\leq(q_{n1m}q_{n3m})^{\frac{1}{2}}$, so that from Table III $q_{n1m,\,n3m}\leq0.05q_{n1m}$. In addition, because energy considerations indicate that the contribution, or coefficient $a_{n3m}$, of $f$-type atomic states in the molecular wave function (4) would probably be small, it seems clear that contributions to $\partial^2V/\partial z^2$ in (5) of this type of term can be neglected.

The terms in (5) for which $l=l'$ and $n\neq n'$ are not so easily ruled out. An estimate of $q_{510,\,610}$ for iodine from Table III would make it about $\frac{1}{3}$ the value of $q_{510}$, while $q_{610}\approx q_{510}/10$. Thus, taking as an example a wave function of the two terms $\psi=a_{510}\psi_{510}+a_{610}\psi_{610}$, from (5),

$$\partial^2V/\partial z^2\approx[|a_{510}|^2+|a_{610}|^2/10 + \text{Real Part of } (2a_{510}a_{610}{}^*/3)]q_{510}.$$

If $a_{610}$ is not considerably smaller than $a_{510}$, the third term in brackets may be comparable in magnitude with the first. We must rely on present understanding of the chemical bond which shows that $a_{610}$ probably is much smaller than $a_{510}$. Because an electron makes a bond only to one adjacent atom, the largest and most easily understood distortion of an atomic orbital due to molecular forces results in decreasing electron density on one side of the atom and increasing it on the other side. This may be accomplished by the well recognized addition of an $s$ or $d$ wave function to a $p$ function. Thus a molecular wave function $\psi=(\sqrt{3}/2)\psi_p+\frac{1}{2}\psi_s$ has been

shown by Pauling[8] to give a "stronger" molecular bond than a pure $p$ function or any other combination of $s$ and $p$. There are no similar good reasons for the electronic orbit to be much elongated or contracted in both directions along the bond-axis, which would be the result of adding appreciable atomic wave functions of the same angular symmetry. We shall thus dispose of terms in the second sum of (5) having $l=l'$ by estimating that when the lowest available atomic orbital is a $p$ state the amplitude of higher $p$ states is less than 0.1, or, in the specific example given above, $|a_{610}|<0.1|a_{510}|$.

The only other type of cross-product term which needs consideration involves the $s$ and $d$ states. Here $l=l'-2$, so that the terms are not identically zero, and since an $s$ type wave function is large near the nucleus, the value of $q_{n00,\,n20}$ may be expected to be large. Calculation of its magnitude with hydrogenic wave functions shows that $q_{n00,\,n'20}$ is approximately equal to or slightly less than $q_{n'10}$ when $n\neq n'$. Again if $n=n'$, this term is zero for the hydrogen-like case, but not necessarily zero when screening is taken into account. It is possible that in some of the heavier atoms where $d$ orbits are expected to be important, terms due to mixing of $s$ and $d$ states will contribute appreciably to $\partial^2V/\partial z^2$. However, for such a term, $a_{n00}a_{n'20}q_{n00,\,n'20}$, to be of importance compared with the contribution of the lowest $p$ orbit, neither $a_{n00}$ or $a_{n'20}$ can be small. The molecular wave function must contain sizable components of both $s$ and $d$ atomic states.

Of course, there are other contributors to the value of $q$ besides the valence electrons. Additional effects as mentioned above are due to the presence of other nuclei and shells of electrons associated with these nuclei in the remainder of the molecule, and to the possible polarization and distortion of what we have been calling the closed spherical shell of electrons around the nucleus under consideration.

An approximate magnitude for the effects of other charges in the molecule may be obtained by computing the contribution of one electronic charge placed a distance from the nucleus equal to the minimum internuclear distance. Thus one electronic charge placed one angstrom away contributes $10^{+15}$ e.s.u. to the value of $q$. Table III shows that even for the light atom fluorine this is considerably less than the contribution of a valence electron in a low energy $p$ state, and by comparison may be neglected. The value of $q$ accurately calculated by Nordsieck[4] for the hydrogen molecule makes an interesting comparison. The two hydrogen atoms in the hydrogen molecule are closer (0.74A) than any two atoms in any other molecule. Hence, one might expect the value of $q$ resulting from distortion of the $s$-type electronic orbits and from the nearness of another nucleus to be the largest that would normally occur. Its value is $1.15\times10^{15}$ e.s.u.—approximately equivalent to one electron at a distance of one angstrom, and considerably less that the $q$ produced by a penetrating $p$ electron.

We now turn to an examination of the effects of possible distortion of the core of electrons around the nucleus at which $\partial^2V/\partial z^2$ is to be determined. Consider a closed shell of three $p$ orbits. A dipole may be induced on this shell because of adjacent charges which result, for example, in adding to the $p$ electron with $m=0$ along the axis some of the $s$-type wave function of the lowest available $s$ state. Such a perturbation might give the $s$-type wave function an amplitude of about 0.1. Although this is enough polarization to effectively move 0.2 electron from one side of the core to the other, it does not greatly change the value of $q$ at the nucleus. Contribution to $q$ by this orbit will be decreased by only 1 percent, which is the decrease in the square of the amplitude of its normal $p$ wave function. For the unperturbed spherical core, the two other $p$ type orbits each contribute an amount half as large and opposite in sign to $q$, making it zero. If these orbits are perturbed, an amount similar to the perturbation of the $m=0$ orbit, then their contributions decrease by the same fraction and $q$ remains exactly zero. It may thus be seen that a rather large amount of polarization of this closed shell of electrons probably normally occurs without an appreciable effect on $q$. Of course, forces are present which may induce a quadrupole moment on the closed shell. Thus an $f$-type term might be added to the unperturbed $p$ state. From the discussion of $q_{nlm,\,n'l'm}$ above, it may be shown again that such a term produces only a small effect on $q$, and since the effect will be in the opposite direction from the quadrupole field due to charges adjacent to the atom under consideration, it will probably conveniently result in some reduction of their contribution to $q$.

Estimates show, then, that distortions of the closed shell of electrons surrounding the nucleus will produce contributions to $q$ less than 1 percent of the value due to a single electron of the shell. Since such an electron is nearer the nucleus than the valence electron, this may be as large as 10 percent of the effect of the lowest $p$ state of the valence electron.

Perhaps a more satisfying demonstration of the smallness of uncertainties due to polarization of the closed electron shell is given by examination of a few cases which allow effectively an experimental determination of their magnitude. The alkali halides are largely ionic molecules, so that they may be regarded as made up of two closed shells which are somewhat distorted by their mutual interaction. The amount of distortion may be judged from the dipole moment[9] of cesium fluoride, the alkali halide for which this moment is most accurately known. Its dipole moment is about 60 percent of the moment corresponding to unit positive and negative electronic charges separated by the distance between nuclei in this molecule. This reduction in dipole

[8] L. Pauling, *Nature of the Chemical Bond* (Cornell University Press, Ithaca, 1945).

[9] H. K. Hughes, Phys. Rev. **70**, 570 (1946).

moment must be due to polarization of the ionic shells and possibly some admixture of the covalent state in the molecular wave function. This covalency will be shown below to be very small, but in any case if all three orbits of the outer shell of both Cs and F participate approximately equally in polarization effects, then the reduction in moment corresponds to perturbation or admixture of other states with amplitudes less than about 7 percent. This corresponds to the 10 percent somewhat arbitrarily chosen for the illustrative case above, and would on the same basis give a quadrupole coupling less than one two-hundredth that due to a single electron in one of these $p$ orbits. Although the quadrupole moment of Cs is not known,[10] it would not be expected to be less than $0.1\times10^{-24}$ cm$^2$. Since the quadrupole coupling in CsF has been measured[11] as 1.24 megacycles, $q$ at the Cs nucleus must be less than $0.18\times10^{15}$ e.s.u., or less than one two-hundredth the contribution to be expected from a single $p$ electron in the closed electron shell. Other alkali halides consistently show small quadrupole coupling constants for both the alkali and the halogen nuclei, indicating the smallness of the effects of distortion of the ionic shells on the value of $q$ at the nuclei. Thus NaBr shows a rather small quadrupole coupling of 1.2 Mc due to Na and a coupling constant less than 1 Mc due to Br,[12] although atomic spectra and other molecules containing Br show quadrupole coupling constants of about 700 Mc.

As a result of the above considerations of the magnitudes of the various parts of (5), it can be said that to a fractional accuracy of the order of ten percent, $\partial^2V/\partial z^2$ due to a single valence electron can be regarded as simply a sum of contributions $|a_{nlm}|^2q_{nlm}$ from the various atomic states and, in addition, that if the lowest energy atomic state is a $p$ state, contributions from other states may be neglected unless for some reason the amplitude of this $p$ wave function in the complete molecular wave function is exceptionally small.

### Detailed Example—ICl

The molecule ICl is perhaps the simplest case of a covalently bonded molecule for which nuclear quadrupole coupling constants are known. Since the approximations discussed above for obtaining $q$ should be rather good in this case and an accurate value of the quadrupole moment of Cl is known from atomic data, we shall examine this case in detail as an introduction to the application of our method to other molecules.

For atomic $Cl^{35}$ in the ground state, the measurements of Davis *et al.*[13] give a value +55.2 Mc*** for the nuclear quadrupole coupling constant $(\partial^2V/\partial z^2)_{atom}$ and allow an accurate evaluation of $(\partial^2V/\partial z^2)_{atom}$ from Eq. (3) as $9.6\times10^{15}$ e.s.u. By comparison, the approximation methods of evaluating this quantity indicated by Eqs. (1) and (2) give $6.0\times10^{15}$ and $9.9\times10^{15}$ e.s.u., respectively. Of course, the ground state of chlorine involves one $p$ electron missing from a closed shell, but essentially the same considerations apply to this case as to a single $p$ electron outside closed shells.

The simplest reasonable assumption about the wave function of each of the two bonding electrons in ICl

TABLE IV. Bond distances used and some computed bond characters.

| Molecule | Resonating structures | Percentage importance from bond #1 | Percentage importance from bond #2 | Observed bond distances (in angstroms) | | Reference |
|---|---|---|---|---|---|---|
| ClCN | Cl—C≡N | 75 | 90 | Cl—C | 1.620 | a |
| | $Cl^+$=C=$N^-$ | 25 | 10 | C—N | 1.163 | |
| BrCN | Br—C≡N | 75 | 90 | Br—C | 1.790 | a |
| | $Br^+$=C=$N^-$ | 25 | 10 | C—N | 1.158 | |
| ICN | I—C≡N | 76 | 90 | I—C | 1.995 | a |
| | $I^+$=C=$N^-$ | 24 | 10 | C—N | 1.158 | |
| NNO | $N^-$=$N^+$=O | 50 | 100 | N—N | 1.126 | b |
| | N≡$N^+$—$O^-$ | 50 | 0 | N—O | 1.191 | |
| ICl | | | | I—Cl | 2.321 | c |
| $CH_3Cl$ | | | | C—H<br>C—Cl | 1.107<br>1.779 | d |
| $CH_3Br$ | | | | C—H<br>C—Br | 1.100<br>1.940 | d |
| $CH_3I$ | | | | C—H<br>C—I | 1.100<br>2.136 | d |
| $AsF_3$ | | | | As—F | 1.712 | e |
| $CH_3CN$ | | | | C—C<br>C—N | 1.49<br>1.16 | f |
| $CH_3NC$ | | | | C—N<br>N—C | 1.44<br>1.18 | g |
| $NH_3$ | | | | N—H | 1.014 | h |
| HCN | | | | C—H<br>C—N | 1.058<br>1.157 | h |

[a] C. H. Townes, A. N. Holden, and F. R. Merritt, Phys. Rev. **74**, 1113 (1948); A. G. Smith, H. Ring, W. V. Smith, and W. Gordy, Phys. Rev. **74**, 370 (1948).
[b] D. K. Coles, E. S. Elyash, and J. G. Gorman, Phys. Rev. **72**, 973 (1947).
[c] G. Herzberg, *Molecular Spectra and Molecular Structure* (Prentice-Hall, Inc., New York, 1939).
[d] W. Gordy, J. W. Simmons, and A. G. Smith, Phys. Rev. **74**, 243 (1948).
[e] B. P. Dailey, K. Rusinow, R. Shulman, and C. H. Townes, Phys. Rev. to be published.
[f] L. Pauling, H. D. Springall, and K. J. Palmer, J. Am. Chem. Soc. **61**, 927 (1939).
[g] W. Gordy and L. Pauling, J. Am. Chem. Soc. **64**, 2952 (1942).
[h] G. Herzberg, *Infrared and Raman Spectra* (D. Van Nostrand Company, Inc., New York, 1945).

[10] T. Schmidt, Naturwiss. **28**, 565 (1940).
[11] J. W. Trischka, Phys. Rev. **74**, 718 (1948).
[12] W. A. Nierenberg and N. F. Ramsey, Phys. Rev. **72**, 1075 (1947).
[13] L. Davis, Jr., B. T. Feld, C. W. Zabel, and J. R. Zacharias, Phys. Rev. **73**, 525 (1948).

*** Note that the value +55.2 given here differs from the value −110.4 of Table I by the factor $-(l+1/2l-1)$ or $-2$ because in the atomic state $\partial^2V/\partial z^2$ is usually evaluated for the state $m=l$, whereas in the molecular case the value for $m=0$ is more convenient. In Table I the atomic value for the state $m=0$ is needed to compare properly with molecular values of $q$.

TABLE V. Probable molecular structures and comparison of resulting quadrupole coupling constants with the observed values.

| Nucleus | Molecule | Resonating structures | Percentage importance | No. of "unbal." $p$ electrons | No. for hybrid struc. | Assumed $eqQ$ per $p$ elec. | Coupling constant calculated | Coupling constant observed | Reference |
|---|---|---|---|---|---|---|---|---|---|
| $Cl^{35}$ | ICl | I—Cl | 91 | 0.82 | 0.75 | − 110.4 Mc | − 83 Mc | − 82.5 Mc | a |
| | | $\overset{+}{I}\overset{-}{Cl}$ | 9 | 0 | | | | | |
| $Cl^{35}$ | $CH_3Cl$ | $CH_3$—Cl | 80 | 0.82 | 0.66 | − 110.4 | − 73 | − 75.13 | b |
| | | $\overset{+}{C}H_3\overset{-}{Cl}$ | 20 | 0 | | | | | |
| $Cl^{35}$ | ClCN | Cl—C≡N | 83 | 0.82 | 0.75 | − 110.4 | − 83 | − 83.2 | c,d |
| | | $\overset{+}{Cl}$=C=$\overset{-}{N}$ | 17 | 0.40 | | | | | |
| $Cl^{35}$ | NaCl | $\overset{+}{Na}\overset{-}{Cl}$ | 97 | 0 | <0.03 | − 110.4 | < 3 | < 1 | e |
| | | Na—Cl | <3 | 1 | | | | | |
| $Br^{79}$ | $CH_3Br$ | $CH_3$—Br | 82 | 1 | 0.82 | + 720 | + 590 | + 577 | b |
| | | $\overset{+}{C}H_3\overset{-}{Br}$ | 18 | 0 | | | | | |
| $Br^{79}$ | BrCN | Br—C≡N | 85 | 1 | 0.96 | + 720 | + 680 | + 686.5 | c, d |
| | | $\overset{+}{Br}$=C=$\overset{-}{N}$ | 15 | 0.625 | | | | | |
| $Br^{79}$ | NaBr | $\overset{+}{Na}\overset{-}{Br}$ | 97 | 0 | <0.03 | + 720 | < 21 | < 1 | e |
| | | Na—Br | <3 | 1 | | | | | |
| $I^{127}$ | ICl | I—Cl | 91 | 1 | 1.135 | −2500 | −2840 | −2944 | a |
| | | $\overset{+}{I}\overset{-}{Cl}$ | 9 | 2.5 | | | | | |
| $I^{127}$ | ICN | I—C≡N | 87 | 1 | 0.951 | −2500 | −2380 | −2420 | c, d |
| | | $\overset{+}{I}$=C=$\overset{-}{N}$ | 13 | 0.625 | | | | | |
| $I^{127}$ | $CH_3I$ | $CH_3$—I | 84 | 1 | 0.84 | −2500 | −2100 | −1931.5 | b |
| | | $\overset{+}{C}H_3\overset{-}{I}$ | 16 | 0 | | | | | |
| $As^{75}$ | $AsF_3$ | $\overset{-}{F}$ / $\overset{+}{As}$—F / F | 100 | −0.4 | −0.4 | 600 | − 240 | − 235 | f |

[a] C. H. Townes, F. R. Merritt, and B. D. Wright, Phys. Rev. **73**, 1338 (1948).
[b] W. Gordy, J. W. Simmons, and A. G. Smith, Phys. Rev. **74**, 243 (1948).
[c] C. H. Townes, A. N. Holden, and F. R. Merritt, Phys. Rev. **74**, 1113 (1948).
[d] A. G. Smith, H. Ring, W. V. Smith, and W. Gordy, Phys. Rev. **74**, 370 (1948).
[e] W. A. Nierenberg and N. F. Ramsey, Phys. Rev. **72**, 1075 (1947).
[f] B. P. Dailey, K. Rusinow, R. Shulman, and C. H. Townes, Phys. Rev. to be published.

is that it represents a pure covalent bond made up only of the atomic ground states of I and Cl. Using a Heitler-London (atomic orbital) type of wave function for the two electrons involved in the covalent band, and indicating coordinates of the first electron by (1) and those of the second electron by (2),

$$\psi = a\{[\psi_{310}{}^{(1)}]_{Cl}[\psi_{510}{}^{(2)}]_I + [\psi_{310}{}^{(2)}]_{Cl}[\psi_{510}{}^{(1)}]_I\}. \quad (8)$$

The constant $a$ is approximately $1/\sqrt{2}$, but must be modified a small amount because of the overlap of the iodine and chlorine wave functions, and will be $1/(2+2S^2)^{\frac{1}{2}}$, where $S=\int[\psi_{310}]_{Cl}{}^*[\psi_{510}]_I d\tau$ is assumed for convenience to be real.

The value of $q$ contributed by the first electron is

$$q_1 = e\int \psi^*[[3\cos^2\theta - 1]/r^3]\psi d\tau, \quad (9)$$

where $\theta$ and $r$ are coordinates of this electron. Inserting expression (8) for $\psi$ and integrating, $q_1=[(q_{310}+Sq_s)/2(1+S^2)]$, where $q_s=\int[\psi^*{}_{310}]_{Cl}(3\cos^2\theta-1)/r^3[\psi_{510}]_I d\tau$. The contribution due to the second electron is similar, so that both valence electrons in the state (8) give

$$q=[(q_{310}+Sq_s)/(1+S^2)]\approx q_{310}(1-S^2)+Sq_s. \quad (10)$$

To evaluate $q_s$, one might first try expanding $[\psi_{510}]_I$ in terms of atomic wave functions about the Cl nucleus. This procedure is not very helpful because $[\psi_{510}]_I$ will involve not only the Cl $3p$ wave function, but also the $2p$ and $4p$ functions, which will give appreciable contributions to $q_s$. A more illuminating approach is to consider the character of the $\psi_{310}$ wave function and the relative importance of its parts in contributing to $\langle 1/r^3\rangle$. For hydrogen, $\psi_{310}$ has the form $(2-r/3a_0)$

$\times re^{-r/2a_0}\cos\theta$, so that when $\pi/2<\theta<-\pi/2$, there is a maximum at approximately $r=1.8a_0$, a minimum at $r=10a_0$, and a null at $r=6a_0$. Integration shows that, although there is 90 percent probability of finding the electron at a distance $r>6a_0$, or in the outer lobe of the probability distribution given by $\psi_{310}$, only 4 percent of the contribution to $\langle 1/r^3\rangle$ comes from the region $r>6a_0$. Furthermore, only 14 percent of the contribution to $\langle 1/r^3\rangle$ comes from regions farther away than the first maximum, i.e. $r>1.8a_0$. Again, simplification can be achieved because of the rapid variation of the function $1/r^3$, and only those parts of the integral for $q_s$ need be considered which are closer to the nucleus than $1.8a_0$, or than the first maximum in the $\psi_{310}$ probability distribution. If $[\psi_{510}]_I$ were constant over this small region near the Cl nucleus, $q_s$ would be essentially zero because of the reversal of the sign of $\psi_{310}$ due to its dependence on $\cos\theta$. Actually $[\psi_{510}]_I$ is not constant, but is small and slowly varying near the Cl nucleus. Using hydrogenic wave functions and appropriate screening constants, $q_s$ can be roughly estimated as $q_s=-.05q_{310}$. The sign of $q_s$ is uniquely determined because of the relative phases of $[\psi_{510}]_I$ and $[\psi_{310}]_{Cl}$ must give a positive value to $S$. For the conclusions which follow, an exact evaluation of $q_s$ is not as important as its sign, which depends primarily on the presence of one radial node in the $\psi_{310}$ wave function, and not otherwise on its exact form.

Consider now the appropriateness of the wave function (8) or (9). It represents the lowest energy atomic state and a wave function which will at the same time contribute strongly to the exchange energy which is largely responsible for the chemical bond. The other lowest energy atomic states ($m=\pm1$) would contribute so little to chemical bonding that it is generally supposed they would be occupied by non-bonding electrons only. Some contributions to $\psi$ may be made by higher energy atomic states, and in addition some of the lower energy atomic states such as the $3s$ state of Cl might be added to $\psi$ by displacing the non-bonding electrons which would otherwise occupy these orbits. Since addition of an $s$ or $d$ wave function would increase the bond strength more than would a $p$ function, the most likely additions to $\psi$ would be $3s$, $4s$, and $3d$ wave functions. To allow for this hybridization, $[\psi_{310}]_{Cl}$ in (8) may be replaced by

$$(1-b)^{\frac{1}{2}}[\psi_{310}]_{Cl}+\sum_{nlm} a_{nlm}[\psi_{nlm}]_{Cl},$$

where the sum is again over all chlorine atomic states except $\psi_{310}$, and the constant $b$ is inserted to allow for the necessary renormalization of $\psi$. If no states lower than the $3s$ state are included in this hybridization, then to a good approximation the only effect of hybridization is through the renormalization constant $b$, and it may be shown that (10) is simply replaced by $q=(1+2S^2-b)q_{310}$.

Possible ionic character of the ICl bond has not yet been considered and terms in the wave function corresponding to a negatively charged chlorine and positively charged iodine ion must be included because chlorine is somewhat more electronegative than iodine. Ionic character of a bond or wave function has been used with several meanings and is not always precisely defined. As the quantity of importance in producing molecular dipoles, and whose magnitude is closely connected with electronegativity differences, it generally means the difference between the probabilities of finding a bonding electron on the two atoms with which it is associated. The same quantity is of importance in quadrupole coupling constants and is what is here referred to as "ionic character." This ionic character for a bonding wave function $\psi$ constructed of atomic states $\psi_1$ and $\psi_2$ of each of two atoms as in (8) can be satisfactorily defined mathematically as

$$i=\int\left[\int\psi_1^*\psi d\tau_1\int\psi_1\psi^*d\tau_1-\int\psi_2^*\psi d\tau_1\int\psi_2\psi^*d\tau_1\right]d\tau_2,$$

where $d\tau_1$ and $d\tau_2$ represent volume elements for electrons 1 and 2, respectively, and $\psi_1$, $\psi_2$ represent atomic states of atoms 1 and 2, respectively. If wave functions $\psi_1$ and $\psi_2$ for the two atoms enter symmetrically in the molecular wave function, this definition gives zero as the ionic character of the bond. Ionic character is allowed for in the wave function (8) by adding a term $c[\psi_{310}^{(1)}]_{Cl}[\psi_{310}^{(2)}]_{Cl}$ corresponding to both electrons on the chlorine atom. After renormalization, this gives

$$\psi=\frac{1}{(1+S^2+c^2+2\sqrt{2}cS)^{\frac{1}{2}}}\times\left\{\frac{[\psi_{310}^{(1)}]_{Cl}[\psi_{510}^{(2)}]_I+[\psi_{310}^{(2)}]_{Cl}[\psi_{510}^{(1)}]_I}{\sqrt{2}}+c[\psi_{310}^{(1)}]_{Cl}[\psi_{310}^{(2)}]_{Cl}\right\}$$

and $i$ as defined above is $c^2+\sqrt{2}cS$ omitting cubic terms in $c$ and $S$. The constant $c$ is presumably positive to increase the exchange integral and produce a stronger chemical bond.

If the value of $q$ contributed by two bonding electrons is computed for a molecular wave function including both hybridization and ionic character, it can, after some manipulation, be shown to be $q=(1-S^2+c^2)\times q_{310}+2(S+\sqrt{2}c)q_s$ neglecting powers of $S$ and $c$ higher than the second.

Although the inner closed shells of chlorine are expected to contribute a negligible amount to $q$, the other non-bonding electrons in the valence shell must be considered. It is customary to assume that the four non-bonding $p$ electrons of Cl remain essentially in their atomic orbits if the chlorine is bonded normally in a molecule. We shall for the moment make this assumption so that their combined contribution to $q$ is

$2q_{31-1}+2q_{31+1}$. Similarly, the two non-bonding $s$ electrons of the valence shell remain in their atomic $s$ orbits unless some of this orbit has been used by the bonding electrons, in which case they would occupy the lowest available energy level, corresponding to a hybrid $s$ and $p$ orbit,

$$\psi=(d)^{\frac{1}{2}}\psi_{300}+(j)^{\frac{1}{2}}\psi_{310}.$$

Their contribution to $q$ is then $2fq_{310}$. Now since for a completely filled shell, $q=0$, it can easily be seen that $q_{31-1}=q_{31+1}=-\frac{1}{2}q_{310}$. Therefore, $q=(-1-S^2b+c^2)q_{310}+2(S+\sqrt{2}c)q_s$. Since $f$ is non-zero primarily because part of the $3s$ wave function has been used in producing a hybridized bond, $b\geq f$, and $b$ may be written $b=b'-f$, so that

$$eQq=(-1-S^2+c^2-b'+f)eQq_{310}+2(S+\sqrt{2}c)eQq_s \quad (11)$$

where all the quantities in the bracket are positive and real except $c$, for which the sign is unknown. Now $eQq_{310}$ is just the quadrupole coupling constant in the atomic case for $m=0$ and equals $-(l+1)/(2l-1)$ or $-2$ times the coupling constant 55.2 Mc found for atomic $Cl^{35}$ by Davis *et al.*[13] The measured value of the $Cl^{35}$ quadrupole coupling in ICl is $-82.5$ Mc, so that

$$1+S^2-c^2+b'-f-2(S+\sqrt{2}c)q_s/q_{310}=0.723 \quad (12)$$

The ionic character may be obtained approximately from the curve of ionic character *versus* difference in electronegativity, which gives $i=0.08$, or from the dipole moment of ICl which gives $i=0.06$ if depolarizing and other disturbing effects are neglected. Substituting $i=0.08$, Eq. (12) becomes

$$1+b'+S^2+\sqrt{2}cS-2(S+\sqrt{2}c)q_s/q_{310}-f=0.80. \quad (13)$$

Equation (13) shows that hybridization of the bonding orbit with atomic orbits of higher energy would tend to increase the ICl quadrupole coupling constant, since this represents an increase in $b'$, whereas $3s$-$3p$ hybridization of the bond gives a decrease in this constant. Since $S$, $b'$, and $c$ are positive and $q_s/q_{310}$ negative, $f\geq 0.20$, corresponding to considerable $3s-3p$ hybridization.

A similar type of calculation may be made using as a basis the Hund-Mulliken molecular orbital type of

TABLE VIa. Coupling constants for molecules containing nitrogen. $\frac{1}{2}\psi_s+(\frac{3}{2})^{\frac{1}{2}}\psi_p$ hybridization is assumed for $\sigma$-component of multiple bonds (see text).

| Molecule | Resonating structures | % Importance | No. of "unbal." $p$ electrons | No. for hybrid struc. | Assumed $eqQ$ per $p$ elec. | Coupling constant calculated | Coupling constant observed | Reference |
|---|---|---|---|---|---|---|---|---|
| $NH_3$ | $N\equiv H_3$ | 100 | −0.16 | −0.16 | +24 Mc | −3.9 | ±4.10 Mc | a |
| | | (100) | (−0.40) | (−0.40) | (+24) | (−9.6) | (±4.10) | |
| $CH_3CN$ | $CH_3-C\equiv N$ | 85 | −0.25 | −0.18 | +24 | −4.4 | −4.67 | b |
| | $CH_3-\overset{+}{C}=\overset{-}{N}$ | 5 | +0.20 | | | | | |
| | $\overset{+}{H}CH_2=C=\overset{-}{N}$ | 10 | +0.20 | | | | | |
| HCN | $H-C\equiv N$ | 90 | −0.25 | −0.20 | +24 | −4.8 | −4.7 | c |
| | $H-\overset{+}{C}=\overset{-}{N}$ | 10 | +0.20 | | | | | |
| $CH_3NC$ | $CH_3-N=C$ | 5 | +0.25 | +0.025 | +24 | +0.62 | <0.5 | b |
| | $CH_3-\overset{+}{N}\equiv\overset{-}{C}$ | 95 | 0 | | | | | |
| BrCN | $Br-C\equiv N$ | 80 | −0.25 | −0.166 | +24 | −3.8 | −3.83 | d |
| | $\overset{+}{Br}=C=\overset{-}{N}$ | 20 | +0.20 | −0.16 | | | | |
| NNO | $\overset{-}{N}=\overset{+}{N}=O$ | 45 | +0.20 | −0.05 | +24 | −1.2 | −1.03 | e |
| (end nitrogen) | $N\equiv\overset{+}{N}-\overset{-}{O}$ | 55 | −0.25 | | | | | |
| NNO | $\overset{-}{N}=\overset{+}{N}=O$ | 45 | 0.0 | 0.0 | +24 | 0.0 | −0.27 | f |
| (central nitrogen) | $N\equiv\overset{+}{N}-\overset{-}{O}$ | 55 | 0.0 | | | | | |

[a] R. S. Henderson, Phys. Rev. **74**, 107 (1948); The sign of $eqQ$ in $NH_3$ has not definitely been established experimentally. However, if it is assumed that the magnetic field produced by molecular rotation is in the same direction as in other known cases, then the combination of nuclear quadrupole and dipole effects show that $eqQ$ is negative as is expected here.
[b] H. Ring, H. Edwards, M. Kessler, and W. Gordy, Phys. Rev. **72**, 1262 (1947).
[c] W. Gordy, Phys. Rev. to be published.
[d] C. H. Townes, A. N. Holden, and F. R. Merritt, Phys. Rev. **74**, 1113 (1948).
[e] A. G. Smith, H. Ring, W. V. Smith, and W. Gordy, Phys. Rev. **73**, 633 (1948).
[f] D. K. Coles, E. S. Elyash, and J. G. Gorman, Phys. Rev. **72**, 973 (1947).

TABLE VIb. Coupling constants for molecules containing nitrogen. $(\frac{1}{2})^{\frac{1}{2}}\psi_s+(\frac{1}{2})^{\frac{1}{2}}\psi_p$ hybridization is assumed for $\sigma$-component of multiple bonds (see text).

| Molecule | Resonating structures | % Importance | No. of "unbal." $p$ electrons | No. for hybrid struc. | Assumed $eqQ$ per $p$ elec. | Coupling constant calculated | Coupling constant observed |
|---|---|---|---|---|---|---|---|
| $NH_3$ | $\begin{matrix}\overset{+}{H}\\ \overset{-}{N}\!-\!H\\ \diagdown\\ H\end{matrix}$ | 100 | −0.40 | −0.40 | 10.0 | 4.0 Mc | ±4.10 Mc |
| $CH_3CN$ | $CH_3\!-\!C\equiv N$ | 85 | −0.50 | −0.425 | 10.0 | −4.25 | −4.67 |
| | $CH_3\!-\!\overset{+}{C}\!=\!\overset{-}{N}$ | 5 | 0 | | | | |
| | $\overset{+}{H}CH_2\!=\!C\!=\!\overset{-}{N}$ | 10 | 0 | | | | |
| HCN | $H\!-\!C\equiv N$ | 90 | −0.50 | −0.45 | 10.0 | −4.5 | −4.7 |
| | $H\!-\!\overset{+}{C}\!=\!\overset{-}{H}$ | 10 | 0 | | | | |
| $CH_3NC$ | $CH_3\!-\!N\!=\!C\!:$ | 5 | +0.50 | +0.025 | 10.0 | +0.25 | <0.5 |
| | $CH_3\!-\!\overset{+}{N}\!\equiv\!\overset{-}{C}$ | 95 | 0 | | | | |
| BrCN | $Br\!-\!C\equiv N$ | 80 | −0.50 | −0.40 | 10.0 | −4.0 | −3.85 |
| | $\overset{+}{Br}\!=\!C\!=\!\overset{-}{N}$ | 20 | 0 | | | | |
| NNO | $\overset{-}{N}\!=\!\overset{+}{N}\!=\!O$ | 45 | 0 | −0.22 | 10.0 | −2.2 | −1.03 |
| (end nitrogen) | $N\equiv\overset{+}{N}\!-\!\overset{-}{O}$ | 55 | −0.50 | | | | |
| NNO | $\overset{-}{N}\!=\!\overset{+}{N}\!=\!O$ | 45 | 0 | 0.0 | 10.0 | 0.0 | −0.27 |
| (central nitrogen) | $N\equiv\overset{+}{N}\!-\!\overset{-}{O}$ | 55 | 0 | | | | |

wave function,

$$\psi=a\{[\psi_{310}{}^{(1)}]_{Cl}+[\psi_{510}{}^{(1)}]_I\}\{[\psi_{310}{}^{(2)}]_{Cl}+[\psi_{510}{}^{(2)}]_I\}.$$

As long as the definition of ionic character given above is used, there is no great difference in the results with this type of wave function except in the way in which overlap effects appear, and again $f\geq 0.20$.

The method of treatment is probably too rough to allow an actual evaluation of the amount of hybridization from (13). This equation was developed, however, to show that overlap and other small effects obtained from a standard type of treatment are in the wrong direction to account for the discrepancy between the molecular and atomic coupling constants for Cl, hence $s$-$p$ hybridization is indicated.

The $s$-$p$ hybridization of the tetrahedral bonds of carbon is well recognized and produces orbitals which are one-quarter $s$, or with $f=0.25$. In addition, the "strongest" bond[8] using $s$-$p$ hybridization occurs when $f=0.25$. It has hitherto not been clear, however, whether the bond energy is sufficient to outweigh the energy required to displace some of the non-bonding electrons of an atom from the $s$ orbit so that this orbit becomes available for bonding. In ICl apparently considerable $s$-$p$ hybridization occurs in the chlorine orbital, the bond possibly corresponding fairly closely to a tetrahedral carbon bond. Other molecules containing Cl which will be discussed below are consistent with this conclusion. In addition, $s$-$p$ hybridization will be shown from a somewhat different and still clearer type of evidence to occur in nitrogen and arsenic, and presumably is rather common.

Before proceeding to other molecules, we shall review the assumptions involved in the conclusion that the chlorine bond is approximately a 20 percent–80 percent $3s$-$3p$ hybrid. Although chlorine is not a heavy atom, the measured atomic and molecular values of $q$ are large enough that the effect of charges on the adjacent iodine atom is comparatively small, probably less than $0.03q_{310}$. Since the closed shells of electrons about the chlorine nucleus are inside of a valence shell of five electrons, they are very tightly bound and effects due to distortions of these shells are most probably less than $0.01q_{310}$. Electrons of the valence shell alone, then, are responsible for the observed quadrupole coupling. The fact that the molecular quadrupole coupling is 28 percent less than the atomic coupling and that the small effect of ionic character of the bond can account for only part of the discrepancy shows that either there is effectively more than one $3p$ electron with $m=0$ ($s$-$p$ hybridization), or that there are less than four $3p$ electrons in the $m=\pm 1$ states. Hybridization of the bonding orbital with any atomic orbit other than the $3s$ would result in an increase rather than the observed decrease in the value of $q$. One is therefore forced into either $s$-$p$ hybridization or aban-

doning the assumption (made tentatively above) that the non-bonding $p$ electrons remain essentially undisturbed. The latter choice seems much less likely because twice as many electrons must be removed from the $m=1$ orbits as have been added to the $3p,m=0$ orbit to account for the observed effect. Although hybridization of the orbit of the bonding electron appears rather natural because of the advantage of increasing the bond energy, there would appear to be no good energetic reason for promoting a sizable fraction of an electron from the $3p$, $m=\pm 1$ orbits. In addition, the small amount of distortion and resulting quadrupole coupling for the case of non-bonding electrons in the alkali halides even in the presence of a strong electrostatic dipole affords good empirical evidence against the perturbation of the non-bonding $p$ electrons in ICl to the extent needed to explain the observed effect.

## MOLECULAR ELECTRONIC STRUCTURES DETERMINED FROM QUADRUPOLE COUPLING DATA

Rather than a detailed examination of each molecule such as has been given in ICl, we shall for the remainder of this discussion accept the general method of approximating $q$, and show how it may be rather simply applied to determine or verify the electronic structure of molecules from the measured quadrupole coupling constants. To correlate electronic structure and quadrupole coupling values we first describe the molecule as resonating between several structures or valence bond combinations and obtain the percentage importance of each structure from more or less standard types of evidence. For each structure the number of "unbalanced" electrons in $p$ states around the nucleus in question is determined (a completely filled $p$ shell containing six electrons has no unbalanced $p$ electrons, a structure involving one bonding $p_z$ orbital has one unbalanced $p$ electron). Next the average number of unbalanced $p$ electrons for the molecule—the weighted average of the values for the various resonant structures—is calculated. Finally, a value of the coupling constant per $p$ electron is chosen to produce the best fit with the observed values for all molecules involving the same nucleus and the final "calculated" coupling constants obtained. In the two cases of Cl and As values of coupling constant per $p$ electron are available from other types of data and these values are used.

For most nuclei values of the nuclear quadrupole moment are unknown and comparisons of measured and calculated values of $q$, of the sort made for chlorine in ICl in a previous section, cannot be carried out. It is still possible, however, to obtain information concerning the molecular electronic structure from the measured quadrupole coupling constants. If a value of the coupling constant for a single $p$ electron is chosen to fit the measured values for the individual molecules, the consistency of the assumptions involved in setting up the molecular electronic structures may be tested.

The contribution of the individual structures has been determined as far as possible from bond distances and the Pauling table of covalent radii as modified by Schomaker and Stevenson.[14] The modified radii for carbon and nitrogen suggested by Gordy[15] have also been accepted. Bond distances used are listed in Table IV. The contribution of ionic structures and structures involving atoms bearing formal charges has been calculated using the table correlating "partial ionic character" and differences in electronegativity given in Pauling's "Nature of the Chemical Bond" and to some extent dipole moment data. In a number of interesting cases modifications in these structures, suggested by a consideration of quadrupole coupling information, have been made.

Table V gives the structures of all molecules involving the halogens and arsenic whose quadrupole couplings are known. They have been chosen from a consideration of all structural information including nuclear quadrupole effects, and although differing in some cases from those proposed by earlier investigators, they appear just as consistent with previously available information. In addition, as shown in Table V, these structures give good agreement between measured and calculated quadrupole coupling constants, whereas some of the alternative proposals would give coupling constants in striking disagreement with the measured values. Data are given for only one isotope of each chemical element. While the individual isotopes of an element may have different values of the nuclear quadrupole moment, in the same molecule they will have identical values of $q$ and therefore contribute no new information concerning the molecular electronic structure.

The halogen cyanides have been assumed to resonate between the structures X—C≡N and $\overset{+}{\text{X}}$=C=$\overset{-}{\text{N}}$. The percent contribution of each configuration has been determined from the observed internuclear distances and the table of covalent radii. Since the percentages obtained by using the C—N distance differs from that derived from the C—X distance, an average has been taken. The data on the percent contribution of individual valence bond structures calculated from independent bond distances for several molecules are given in Table IV. The discrepancies observable in this table as well as the difficulties pointed out below in bond lengths of the methyl halides indicate some lack of internal consistency in the table of covalent radii or their use with simple structural approximations. Since the calculation of bond distances from bond radii neglects a number of important considerations, this apparent lack of consistency—pointed out clearly by the rather accurate bonds distances obtained from microwave spectra—is not surprising.

[14] V. Schomaker and D. P. Stevenson, J. Am. Chem. Soc. **63**, 37 (1941).
[15] W. Gordy, J. Chem. Phys. **15**, 81 (1947).

A double bond involving one of the halogen atoms is assumed in Table V to consist of a $\sigma$-bond (in Mulliken's notation) of the same character (hybridized $s$-$p$ or pure $p$) as the single bond to that atom and a $\pi$-bond of pure $p$ character. A positive formal charge on an atom, since it pulls the electrons closer to the nucleus, is taken into account by multiplying the number of unbalanced $p$ electrons by a factor 1.25 estimated from atomic fine structure. Similarly for a negative formal charge, a factor 1/1.25 is introduced.

The methyl halides, in Table V, have been considered as containing a single covalent bond between carbon and halogen, having some "ionic character." The problem of evaluating the ionic character of the carbon halogen bonds is somewhat difficult as can be seen in the case of the C—I bond in $CH_3I$ which should have zero moment on the basis of the electronegativity differences and which has an observed bond moment of 1.2 Debye units. Complications such as interaction between the C—H and C—X bonds, as well as effect on electronegativity of possible hybridization,[16] are presumably responsible. Since the ionic character of the carbon-halogen cannot be correctly assigned from a simple consideration of the carbon-halogen electronegativity differences, the decision has been based on the dipole moment and the quadrupole data. These indicate 15–20 percent ionic character. It should perhaps be mentioned that this picture fails to account for the anomalous carbon halogen bond lengths in these molecules which are significantly greater than the covalent single bond radii. A shortening of the bond due to resonance with ionic states would generally be expected.

In the case of the sodium halides the quadrupole coupling constant is an especially sensitive indication of the amount of covalent character. From a consideration of the quadrupole coupling data, one can with some confidence assign a maximum of 4 percent covalent character in NaCl and 3 percent in NaBr. While these values are quite different from the figures which would have been chosen on the basis of electronegativity differences alone, they are of the same order of magnitude as the 5–10 percent figure quoted by Pauling[17] for alkali halide gas molecules based on a consideration of curves of energy *versus* internuclear distance for the ionic and covalent molecules. The observed dipole moment of gaseous cesium fluoride indicates only 60 percent ionic character if polarization is completely neglected. However, the quadrupole coupling constants give rather clear evidence that the alkali halides should be considered as almost purely ionic with a large amount of polarization responsible for reducing the dipole moment. This is in agreement with similar conclusions of Mulliken[18] from a study of the electronic spectra of these molecules.

[16] R. S. Mulliken, J. Chem. Phys. **3**, 573 (1935).
[17] See reference 8, p. 46.
[18] R. S. Mulliken, Phys. Rev. **51**, 310 (1937).

Because the quadrupole coupling was known in the atomic case for $Cl^{35}$, it was shown above that $s$-$p$ hybridization occurs in the Cl bond and for this reason we have taken the pure covalent single Cl bond as of 82 percent $p$-character and used the value $-110.4$ Mc obtained from atomic data for the coupling per $p$ electron. In the cases of Br and I, although hybridization may be expected, the degree or character of hybridization is not yet known and we have assumed the covalent single bonds to involve pure $p$ orbitals. This assumption does not introduce much error in the relative values of quadrupole couplings as long as the amount of hybridization of a single bond does not vary from molecule to molecule.

Possible structures considered for arsenic trifluoride were

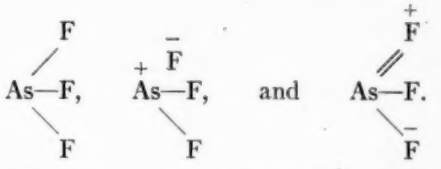


Both the dipole moment and bond distance allow only negligible contributions from structures other than

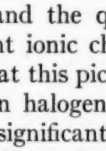


Accepting this structure, the degree of $s$-$p$ hybridization can be estimated from the quadrupole coupling, since in this case the value of the quadrupole moment is known,[19] at least roughly, from atomic data to be $0.3\times10^{-24}$ cm$^2$. The resulting wave function for the bonding orbitals is of the form $(\frac{1}{5})^{\frac{1}{2}}\psi_s+2(\frac{1}{5})^{\frac{1}{2}}\psi_p$. This wave function would not be very much changed if some importance is given the other two molecular structures mentioned above.

If the $p$ orbitals of $AsF_3$ were not hybridized, there would be a very small or zero coupling constant since the three perpendicular $p$ orbits would be equally filled and produce a spherical charge distribution around the nucleus. Consider now the three $p$ orbits of the valence shell referred to axes with $z$ oriented along the molecular axis rather than any of the As—F bonds. If hybridization occurs and increases the angle between bonds to a value greater than 90° (100° is the best available value of bond angle for $AsF_3$), then a defect of electrons along the molecular axis might be expected since the $p_z$ orbit oriented along this axis would not be as much occupied by bonding electrons as the $p_x$ and $p_y$ orbits perpendicular to the axis. However, if this hybridization is produced by use of the $s$ orbit of the valence shell—and only in this case—the two non-bonding electrons of the valence shell must be promoted to an orbit which contains a $p_z$ component. Since this non-bonding orbit contains two electrons whereas the bonding orbits

[19] H. Schuler and M. Marketu, Zeits. f. Physik **103**, 434 (1937).

contain on the average only one electron, there is an excess of electrons along the molecular axes instead of a defect. Such an excess is proved by the sign of the quadrupole coupling constant in $AsF_3$, showing definitely that the bonding orbitals are *s-p* hybrids.

Thus as in the case of Cl, a considerable amount of *s* character is demanded in the As bonds. Together with the observed bond angle (100°), this indicates the correctness of Pauling's suggestion[20] that a compromise results between the tendency of the molecule to form the "strongest possible" bonds (tetrahedral bonds) and the tendency in the case of atoms with an unshared pair to keep the unshared pair in the lower energy orbital.

The approximations involved in the calculation of the quadrupole coupling constants are less valid for the case of the lighter nucleus, nitrogen, than for the halogens and arsenic. This is primarily because in a light atom the contribution to $q$ of a $p$ electron is large but not overwhelmingly large by comparison with other neglected effects. The data for molecules containing nitrogen have been collected in Table VI (a and b). Any conclusions drawn from these data must be somewhat more tentative than those presented in the preceding sections, both because of less accuracy in the approximations and because the double and triple bond structures characteristic of N are less well understood than are single bonds.

Most authors have discussed the nitrogen bonds in ammonia and related molecules in terms of pure $p$ bonds with some ionic character.[21] If such structures were assumed in Table VI, however, the resulting coupling constants would all be uniformly very small or zero in contradiction to experiment. Consequently, in Table VI we have adopted the next least radical assumption—that the nitrogen bonds are *s-p* hybrids. Nitrogen single bonding orbitals are assumed to have tetrahedral wave functions $\psi=\frac{1}{2}\psi_s+(\sqrt{3}/2)\psi_p$.

In Table VIa the $\sigma$-component of multiple bonds has been assigned a similar tetrahedral wave function $(\frac{1}{2}\psi_s+(\sqrt{3}/2)\psi_p)$ while in Table VIb calculations are presented for $\sigma$-wave functions of the form $(\frac{1}{2})^{\frac{1}{2}}\psi_s+(\frac{1}{2})^{\frac{1}{2}}\psi_p$. The $\pi$-components of multiple bonds are assumed to be pure $p$ orbitals.

The amount of ionic character of the N—H bonds in ammonia has been calculated from electronegativity differences and the Pauling curve as 20 percent. The observed dipole moment would indicate 33 percent ionic character, but is considered less reliable. For HCN, $CH_3CN$, and $CH_3NC$ the contributions of the various resonating structures were obtained from the values of bond distances. In $N_2O$ not only do the contributions of the individual bond structures calculated from the two different bond distances fail to agree but one of them leads to a value of the dipole moment in poor agreement with experiment. The structure suggested by the dipole moment (as well as one of the bond distances) gives approximately equal importance to the two structures listed in Table VIa. The relative importances 45 percent–55 percent are chosen to best fit the quadrupole coupling data.

For the nitrogen-containing molecules there are three possible sets of molecular electronic structures which might be consistent with the quadrupole coupling data. In the first of these a rather poor agreement (especially in the case of $N_2O$) may be obtained by assuming less than 25 percent *s* character for the bond orbitals in ammonia and about 50 percent *s* character for the bonds in the other molecules. These are the bond types used in Table VIb. The poorness of fit to the experimental data and the relative implausibility of these assumptions tend to rule out this set of structures.

The second possibility, while yielding excellent agreement between calculated and observed coupling constants, involves the assumption of tetrahedral bonds for both single and multiple bonds in these nitrogen compounds. Penney[22] has presented calculations which argue against this picture of multiple bonds.

The structural assumptions used in Table VIa, while apparently rather plausible, lead to poor agreement with ammonia when tetrahedral bonding orbitals are assumed for the $NH_3$ molecule. They lead to a quite satisfactory agreement when the following electronic structure roughly similar to that proposed by Mulliken[23] is adopted. Four molecular orbitals are set up; three bonding $[\pi]^2[\pi]^2[z]^2$ and one non-bonding $[s]^2$. The two $[\pi]$ orbitals are approximated in the immediate neighborhood of the N atom by nitrogen $2p$ orbitals. The $[z]$ orbital is assumed to possess 75 percent $p$ character, while the $[s]$ orbital is equivalent in the region near N to an orbital containing 25 percent $p$ character and 75 percent *s* character. In assigning ionic character a figure of 20 percent was estimated as described above so that we have added $\frac{1}{5}$ of an electron to each of the three bonding orbitals.

It is this structure which is designated in Table VIa as $N{\equiv}H_3$ and which is considered most probable. It gives a quadrupole coupling for ammonia which is consistent with the nitrogen quadrupole couplings in other molecules assuming the usual picture for multiple bonds but with a hybridized component as discussed above. Such a structure for the nitrogen bonds in ammonia makes them closely similar to the nitrogen bonds in the C≡N group. This similarity is suggested directly by the observation that the quadrupole coupling constants for N in ammonia and in the cyanides are substantially the same. Since no other reasonable structure for $NH_3$ seems to give the correct coupling constants, the electronic environments of N in $NH_3$ and C≡N must be very similar.

[20] See reference 8, p. 87.
[21] E.g. W. C. Price, Ann. Rep. Chem. Soc. **36**, 50 (1939).
[22] W. G. Penney, Proc. Roy. Soc. **A144**, 166 (1934) and **A146**, 223 (1934).
[23] R. S. Mulliken, J. Chem. Phys. **3**, 506 (1935).

The small values of the coupling constants for N in methyl isocyanide and the inner N atom in $N_2O$, while casting no special light on the nature of the bonding orbitals, furnish new evidence of the correctness of the resonant structures involving quadrivalent nitrogen and of the correctness of the basic assumptions underlying the calculations of coupling constants.

It may be noted that very good agreement is obtained in Tables IV and VIa between "calculated" and measured coupling constants for all molecules for which quadrupole coupling data are at present available. The only known cases which are not listed and considered are some additional alkali halides which all show very small couplings just as do the alkali halides discussed here, and the nuclei $S^{33}$, $B^{10}$, and $B^{11}$. In each of the latter three cases, a coupling constant in only one molecule has been obtained, and since in addition no atomic data on their quadrupole couplings are available for comparison, very little useful molecular information can be obtained by discussing them. The good agreement shown in Tables IV and VIa, using molecular electronic structures which are very reasonable in the light of other reliable evidence, is a satisfying argument for the correctness of the method and principles underlying the calculation of quadrupole coupling constants.

## SUMMARY

Thus, an examination of nuclear quadrupole couplings in molecules in terms of the approximate method discussed above leads to the following conclusions:

1. At least 15 percent hybridization of $p$ bonding orbitals with $s$ orbitals occurs in N, Cl, and As bonds and presumably is rather common in other elements.
2. The electronic structures of the three nitrogen bonds in ammonia is very similar to that of nitrogen in the —C≡N group.
3. Bonds of most of the alkali halides show less than 3 percent true covalent character, and the molecules should be considered primarily ionic with a considerable amount of polarization of each ion.

Further measurements of quadrupole coupling constants should afford additional useful tests of molecular structure.

Nuclear quadrupole moments may be approximated by combining the data of Tables V and VI on the quadrupole coupling per $p$ electron with estimates of $\partial^2V/\partial z^2$ for a $p$ electron in the atomic state. This yields the values given in Table VII and discussed in the appendix.

## APPENDIX

*Determination of nuclear quadrupole moments.*—The values given in Tables V–VI for quadrupole coupling per $p$ electron may be used to evaluate nuclear quadrupole moments if the magnitude of $\partial^2V/\partial z^2$ produced at the nucleus by a $p$ electron is known. The latter quantity can be approximately obtained from expression (1) or (2).

For the halides, $\partial^2V/\partial z^2$ can be readily evaluated from expression (2) and has already been given above for F, Cl, and I as $21\times10^{15}$, $19.8\times10^{15}$, and $45\times10^{15}$ e.s.u., respectively. The values for $\Delta\nu$ used for these elements are well known as 404, 881, and 7603 $cm^{-1}$. The numbers 49, 13, and 6 were taken for $Z_i$. For Br, $\Delta\nu$ is 3685 $cm^{-1}$ and if $Z_i$ is taken as 31, $\partial^2V/\partial z^2=34\times10^{15}$ e.s.u. It must be remembered that the values here are for the molecular case (or for an atomic case with $m=0$), so that expression (2) must be multiplied by $-2l/(2l-1)$ or $-2$. These values immediately allow determination of the Cl, Br, and I quadrupole moments as given in Table VII.

TABLE VII. Nuclear quadrupole moments derived from measured quadrupole coupling constants in molecules and approximate evaluation of $\frac{\partial V^2}{\partial z^2}$.

| Nuclei | Quadrupole moment | Ratio of moments |
|---|---|---|
| $N^{14}$ | $\sim0.02\times10^{-24}$ cm² | |
| $S^{33}$ | $\sim-0.08$ | |
| $Cl^{35}$ | $-0.077$ | |
| $Cl^{35}/Cl^{37}$ | | 1.27 |
| $As^{75}$ | 0.3 | |
| $Br^{79}$ | 0.28 | |
| $Br^{79}/Br^{81}$ | | 1.198 |
| $I^{127}$ | $-0.75$ | |

The $Cl^{35}$ quadrupole moment given in Table VII is close to the true value $-0.079\times10^{-24}$ cm² (cf. reference 13) because the true value was known and hybridization could be allowed for. A previous estimate[5] of the $Cl^{35}$ quadrupole moment without allowing for hybridization was $-0.067\times10^{-24}$ cm². The estimated quadrupole moments of Br and I will also be too small if these atoms exhibit $s$-$p$ hybridization, but too large if $p$-$d$ hybridization occurs. At least in the case of the heavy atom I, some $p$-$d$ hybridization is not unlikely, and may explain why the $I^{127}$ quadrupole moment given in Table VII is larger than the approximate value $-0.45\pm.15\times10^{-24}$ cm² obtained from atomic spectra.[24]

Determination of $\partial^2V/\partial z^2$ for N requires a somewhat more lengthy procedure than did the halogens. Probably the most reliable and simplest estimate is obtained by noticing that for double ionized N, $\Delta\nu=174.5$ $cm^{-1}$, and that for quadruply ionized F, $\Delta\nu=746$ $cm^{-1}$, or just 1.85 times the value of $\Delta\nu$ for neutral F. An equivalent $\Delta\nu$ for neutral N for substitution in expression (2) may then be taken as $174.5/[1+(0.85/2)]$ $cm^{-1}$. If $Z_i$ is assumed to be 4, $\partial^2V/\partial z^2=9.9\times10^{15}$ e.s.u. A similar, but less reliable, value can be obtained using formula (1) and estimating an effective value of $n$ from the ionization potential of N. Using the value 24 Mc of Table VIa for the coupling constant per $p$ electron, the $N^{14}$

[24] K. Murakawa, Zeits. f. Phys. 114, 651 (1939).

quadrupole moment would be $0.033\times10^{-24}$ cm$^2$. However, using the value 9.0 Mc indicated by Table VIb, its quadrupole moment is $0.012\times10^{-24}$ cm$^2$. The value $0.02\times10^{-24}$ cm$^2$ chosen for the table is thus seen to be more uncertain than are the halide quadrupole moments.

The quadrupole moment of $As^{75}$ given in Table VII represents no new determination because the structure of $AsF_3$, the only molecule for which the As coupling constant is available, has been determined so that the coupling constant will give the correct, known $As^{75}$ quadrupole moment.

Evaluation of $\partial^2V/\partial z^2$ for $S^{33}$ is done in essentially the same way as for $N^{14}$. For triply ionized $S$, $\Delta\nu=950.2$ cm$^{-1}$. The ratio between for quadruply ionized Cl and singly ionized Cl is 1.70. An equivalent for neutral $S$ is taken as $950.2/(1+\frac{3}{4}\times0.70)$ cm$^{-1}$, and $Z_i$ as 12.5. This yields $\partial^2V/\partial z^2=14.7\times10^{15}$ e.s.u. The structure of OCS, in which the $S^{33}$ coupling constant has been measured as $-28.5$ Mc, has not been discussed above. The molecule is assumed to resonate between the structures $O{=}C{=}S$, $\overset{-}{O}{-}C{\equiv}\overset{+}{S}$, and $\overset{+}{O}{\equiv}C{-}\overset{-}{S}$. A calculation from bond distances gives importances of 58 percent, 14 percent, and 28 percent, respectively, to these three structures. Assuming the double and triple bonds are similar to those indicated for N in Table VIa, and that the single bond is a 25 percent–75 percent $s$-$p$ hybrid, the calculated average fraction of unbalanced $p$ electron is then 0.27, giving a quadrupole moment $-0.098\times10^{-24}$ cm$^2$. On the other hand, if all bonds involve pure $p$ orbits only, the calculated average fraction of unbalanced $p$ electron is 0.52, giving a quadrupole moment $-0.052\times10^{-24}$ cm$^2$. The value $-0.08\times10^{24}$ cm$^2$ chosen for the table thus may involve considerable error because of uncertainty in the bond structure of OCS, but the sign appears to be definitely determined, and the magnitude is probably not in error by more than 50 percent. Measurement of the $S^{33}$ coupling in other molecules may allow a more accurate determination of its quadrupole moment.

### ACKNOWLEDGMENT

The authors are grateful for very helpful discussions with Professors G. E. Kimball, R. S. Halford, and R. S. Mulliken.

# Mass Spectrometric Study of a Mixture of Deuterated Acetaldehydes

ROBERT K. BRINTON AND FRANCIS E. BLACET
*Division of Chemistry, University of California, Davis, California*
*Department of Chemistry, University of California, Los Angeles, California*

(Received November 29, 1948)

An investigation of the composition of samples of deuterium containing acetaldehyde was made by mass spectrometric methods. The complete determination of the relative abundance of all possible heavy acetaldehyde species was accomplished by combining data from the direct mass spectrometric analysis with information on the relative amounts of heavy methyl iodides produced when the gaseous heavy acetaldehyde mixture was photolyzed with ultraviolet light in the presence of iodine vapor. The distribution of the various acetaldehydes in the mixture was about 80 percent $CH_3CDO$ and 17 percent $CH_3CHO$ with small amounts of acetaldehydes of higher deuterium content. The mass spectrum of the acetaldehyde mixture was corrected to give the spectrum of the single species, $CH_3CDO$. Inspection of the corrected spectrum indicated that on impact by 60 electron-volt electrons the split of the C—H bond of $CH_3CHO$ is more probable than the corresponding split of C—D bond in $CH_3CDO$ in agreement with the findings of Delfosse and Hipple who first reported this difference in the behavior of C—H and C—D bonds for *cis* and *trans* ethene-1,$2d_2$. The formation of formyl positive ion in the case of $CH_3CDO$ is evidently by a clean split of the C—C bond with little exchange of hydrogen and deuterium between carbon atoms at the time of electron impact. The formation of methyl positive ion, on the other hand, is accompanied by a large interchange of hydrogen and deuterium between carbon atoms.

## INTRODUCTION

THE mass spectrometric study of *cis* and *trans* ethene-1,$2d_2$ by Delfosse and Hipple,[1] methane-*d* by Evans, Bauer, and Beach,[2] acetylene-*d* and acetylene-$d_2$ by Mohler and Dibeler,[3] and ethane-*d*, propane-1*d*, and propane-2*d* by Turkevich, Friedman, Soloman, and Wrightson[4] has clearly indicated that a splitting of the C—H bond is more probable than a corresponding C—D rupture on dissociation by electron impact. Additional data substantiating these studies have been obtained in this laboratory in the study of acetaldehyde-*d* ($CH_3CDO$) which was prepared[5] for photochemical studies. The compound as prepared was unfortunately not a single isomer but contained normal acetaldehyde, acetaldehyde-*d*, and small amounts of acetaldehyde of higher deuterium content. The relative proportions of molecules in the heavy acetaldehyde mixture containing one, two, three and four deuterium atoms could be determined rather simply by making use of the observation of these same workers[1–4] that the specific intensities (intensity per unit pressure against the spectrometer leak) of the parent mass ions of a corresponding protium and deuterium compound were equal. However, such a determination does not uniquely fix the position of a deuterium atom on the two available carbon atoms in the molecule. In addition, the relative intensities of the fragmentation ions obtained in the mass spectrum of acetaldehyde-*d* were contradictory in the sense that certain ion intensities seemed to indicate a large amount of deuterium on the methyl carbon atom while certain other ion intensities indicated the deuterium to be present substantially only on the carbonyl carbon atom.

In order to obtain a complete analysis of the heavy acetaldehyde mixture use was made of the observation of Gorin[6] and Blacet and co-workers[7] that methyl radicals formed on the irradiation of acetaldehyde vapor could be effectively trapped by iodine vapor to yield methyl iodide. Combination of the data from the analysis of the original heavy acetaldehyde mixture with the mass spectrometric determination of the relative abundance of normal and heavy methyl iodides present in the products of the photolysis would allow a calculation of the amounts of all types of acetaldehyde present. The spectrum of $CH_3CDO$ could be obtained by correcting the spectrum of the heavy acetaldehyde mixture for contributions of all other acetaldehyde species present. A study of the $CH_3CDO$ spectrum should give some evidence as to possible mechanisms of electron impact dissociation.

## EXPERIMENTAL

The mass spectrometric analyses were carried out in the Westinghouse Type LV instrument described by Hipple and coworkers.[8] The operating conditions which were maintained constant in all trials were: Ion source temperature, 200°C; electron energy, 60 ev; electron current, 10 $\mu$a; and ion draw out voltage, 3v. The magnet flux was adjusted so that $m/e$ peaks (mass to charge ratios) from 13 to 55 could be covered by scanning electrically from 1300 to 300 volts. It was found that the cracking pattern of both the heavy acetaldehyde mixture

[1] J. Delfosse and J. A. Hipple, Phys. Rev. **54**, 1060 (1938).
[2] M. W. Evans, N. Bauer, and J. Y. Beach, J. Chem. Phys. **14**, 701 (1946).
[3] F. L. Mohler and V. Dibeler, Phys. Rev. **72**, 158 (1947).
[4] J. Turkevich, L. Friedman, E. Soloman, and F. M. Wrightson, J. Am. Chem. Soc. **70**, 2638 (1948).
[5] The method of preparation to be submitted for publication elsewhere.
[6] E. Gorin, Acta. Physicochimica **9**, 681 (1938).
[7] (a) F. E. Blacet and J. D. Heldman, J. Am. Chem. Soc. **64**, 889 (1942). (b) F. E. Blacet and D. E. Loeffler, *ibid.* **64**, 893 (1942).
[8] J. A. Hipple, D. J. Grove, and W. M. Hickam, Rev. Sci. Inst. **16**, 69 (1945); J. A. Hipple, Electronics **16**, 120 (1943).

and normal acetaldehyde changed somewhat over a period of time apparently as a result of small differences in operating conditions. For this reason the mass spectra of both products were run one following the other in as short a period of time as possible.

A check on the accuracy of using the parent peak intensities as a measure of the relative abundance of the various acetaldehyde species was made by an independent method. The heavy acetaldehyde mixture was ignited in a stream of oxygen and the heavy water purified after the method described by Keston, Rittenberg, and Schoenheimer.[9] The composition of the water was determined by the falling drop method[10] of density measurement. The water composition of 79.1 percent $H_2O$—20.9 $D_2O$ (ignoring for simplicity the existence of HDO) calculated from this method agreed within experimental error (0.5 percent) with a hypothetical water composition of 78.7 percent $H_2O$—21.3 percent $D_2O$ which would have been obtained on basis of the mass spectrometric analysis.

TABLE I. Relative intensities of ions produced by 60-volt electrons on normal and heavy acetaldehydes.

| Ion mass $m/e$ | Heavy acetaldehyde mixture | $CH_3CHO$ | Calculated $CH_3CDO$ |
|---|---|---|---|
| 48 | 4 | | |
| 47 | 9 | | |
| 46 | 24 | | |
| 45 | 1000 | | 1000 |
| 44 | 288 | 1000 | 67 |
| 43 | 409 | 530 | 310 |
| 42 | 135 | 147 | 105 |
| 41 | 55 | 63 | 39 |
| 40 | 13 | 14 | 10 |
| 30 | 1820 | | 1770 |
| 29 | 493 | 1620 | 140 |
| 28 | 279 | 196 | 242 |
| 27 | 113 | 53 | 102 |
| 26 | 75 | 98 | 53 |
| 25 | 33 | 42 | 22 |
| 24 | 11 | 9 | 9 |
| 19 | 7 | | 5 |
| 18 | 31 | 35 | 17 |
| 17 | 100 | 7 | 86 |
| 16 | 371 | 107 | 336 |
| 15 | 664 | 800 | 490 |
| 14 | 183 | 274 | 123 |
| 13 | 79 | 88 | 60 |

The apparatus used in the photolysis of the heavy acetaldehyde mixture was identical to that described by Blacet and Heldman.[7a] Radiation from the 2537A and 2654A lines of an atmospheric pressure mercury arc used in conjunction with a crystal quartz monochromator was used to photolyze a gaseous mixture of the acetaldehydes at about 300 mm pressure and iodine maintained at a pressure greater than 2 mm. The products of the photolysis which were condensable at −190°C were collected when the decomposition of the acetaldehydes was about 2 percent completed and analyzed by the mass spectrometer. In one determination the large excess of aldehyde was removed previous to the analysis by polymerization over solid potassium hydroxide. Other determinations were made directly on the photolysis products since the aldehyde did not interfere in the high $m/e$ region of the parent peaks of the methyl iodides.

## RESULTS

The mass spectra of the heavy acetaldehyde mixture and fractionated Eastman "White Label" acetaldehyde are shown in columns two and three of Table I. The intensities of mass peaks 39 to 36 were very small and are not shown. In all cases the spectra are corrected for the naturally occurring amounts of $C^{13}$, $O^{17}$, and $O^{18}$ isotopes. The absolute accuracy in the intensity range 0 to 100 is about ±2, in the 100 to 500 range about ±4, and ±8 above intensity 500.

The calculation of the relative amounts of the various heavy acetaldehydes present was made on the basis of the specific intensities of the 48, 47, 46, and 45 peaks of the heavy acetaldehyde mixture in relation to the specific intensity of the 44 peak of normal acetaldehyde ($CH_3CHO$). It was necessary to make small corrections in the 46 and 45 peaks for aldehydes of higher deuterium content. This was done by making reasonable assumptions as to the spectra of these aldehydes. The corrections were small in all cases and only the percentage of the acetaldehyde with two deuterium atoms per molecule could be in error by an appreciable amount. Table II shows the composition of the heavy acetaldehyde mixture obtained by this analysis. The percentage of normal acetaldehyde present is by difference.

Two separate samples of the heavy acetaldehyde mixture whose composition is given in Table II were photolyzed in the presence of iodine vapor. The methyl iodide from these photolyses was analyzed by the mass spectrometer and the relative amounts of the various methyl iodide species found are shown in Table III.

The data of Tables II and III allow the calculation of the amounts of all different acetaldehyde species in the heavy acetaldehyde mixture. The method is apparent from the following schematic representations where the percentages shown on the left are from the direct spectrometric analysis

| | | |
|---|---|---|
| 0.4% | $CD_3CDO$ | 0.4% |
| 0.7% | $CD_3CHO$ | |
| | $CD_2HCDO$ | 1.1% |
| 1.8% | $CD_2HCHO$ | |
| | $CDH_2CDO$ | 3.2% |
| 80.0% | $CDH_2CHO$ | |
| | $CH_3CDO$ | 95.3% |
| 17.1% | $CH_3CHO$ | |

and those on the right from the methyl iodide composition. Table IV indicates the percentages of each species

[9] A. S. Keston, D. Rittenberg, and H. Shoenheimer, J. Biol. Chem. 122, 227 (1937).

[10] K. Fenger-Ericksen, A. Krough, and H. Ussing, Biochem. J. 30, 1264 (1936).

of acetaldehyde present in the mixture as calculated from these data.

The mass spectrum of $CH_3CDO$ shown in column 4 of Table I was obtained by correcting the spectrum of the heavy acetaldehyde mixture in column 2 for contributions of $CH_3CHO$ (17.1 percent) and the additional deuterium containing acetaldehydes (1) through (6) by the amounts shown in Table IV. The corrections were made by an estimation of the most probable individual spectra of these individual compounds. In no case was the correction of large magnitude, so possible errors made in the correction were not of significant importance.

## DISCUSSION

A comparison of the spectra of $CH_3CHO$ and $CH_3CDO$ reveals several interesting aspects on the mechanism of the dissociation by electron impact.

1. The loss of a single hydrogen atom by acetaldehyde on electron impact occurs mainly by a C−H bond rupture on the functional group. The low intensity of peak 44 in the $CH_3CDO$ spectrum seems to indicate that approximately 85 percent of the acetyl type positive ion is formed by such a process. In addition the split of the C−H bond of the functional group in $CH_3CHO$ is considerably more likely than the corresponding split of the C−D bond in $CH_3CDO$ as shown by the smaller peak 43 intensity for $CH_3CDO$ than for $CH_3CHO$. A quantitative evaluation of the relative probability of these two processes is not possible since the 43 peak from $CH_3CDO$ is made up of both $CHCDO^+$ and $CH_3CO^+$ ions while the 43 peak from $CH_3CHO$ has contribution from $CH_2CHO^+$ and $CH_3CO^+$ ions. If the probability of the loss of a single hydrogen atom from the methyl group accompanied by formation of a positive ion of the remaining fragment is assumed equal for the two aldehydes, then $CH_3CO^+$ ion from $CH_3CHO$ would be $530-67=463$. The intensity of $CH_3CO^+$ from $CH_3CDO$ is less than 310 depending on the abundance of $CHCDO^+$ ion, which is probably small. It would appear that the rupture of the C−D bond of the functional group of $CH_3CDO$ is about 0.6 as probable as the corresponding C−H bond split of $CH_3CHO$.

2. The formation of the formyl type positive ion seems to occur mainly (more than 90 percent) by a simple fission of the C−C bond of the molecule. However, the existence of a relative intensity for peak 29 of 140 for $CH_3CDO$ may indicate that the process is more complicated for the remaining 10 percent of formyl positive ions formed. A protium-deuterium rearrangement after electron impact and before fragmentation would be necessary to account for this intensity. The probability of formation of the formyl positive ion is somewhat greater for $CH_3CDO$ than $CH_3CHO$ since the relative intensity of $CHO^+$ ion of $CH_3CHO$ is about 85 percent of the combined $CDO^+$ and $CHO^+$ intensities of $CH_3CDO$. The proportion of the 29 peak of $CH_3CDO$ due to the $CH_3CD^+$ ion is in doubt, but comparison of the two spectra seems to indicate that this type ion is of small abundance.

3. The process taking place for the formation of the methyl type positive ion is not a simple split of the C−C bond of the molecule. In order to inspect this process more thoroughly it is first necessary to make more specific assignment to individual ions in this region of the spectra. From the $CH_3CDO$ spectrum the intensity at $m/e=17$

$$OH^+ + CH_3D^+ = 86$$

but $OH^+$ must be less than 7 since the $OH^+$ intensity would not be as great for $CH_3CDO$ as for $CH_3CHO$. Then

$$CH_3D^+ \simeq 80.$$

If an equal probability of methane type ion and $O^+$ ion is assumed for both aldehydes,

$$CH_4^+ \simeq 80$$

in the $CH_3CHO$ spectrum. Since $CH_4^+ + O^+ = 107$ ($CH_3CHO$ spectrum)

$$O^+ \simeq 27$$

for both aldehydes. Correction of mass peaks 16 and 17 for contributions of $OH^+$ and $O^+$ leads to the ion intensities shown in Table V.

The ion intensities shown in parentheses in Table V arise by adding the further assumption that intensities of ions of $CH^+$ and $CH_2^+$ types are identical whether

TABLE II. The composition of the heavy acetaldehyde mixture.

| Deuterium atoms per molecule | Percentage composition |
|---|---|
| 4 | 0.4% |
| 3 | 0.7 |
| 2 | 1.8 |
| 1 | 80.0 |
| 0 | 17.1 |

TABLE III. The composition of methyl iodides from photolysis of the heavy acetaldehyde mixture in presence of iodine vapor.

| | Trial 1 | Trial 2 | Average |
|---|---|---|---|
| $CD_3I$ | 0.4% | 0.4% | 0.4% |
| $CD_2HI$ | 1.2 | 1.0 | 1.1 |
| $CDH_2I$ | 3.5 | 3.0 | 3.2 |
| $CH_3I$ | 94.9 | 95.6 | 95.3 |

TABLE IV. Acetaldehydes present in heavy acetaldehyde mixture.

| | | |
|---|---|---|
| (1) | $CD_3CDO$ | 0.4% |
| (2) | $CD_3CHO$ | Trace |
| (3) | $CD_2HCDO$ | 0.7 |
| (4) | $CD_2HCHO$ | 0.4 |
| (5) | $CDH_2CDO$ | 1.4 |
| (6) | $CDH_2CHO$ | 1.8 |
| (7) | $CH_3CDO$ | 78.2 |
| (8) | $CH_3CHO$ | 17.1 |

TABLE V. Relative intensities of individual ions of acetaldehyde and acetaldehyde-*d*.

| *m/e* | $CH_3CHO$ | $CH_3CDO$ |
|---|---|---|
| 17 | | $CH_3D^+=80$ |
| 16 | $CH_4^+=80$ | $CH_2D^+=309$ |
| 15 | $CH_3^+=800$ | $CH_3^+(311)+CHD^+(179)=490$ |
| 14 | $CH_2^+=274$ | $CH_2^+(95)+CD^+(28)=123$ |
| 13 | $CH^+=88$ | $CH^+=60$ |

deuterium or protium is present in them. $CH^+=88$ from the $CH_3CHO$ spectrum and $CH^+ + CD^+ = 88$ by this assumption.

Thus

$$CD^+ = 88 - 60 = 28$$

and

$$CH_2^+ = 123 - 28 = 95, \text{ from } CH_3CDO.$$

$CH_2^+=274$ from the $CH_3CHO$ spectrum and $CH_2^+ + CHD^+ = 274$ by a similar assumption as to the equality of $CH_2^+$ type ion formation.

$$CHD^+ = 274 - 95 = 179$$
$$CH_3^+ = 490 - 179 = 311, \text{ from } CH_3CDO.$$

Although the imposition of the restrictive of equal $CH^+$ and $CH_2^+$ ion probabilities from the two aldehydes is not completely valid, the magnitude of the $CH_3^+$, $CHD^+$, $CH_2^+$, and $CD^+$ ion intensities is at least close to the values shown in Table V. It is interesting to note that the formation of $CH_3^+$ and $CH_2D^+$, methyl type ions from $CH_3CDO$, is almost equally probable. In the formation of the methyl type radical by electron impact on acetaldehyde, the over-all mechanism must accommodate a rapid exchange of hydrogen atoms between the two carbon atoms. The final methyl ion must contain hydrogen atoms originally present on the functional carbon atom as well as on the methyl carbon atom. It is perhaps possible to postulate more exact mechanisms for this ionization process but little justification is forthcoming from the experimental evidence. Evidence for a similar mobility of hydrogen atoms during an electron impact may be found in the mass spectra of various hydrocarbon compounds. The existence of considerable ethyl positive ion from the fragmentation of isobutane as reported by Stevenson and Hipple[11] is an example of this type of exchange.

The result of C—C bond splitting in the two type acetaldehydes is somewhat different. The ratio of methyl type ion/formyl type ion is about 0.49 for $CH_3CHO$ and 0.33 for $CH_3CDO$.

## ACKNOWLEDGMENT

The mass spectrometer which made this study possible was a gift to the University of California, Los Angeles, by the Signal Oil and Gas Company of Los Angeles, California. During the time he was engaged in this study the first-named author held the H. M. Mosher Fellowship which was established by the same company.

[11] D. P. Stevenson and J. A. Hipple, J. Am. Chem. Soc. **61**, 1588 (1942).

# Isomer Distribution in Hydrocarbons from the Fischer-Tropsch Process*

SOL WELLER** AND R. A. FRIEDEL**
*Bureau of Mines, Central Experiment Station, Pittsburgh, Pennsylvania*
(Received December 13, 1948)

The isomer distribution experimentally found for the saturated-hydrocarbon products (pentane to octane range) from a cobalt Fischer-Tropsch catalyst have been deduced from probability considerations. With certain restrictions, it is assumed that the carbon skeleton is built up by addition to any terminal carbon atom (for which the *a priori* probability has a constant value $a$) or to any penultimate carbon atom (with *a priori* probability $b$). Values of $a$ and $b$, determined from experimental data, led to deduced isomer concentrations in each molecular-weight cut agreeing with experimental concentrations with an average deviation of 0.7 percent. Peculiarities in the observed isomer distribution were also reproduced.

A RECENT mass-spectrometric investigation of the paraffinic product obtained with a cobalt Fischer-Tropsch catalyst[1] has permitted quantitative determination of the isomer distribution in each of the molecular-weight cuts from pentane to octane ($C_5$ to $C_8$). It is the purpose of this paper to show that, on the basis of a few not unreasonable assumptions about the manner in which the carbon chains are built up, the observed isomer distribution can be deduced by probability considerations. The deductions concern only the isomer distribution in each molecular-weight cut, not the distribution of molecular weights in the total product. The latter concerns the relative probabilities that a chain of given length on the surface is desorbed or stays on the surface to react further; this problem has been considered by Herington.[2] Furthermore, the discussion applies only to the building up of the carbon skeleton and not to the degree of saturation of the products. For example, when the terms "*n*-butane" or "*i*-pentane" are used below, they are to be understood as designating only the carbon skeleton corresponding to those compounds.

The following assumptions will be made concerning the manner in which the synthesis occurs:

(1) The carbon skeleton is built up by successive one-step additions to the carbon chain of groups containing a single carbon atom. It is irrelevant here whether the group which adds is $CH_2$, CO, or any other; for convenience, the group added will be referred to as a carbon atom.

(2) Addition occurs at any terminal or next to terminal (penultimate) carbon atom, with two restrictions:

(a) Addition to a tertiary carbon atom does not occur.
(b) Addition to a side chain occurs only if the side chain is attached to a penultimate carbon.

These two limitations are introduced to explain the experimental result that no appreciable amounts of quaternary carbon atoms or of side chains longer than methyl are found. No explanation for these rules will be discussed here, other than to state that the rules may arise from steric effects if certain detailed mechanisms of the synthesis are valid.

(3) The probability of addition to a terminal carbon atom is intrinsically different from that for addition to a penultimate one. This *a priori* probability of addition to a terminal carbon may be designated $a$, that of addition to a penultimate carbon, $b$. Since addition must occur to either a terminal or a penultimate carbon atom, $a+b=1$. All terminal atoms, however, have the same *a priori* probability, as have all penultimate atoms. The probabilities $a$ and $b$ are assumed to be independent of chain length, but they may depend on the nature of the catalyst.

(4) The distribution of isomers in the final product is identical with the distribution on the catalyst surface.

The rules for addition may be illustrated by consideration of the generation of $C_8$ isomers from a particular $C_7$ isomer, say 2, 3-dimethyl pentane, shown below.

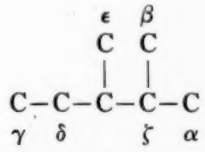


Addition of a carbon atom occurs at the positions designated $\alpha$, $\beta$, or $\gamma$ with an *a priori* probability of $a$, and at position $\delta$ with an *a priori* probability $b$. Addition does not occur at $\zeta$ because the carbon atom is tertiary; it does not occur at $\epsilon$ because that carbon atom constitutes a side chain not attached to a penultimate carbon (assumption (2), above). If this $C_7$ isomer constituted a fraction $x$ of the $C_7$ cut, it would generate the only permitted $C_8$ isomers in the following ways:

| Isomer | Formed by addition to atom | Weighted relative probability | Percent in $C_8$ cut |
|---|---|---|---|
| 3,4-dimethyl hexane | $\alpha$ or $\beta$ | $2a$ | $\frac{2a}{3a+b}x=\frac{2a}{2a+1}x$ |
| 2,3-dimethyl hexane | $\gamma$ | $a$ | $\frac{a}{2a+1}x$ |
| 2,3,4-trimethyl pentane | $\delta$ | $b$ | $\frac{b}{2a+1}x$ |

* Work on manuscript completed December 1, 1948.
** Physical chemist, Bureau of Mines, Central Experiment Station, Pittsburgh, Pennsylvania.
[1] R. A. Friedel and R. B. Anderson, J. Am. Chem. Soc., submitted for publication.
[2] E. F. G. Herington, *Chemistry and Industry*, 65, 346 (1946).

With establishment of these "building-up" principles, the distribution of isomers for any cut may now be deduced, starting with methane. The $C_1$, $C_2$, and $C_3$ cuts are each made up of a single isomer, of course. Propane, however, can lead to *n*-butane in $2a$ ways (by addition to either end) or to *i*-butane in $b$ ways (by addition to the middle carbon). The fractions of *n*-butane and *i*-butane in the $C_4$ cut will, therefore, be $2a/(2a+b)(=2a/(a+1))$ and $b/(a+1)$, respectively.

The $C_5$ isomers are similarly derived. *n*-Butane can give *n*-pentane in $2a$ ways and *i*-pentane in $2b$ ways, while *i*-butane yields only *i*-pentane on addition. The fractions of *n*- and *i*-pentane in the $C_5$ cut are, therefore,

$$n\text{-pentane:}\quad \frac{2a}{2a+2b}\cdot\frac{2a}{a+1}=\frac{2a^2}{a+1},$$

$$i\text{-pentane:}\quad \frac{2b}{2a+2b}\cdot\frac{2a}{a+1}+\frac{b}{a+1}=\frac{b(2a+1)}{a+1}.$$

It is to be noted here that *i*-pentane can be formed in two mutually exclusive ways, that is, from either *n*-butane or *i*-butane; its total probability is the sum of the probabilities for the individual ways.

The isomer distributions for higher molecular-weight cuts are deducible in the same way. For convenience, the results through the $C_8$ cut are summarized in Table I; obviously, the method could be extended beyond this cut. The table includes all of the isomers possible according to the rules that have been set up above. Clearly, the fraction of every isomer in a cut can be calculated if values for the *a priori* probabilities $a$ and $b$ can be found. The procedure adopted here was to obtain empirically values of $a$ and $b$, by the method of averages, from an application of the formulas in Table I to the observed concentration values for all isomers found in appreciable quantity in the $C_5$–$C_8$ cuts. The best values of $a$ and $b$ were 0.961 and 0.039, respectively. These values were then used to back-calculate the individual concentrations; this is essentially a test of the self-consistency of the entire calculation. The calculated and observed values of the mole percentages[3] are compared in Table II.

TABLE I.—Calculation of isomer distributions.

| Isomer | Fraction in cut | Isomer | Fraction in cut |
|---|---|---|---|
| *n*-butane | $\frac{2a}{a+1}$ | *n*-octane | $\frac{2a^5}{a+1}$ |
| *i*-butane | $\frac{b}{a+1}$ | 2-methyl heptane | $\frac{a^3b(2a+1)}{a+1}$ |
| *n*-pentane | $\frac{2a^2}{a+1}$ | 3-methyl heptane | $\frac{4a^3b}{a+1}$ |
| *i*-pentane | $\frac{b(2a+1)}{a+1}$ | 4-methyl heptane | $\frac{2a^3b}{a+1}$ |
| *n*-hexane | $\frac{2a^3}{a+1}$ | 2,3-dimethyl hexane | $\frac{ab^2(2a+1)}{a+1}$ |
| 2-methyl pentane | $\frac{ab(2a+1)}{a+1}$ | 2,4-dimethyl hexane | $\frac{ab^2(2a+1)}{a+1}$ |
| 3-methyl pentane | $\frac{2ab}{a+1}$ | 2,5-dimethyl hexane | $\frac{a^2b^2}{a+1}$ |
| 2,3-dimethyl butane | $\frac{b^2}{a+1}$ | 3,4-dimethyl hexane | $\frac{2ab^2}{a+1}$ |
| *n*-heptane | $\frac{2a^4}{a+1}$ | 2,3,4-trimethyl pentane | $\frac{b^3}{a+1}$ |
| 2-methyl hexane | $\frac{a^2b(2a+1)}{a+1}$ | | |
| 3-methyl hexane | $\frac{4a^2b}{a+1}$ | | |
| 2,4-dimethyl pentane | $\frac{ab^2}{a+1}$ | | |
| 2,3-dimethyl pentane | $\frac{b^2(2a+1)}{a+1}$ | | |

Several points may be noted. First, the agreement between calculated and observed values is probably within the experimental error in all cases. The average deviation for all the isomers experimentally found in appreciable concentration is 0.7 percent. Furthermore, a number of peculiarities in the observed distributions are reproduced. These include: the decrease in concentration of the *n*-isomer with increase in molecular weight; the fact that the concentration of 2-methyl pentane is greater than that of 3-methyl pentane, while in the $C_7$ cut the 3-methyl isomer is in larger amount; and the high concentration of 3-methyl heptane in the $C_8$ cut. The reason for the reversed order of 2- and 4-methyl heptane is not known; it is quite possible that the discrepancy is within the experimental errors for determination of these constituents. It is interesting that all the predicted isomers which are not found experimentally are predicted to occur in quantities too small to be detected under the conditions of the analysis.

## DISCUSSION

The calculation has been shown to describe satisfactorily the saturated products from a cobalt Fischer-Tropsch catalyst; thus far these are the only reliable quantitative data available. If the same general mechanism holds on iron catalysts, it should be possible to deduce the isomer distribution in products from iron catalysts also, when these data have been obtained; slightly different values of $a$ and $b$ may be required. Furthermore, since the discussion has concerned only the development of the carbon skeleton, it may be anticipated that data for the skeleton isomerism of the olefinic products will also be describable in similar terms.

The agreement of the calculation with available data may be coincidental. If sufficient agreement is found in other cases (as, for example, the products from iron

[3] The volume percentages given in reference 1 were re-calculated on a mole percent basis. This resulted in shifts of 0.1 percent in the concentrations of some of the isomers. The table begins with the pentanes because the butane isomers were not determined by Friedel and Anderson, reference 1.

TABLE II.—Comparison of calculated and observed isomer concentrations.

| Isomer | Mole percent in cut observed | Mole percent in cut calculated ($a$ =0.961 $b$ =0.039) | Isomer | Mole percent in cut observed | Mole percent in cut calculated ($a$ =0.961 $b$ =0.039) |
|---|---|---|---|---|---|
| *n*-pentane | 95.0 | 94.2 | *n*-octane | 84.5 | 83.6 |
| *i*-pentane | 5.0 | 5.8 | 2-methyl heptane | 3.9 | 5.2 |
| | | | 3-methyl heptane | 7.2 | 7.1 |
| *n*-hexane | 89.6 | 90.5 | 4-methyl heptane | 4.4 | 3.5 |
| 2-methyl pentane | 5.7 | 5.6 | 2,3-dimethyl hexane | 0 | 0.24 |
| 3-methyl pentane | 4.7 | 3.8 | 2,4-dimethyl hexane | 0 | 0.24 |
| 2,3-dimethyl butane | 0 | 0.09 | 2,5-dimethyl hexane | 0 | 0.07 |
| | | | 3,4-dimethyl hexane | 0 | 0.16 |
| *n*-heptane | 87.7 | 87.0 | 2,3,4-trimethyl pentane | 0 | 0.004 |
| 2-methyl hexane | 4.6 | 5.4 | | | |
| 3-methyl hexane | 7.7 | 7.3 | | | |
| 2,4-dimethyl pentane | 0 | 0.08 | | | |
| 2,3-dimethyl pentane | 0 | 0.25 | | | |

catalysts), the argument may become sufficiently strong that the assumed rules for chain building-up are really valid. If this occurs, any detailed mechanism for the Fischer-Tropsch synthesis would have to be consistent with these rules, and any scheme such as the cracking of a giant polymethylene molecule probably would be ruled out.[4]

[4] It may be incidentally noted that the observed isomer distribution is completely contrary to that predictable from the relative thermodynamic stabilities of the isomers.

# Photomagnetism. Determination of the Paramagnetic Susceptibility of a Dye in Its Phosphorescent State*

G. N. LEWIS, M. CALVIN, AND M. KASHA†
*Department of Chemistry, University of California, Berkeley, California*

(Received December 16, 1948)

The molar paramagnetic susceptibility of acid fluorescein dye in its 2-sec. phosphorescent state in boric acid glass at 25°C has been measured directly by means of a modified Theorell microbalance. The steady state concentration of phosphorescent state molecules was $1.96\times10^{-8}$ mole per cm length of sample, calculated from optical intensity integrals and phosphorescence saturation curve data. The measured boom displacement was $4.04\times10^{-3}$ cm, corresponding to a force of $1.07\times10^{-2}$ dyne. The calculated value of the molar paramagnetic susceptibility is $3090\times10^{-6}$ c.g.s. units, which agrees with the measured value for the susceptibility of the $^3\Sigma$ ground state of oxygen within the estimated maximum experimental error of 13 percent.

## I. INTRODUCTION

THE phenomenon of phosphorescence of complex molecules was interpreted to be a lowest-triplet→singlet emission as the result of a spectroscopic study of this luminescence.[1,2] Simultaneously, the inviting possibility of measuring the paramagnetic susceptibility of the molecule in the phosphorescent state presented itself. Preliminary experiments demonstrated the existence of a genuine photomagnetism and indicated that this was within a measurable range, although requiring experiments of great delicacy.[3] The present report marks the completion of the quantitative determination of the molar paramagnetic susceptibility of acid fluorescein dye in its phosphorescent state.[4,5]

Although the present experiments were done on a dye molecule, it is to be emphasized that the phenomena studied are characteristic of unsaturated complex molecules in general, rather than being peculiar to dyes. The absorption bands usually observed in the near ultraviolet spectra of unsaturated complex molecules are attributed to singlet-singlet transitions between the $\pi$-electron energy levels of the molecule. When these bands are intense and occur in the visible region, the molecule is called a dye. In addition to the set of singlet levels, there is commonly a corresponding set of triplet levels. The lowest triplet level and the ground level are involved in the phosphorescence emission. The paramagnetism of the molecule in this lowest triplet level is the subject of this study.

A direct measurement of the paramagnetic susceptibility of the phosphorescent state is possible in the case of complex molecules as a consequence of the phosphorescence saturation phenomenon.[6,7] Because of the relatively long phosphorescence lifetime (seconds) and the large quantum yield of phosphorescence (approaching unity) of many complex molecules, a large concentration of molecules may be maintained in the phosphorescent state by illumination with an intense light source. All such experiments require the use of rigid glass solutions of the molecule, in order that viscosity dependent quenching processes be limited or eliminated. The name "phosphor" has been given to these rigid glass materials because of their luminescence properties (by analogy to inorganic phosphorescent materials), but it must be remembered that the properties of the dissolved molecule, and not of the rigid glass system, are so studied.[5]

A quantitative determination of a molar property of a molecule in its phosphorescent state requires a knowledge of the absolute concentration of the molecules in this state. The straightforward approach to this measurement would be to determine the absolute quantum efficiency of the phosphorescence as a primary datum; this, however, involves geometry-dependent factors which greatly complicate the evaluation. The need for a determination of absolute quantum efficiency has been disposed of in the present work by making use of the mathematical properties of the equations for the phosphorescence saturation curve. This permitted a direct evaluation of the absolute concentration of molecules in the phosphorescent state by a simple measurement of source intensity used in the paramagnetic apparatus relative to the maximum source intensity used in ob-

* Most of the experimental work of this paper was done after the death of Professor Lewis; however, the theoretical treatment and design of the experiments are largely his.

† Work done during first four months as a University Postdoctoral Fellow. The large part of this author's work was done subsequently under a contract between the Office of Naval Research and the University of California.

[1] G. N. Lewis and M. Kasha, J. Am. Chem. Soc. **66**, 2100 (1944).

[2] G. N. Lewis and M. Kasha, J. Am. Chem. Soc. **67**, 994 (1945).

[3] G. N. Lewis and M. Calvin, J. Am. Chem. Soc. **67**, 1232 (1945).

[4] A preliminary report of this work was made by M. Calvin, Symposium on the Color and Electronic Structure of Complex Molecules, Northwestern University, Chicago, December 31, 1946. See reference 5, Section V.

[5] M. Kasha, Chem. Rev. **41**, 401 (1947).

[6] V. L. Levshin and L. A. Vinokurov, Physik. Zeits. Sowjetunion **10**, 10 (1936) (English); L. A. Vinokurov and V. L. Levshin, J. Phys. Chem. (U.S.S.R.) **8**, 181 (1936) (Russian). [The two articles are identical in content; nevertheless, although the abstract of the first (Chem. Abs. **31**, 2100 (1937)) is exemplary for its accuracy and completeness, the abstract of the Russian version (Chem. Abs. **31**, 1298 (1937)) is ambiguous and in error, owing partly to the mistranslation of the word for *decay* as *quenching*.]

[7] G. N. Lewis, D. Lipkin, and T. T. Magel, J. Am. Chem. Soc. **63**, 3005 (1941).

taining the phosphorescence saturation curve. We now consider these points in detail.

## II. THEORY AND EXPERIMENTAL DETERMINATION OF PARAMAGNETISM

### A. The Phosphorescence Saturation Curve

*Theory*

Consider the energy level scheme of Fig. 1 which represents the three lowest electronic states of a typical complex molecule (zero-point vibrational levels). The phosphorescent or triplet state $T$ is reached by primary absorption $S' \leftarrow S$ followed by the radiationless transition[5] $S' \rightarrow T$. The excitation of the triplet state by direct absorption $T \leftarrow S$ is improbable in most molecules containing atoms of low atomic number.

The ratio of the concentration of molecules in the triplet state relative to those in the ground state is given by

$$C_T/C_S = k_1 I_s,$$

where $I_s$ is the source intensity used in the optical excitation, and $k_1$ is a collection of constants. Now define the magnitude

$$i = C_T/C_S = I_s/I_{s,m}, \tag{1}$$

where $I_{s,m}$ is a median *source* intensity corresponding to the half-value of the maximum *phosphorescence* intensity (see Fig. 2). Let $C = C_S + C_T$, then from (1)

$$C_T = C(i/i+1). \tag{2}$$

The intensity of phosphorescence is given by[8]

$$I_p = k_2 C_T$$

which by (2) is equivalent to

$$I_p = k_2 C(i/i+1). \tag{3}$$

Now define the half- or median-phosphorescence intensity $I_{p,m} = I_p$ when $C_T = C_S$; i.e., when $i = 1$. Then[8]

$$I_{p,m} = k_2(C/2). \tag{4}$$

Defining the magnitude

$$j = I_p/I_{p,m}, \tag{5}$$

we obtain from (3) and (4)

$$j = 2i/(i+1). \tag{6}$$

This is the equation of the phosphorescence saturation curve. Using (1) and (5), the equation may be written in terms of $I_p$ and $I_s$:

$$\frac{I_p}{I_{p,m}} = \frac{2I_s}{I_s + I_{s,m}}, \tag{7}$$

expressing the relation of the phosphorescence intensity to the exciting source intensity. This is next compared with experiment.

[8] The term for *induced emission* is omitted since the new elements introduced by it cancel in taking the ratio, Eq. (5).

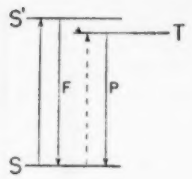


FIG. 1. Schematic energy level diagram for the three lowest electronic states of a complex molecule (zero-point levels).

*Experimental*

A sample of fluorescein dye dissolved in boric acid glass of dimensions 3 cm $\times$1 cm $\times$0.2 mm was prepared by means of the extrusion process described elsewhere.[9] The concentration of dye was extremely low, so that $\log_{10} I_0/I$ was $<0.005$, as measured by means of the Beckman spectrophotometer at 4390A (absorption maximum, see below). In a phosphorescence saturation experiment it is essential that a concentration approaching infinite dilution of the complex molecule be used, in order that >90 percent of the molecules may become excited to the phosphorescent state with the light sources available in the laboratory. As a light source, the AH6 high pressure mercury arc was used, together with a chromium reflector and a 5 cm path of concentrated aqueous solution of $Cu(NO_3)_2$ as a heat absorbing filter (see below). Between the light source and the filter a 10 cm dia. $f1$. quartz condensing lens was placed, concentrating the light of the mercury arc on a 0.5$\times$0.5 cm square of the fluorescein-boric acid sample. The sample was carefully masked with aluminum foil to fix the geometry of the sample. A stream of air was directed at the sample as a further precaution against warming. The phosphorescence light, observed from the back face of the sample by means of a Weston photronic cell (Model 594, barrier layer photocell) and measured by a Rubicon galvanometer (Ser. 805B, resistance 1067$\omega$, sensitivity 0.004$\mu$A/mm), was separated from the exciting light by means of a rotating drum phosphoroscope, previously described.[1] The source intensity was diminished successively for the various readings by means of a calibrated set of oxidized copper screens. The galvanometer and photronic cell combination were tested for linearity of response in the range of measurement. Despite the high dilution of the dye in the glass, the phosphorescence at the maximum source intensity was visible as a strong yellow green emission through the phosphoroscope. The phosphorescence saturation curve obtained is given in Fig. 2. The observed maximum $I_p = 4.10$ is 0.92(4) times the limiting value of $I_p$ (4.44, see below). Thus, in this experiment 88.5 percent of the molecules were in the triplet state at the maximum value of the source intensity used.

*Calculations*

The saturation curve Eq. (7) in $I_p$ and $I_s$ may be written in the reciprocal form[10]

$$\frac{1}{I_p} = \frac{1}{2I_{p,m}} + \frac{I_{s,m}}{2I_{p,m}} \cdot \frac{1}{I_s}. \tag{8}$$

Then, if $1/I_p$ is plotted against $1/I_s$, a straight line intersecting the $1/I_p$ axis should be obtained, with $(1/2I_{p,m})$ as the intercept and $(I_{s,m}/2I_{p,m})$ as the slope. Accordingly the phosphorescence saturation curve data of Fig. 2 were replotted in the reciprocal form in Fig. 3.

[9] M. Kasha, "Fabrication of boric acid glass for luminescence studies," J. Opt. Soc. Am. 38, 1068 (1948).

[10] We are indebted to Dr. Harrison Shull for suggestions regarding the form of this equation.

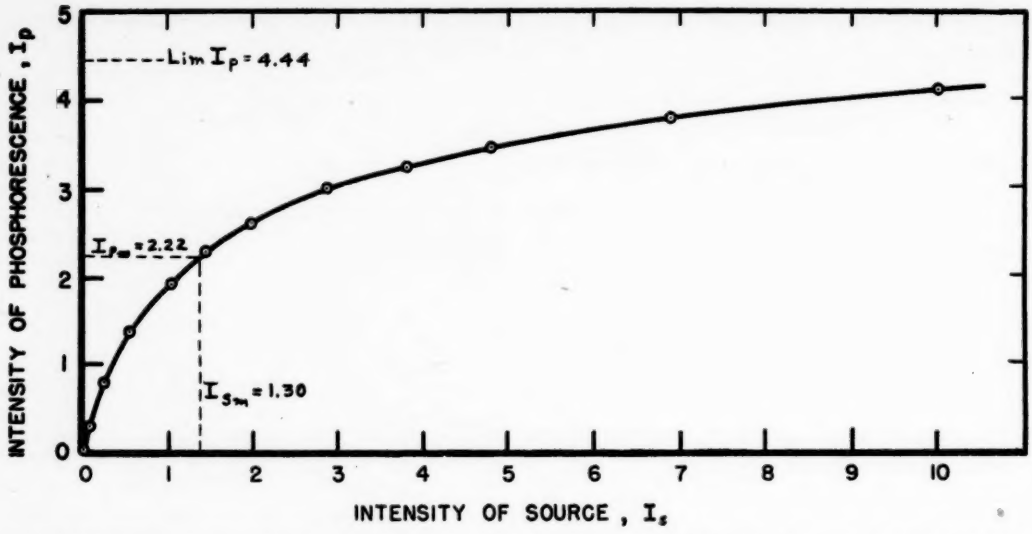


FIG. 2. Phosphorescence saturation curve for an extremely dilute solution of acid fluorescein dye (I) (see Part B, *Experimental*) in boric acid glass at room temperature.

The fit of the points to a straight line verifies the form of the saturation curve equation. The intercept on the $1/I_p$ axis is 0.225, so that $I_{p,m}$ is 2.22. From the slope (0.292) the value of $I_{s,m}$ is calculated to be 1.30. The value of $I_s$ measured in the paramagnetic apparatus (see below) is 0.205 of the maximum value of $I_s$ used in the saturation curve determination. Since the latter value of $I_s=10$ arbitrary units, the value of $I_s=2.05$ for the paramagnetic experiment. Thus, according to equation (1) $i=2.05/1.30$, or 1.58.

## B. Concentration of Triplet State Molecules

### *Theory*

We begin the development of the expression giving the concentration of molecules excited to the triplet state by first considering that the absorbing layer is (a) *very thin*, so that the fraction of the incident light absorbed will be negligibly small, and (b) *very dilute*, so that interaction between excited molecules and neighboring non-excited molecules, which leads to the concentration dependent quenching of the phosphorescent state (see *Calculations*, end of section B, and Fig. 7), will be negligibly small.

For a very thin, very dilute layer of absorbing centers (as used in the determination of the phosphorescence saturation curve) *per unit area* (cm²) the ratio *moles of triplets/moles of absorption acts* is

$$\frac{C_T}{C_S\int_{\nu_1}^{\nu_2} I_{(\nu)}\epsilon_{(\nu)}'d\nu}=\frac{i}{\int_{\nu_1}^{\nu_2} I_{(\nu)}\epsilon_{(\nu)}'d\nu} \tag{9}$$

in which the value of $i=C_T/C_S$ is used to obtain the right member of the equation.

For a very thick, very dilute sample, *per unit area*, the ratio (*total*) *moles of triplets/moles of absorption acts* is

$$\frac{N_T'}{\int_{\nu_1}^{\nu_2} I_{(\nu)}d\nu}, \tag{10}$$

if the light is totally absorbed. In expressions (9) and (10), $I_{(\nu)}$ is the function representing the dependence of intensity of the exciting light on frequency, and $\epsilon_{(\nu)}'$ is the corresponding function for the absorption curve of the complex molecule.

The first ratio (9) is valid for each very thin layer of a thick sample. Although $I_{(\nu)}$ diminishes in each successive layer, ratio (9) remains constant for each very thin layer, since $C_T/C_S=k_1I$. Therefore, ratio (9) is valid for the whole sample, and we may equate it to ratio (10). Then after converting the units of $\epsilon_{(\nu)}'$ to give the ordinary molar absorption coefficient, by

$$\epsilon_{(\nu)}'=1000\cdot 2.303\epsilon_{(\nu)},$$

we obtain

$$N_T'=\frac{i\int_{\nu_1}^{\nu_2} I_{(\nu)}d\nu}{1000\cdot 2.303\int_{\nu_1}^{\nu_2} I_{(\nu)}\epsilon_{(\nu)}d\nu}. \tag{11}$$

If the exciting light were monochromatic the corresponding expression would be

$$N_T'=\frac{i}{1000\cdot 2.303\epsilon_0}, \tag{12}$$

where $\epsilon_0$ is the molar absorption coefficient at the frequency of the exciting light. The values of the integrals

of Eq. (11) are determined experimentally as described below.

### *Experimental*

A sample of fluorescein dye mixed with crystalline boric acid was fused at 240°C and fabricated into glass strips by the extrusion process described elsewhere.[9] The concentration of the dye in the glass was determined by two independent methods. In the *dry* method the concentration is given by

$$C=\frac{1000wd}{WfM},$$

where $C$ = moles of dye/liter of glass, $w$ is the weight of the dye in grams, $d$ is the density[9] of boric acid glass, 1.830 g/cm³, $W$ is the weight of boric acid crystals used, $f$ is the weight fraction of boric acid remaining after fusion,[9] 0.660, and $M$ is the molecular weight of the dye or substance used.

In the *wet* method, a weighed sample of the glass containing the dye was dissolved in alkali of known concentration and the optical density of the solution measured at an appropriate wave-length by means of a spectrophotometer. The concentration of the dye is given by the usual equation

$$C=\frac{\log_{10}I_0/I}{\epsilon_0 d},$$

where $C$ is concentration of dye in moles per liter of solution, $\log_{10}I_0/I$ is determined by the spectrophotometer, $d$ is the cell length in cm, and $\epsilon_0$ is the molar absorption coefficient for the solution at the wave-length used for calibration.

For purposes of analysis and comparison, the absorption spectrum of fluorescein dye was measured in various media and after varied preliminary treatment. The results are summarized in Table I. Comparing experiments (2) and (3) it is evident that fusion of the dye with the boric acid does not destroy the dye, as may be expected from the mode of synthesis of such dyes as fluorescein. Comparison of experiments (4) and (5) shows the close similarity of the absorption spectra of the dye in these two different *acid* media. It is to be emphasized[7] that the species in this latter case is the positive ion (I), whereas in *alkaline* solution the doubly-negative ion (II) is present. Dye I and dye II have quite distinct optical properties as may be seen by comparing experiments (2) and (4) of Table I and by the fact that (I) has a quantum efficiency of *phosphorescence* approaching unity, while (II) has a quantum efficiency of *fluorescence* approaching unity.

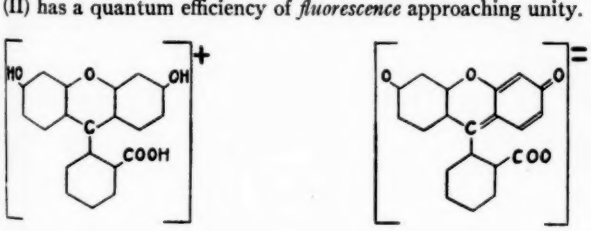


I II

The absorption spectrum of acid fluorescein dye (I) in boric acid glass at room temperature is given in Fig. 4, curve 1. The maximum molar absorption coefficient was calculated to be $\epsilon$=23640 (experiment 5, Table I) by the methods outlined above.

The light source used for excitation of the phosphorescence was an AH6 high pressure mercury arc. Figure 4, curve 2, gives the frequency dependence of emission intensity, determined spectrographically. The light was filtered by 5 cm of a concentrated aqueous solution of $Cu(NO_3)_2$. The transmission curve of this filter solution is given by Fig. 5; by comparison with curve 1, Fig. 4, it may be seen that the transmission region of this filter coincides with the first absorption region of acid fluorescein dye. Figure 4, Curve 3 gives the relative transmission of this filter in the region important in the evaluation of the intensity integrals.

### *Calculations*

In evaluating the integral for the source intensity of Eq. (11) we must multiply each ordinate of curve 2, Fig. 4, by the ordinates for the relative transmission of the $Cu(NO_3)_2$ filter, curve 3. The resulting ordinates are plotted in Fig. 6, curve 1. The value of the intensity integral, determined graphically from this curve is, in arbitrary units

$$\int_{21500}^{25300} I_{(\nu)}d\nu=2.26\times10^{7}. \tag{13}$$

The value of the integral for the $\epsilon I_s$-product curve, obtained by multiplying the ordinates of curves 1, 2, and 3 of Fig. 4 together, plotted as curve 2 of Fig. 6, is, in arbitrary units

$$\int_{21500}^{25300} I_{(\nu)}\epsilon_{(\nu)}d\nu=3.86\times10^{11}. \tag{14}$$

The value of the integral ratio $2.26\times10^{7}/3.86\times10^{11}=5.86\times10^{-5}$, which is to be used in Eq. (11), may be compared with $1/\epsilon_{max}=4.23\times10^{-5}$ (experiment (5), Table I) which would be used in Eq. (12) if monochromatic light of wave-length 4390A had been used in the excitation of the phosphorescence.

The absolute concentration of triplet molecules may now be calculated using a modification of Eq. (11):

$$N_T=\frac{isq\int_{\nu_1}^{\nu_2} I_{(\nu)}d\nu}{1000\cdot2.303\int_{\nu_1}^{\nu_2} I_{(\nu)}\epsilon_{(\nu)}d\nu}, \tag{15}$$

in which $N_T$ is the concentration of triplet molecules in moles/cm length for a strip of width $s$ cm, and $q$ is a "concentration quenching" factor. The factor $q$ must be taken into consideration in order to convert Eq. (11), which is valid for a very thick, very dilute, sample, to an equation valid for a sample of finite thickness and finite *concentration*. The need for such a correction is occasioned by the concentration-dependent quenching of luminescence which occurs in the solid state, as found by Dixon[11] and by Levshin and Vinokurov.[6] A plot of data from the paper by the latter authors for the phosphorescence of fluorescein dye in boric acid glass is given in Fig. 7. The ordinate is light sum (plotted as relative values with $L_{p,max}=1$),

$$L_p=\int_0^{\infty} I_{p,0}\epsilon^{-t/\tau_p}dt=I_{p,0}\tau_p,$$

which is a measure of relative quantum efficiency if the exciting pulse is of constant magnitude in comparable

[11] A. A. Dixon, J. Opt. Soc. Am. **21**, 250 (1931).

experiments. In the previous considerations in this paper it has been assumed that the mean lifetime of phosphorescence is independent of experimental conditions.[12] Here, however, $\tau_p$ changes with concentration of the dissolved dye, so light sum must be used in making comparisons, instead of merely the intensity. The abscissa of Fig. 7 is concentration of dye in grams per grams of boric acid glass. The concentration of dye used in the sample for the paramagnetic experiment was $7.90\times10^{-4}$ g/g glass. Considering the value of $L$ determined by means of a blue filter is low owing to self-absorption of the phosphorescence light, the value of $q$ is determined from the curve for $L_{\text{red}}$ of Fig. 7 to be 0.65 at the pertinent concentration.

Therefore, by Eq. (15), with $i=1.58$, $s=0.75$ cm (measured by vernier caliper), $q=0.65$ and the integral

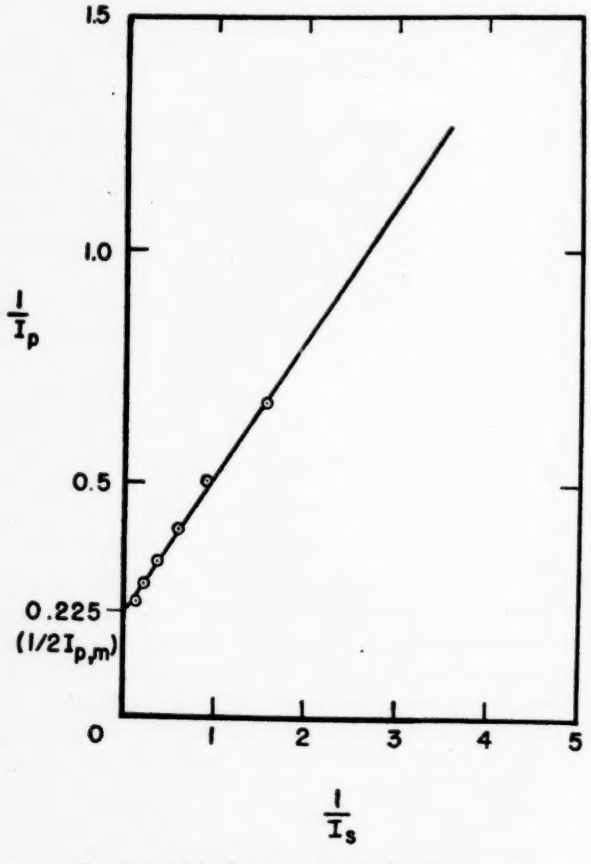


FIG. 3. Straight line form of the phosphorescence saturation curve (see Fig. 2).

ratio $=5.86\times10^{-5}$, we calculate

$$N_T=1.96\times10^{-8}\ \text{mole/cm}$$

as the absolute concentration of molecules excited to the triplet state in the paramagnetic apparatus.

[12] B. Ya. Sveshnikov [Comptes Rendus Acad. Sci. URSS **51**, 429 (1946)] reports a slight dependence of lifetime on initial phosphorescence intensity, for example (see reference 5, Section IV). This is a negligible effect in comparison with the concentration quenching effect.

## C. Measurement of Paramagnetism

### *Theory*

The horizontal boom microbalance used in the paramagnetic measurement (see experimental part, below) was in the form of a double pendulum. From the equations of the pendulum, in which the period is given by

$$T=2\pi(l/g)^{\frac{1}{2}},$$

where $l$ is the length and $g$ the gravitational constant, and the force is given by

$$F=(mg/l)\delta,$$

where $m$ is the mass of the pendulum and $\delta$ is the displacement, the force in dynes may be calculated by

$$F=(4\pi^2m/T^2)\delta. \tag{16}$$

The molar paramagnetic susceptibility of a substance whose magnetic pull is measured in the pendulum balance is then given by

$$\chi_M=\frac{2F}{N_T p(H_m^2-H_0^2)}, \tag{17}$$

where $N_T$ is the concentration per cm length (here, triplet state molecules) as before, $(H_m^2-H_0^2)$ is the field-square-difference for the magnet, and $p$ is an empirical correction factor for percent of maximum pull as a function of the length of the sample.

### *Experimental*

Figure 8 shows a curve depicting the dependence of percent of maximum pull on the length of the sample as measured from the center of the pole piece of the magnet. This was determined experimentally by measuring the pull on a uniform tube filled to different heights with a standard paramagnetic salt solution. The sample of fluorescein in boric acid glass used in the paramagnetic determination protruded 3.1 cm out from each side, measured from the center of the pole pieces. Reading from the curve of Fig. 8, this corresponds to a value of $p=0.84$.

The apparatus used in measuring the magnetic pull was hori-

TABLE I. Optical absorption data for fluorescein dye in various media (using sodium salt of fluorescein as starting material).

| Solution or Treatment | Concentration of Dye | Wavelength of max. Absorption $\lambda_{max}$ | Character of Band | Molar Absorption Coefficient $\epsilon_{max}$ |
|---|---|---|---|---|
| 1. Dye dissolved in water | $1.628\times10^{-5}$ M | 4550A<br>4850 | shoulder<br>peak | 12500<br>16220 |
| 2. Dye dissolved in 0.500 M NaOH | $1.960\times10^{-6}$ M | 4920 | peak | 39800 |
| 3. Dye fused with boric acid 20 min. at 240°C. Final solution 0.440*N* NaOH and 0.0858 M $B_4O_7^=$ | $2.960\times10^{-6}$ M | 4920 | peak | 40900 |
| 4. Dye dissolved in 0.264 M $HClO_4$ | $3.89\times10^{-5}$ M | 4375 | peak | 22030 |
| 5. *Dye in boric acid glass*, 0.055 cm thick | $(3.94\times10^{-4}$ M) | 4390 | peak | 23640 |

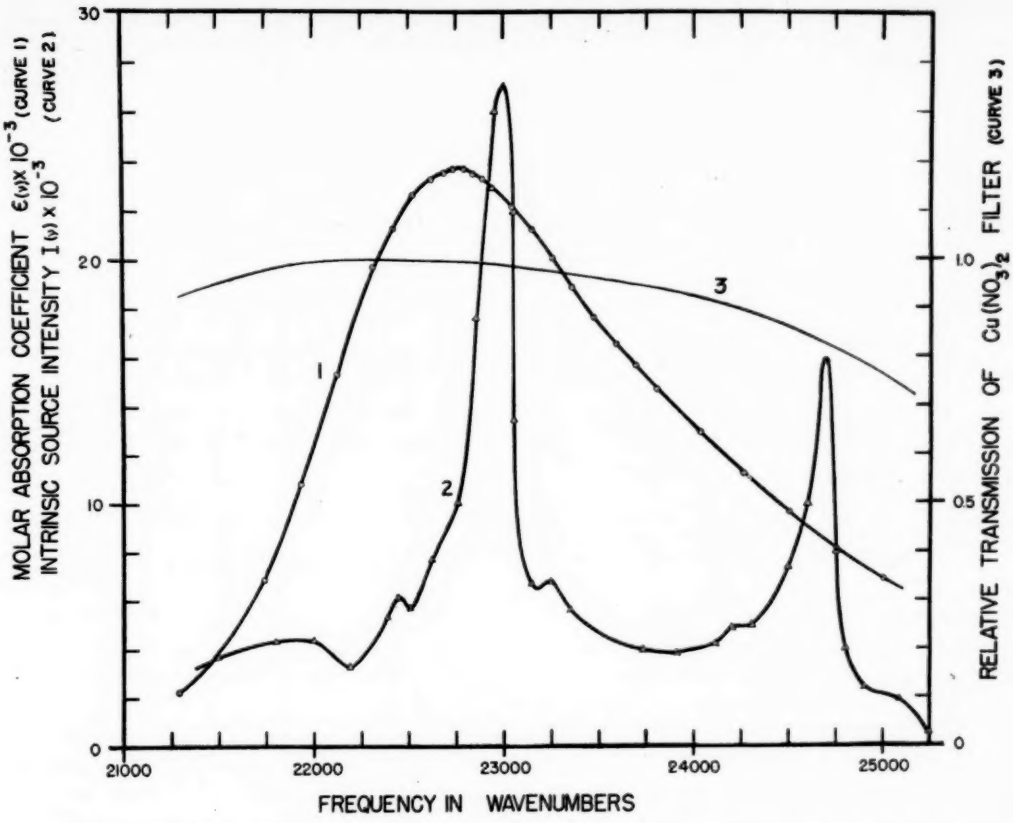


FIG. 4. Miscellaneous spectral curves. Curve 1, absorption curve of acid fluorescein dye (I) in boric acid glass at 25°C. Curve 2, intensity distribution of AH6 high pressure mercury arc. Curve 3, relative transmission of $Cu(NO_3)_2$ filter (see Fig. 5).

zontal boom microbalance patterned after the balance of Theorell,[13] and except for some minor modifications, is identical with that used in the preliminary experiments.[3] This apparatus is diagrammed in Fig. 9. The components are as follows: (1) vernier eyepiece micrometer for measuring displacement of boom, (2) jacket of 20 mm glass tubing for protection against draughts. Inside may be seen the double pendulum suspension, consisting of a horizontal capillary boom—just stout enough to support its own weight plus the weight of the thin strip of phosphor—supported by two extremely fine glass threads (1.40 m long) by means of two hooks of very fine platinum wire. The upper ends of the suspension were the section of 8 mm Pyrex tubing from which the glass thread had been drawn; these sections of tubing were cemented by means of de Khotinsky cement to the glass jacket, so that warming of the cement allowed adjustment of the boom height. The magnet (3), consisting of copper tube conductors cooled by internally circulating kerosene oil, generated a field of about 20,000 gauss ($H_m^2 - H_0^2 = 4.20 \times 10^8$; calibrated by a standard paramagnetic salt solution) with a current of 35.0 amperes. The tapered pole pieces (4), depicted in end view in Fig. 8, were fitted close to each side of the glass jacket of the apparatus. As a light source, the AH6 high pressure mercury arc was mounted in the bed of the magnet (5). The light was directed toward the phosphor sample by means of an $f1.0$ quartz condensing lens (10 cm dia.) (6), then passed through a 5 cm quartz cell (7) of a concentrated aqueous solution of $Cu(NO_3)_2$, for purposes of cooling the light beam (see Fig. 5).

The glass phosphor sample for the paramagnetic determination was a strip of dimensions 6.3 cm $\times$0.75 cm $\times$0.035 cm, prepared by an extrusion process.[9] The weight of the sample and its capillary boom was 0.370 g. The concentration of dye was $7.90 \times 10^{-4}$ g/g boric acid glass, or $6.79 \times 10^{-3}$ mole of dye/$l$ glass. For a thickness of 0.035 cm, using $\epsilon = 23640$ (Table I), we calculate that $\log_{10} I_0/I \gtrsim 5$, so that the light may be considered to have been totally absorbed.

The period of the pendulum, consisting of the glass phosphor strip mounted on the capillary boom and suspended by the two glass thread suspensions, was determined to be 2.35 sec.

After the optics were adjusted to give a uniform and intense illumination of the glass phosphor sample, the paramagnetic apparatus was lifted out of its mount and a piece of glass tubing (of the same size as used in the apparatus and cut to give a half-round end view) was mounted between the pole pieces of the magnet. A small flat rectangular barrier-layer photocell, covered with a dense, uniform screen, and masked to leave a 0.5$\times$1 cm aperture, was adjusted to occupy the same position as the phosphor sample, and the measurements of source intensity were thus

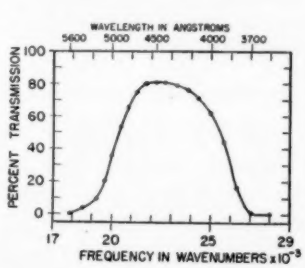


FIG. 5. Transmission curve of a 5-cm path of a concentrated aqueous solution of $Cu(NO_3)_2$ used as a heat absorbing and "monochromatizing" filter.

[13] H. Theorell, Arkiv. f. Kemi. Min. Geol. **16A**, 1 (1943).

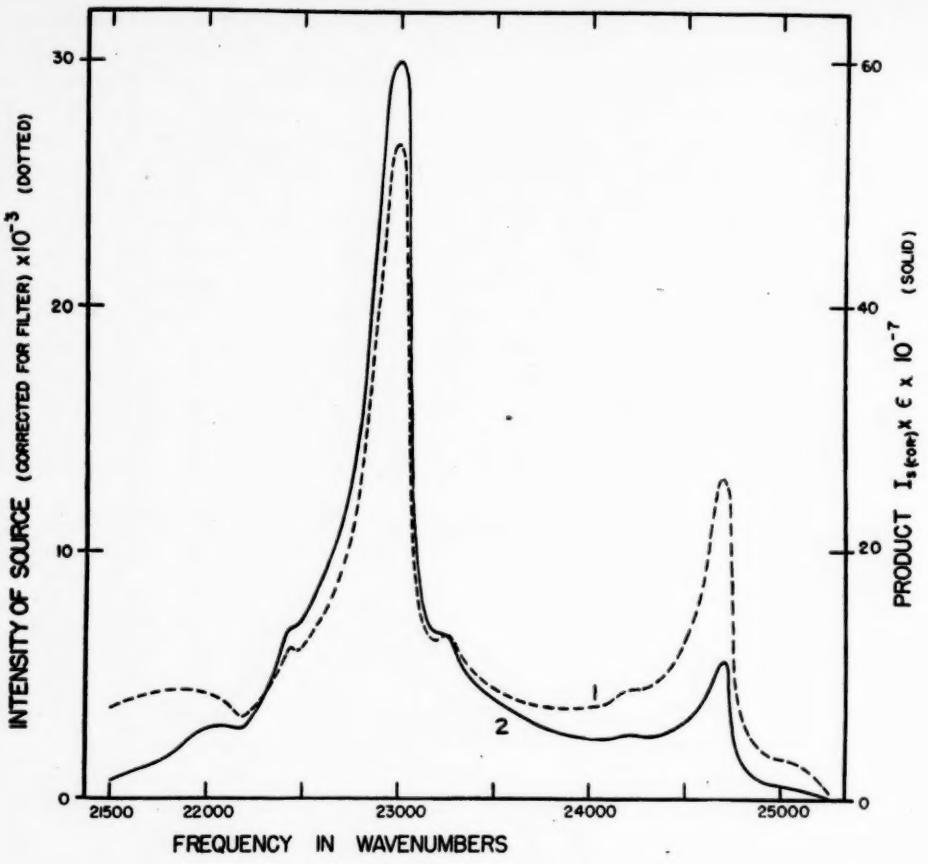


FIG. 6. Intensity curves used in the graphical integration of the theoretical intensity integrals (see Eq. (11)).

obtained. The same masked and screened photocell and galvanometer were used to measure the intense source used in the previous phosphorescence saturation curve determination. By such measurements it was found that the source intensity in the paramagnetic apparatus was 0.205 of the source intensity used in the saturation curve experiment, as previously indicated.

After mounting the phosphor sample in the magnetic balance and adjusting the position of the glass housing for freedom of swing of the suspension, the apparatus was pumped out to a high vacuum. In order to prevent recurrence of the oxygen effect[3] (see below) the apparatus was swept out with hydrogen gas several times and then filled with hydrogen gas to a pressure of 1 atmosphere. In addition to its being diamagnetic, hydrogen presents the additional virtue of relatively high heat conductivity.

The apparatus was covered with opaque black paper in such a way that one half of the phosphor sample would receive the full beam of the filtered high intensity mercury arc and that the other half would be kept dark. A simple shutter permitted complete shutting-off of the light. If the molecules excited to the phosphorescent state were paramagnetic, the illuminated half should be pulled into the field and the deflection could be observed by means of the eyepiece micrometer.

### *Observations and Calculations*

The various experiments performed and the deflections observed with the magnetic balance are summarized in Table II. Experiment 1 was performed to test the effect of the light on the null point of the balance; the effect of the beam was found to be negligible in the absence of the magnetic field. In Experiment 2 observations were made alternately with both halves of the sample dark, and with one half dark and the other illuminated by the full exciting beam. Although a mean deflection of only 0.47 of the smallest scale division of the eye-piece micrometer was observed (read by vernier), the readings were exceptionally steady and reproducible. Experiment 3 repeated Experiment 2, except that the observations were made independently by a second observer. Experiments 4 and 5 were done at a later time at a significantly higher room temperature and were designed to test the effect of a 50 percent screen in the light beam; approximately a half deflection was obtained with the screen, as expected from the kinetics of excitation.

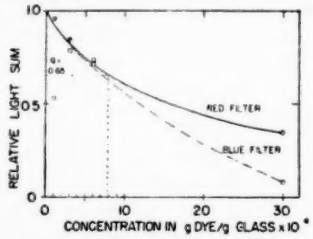


FIG. 7. Concentration quenching curves for the solid state; phosphorescence of acid fluorescein dye in boric acid glass at room temperature (data of Levshin and Vinokurov, reference 6).

From Experiments 2 and 3 of Table II, the average measured displacement is 0.48(5) scale divisions. One division on the eyepiece micrometer corresponds to $\frac{1}{12}$ mm or 0.00833 cm. Therefore, $\delta$ (Eq. 16) = 0.0040(4)

cm is the absolute displacement. Since the mass of the pendulum $m=0.370$ g, and the period $T=2.35$ sec., by Eq. (16) the magnetic pull $F$ is $1.07\times10^{-2}$ dyne.

To calculate the molar paramagnetic susceptibility of acid fluorescein dye in its phosphorescent state, we use Eq. (17), for which $F$ has just been found to be $1.07\times10^{-2}$ dyne, $N_T=1.96\times10^{-8}$ mole/cm length, $p=0.84$, and $(H_m^2-H_0^2)=4.20\times10^8$. From these data we calculate

$$\chi_{M,F}+=3090\times10^{-6} \text{ c.g.s. unit}$$

for the molar paramagnetic susceptibility of acid fluorescein dye in its phosphorescent state at 25°C. For comparison we give the molar paramagnetic susceptibility of molecular oxygen at 25°C, which has a triplet ground state,

$$\chi_{M,O_2}=3340\times10^{-6} \text{ c.g.s. unit.}^{14}$$

## III. DISCUSSION AND CONCLUSION

The measurement of the paramagnetic susceptibility of a complex molecule in its phosphorescent state gives direct physical evidence for the triplet character of the associated electronic level. However, the phenomenon of photomagnetism is a delicate one whose quantitative investigation is susceptible to numerous possibilities for error; a discussion of these is therefore appropriate.

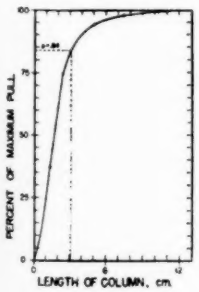


FIG. 8. Magnetic correction curve for length of sample.

### *Errors*

Aside from offering a possibility of measuring extremely small paramagnetic effects, the Theorell balance presents several other desirable features. Not the least of these is the fact that in the present application the angle of incidence of the light beam relative to the direction of displacement of the boom is 90°. This disposes of troublesome corrections for simple thermal effects (see below), radiation pressure, etc.

The largest errors in the present determination are anticipated to occur in $F$, the force in the magnetic balance; in the integral ratio of Eq. (15); and in $q$, the concentration quenching factor. Estimating respective errors of 10 percent, 5 percent, and 5 percent in these quantities (all other errors are estimated to be less than

[14] Calculated from data for the gas at 20°C by Curie's law [*Handbook of Chemistry and Physics* (Chemical Rubber Publishing Company, Cleveland, Ohio, 1944), 28th ed., p. 1912].

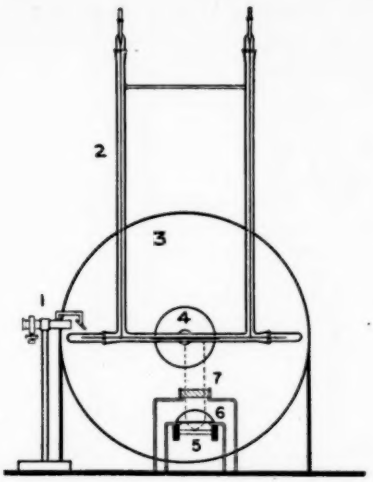


FIG. 9. Modified Theorell horizontal magnetic microbalance for photomagnetism determinations. In actual practice the illuminated half is entirely within the light beam.

1 percent), a propagated error calculation indicates that the error in $\chi_M$, the molar paramagnetic susceptibility, may be a maximum of 13 percent. Thus the precision of measurement is indicated to be

$$\chi_{M,F}+=3090\times10^{-6}\pm400,$$

which covers the theoretical value of $3340\times10^{-6}$.

### *Temperature Effect*

In the case of phosphorescence of dyes, for which the lowest excited singlet and the lowest triplet levels are often less than 10 kcal. apart in energy, there are characteristic phenomena[5,7] associated with changes of temperature of the phosphor. Of importance here is the thermal depopulation which takes place in such a phosphor at temperatures in the range of 290°K. From this, one may anticipate that the chief effect of a temperature increase in the sample, such as may occur in an intense light beam, would be to cause a *diminution* in the concentration of triplet state molecules.[15]

In order to determine whether there was any significant warming of the phosphor, despite the use of the $Cu(NO_3)_2$ filter, a thermocouple element was imbedded in the front surface of a strip of fluorescein-boric acid glass. With the full beam turned on the strip in the paramagnetic apparatus, a temperature rise of less than 2° in five minutes occurred.

As a second approach, a thin strip of mica was covered with carbon black and suspended on the boom of the balance. Duplicating the technique of the paramagnetism determination (hydrogen atmosphere) readings were taken with the strip in total darkness and with half the strip illuminated by the full beam of the AH6 arc (filtered by the $Cu(NO_3)_2$ filter). No measurable deflection occurred.

[15] At the time the preliminary report of the present determination was made (see references 4 and 5) it was thought that this was the reason for the low value of $\chi_M$ obtained. However, the "concentration quenching" correction was not made at that time. If we divide the previously reported result $\chi_M=2100\times10^{-6}$ by 0.65, we obtain $3230\times10^{-6}$. This corresponds to a value of $N_T=2.10\times10^{-8}$ mole/cm, which also is not corrected for the $Cu(NO_3)_2$ transmission (the corrected value is $1.96\times10^{-8}$ mole/cm). Aside from these two corrections and some minor arithmetical corrections, the present results are the same as those previously reported (see reference 5).

TABLE II. Deflections in the Theorell balance.*

| | | | |
|---|---|---|---|
| Experiment 1, no field | | | |
| dark | 2.12 | | |
| full beam | 2.08 | | |
| dark | 2.10 | | |
| Experiment 2,† field on‡ | | Experiment 3,† field on | |
| dark | 1.87 | dark | 2.91 |
| | >0.52 | | >0.55 |
| full beam | 2.39 | full beam | 3.46 |
| | >0.41 | | >0.49 |
| dark | 1.98 | dark | 2.97 |
| | >0.54 | | |
| full beam | 2.52 | dark | 3.03 |
| | >0.41 | | >0.48 |
| dark | 2.11 | full beam | 3.51 |
| | | | >0.46 |
| | mean 0.47 | dark | 3.05 |
| | | | mean 0.50 |
| Experiment 4, field on | | Experiment 5, field on | |
| dark | 3.77 | 50% beam | 3.59 |
| | >0.42 | | >0.16 |
| full beam | 3.35 | dark | 3.43 |
| | >0.36 | | >0.17 |
| dark | 3.71 | 50% beam | 3.60 |
| | >0.41 | | >0.16 |
| full beam | 3.30 | dark | 3.44 |
| | >0.36 | | |
| dark | 3.66 | | mean 0.16 |
| | mean 0.39 | | |

* Each reading is a mean of six settings of the eyepiece micrometer, in units 0.00833 cm.
† Room temperature, 25°C.
‡ The field is turned on before readings are taken, since the null point changes with field owing to diamagnetic asymmetry of the sample.

From these results it was concluded that both thermal depopulation of the excited state, and simple thermal effects, could be disregarded in these experiments.

### *Oxygen Effect*

In the first experiments[3] on the photomagnetism of acid fluorescein in its phosphorescent state, a large negative deflection (the illuminated half of the boom was pushed out of the field) was observed if the gas surrounding the boom of the microbalance was oxygen (or air). A strip of mica, covered with carbon black, and similarly illuminated in an oxygen atmosphere, was driven violently out of the field. With non-paramagnetic atmospheres (argon, carbon dioxide, or hydrogen) the phenomenon was absent. The explanation of this queer phenomenon may be traced[16] to warming of a small layer of oxygen close to the surface of the illuminated part of the sample. The resulting diminution of the volume paramagnetic susceptibility of the oxygen should have a square dependence on the temperature according to Curie's and Charles' law. The more highly paramagnetic cool gas surrounding the dark half of the sample then would be pulled into the field, the flow of gas along the sample dragging it in the indicated direction. This "magnetic wind" phenomenon was avoided in the serious experiments by filling the apparatus with hydrogen gas, as described above.

The satisfactory result obtained in this paramagnetism determination for a molecule in its phosphorescent state substantiates the validity of the theoretical treatment. This method may thus be extended to other cases in which the electronic character of a metastable level is in doubt. An independent determination of the present result would also be desirable, especially since the various determinations were not all carried to the highest refinement.

The specific molecular properties which are requisite for the application of this method are (a) a phosphorescence lifetime on the order of seconds, (b) a high relative quantum yield of phosphorescence, (c) a strong lowest normal absorption band, or a high solubility in the rigid glass medium, and (d) light absorption in an accessible range.

On the other hand, the extended sequence of determinations required for the quantitative evaluation of the paramagnetic susceptibility will put practical limits on its extensive application. In many cases purely qualitative results would be sufficient to deduce the multiplet character of a metastable level. Moreover, purely spectroscopic criteria which are now being developed offer methods of great experimental simplicity for deductions concerning the electronic characteristics of the energy levels of complex molecules.

[16] We are indebted to Professor W. F. Giauque for this explanation.

THE JOURNAL OF CHEMICAL PHYSICS VOLUME 17, NUMBER 9 SEPTEMBER, 1949

# Magnetic Study of Some Hydrates

MATA PRASAD, S. S. DHARMATTI, C. R. KANEKAR, AND N. S. BIRADAR
*Chemical Laboratories, Royal Institute of Science, Bombay, India*

(Received January 3, 1949)

Magnetic susceptibilities of a number of hydrates have been measured by the Gouy technique. In several hydrates of the same salt it has been found that the deviation in the observed molecular susceptibility from additivity, per molecule of water of crystallization, is greatest in the hydrate containing the least number of molecules of water of crystallization and tends to decrease as the number of molecules of water of hydration increases. A relation has been shown to exist between the heat of hydration per molecule of water of crystallization and the deviation in $\chi_m$ per molecule, in these hydrates. The departure from the additivity rule in hydrates has been explained on the basis of bindings between the molecules of water of crystallization and the anhydrous salt.

COMPARATIVELY few workers have studied the effect of water of crystallization on the diamagnetic susceptibility of hydrates. Duchemin[1] found that although monohydrate of $MgSO_4$ is complex, the susceptibilities of the di- and heptahydrates follow the additivity rule. Zimens and Hedvall[2] concluded from the study of the susceptibilities of $Na_2CO_3 \cdot 10H_2O$ and alum that the water of crystallization does influence the susceptibilities of the hydrates; however, in a later communication,[3] the same authors have reported that the water in these hydrates behaves in an additive fashion. Raychaudhari[4] finds that there is a loss in diamagnetism when a hydrate is formed, and therefore the susceptibility of the hydrated salt is generally less than its value calculated from the anhydrous molecule on the basis of strict addivitity. Varadachari[5] considers that Raychaudhari's method of preparing the hydrates and anhydrous substances separately for magnetic measurement makes his results doubtful. He suggests that an obviously better method would be to prepare the hydrated salt and determine its magnetic susceptibility before and after dehydration; the water will be in the combined state in one case and free in the other, and hence the effect of binding alone will be recorded by the change in the magnetic susceptibility. According to this method, Varadachari studied the effect of binding of molecules of water of crystallization on the susceptibility of sodium sulphate decahydrate, by determining the changes in the susceptibility of sodium sulphate in solution below and above the temperature at which transition, from the decahydrate to the anhydrous substance, takes place. From the results obtained, Varadachari concluded that the binding of water molecules with sodium sulphate is very loose.

Varadachari's method of studying the effect of hydration is not always easy to follow. Further, according to this method, the susceptibilities of hydrates should be studied in the state of solution. Many factors other than the effect due to water of crystallization influence the susceptibilities of salts in solutions. For instance, water consists of associated molecules, and at higher concentrations these molecules tend to depolymerize, producing a slight increase in the magnetic susceptibility. Further, the effect produced by the hydration of ions on the susceptibilities of the salts in solutions is also considable. It therefore appears likely that the conclusions obtained, regarding the effect of water of crystallization on the susceptibility of a hydrate from the measurements on solutions of the hydrate below and above the transition temperature, may be erroneous in some cases. Thus, the method adopted by Raychaudhari appears to be the best approach to the problem of the effect of hydration.

Raychaudhari[4] has tried to establish a qualitative relation between the heat of hydration of a salt and the percentage deviation in susceptibility from the additivity rule, and has come to the conclusion that in cases where the heat of hydration is in the neighborhood of 20 calories, the percentage deviation is as great as 20 percent.

In the present investigation, the authors have determined the susceptibilities of a number of hydrates and their corresponding anhydrous salts in the solid state. Attempts have also been made to find how far the conclusions arrived at by Raychaudhari are correct.

The susceptibilities of a number of hydrates of the same salt, containing different number of molecules of water of crystallization, were also determined with a view to find a relation between the deviation in the susceptibility from additivity and the number of molecules of water of crystallization associated with the salt.

In order to test how far the additivity rule holds good for the hydrates in solution, susceptibilities of some hydrates and their corresponding anhydrous salts were also calculated from the measured susceptibilities of their aqueous solutions.

## EXPERIMENTAL

The susceptibilities of the hydrated and anhydrous salts were measured in the solid state and in solutions

[1] E. Duchemin, Comptes Rendus **199**, 571 (1934).
[2] K. E. Zimens and J. A. Hedvall, Svensk, Kem. Tid. **53**, 12 (1941).
[3] K. E. Zimens and J. A. Hedvall, Trans. Chalmers. Univ. Technd. (Gothinburg) No. 9, 3–26 (1942).
[4] D. P. Raychaudhari, Zeits. f. Physik **7**, 393 (1932).
[5] P. S. Varadachri, Proc. Ind. Acad. Sci. **2A**, 161 (1935).

by using the modified form of Gouy's balance described by Prasad, Dharmatti, and Gokhale.[6] All stable hydrates, containing the maximum number of molecules of water of crystallization, used in this investigation were extra pure compounds of either Merck or Kahlbaum. The anhydrous substances were prepared from the hydrates by heating them in an oven to constant weight at temperatures at which the transformation from the hydrate to the anhydrous substances takes place. In addition to these stable hydrates, several intermediate hydrates of some salts, containing various molecules of water of crystallization, were also prepared by heating the stable hydrates at definite temperatures at which the transition from one hydrate to the other takes place, until constant weights were obtained. As some of these intermediate hydrates are not quite stable and tend to pass into a hydrate containing a larger number of molecules of water of crystallization if kept for a long time, they were introduced in the specimen tube as soon as they were prepared, and their susceptibilities were measured immediately without allowing them to absorb moisture. As it does not generally take a long time to pack the substance in the specimen tube for susceptibility measurement, the authors' measurements for these hydrates can be taken as quite reliable. As an additional evidence to show that the substances did not absorb moisture during the susceptibility measurement, it was noted that no increase in the weight of the sample took place during the period of measurement in the solid state. The susceptibilities

TABLE I(a).

| Substance | $\chi_a$ (obs.) | $\chi_m$ (obs.) | $\chi_a$ (cal.) | $\chi_m$ (cal.) | $\frac{\Delta\chi_a}{\chi_a}\times 100$ | $Q$ | $\frac{\Delta\chi_a\times 100}{\chi_a\times n}$ | $\frac{Q}{n}$ |
|---|---|---|---|---|---|---|---|---|
| $BaCl_2\cdot 2H_2O$ | 0.410 | 100.16 | 0.411 | 100.49 | — | 7.0 | — | 3.5 |
| $BaCl_2$ | 0.358 | 74.57 | | | | | | |
| $3CdSO_4\cdot 8H_2O$ | 0.380 | 292.4 | 0.358 | 275.5 | +6.1 | 8.1 | +2.28 | 3.0 |
| $3CdSO_4$ | 0.28 | 175.16 | | | | | | |
| $CdCl_2\cdot 2H_2O$ | 0.45 | 98.68 | 0.427 | 93.74 | +5.38 | 5.6 | +2.69 | 2.8 |
| $CdCl_2$ | 0.370 | 67.82 | | | | | | |
| $CdBr_2\cdot 4H_2O$ | 0.432 | 148.73 | 0.406 | 139.76 | +6.4 | 6.86 | +1.6 | 1.71 |
| $CdBr_2$ | 0.323 | 87.92 | | | | | | |
| $SrCl_2\cdot 6H_2O$ | 0.545 | 145.31 | 0.531 | 141.8 | +2.63 | 18.6 | +0.43 | 3.1 |
| $SrCl_2$ | 0.404 | 64.05 | | | | | | |
| $SrBr_2\cdot 6H_2O$ | 0.462 | 164.27 | 0.501 | 178.16 | −7.78 | 23.3 | −1.29 | 3.88 |
| $SrBr_2$ | 0.406 | 100.40 | | | | | | |
| $Ba(ClO_3)_2H_2O$ | 0.350 | 112.8 | 0.361 | 116.41 | −3.0 | 4.8 | −3.0 | 4.8 |
| $Ba(ClO_3)_2$ | 0.340 | 103.45 | | | | | | |
| $K_2SO_4Al_2(SO_4)_3\cdot 24H_2O$ | 0.530 | 502.50 | 0.53 | 503.24 | 0.0 | — | 0 | — |
| $K_2SO_4Al_2(SO_4)_3$ | 0.370 | 191.00 | | | | | | |
| $Zn_3(PO_4)_2\cdot 4H_2O$ | 0.360 | 165.0 | 0.383 | 175.34 | −6.0 | — | −1.5 | — |
| $Zn_3(PO_4)_2$ | 0.320 | 123.50 | | | | | | |
| $Al_2(SO_4)_3\cdot 18H_2O$ | 0.485 | 323.20 | 0.489 | 326.33 | −0.81 | — | −0.04 | — |
| $Al_2(SO_4)_3$ | 0.272 | 93.05 | | | | | | |
| $Na_2S_2O_3\cdot 5H_2O$ | 0.490 | 121.62 | 0.512 | 127.28 | −4.29 | 13.3 | −0.85 | 2.66 |
| $Na_2S_2O_3$ | 0.395 | 62.48 | | | | | | |

TABLE I(b).

| Substance | $\chi_a$ (obs.) | $\chi_m$ (obs.) | $\chi_a$ (cal.) | $\chi_m$ (cal.) | $\frac{\Delta\chi_a\times 100}{\chi_a}$ | $Q$ | $\frac{\Delta\chi_m}{n}$ | $\frac{\Delta\chi_a\times 100}{\chi_a\times n}$ | $\frac{Q}{n}$ |
|---|---|---|---|---|---|---|---|---|---|
| $CaSO_4\cdot 2H_2O$ | 0.424 | 73.02 | 0.432 | 74.36 | −1.9 | 4.74 | −0.67 | −0.95 | 2.37 |
| $CaSO_4\cdot \frac{1}{2}H_2O$ | 0.365 | 52.97 | 0.378 | 54.94 | −3.43 | — | −4.34 | −6.86 | — |
| $CaSO_4$ | 0.356 | 48.44 | | | | | | | |
| $ZnSO_4\cdot 7H_2O$ | 0.480 | 137.97 | 0.506 | 145.6 | −5.1 | 22.69 | −1.09 | −0.73 | 3.24 |
| $ZnSO_4\cdot H_2O$ | 0.353 | 63.34 | 0.378 | 67.86 | −6.6 | 8.48 | −4.52 | −6.60 | 8.48 |
| $ZnSO_4$ | 0.340 | 54.88 | | | | | | | |
| $MgSO_4\cdot 7H_2O$ | 0.550 | 135.5 | 0.578 | 142.40 | −4.8 | 24.08 | −0.99 | −0.69 | 3.44 |
| $MgSO_4\cdot 5H_2O$ | 0.517 | 108.7 | 0.554 | 116.56 | −6.7 | 18.0 | −1.57 | −1.34 | 3.60 |
| $MgSO_4H_2O$ | 0.440 | 60.78 | 0.467 | 64.72 | −5.8 | 6.98 | −3.94 | −5.80 | 6.98 |
| $MgSO_4$ | 0.430 | 51.76 | | | | | | | |
| $BaBr_2\cdot 2H_2O$ | 0.385 | 128.3 | 0.400 | 132.90 | −3.46 | 9.11 | −2.30 | −1.73 | 4.56 |
| $BaBr_2H_2O$ | 0.370 | 116.6 | 0.380 | 119.95 | −2.6 | — | −3.35 | −2.60 | — |
| $BaBr_2$ | 0.360 | 107.0 | | | | | | | |
| $Na_2B_4O_7\cdot 10H_2O$ | 0.592 | 225.7 | 0.551 | 210.10 | 7.4 | 36.1 | 1.56 | 0.74 | 3.61 |
| $Na_2B_4O_7\cdot 2H_2O$ | 0.486 | 115.3 | 0.448 | 106.42 | 8.5 | — | 4.45 | 4.25 | — |
| $Na_2B_4O_7H_2O$ | 0.450 | 98.68 | 0.426 | 93.46 | 5.6 | — | 5.22 | 5.60 | — |
| $Na_2B_4O_7$ | 0.400 | 80.5 | | | | | | | |

$\chi_a$ = specific susceptibility; $\chi_m$ = molecular susceptibility; $\Delta\chi_a$ = difference between the calculated and observed specific susceptibility; $\Delta\chi_m$ = difference between calculated and observed molecular susceptibility; $n$ = number of molecules of water of crystallization; $Q$ = heat of hydration in kcals.

[6] Prasad, Dharmatti, and Gokhale, Proc. Ind. Acad. Sci. **20**, 224 (1940).

of the anhydrous substances were also measured in the solid state after taking the same precautions against the absorption of moisture.

Results obtained from the measurement of the hydrated and the anhydrous salts in the solid state are given in Tables I(a) and I(b) and are a mean of six independent readings. Throughout this paper, the susceptibility values have been expressed in terms of $-1\times10^{-6}$ c.g.s. units.

For the measurement of the susceptibilities in solutions, about five solutions of different concentrations were prepared by dissolving a known weight of the anhydrous or the hydrated salt in a known weight of conductivity water. Throughout the investigation, the concentration ($C_s$) of a solution has been expressed as the weight of the solute divided by the weight of the solution. The susceptibility of pure conductivity water has also determined and was found to be $-0.72\times10^{-6}$. It was not possible to determine the susceptibilities of solutions of more than 4 or 5 concentrations because of the following experimental difficulties:

(1) The solubilities of some of the compounds are quite low and, therefore, it was not possible to prepare their solutions of concentrations beyond a certain range.

(2) It was necessary to use solutions of widely different concentrations since the differences in the susceptibilities of solutions of concentrations very near to each other were very small.

(3) Concentrated solutions were not used as there is a possibility that mixture law may not hold at high concentrations.

(4) Solutions of concentrations lower than about 5 percent were also not employed because, in such solutions, the quantity of the solute is so small that the differences between the specific susceptibilities of water and these solutions will be quite small, and the experimental error involved in the measurement of susceptibility will appreciably vitiate the correctness of the values of the susceptibility of the solid deduced from such solutions.

The susceptibilities of the solutes were calculated from the observed susceptibilities of the solutions by a graphical method. The values of the susceptibilities of solutions ($\chi_{sol}$) were plotted against their concentrations ($C_s$) and the plotted points were found to lie on straight lines. According to the mixture law, $\chi_{sol}=C_s\chi_a+(1-C_s)\chi_\omega$, which evidently holds in these cases, the intercepts of these straight lines on the susceptibility axis give the value of the specific susceptibility of water, and the slopes are the values of $(\chi_\omega-\chi_a)$ where $\chi_a$ is the specific susceptibility of the solute. It was found that the value of the intercepts in all cases was $-0.72\times10^{-6}$, which is the standard value of the susceptibility of water. The values of $\chi_a$, calculated from the slopes, are given in the 4th column of Table II, and the values of the molecular susceptibility $\chi_m$ in the 5th column.

## DISCUSSION OF RESULTS

The specific or molecular susceptibilities of the compounds, studied in this investigation by the authors either in the solid state or in solutions, were compared, wherever available, with the values obtained by other workers (cf. Table III). It will be seen from the table that the authors' values for the solids do not agree with those reported by Raychaudhari for many compounds, but the agreement between their values and those reported by other workers is quite good. The authors' values deduced from solutions of anhydrous $BaCl_2$ and $SrCl_2$ agree well with those obtained by Flordal and Frivold[7] but the values of $\chi_m$ obtained for the anhydrous $BaBr_2$ and $SrBr_2$ are slightly higher than those of other workers. Whenever the difference between the authors' values and those reported by other workers was quite large, the experiments were carefully repeated with different samples and the reliability of the authors' values has been established.

### (a) Susceptibilities of Hydrates in the Solid State

If Pascal's additivity rule holds good in the case of hydrates, the molecular susceptibility of a hydrate

TABLE II.

| Substance | $C_s$ % | $\chi_{sol}$ | $\chi_a$ | $\chi_m$ |
|---|---|---|---|---|
| $BaCl_2\cdot2H_2O$ | 25 | 0.6413 | | |
| | 16.66 | 0.6728 | 0.42 | 102.8 |
| | 12 | 0.6861 | | |
| | 6 | 0.7025 | | |
| $BaCl_2$ | 19.37 | 0.654 | | |
| | 14.4 | 0.6703 | 0.37 | 78.05 |
| | 10.8 | 0.6861 | | |
| | 6 | 0.700 | | |
| $BaBr_2\cdot2H_2O$ | 42 | 0.583 | | |
| | 40 | 0.598 | 0.40 | 132.11 |
| | 30 | 0.624 | | |
| | 13 | 0.6803 | | |
| | 7 | 0.6969 | | |
| $BaBr_2$ | 40 | 0.5828 | | |
| | 32 | 0.6062 | 0.37 | 110.00 |
| | 25 | 0.6413 | | |
| | 20 | 0.6546 | | |
| | 10 | 0.685 | | |
| $SrCl_2\cdot6H_2O$ | 25 | 0.6839 | | |
| | 12 | 0.6998 | 0.55 | 147.00 |
| | 6 | 0.7108 | | |
| $SrCl_2$ | 20 | 0.6624 | | |
| | 13 | 0.684 | 0.425 | 67.38 |
| | 10 | 0.6922 | | |
| | 8 | 0.6982 | | |
| $SrBr_2\cdot6H_2O$ | 47.4 | 0.6087 | | |
| | 32 | 0.6428 | 0.48 | 170.6 |
| | 24 | 0.6631 | | |
| | 20 | 0.6711 | | |
| | 8 | 0.7003 | | |
| $SrBr_2$ | 40 | 0.6033 | | |
| | 32 | 0.6229 | 0.42 | 103.9 |
| | 20 | 0.6591 | | |
| | 10 | 0.6933 | | |
| | 5 | 0.7046 | | |
| $Na_2S_2O_3\cdot5H_2O$ | 48 | 0.6159 | | |
| | 24 | 0.6764 | 0.50 | 125.1 |
| | 12 | 0.6946 | | |
| | 8 | 0.7023 | | |
| $Na_2S_2O_3$ | 45 | 0.5764 | | |
| | 40 | 0.608 | 0.42 | 66.91 |
| | 24 | 0.646 | | |
| | 20 | 0.664 | | |
| | 6 | 0.7031 | | |

[7] M. Flordal and O. E. Frivold, Ann. d. Physik **23**, 425 (1935).

TABLE III.

| Substance | Authors' values $\chi_a$ and $\chi_m$ | Values of other workers $\chi_a$ or $\chi_m$ | |
|---|---|---|---|
| | *Values obtained from solids* | | |
| $BaCl_2 \cdot 2H_2O$ | 0.41 | 0.41 | *International Critical Tables* |
| | 100.16 | 0.39 | Raychaudhari[a] |
| | | 0.407 | Prasad, Dharmatti, and Kanekar[b] |
| $BaCl_2$ | 0.358 | 0.36 | *International Critical Tables* |
| | 74.57 | 0.33 | Raychaudhari[a] |
| $3CdSO_4 \cdot 8H_2O$ | 0.380 | 0.27 | Raychaudhari[a] |
| | 292.4 | 0.374 | Hollens and Spencer[c] |
| $3CdSO_4$ | 0.28 | 0.22 | Raychaudhari[a] |
| | 175.16 | 0.281 | Kido[d] |
| | | 0.284 | Hollens and Spencer[c] |
| $CdCl_2$ | 0.370 | 0.368 | Kido[d] |
| | 67.82 | 0.378 | Hollens and Spencer[c] |
| $CdBr_2$ | 0.323 | 0.32 | Kido[d] |
| | 87.92 | 0.343 | Hollens and Spencer[c] |
| $SrCl_2$ | 0.404 | 61.3 | Kido[d] |
| | 64.05 | 69.6 | Hollens and Spencer[c] |
| | | 0.402 | Prasad, Dharmatti, and co-workers[e] |
| $SrBr_2$ | 0.406 | 0.39 | *International Critical Tables* |
| | 100.4 | 96.28 | (Meyer) *International Critical Tables* |
| $Ba(ClO_3)_2 \cdot H_2O$ | 0.350 | 0.358 | Prasad, Dharmatti, and Kanekar[b] |
| | 112.8 | | |
| $CaSO_4 \cdot 2H_2O$ | 0.424 | 0.433 | Prasad, Dharmatti, and Gokhale[e] |
| | 73.02 | | |
| $CaSO_4$ | 0.356 | 0.38 | Raychaudhari[a] |
| | 48.44 | 0.364 | Pascal |
| $BaBr_2 \cdot 2H_2O$ | 0.385 | 0.39 | Prasad, Dharmatti, and Kanekar[b] |
| | 128.28 | | |
| $BaBr_2$ | 0.36 | 0.39 | *International Critical Tables* |
| | 106.99 | 0.32 | Kido[d] |
| | 0.395 | 0.391 | *International Critical Tables* |
| $Na_2S_2O_3$ | 62.48 | | |
| $MgSO_4 \cdot 7H_2O$ | 0.550 | 0.43 | Raychaudhari[a] |
| | 135.5 | 0.557 | Pascal |
| | | 0.546 | Prasad, Dharmatti, and Amin[f] |
| $MgSO_4$ | 0.430 | 54.18 | *International Critical Tables* |
| | 51.76 | 0.37 | Raychaudhari[a] |
| | | 45.08 | Pascal |
| | | 47.2 | Ishiwara[g] |

TABLE III—(*Continued*).

| Substance | Authors' values $\chi_a$ and $\chi_m$ | Values of other workers $\chi_a$ or $\chi_m$ | |
|---|---|---|---|
| | *Values obtained from solids* | | |
| $ZnSO_4 \cdot 7H_2O$ | 0.480 | 0.45 | Raychaudhari[a] |
| | 137.97 | 0.496 | Prasad, Dharmatti, and Amin[f] |
| | | 0.48 | *International Critical Tables* |
| $ZnSO_4$ | 0.340 | 61.88 | *International Critical Tables* |
| | 54.88 | 0.32 | Raychaudhari[a] |
| | | 52.08 | Prasad, Dharmatti, and Amin[f] |
| $K_2SO_4$, $Al_2(SO_4)_3 \cdot 24H_2O$ | 0.530 | 0.53 | Raychaudhari[a] |
| | 502.50 | 493.00 | Trew[h] |
| | | 510.00 | B. N. Ghosh |
| $K_2SO_4 \cdot Al_2(SO_4)_3$ | 0.370 | 0.37 | Raychaudhari[a] |
| | 191.00 | 197.00 | B. N. Ghosh |
| $Na_2B_4O_7 \cdot 10H_2O$ | 0.592 | 0.59 | *International Critical Tables* |
| | 225.7 | | |
| $Al_2(SO_4)_3 \cdot 18H_2O$ | 0.485 | 0.46 | Raychaudhari[a] |
| | 323.2 | | |
| $Al_2(SO_4)_3$ | 0.272 | 0.48 | *International Critical Tables* |
| | 93.05 | | |
| | *Values obtained from solution data* | | |
| $BaCl_2$ | 78.05 | 74.0 | Ikenmeyer[i] |
| | | 76.3 | Flordal and Frivold[j] |
| | | 72.6 | Hocart[k] |
| $BaBr_2$ | 110.00 | 100.7 | Veiel[l] |
| | | 103.6 | Ikenmeyer[i] |
| $SrCl_2$ | 67.38 | 64.2 | Veiel[l] |
| | | 61.6 | Ikenmeyer[i] |
| | | 65.3 | Flordal and Frivold[j] |
| | | 63.0 | Hocart[k] |
| $SrBr_2$ | 103.9 | 87.9 | Veiel[l] |
| | | 85.3 | Ikenmeyer[i] |
| | | 87.9 | Flordal and Frivold[j] |

[a] See reference 4.
[b] N. Prasad, S. S. Dharmatti, and C. R. Kanekar, Proc. Ind. Acad. Sci. **15**, 307 (1942).
[c] W. R. A. Hollens and J. F. Speneer, J. Chem. Soc. **147**, 495 (1935).
[d] K. Kido, Sci. Rep. Tohoku Imp. Univ. **21**, 149, 289 (1932); **22**, 835 (1935).
[e] Prasad, Dharmatti, and Gokhale, Proc. Ind. Acad. Sci. **20**, 224 (1940).
[f] Prasad, Dharmatti, and Amin, Proc. Ind. Acad. Sci. **26**, 312 (1947).
[g] J. T. Ishiwara, Sci. Rep. Tohoku Imp. Univ. Series 1, **3**, 303 (1914); **5**, 53 (1916); **9**, 232 (1920).
[h] V. C. J. Trew, Trans. Faraday Soc. **32**, 1658 (1936).
[i] K. Ikenmeyer, Ann. d. Physik **1**, 169 (1929).
[j] See reference 7.
[k] See reference 8.
[l] Veiel, Ann. d. Physik **24**, 697 (1935).

should be equal to the sum of the molecular susceptibilities of the anhydrous salt and the molecules of water of crystallization ($\chi_m = -12.96 \times 10^{-6}$). Values calculated for the molecular susceptibilities of different hydrates on the additivity basis, using authors' values for the molecular susceptibilities of anhydrous salts, are given in column 5 of the Tables I(a) and I(b). From these values the specific susceptibilities have been calculated and are given in column 4 of the tables. It will be seen that the calculated values of $\chi_a$ (column 4) depart from the observed ones (column 2). These departures may be due to factors such as the strength of the binding of water molecules (tighter the binding, the greater the departure) and distribution of charge in the molecule of the hydrate.

The percentage deviations of the observed $\chi_a$ values from the calculated ones are given in column 6 of the tables. Data for the heats of hydration ($Q$) of the hydrates studied in this investigation have been collected, wherever available, from the literature and are given in column 7 of the tables. It will be seen from the values given in columns 6 and 7 that the percentage deviation from additivity does not bear any relation to the heat of hydration as pointed out by Raychaudhari.[4]

Since the substances investigated have different number of molecules of water of crystallization, a comparison between the percentage deviation and the total heat of hydration will not be quite correct. Values were, therefore, calculated for the percentage deviation in $\chi_a$ from additivity per molecule of water of crystallization, and were plotted against the values for the heat of hydration per molecule of water of crystallization. The curve obtained is shown in Fig. 1; the plotted points lie slightly scattered about a mean curve. The curve shows that on an average the percentage deviation tends to decrease, approaches to zero, and then tends to become more and more negative as the heat of hydration per molecule increases. These conclusions are

general as they have been drawn from the consideration of the different hydrates of several substances.

Interesting observations are made when the values for $(\Delta\chi_m/n)$ (Cf. column 8, Table I(b)), in the case of several hydrates of the same salt, are considered. It will be seen that in all cases these values numerically increase as the number $(n)$ of molecules of water of crystallization decreases. It is worth mentioning here that, in some cases, the deviations $(\Delta\chi_m/n)$ are negative, that is, the observed values are greater than the calculated ones, while in others, the reverse is the case. However, in both cases the values of $(\Delta\chi_m/n)$ tend towards zero as $n$ increases. As stated previously, the deviations from additivity rule are caused as a result of the variability of the binding strength between the ions of the anhydrous salt and the molecules of the water of crystallization. If the binding between the two is tight, it will appreciably affect the distance between them and will bring about a strain because of the overlapping of the electronic orbits in the anhydrous salt and the molecules of the water of crystallization, and, hence, cause a deformation of the whole molecule of the hydrate which will give rise to a large deviation in the value of $\chi_m$ from additivity. However, if the binding is weak these deviations will be comparatively small. The observations stated in the previous paragraph, therefore, show that in the case of a hydrate containing

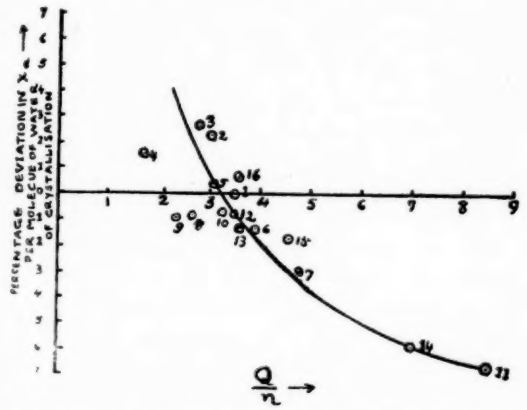


FIG. 1. 1—$BaCl_2$, $2H_2O$; 2—$3CdSO_4$, $8H_2O$; 3—$CdCl_2$, $2H_2O$; 4—$CdBr_2$, $4H_2O$; 5—$SrCl_2$, $6H_2O$; 6—$SrBr_2$, $6H_2O$; 7—$Ba(ClO_3)_2$, $H_2O$; 8—$Na_2S_2O_3$, $5H_2O$; 9—$CaSO_4$, $2H_2O$; 10—$ZnSO_4$, $7H_2O$; 11—$ZnSO_4$, $H_2O$; 12—$MgSO_4$, $7H_2O$; 13—$MgSO_4$, $5H_2O$; 14—$MgSO_4$, $H_2O$; 15—$BaBr_2$, $2H_2O$; 16—$Na_2B_4O_7$, $10H_2O$.

the smallest number of molecules of water of crystallization [largest values of $(\Delta\chi_m/n)$] the binding of the molecules of water with the anhydrous salt is quite tight. The decrease in the value of $(\Delta\chi_m/n)$, when $n$ increases, that is, more molecules of water of crystallization are added on, shows that the binding is considerably weakened, probably because the ions are now further apart and hence do not cause as much deformation as when the number of molecules of the water of crystallization is smaller. The behavior observed for the several hydrates of the same salt appears to be a general phenomenon (true for the hydrates of any substance) as shown in Fig. 2 by plotting the numerical values irrespective of signs of $(\Delta\chi_m/n)$ for all the hydrates, against the ratio of the weight of molecules of water of crystallization to the weight of the anhydrous salt, which is the factor of association of water of crystallization with the salt. The graph is a smooth curve drawn through the plotted points.

Table I(b) also shows that the values of $(Q/n)$, wherever available (given in column 9 of the table), increase with an increase in the numerical values of $(\Delta\chi_m/n)$ for the several hydrates of the same salt, that is, they increase as $n$ decreases. Thus, there appears to be a direct relation between the two quantities. It has not been possible to determine the exact nature of this relation for want of sufficient data.* The heat of hydration of any substance is a measure of the energy of the association of water molecules with the ions of the anhydrous salt in the hydrate. It follows, therefore, from the observation made above that the energy per molecule of water of crystallization decreases as the number of molecules of water of crystallization increases. Thus, the amount of energy required to drive out a molecule of water of crystallization from a hydrate salt containing a large number of molecules of water of crystallization will be small, and this amount will increase for the same salt containing less water of crystallization. This conclusion is supported by the fact that a hydrate containing several molecules of water of crystallization will dehydrate easily and form a hydrate of smaller content of water of crystallization at comparatively low temperatures, but the latter hydrate requires a higher temperature for further dehydration; this discussion, there-

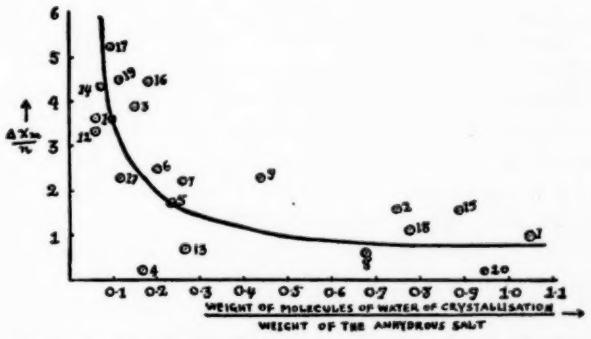


FIG. 2. 1—$MgSO_4$, $7H_2O$; 2—$MgSO_4$, $5H_2O$; 3—$MgSO_4$, $H_2O$; 4—$BaCl_2$, $2H_2O$; 5—$8CdSO_4$, $3H_2O$; 6—$CdCl_2$, $2H_2O$; 7—$CdBr_2$, $4H_2O$; 8—$SrCl_2$, $6H_2O$; 9—$SrBr_2$, $6H_2O$; 10—$Ba(ClO_3)_2$, $H_2O$; 11—$BaBr_2$, $2H_2O$; 12—$BaBr_2$, $H_2O$; 13—$CaSO_4$, $2H_2O$; 14—$CaSO_4$, $\frac{1}{2}H_2O$; 15—$Na_2B_4O_7$, $10H_2O$; 16—$Na_2B_4O_7$, $2H_2O$; 17—$Na_2B_4O_7$, $H_2O$; 18—$ZnSO_4$, $7H_2O$; 19—$ZnSO_4$, $H_2O$; 20—$Al_2(SO_4)_3$, $18H_2O$.

* The heat of hydration of a salt is not an exact measure of the interaction of the ions with the solvated water molecules, since the crystal structure of the anhydrous salt is usually different from that of the hydrate. However, it would appear that the difference in the crystal energy of the two structures, which constitutes part of the energy of hydration, is not the predominant term since there is a definite correlation between the overall energy of hydration of water molecules and $\Delta\chi/n$.

TABLE IV.

| Substance | $\chi_m$(obs.) | $\chi_m$(cal.) | $\Delta\chi_m$ |
|---|---|---|---|
| $BaCl_2 \cdot 2H_2O$ | 102.8 | 103.97 | −1.17 |
| $BaBr_2 \cdot 2H_2O$ | 132.1 | 135.92 | −3.82 |
| $SrCl_2 \cdot 6H_2O$ | 147.0 | 145.14 | 1.86 |
| $SrBr_2 \cdot 6H_2O$ | 170.6 | 181.60 | −11.00 |
| $Na_2S_2O_3 \cdot 5H_2O$ | 125.10 | 131.70 | −6.60 |

fore, establishes that in the lower hydrate of the same salt, the binding of the water molecules with the anhydrous salt must be stronger than the binding in the case of a higher hydrate.

### (b) Susceptibilities of Hydrates in Solutions

It is apparent that by applying the mixture law, one can calculate a formal value of $\chi_a$ and hence $\chi_m$ for either an anhydrous salt or its hydrate from the susceptibility of the respective solution.

A comparison of the values of the molecular susceptibilities given in column 3 of tables I(a) and I(b) and those in column 5 of Table II indicates that the values of the molecular susceptibilities obtained for substances from solutions are in all cases higher than those obtained for the same salts from the measurements in the solid state. This observation confirms the findings of Flordal and Frivold[7] and Hocart.[8] The differences between the two sets of values are, however, small, but since they are observed in all cases they may be quite significant. These differences are possibly due to the fact that the forces which keep the ions of a salt together and thus exert a strain on these ions in the solid state are weakened when the salt is dissolved in water. The effect would probably be much greater if it were not for the fact that the interaction of ions with the salt is almost as pronounced as the interaction of the ions with each other in the anhydrous crystal.

The molecular susceptibilities of the hydrates have been calculated on the additivity basis using the observed values of the susceptibilities of the anhydrous substances obtained from solutions. These calculated values are given in column 3 of Table IV with the observed $\chi_m$ values for the hydrates obtained from solutions (column 2). It will be seen from the table that the calculated values of $\chi_m$ are definitely higher than the observed ones in all cases excepting $SrCl_2 \cdot 6H_2O$. These differences are shown in column 4 of the table. The significance of these differences cannot be definitely understood at this stage.

[8] R. Hocart, Comptes Rendus **188**, 1151 (1929).

## SUMMARY

Magnetic susceptibilities of a number of hydrates have been measured by modified form of Guoy's balance along with the susceptibilities of their corresponding anhydrous salts, in the solid state. The values obtained have been compared with those calculated for the hydrates on the strict additivity basis. The results indicate that the percentage deviation from additivity of the observed values, for specific susceptibilities of the hydrates from the calculated ones, bears no generalized relation of any nature with the total heat of hydration. The percentage deviation in specific susceptibility per molecule of water of crystallization has, however, been found to decrease as the heat of hydration per molecule of water of crystallization increases in the case of several hydrates.

In the case of several hydrates of the same salt, it has been found that the deviation in the observed molecular susceptibility from additivity, per molecule of water of crystallization, is greatest in the hydrate containing the least number of molecules of water of crystallization and tends to decrease as the number of molecules of water of hydration increases. There appears to be some relation between the heat of hydration per molecule of water of crystallization and the deviation in $\chi_m$ per molecule, in the case of these salts.

The departure from the additivity rule in hydrates has been explained on the basis of bindings between the molecules of water of crystallization and the anhydrous salt. Susceptibilities of some hydrates have also been calculated, with their corresponding anhydrous salts, from the susceptibilities of their aqueous solutions. The values obtained in solution are in all cases higher than those obtained for the same salts from the measurement in the solid state. The molecular susceptibilities of the hydrates, calculated on the additivity basis using the observed values of the susceptibilities of the anhydrous salts obtained from solutions, are higher in most cases than the observed values of hydrates measured from solutions.

The authors are indebted to Dr. W. K. Wilmarth of the University of Southern California for valuable discussion and suggestions.

THE JOURNAL OF CHEMICAL PHYSICS VOLUME 17, NUMBER 9 SEPTEMBER, 1949

# Diamagnetic Susceptibilities of Mercuric and Mercurous Ions

MATA PRASAD, S. S. DHARMATTI, AND A. K. GHOSE
*Chemical Laboratories, Royal Institute of Science, Bombay, India*

(Received January 3, 1949)

Magnetic susceptibilities of a number of pure mercuric and mercurous salts of inorganic and organic acids have been measured and it has been shown that Ikenmeyer's relation does not hold true in these compounds. A linear relation has been established between the molecular susceptibilities of salts of Mg, Zn, Cd, and Hg (*ic*) containing the same anion and the number of electrons contained in the cations. The significance of this relation is discussed in detail primarily with a view to finding out the susceptibilities of mercuric and mercurous ions.

A STUDY of the literature shows that a number of widely different theoretical and experimental values have been assigned to the susceptibility of an ion or an atom by various authors. These divergences may be attributed to (i) the use of different methods for the evaluation of $\Sigma \bar{r}^2$ in calculating the theoretical values, (ii) the choice of a value of the susceptibility of an ion from a number of widely different reported values on a more or less arbitrary principle for the calculation of the values of the susceptibilities of other ions on the additivity basis, (iii) the inaccuracy of the methods employed for the measurement of the susceptibilities, and (iv) the use of substances of different purities by different workers for measurement. Systematic investigations have been carried out by Prasad, Dharmatti, and co-workers[1] on the magnetic properties of a large number of Ca, Sr, Ba, Mg, Zn, and Pb salts of inorganic and organic acids for the determination of the susceptibilities of these cations, on the basis that the molecular susceptibility of a heteropolar salt is the sum of susceptibilities of the constituent ions. In order to obviate errors caused by the choice of a particular value for an anion as a standard, they subtracted all the known values of several anions from the molecular susceptibilities of the compounds and have taken an arithmetic mean of the values thus obtained as the standard value for the cation. They found that the mean value of the susceptibility for the cation deduced from salts of inorganic acids is lower than that deduced from its salts of organic acids.

The present investigation deals with the measurement of the susceptibilities of a large number of inorganic and organic salts of mercuric and mercurous mercury. The ionic susceptibility of divalent mercury, given in the *International Critical Tables*, is $-33.4 \times 10^{-6}$ [Pascal], while Kido's[2] values are $-36.6 \times 10^{-6}$ and $-40.3 \times 2 \times 10^{-6}$ for the mercuric and mercurous ions (calculated for the unit $Hg^{+}$), respectively. The theoretical values, calculated for the mercuric ion, according to Slater's and Angus' methods, are $-47.77 \times 10^{-6}$ and $-47.57 \times 10^{-6}$, respectively, thus showing that there is a great divergence between the various theoretical and experimental values. This calls for a confirmation of the reported experimental values for these ions.

## EXPERIMENTAL

The susceptibilities of the compounds were measured by using a modified Gouy's balance, specially constructed by Prasad and co-workers[1] for their investigations. The details of the design and the necessary precautions to be taken are described by Prasad, Dharmatti, and Gokhale.[1a]

All the salts used in this investigation were chemically pure. Most of the compounds were of Merck's extra pure quality stored up for this work and those which could not be obtained in the purest form were prepared in the laboratory and their purity was ascertained before use.

## RESULTS

The results obtained for mercuric salts are given in Tables I(a) and I(b) and for mercurous salts in Tables II(a) and II(b). In these tables, column I gives the chemical formulas of the substances—together with their analysis in the case of the substances prepared in the laboratory. Column 2 gives the total number of electrons ($Z$) in the compounds. The observed values of the specific susceptibilities ($\chi_s$) and the molecular susceptibilities ($\chi_m$) are given in the third column, one below the other. The only hydrated salt investigated was mercurous nitrate. $\chi_m$ value given for this compound in column 3 is that of the anhydrous salt and has been obtained by subtracting the susceptibility value for two molecules of water from the molecular susceptibility value of the hydrated salt. Columns 4 and 5 give, respectively, the experimental values obtained by previous workers and those computed for the salts by adding up the susceptibility values of anions and cations reported by the same authors. The values computed by using the theoretical ionic values of Pauling, Slater, and Angus are given in the last column and have been indicated by letters $P$, $S$, and $A$, respectively. For the organic compounds, the method of Angus and Farqu-

[1] Prasad, Dharmatti, and Kanekar, Proc. Acad. Sci. **16**, 307 (1942). [a] Prasad, Dharmatti, and Gokhale, *ibid.* **20**, 224 (1944). [b] Prasad, Dharmatti, and Amin, *ibid.* **26**, 312 (1947). [c] Prasad, Dharmatti, and Khanolker, *ibid.* **26**, 328 (1947).
[2] Kido, Sci. Rep. Tohoku. Imp. Univ. **21**, 149 (1922); **21**, 288–97 (1932).

TABLE I(a). Mercuric salts of inorganic acids.

| Compounds | Z | Author's values | Other workers | $\chi_m$ Computed, using the experimental ionic values of the constituents by the same author | Computed from theoretical ionic values |
|---|---|---|---|---|---|
| $HgCl_2$ | 114 | 0.3028<br>82.21 | 65.16(4)<br>51.59(5)<br>80.90(2)<br>86.30(6) | 73.6 Pascal | $Hg^{+2}+2(Cl)^{-1}$<br>113.00(*P*)<br>99.35(*S*)<br>93.29(*A*) |
| $HgBr_2$<br>Hg found: 55.49%<br>Hg theory: 55.64% | 150 | 0.2914<br>105.10 | 93.74(4)<br>108.10(5)<br>109.20(6) | 106.00 Kido<br>94.40 Pascal | $Hg^{+2}+2(Br)^{-1}$<br>163.00(*P*)<br>127.79(*S*)<br>120.87(*A*) |
| $HgI_2$<br>Hg found: 43.92%<br>Hg theory: 44.12% | 186 | 0.2931<br>133.20 | 123.70(6)<br>134.10(2) | 143.00 Kido<br>122.60 Pascal | $Hg^{+2}+2(I)^{-1}$<br>215.00(*P*)<br>167.43(*S*)<br>158.21(*A*) |
| HgO | 88 | 0.2343<br>50.76 | 51.99(5)<br>52.70(6)<br>52.64(7) | | $Hg^{+2}+O^{-2}$<br>67.60(*P*)<br>60.92(*S*)<br>58.82(*A*) |
| HgS | 96 | 0.2382<br>55.44 | 53.42(5) | | $Hg^{+2}+S^{-2}$<br>95.00(*P*)<br>85.18(*S*)<br>80.20(*A*) |
| $HgSO_4$ | 128 | 0.2484<br>73.70 | 64.80(2) | 75.60 Kido<br>67.00 Pascal | $Hg^{+2}+(SO_4)^{-2}$<br>106.80(*P*)<br>101.78(*S*)<br>93.88(*A*) |
| $Hg(NO_3)_2$ | 142 | 0.2391<br>77.61 | 74.00(2) | 76.80 Kido<br>61.80 Pascal | $Hg^{+2}+2(NO_3)^{-1}$<br>130.82(*P*)<br>126.89(*S*)<br>115.29(*A*) |
| $Hg(CN)_2$ | 106 | 0.2613<br>66.00 | | 69.80 Kido<br>55.00 Pascal | $Hg^{+2}+2(CN)^{-1}$<br>99.30(*P*)<br>95.95(*S*)<br>87.79(*A*) |
| $Hg(CNS)_2$<br>Hg found: 63.19%<br>Hg theory: 63.31% | 138 | 0.3046<br>96.51 | | 112.60 Kido<br>86.60 Pascal | $Hg^{+2}+2(CNS)^{-1}$<br>179.30(*P*)<br>170.77(*S*)<br>153.05(*A*) |
| $HgCrO_4$<br>Hg found: 63.16%<br>Hg theory: 63.36% | 136 | 0.0396<br>12.54 | | | $Hg^{+2}+(CrO_4)^{-2}$<br>112.00(*P*)<br>105.87(*S*)<br>97.72(*A*) |

harson[3] was followed. Throughout this paper all the susceptibility values are expressed in $-1\times10^{-6}$ c.g.s. unit.

## DISCUSSION OF RESULTS

It will be observed from the above tables that the molecular susceptibilities of many compounds obtained by the authors agree quite well with those found by previous workers. Further, in general, there is a large difference between the authors' values of $\chi_m$ and those computed from theoretical values, especially in the case of the mercurous salts. These theoretically computed values represent the sum of the susceptibilities of the free ions which are not influenced by external factors, whereas when a compound is formed the ions are influenced by one another and this causes an alteration in the effective external charge distribution of the ions and hence the departure from strict additivity. It will be noticed from the tables that the agreement between the experimental values and those computed in column 5 by adding up the cation and anion values given by the same author is fairly good.

[3] Angus and Farquharson, Proc. Roy. Soc. **136A**, 579 (1932).

### (a) Graphical Discussion of the Molar Susceptibilities

Prasad and co-workers[1] have shown that when the molecular susceptibilities of compounds containing the cations belonging to a particular group or subgroup in the periodic table are plotted against the total number of electrons in the compounds, the plots obtained form a pattern which is characteristic of the cations of the group or the subgroup. This has been found to be true in the case of salts of (i) Ca, Sr, Ba;[1a] (ii) Mg, Zn, Cd;[1b] and Tl and Pb.[1c] Hence, the values of the susceptibilities of the mercuric salts were plotted against the total number of electrons in the compounds and the graph obtained is shown in Fig. 1, along with similar graphs for salts of Mg, Zn, and Cd. The susceptibility values of Mg and Zn salts used for plotting these graphs have been taken from the data of Prasad, Dharmatti, and Amin[1b] and the values for Cd salts have been taken from an unpublished work done in the laboratory. It is clearly seen from the figure that all the graphs are similar in nature. Since magnetic susceptibility is essentially a physical property, depending on the electrons in the atoms, it is reasonable to expect a similarity in the magnetic behavior of the salts of a particular group of cations having similar electronic configuration.

TABLE I(b). Mercuric salts of organic acids.

| Compounds | Z | Author's values | Other workers | $\chi_m$ Computed, using the experimental ionic values of the constituents by the same author | Computed from theoretical ionic values |
|---|---|---|---|---|---|
| $Hg(HCOO)_2$<br>Hg found: 68.91%<br>Hg theory: 69.02% | 126 | 0.2512<br>73.00 | — | 67.4 Pascal | $Hg^{+2}+2(HCOO)^{-1}$<br>88.50(*P*)<br>81.27(*S*)<br>81.07(*A*) |
| $Hg(CH_3COO)_2$<br>Hg found: 62.76%<br>Hg theory: 62.94% | 142 | 0.3086<br>98.37 | 100.2 (2) | 100.6 Kido<br>91.2 Pascal | $Hg^{+2}+2(CH_3COO)^{-1}$<br>112.0 (*P*)<br>104.77(*S*)<br>104.57(*A*) |
| $Hg(C_6H_5COO)_2$<br>Hg found: 45.17%<br>Hg theory: 45.31% | 206 | 0.3974<br>175.90 | — | 168.60 Pascal | $Hg^{+2}+2(C_6H_5COO)^{-1}$<br>186.10(*P*)<br>178.87(*S*)<br>178.67(*A*) |
| $HgC_2O_4$<br>Hg found: 69.29%<br>Hg theory: 69.50% | 124 | 0.2378<br>68.63 | — | 61.34 Pascal | $Hg^{+2}+(C_2O_4)^{-2}$<br>82.70(*P*)<br>75.47(*S*)<br>75.27(*A*) |
| $Hg(CHOHCOO)_2$<br>Hg found: 57.31%<br>Hg theory: 57.51% | 156 | 0.3002<br>104.70 | — | 94.28 Pascal | $Hg^{+2}+(CHOHCOO)^{-2}$<br>115.40(*P*)<br>108.17(*S*)<br>107.97(*A*) |
| $Hg(C_{18}H_{33}O_2)_2$<br>Hg found: 25.92%<br>Hg theory: 26.13% | 398 | 0.5957<br>457.10 | — | — | $Hg^{+2}+2(C_{18}H_{33}O_2)^{-1}$<br>488.00(*P*)<br>480.77(*S*) *V*<br>480.57(*A*) |
| $Hg(C_{16}H_{31}O_2)_2$<br>Hg found: 28.02%<br>Hg theory: 28.19% | 366 | 0.5776<br>410.90 | — | — | $Hg^{+2}+(C_{16}H_{31}O_2)^{-1}$<br>441.00(*P*)<br>433.77(*S*)<br>433.57(*A*) |

TABLE II(a). Mercurous salts of inorganic acids.

| Compounds | Z | $\chi_m$ Author's values | Other workers | Computed, using the experimental ionic values of the constituents by the same author | Computed from theoretical ionic values |
|---|---|---|---|---|---|
| $Hg_2Cl_2$ | 194 | 0.2440<br>115.20 | 143.46(6)<br>119.60(2)<br>108.60(5) | 124.80 Kido | $Hg_2^{+2}+2(Cl)^{-1}$<br>168.00(*P*)<br>147.12(*S*)<br>140.86(*A*) |
| Hg found: 84.79%<br>Hg theory: 84.98% | | | | | |
| $Hg_2Br_2$ | 230 | 0.2576<br>144.50 | — | 150.00 Kido | $Hg_2^{+2}+2(Br)^{-1}$<br>218.00(*P*)<br>175.56(*S*)<br>168.44(*A*) |
| Hg found: 71.26%<br>Hg theory: 71.48% | | | | | |
| $Hg_2I_2$ | 266 | 0.2614<br>171.20 | 196.18(6)<br>160.10(2) | 187.00 Kido | $Hg_2^{+2}+2(I)^{-1}$<br>270.00(*P*)<br>215.20(*S*)<br>205.78(*A*) |
| $Hg_2SO_4$ | 208 | 0.2568<br>127.70 | 122.70(2) | 119.60 Kido | $Hg_2^{+2}+(SO_4)^{-2}$<br>161.80(*P*)<br>149.55(*S*)<br>141.45(*A*) |
| $Hg_2(NO_3)_2$<br>$2H_2O$ | 222 | 0.2621<br>121.18 | 118.20(2) | 120.80 | $Hg_2^{+2}+2(NO_3)^{-1}$<br>185.82(*P*)<br>174.66(*S*)<br>162.86(*A*) |
| $Hg_2(BrO_3)_2$ | 278 | 0.2393<br>157.30 | — | — | $Hg_2^{+2}+2(BrO_3)^{-1}$<br>198.26(*S*)<br>186.32(*A*) |
| Hg found: 60.87%<br>Hg theory: 61.03% | | | | | |
| $Hg_2(IO_3)_2$ | 314 | 0.2449<br>184.00 | — | — | $Hg_2^{+2}+2(IO_3)^{-1}$<br>— |
| Hg found: 53.24%<br>Hg theory: 53.40% | | | | | 219.00(*S*)<br>206.98(*A*) |
| $Hg_2CrO_4$ | 216 | 0.1217<br>62.94 | | | $Hg_2^{+2}+CrO_4^{-2}$<br>167.00(*P*)<br>153.64(*S*)<br>145.29(*A*) |
| Hg found: 77.38%<br>Hg theory: 77.56% | | | | | |

TABLE II(b). Mercurous salts of organic acids.

| Compounds | $\chi_m$ Author's values | Other workers | Computed, using the experimental ionic values of the constituents by the same author | Computed from theoretical ionic values |
|---|---|---|---|---|
| $Hg_2(HCOO)_2$ | 0.2443<br>120.00 | — | — | $Hg_2^{+2}+2(HCOO)^{-1}$<br>143.50(*P*)<br>129.04(*S*)<br>128.64(*A*) |
| Hg found: 81.51%<br>Hg theory: 81.66% | | | | |
| $Hg_2(CH_3COO)_2$ | 0.2787<br>144.70 | 144.0 (2) | 144.6 Kido | $Hg_2^{+2}+2(CH_3COO)^{-1}$<br>167.00(*P*)<br>152.54(*S*)<br>152.14(*A*) |
| $Hg_2C_2O_4$ | 0.2436<br>119.20 | — | — | $Hg_2^{+2}+(C_2O_4)^{-2}$<br>137.70(*P*)<br>123.24(*S*)<br>122.84(*A*) |
| Hg found: 81.78%<br>Hg theory: 82.00% | | | | |
| $Hg_2(CHOHCOO)_2$ | 0.2769<br>152.10 | — | — | $Hg_2^{+2}+(CHOHCOO)^{-2}$<br>170.40(*P*)<br>155.94(*S*)<br>155.54(*A*) |
| Hg found: 72.87%<br>Hg theory: 73.03% | | | | |
| $Hg_2(C_{15}H_{33}O_2)_2$ | 0.5213<br>504.40 | — | — | $Hg_2^{+2}+2(C_{15}H_{33}O_2)^{-1}$<br>543.00(*P*)<br>528.54(*S*)<br>528.14(*A*) |
| Hg found: 41.24%<br>Hg theory: 41.45% | | | | |
| $Hg_2(C_{15}H_{31}O_2)_2$ | 0.5036<br>459.20 | — | — | $Hg_2^{+2}+2(C_{15}H_{31}O_2)^{-1}$<br>496.00(*P*)<br>481.54(*S*)<br>481.14(*A*) |
| Hg found: 43.72%<br>Hg theory: 43.99% | | | | |

### (b) Ikenmeyer's Relation[4]

According to Ikenmeyer, the molar susceptibilities ($\chi_m$) of salts are a linear function of the total number ($Z$) of electrons contained in their molecule, that is,

$$\chi_m = C_1 Z + C_2,$$

where $C_1$ and $C_2$ are constants. To test this relationship graphs have been plotted for the values of $\chi_m$ against $Z$ in the case of inorganic salts of mercuric and mercurous mercury separately, and are shown in Figs. 2, 3, and 4. A study of these curves leads to the following conclusions:

(1) The Ikenmeyer's relation does not hold true for all mercuric and mercurous salts. Similar observations have been made by previous workers.

(2) The points corresponding to $HgCl_2$, $HgBr_2$, $HgI_2$, and $Hg(CNS)_2$ (Fig. 2) fall on a straight line. Similarly, the points corresponding to (i) $Hg_2Cl_2$, $Hg_2Br_2$, $Hg_2I_2$ (Fig. 3) also lie on a straight line: (shown by dotted lines). Thus it appears that only compounds containing anions having similar constitution obey the linear law. Such a behavior has also been found in the case of lead salts.[1c]

(3) In the case of organic compounds (Fig. 4) of both mercuric and mercurous mercury many points lie on straight lines.

The values of the slopes ($C_1$) of the several straight lines drawn in Figs. 2, 3, and 4 have been determined from the graphs and are given in the second and fourth columns of Table III. These values of $C_1$ have been used

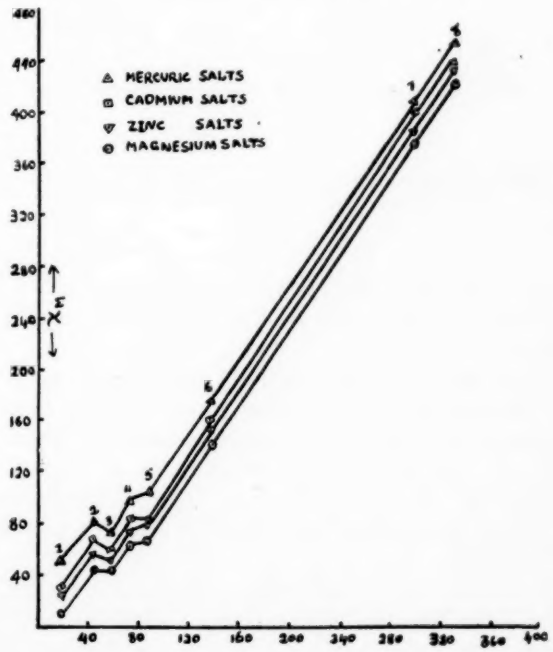


FIG. 1. (To bring out the similarity in curves very prominently, the abscissa for the same anions is kept the same in all compounds.) 1—oxide; 2—chloride; 3—sulfate; 4—acetate; 5—tartrate; 6—benzoate; 7—palmitate; 8—stearate.

[4] K. Ikenmeyer, Ann. d. Physik **5**, 1, 190 (1929).

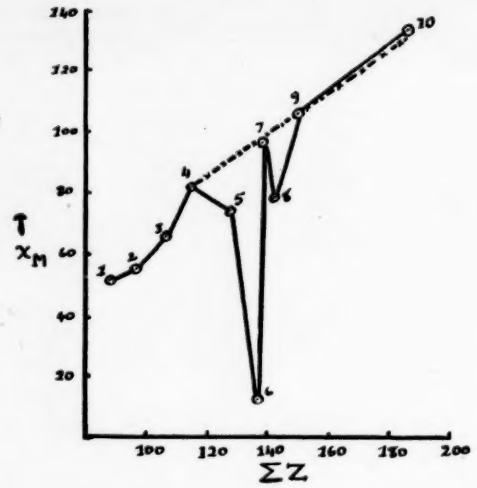


FIG. 2. Mercuric salts of inorganic acids. 1—oxide; 2—sulfide; 3—cyanide; 4—chloride; 5—sulfate; 6—chromate; 7—thiocyanate; 8—nitrate; 9—bromide; 10—iodide.

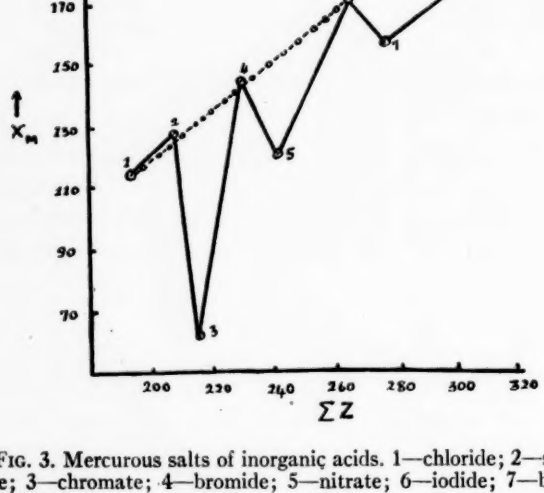


FIG. 3. Mercurous salts of inorganic acids. 1—chloride; 2—sulfate; 3—chromate; 4—bromide; 5—nitrate; 6—iodide; 7—bromate; 8—iodate.

to calculate the values of $C_2$ in Ikenmeyer's relation for every plotted point, and are given in the third and fifth columns of the table.

It will be seen from Table III that the values of $C_1$ are different for corresponding sets of inorganic salts of mercuric and mercurous mercury, showing probably that the susceptibility contributions of the anions of different groups are not the same. However, in the case of organic compounds the values of $C_1$ are the same for salts of both mercuric and mercurous mercury.

The values of $C_2$ are very nearly the same for salts of a given series, but the average value is different for each series. The values of $C_2$ for mercurous salts of both inorganic and organic acids are numerically higher than those for corresponding mercuric salts. Further, in both the mercuric and mercurous compounds the values of $C_2$ are considerably higher for organic salts than those for inorganic ones. These results are in conformity with those found in the case of lead salts.[10]

From the comparison of Ikenmeyer's relation with the Pascals' law ($\chi_m = \Sigma\chi_a + \lambda$) one may infer that $C_2$ is of the nature of the constitutive correction constant; however, the variation of the value of $C_2$ from 4 to 183 for mercury salts of different series does not substantiate this view. Under these circumstances it is difficult to assign any physical meaning to $C_2$ at this stage.

### (c) Ionic Susceptibilities of Mercuric and Mercurous Ions

1. *Statistical method.*—The ionic susceptibilities of mercuric and mercurous ions were determined by the method followed by Prasad and co-workers.[1] In this method, to give weight to all available values, various values of susceptibilities of the anions reported in the literature are collected and the values of the susceptibilities of mercuric and mercurous ions are obtained by subtracting these anion values from the molar susceptibilities. The means of such values are perhaps the most probable values of susceptibility of mercuric and mercurous ion. The mean values calculated for mercuric and mercurous ions separately from salts of inorganic and organic acids come out to be 36.92 and 37.99 and 37.21 and 41.97, respectively.

By applying a statistical test it has been found that the difference in the values for the mercuric ion obtained from inorganic and organic salts is not quite significant.

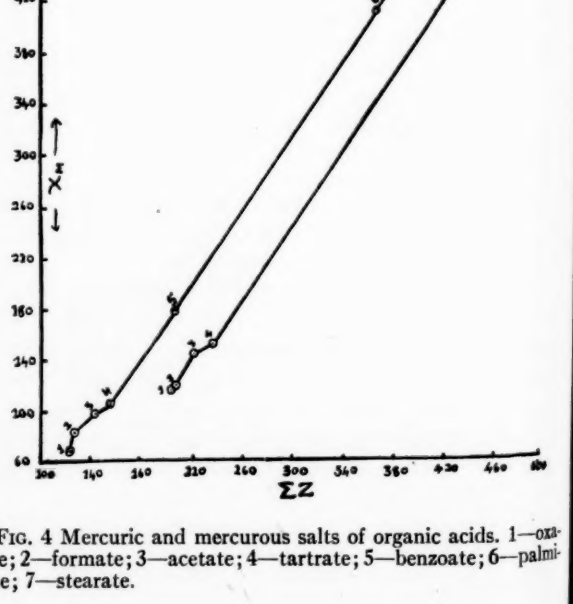


FIG. 4 Mercuric and mercurous salts of organic acids. 1—oxalate; 2—formate; 3—acetate; 4—tartrate; 5—benzoate; 6—palmitate; 7—stearate.

In the case of mercurous ion, however, the difference (3.96) is evidently significant.

(2) *Bhatnagar, Nevgi, and Ohri's method.*—Bhatnagar, Nevgi, and Ohri[5] have suggested that as mercury forms covalent compounds it is necessary for the evaluation of cation values to take only Pascal's values of the anions, since these anion values have been derived from covalent compounds. The mean values of susceptibilities of mercurous and mercuric ions obtained from such consideration from salts of inorganic and organic acids separately have been found to be 44.03 and 42.70×2 (inorganic) and 35.20 and 41.05×2 (organic), respectively.

This method is, however, statistically not very consistent because mercury compounds are considered partly covalent and partly electrovalent, and hence it will not be justifiable to use only Pascal's values for the anions.

(3) *Graphical method.*—Prasad and co-workers[1b] have found that almost straight line graphs are obtained when the molar susceptibilities ($\chi_m$) of compounds having the same anions, and cations belonging to the same family of elements in periodic table, are plotted against the number of electrons ($N$) in the cations, that is, $\chi_m = p_1 N + p_2$, where $p_1$ is the tangent of the inclination (the contribution to the susceptibility ($\chi_m$) per electron of the cation of the same group), and $p_2$ is the intercept of the line on the $\chi_m$ axis. This relation was also observed by Kido. Prasad and co-workers and also Kido extrapolated the straight lines to meet the $\chi_m$ axis ($N=0$); the intercepts $p_2$ of the lines obtained in this manner are the measure of the susceptibilities of the anion with which the cations in the group combine. The values of the anions thus obtained were utilized by these workers to deduce the values of $\chi$-cations.

Graphs were, therefore, drawn between the molecular susceptibilities of the salts of Mg, Zn, Cd, and Hg (*ic*), having the same anion against the total number of electrons in the cations, for salts of inorganic and the organic acids and are shown in Figs. 5 and 6, respectively. The susceptibility values of the salts of Mg, Zn, and Cd used for drawing these graphs are the same as those used in Fig. 1 with the exception of the values of $MgBr_2$ and $ZnCl_2$ which are Kido's.[2] It will be seen that in all cases the graphs are straight lines. The straight lines are produced to meet the $\chi_m$ axis and the values of the intercepts ($p_2$) thus obtained have been given in column 3 of Table IV along with the slopes $p_1$ column (2). In order to show that the plotted points corresponding to mercuric salts definitely lie on straight lines, the molecular susceptibilities of these salts have been calculated by multiplying the values of the slope ($p_1$) by the number of electrons in the cation and adding the value of $p_2$ (the susceptibility of anions).

The values thus obtained are given in Table IV. The excellent agreement between the observed and calculated values shows that the plotted points definitely lie on the straight lines drawn for $\chi_m$ against $N$.

The values of the anions obtained from the intercepts $p_2$ were used to calculate the susceptibility of mercuric ion and the values thus obtained are given in the last column of Table IV. The mean of these values calculated for salts of inorganic and organic acids separately comes out to be 40.19 and 38.77, respectively.

The linear relation between $\chi_m$ and $N$ shows that the contribution per electron in the cations belonging to the group of Mg, Zn, Cd, and Hg is a fixed quantity for a particular anion; it also shows that the anion has a fixed value in combination with a particular group of cations. Hence it appears that if these two constants are known for a particular group of the cations, the molecular susceptibilities of the salts of all the elements in that group corresponding to the anion can be easily calculated.

TABLE III.

| Compound | Mercuric compounds $C_1$ | Mercuric compounds $C_2$ | Mercurous compounds $C_1$ | Mercurous compounds $C_2$ |
|---|---|---|---|---|
| Chloride | 0.67 | +5.83 | 0.84 | −47.7 |
| Bromide | 0.67 | +4.60 | 0.84 | −48.7 |
| Iodide | 0.67 | +4.05 | 0.84 | −52.1 |
| Oxalate | 1.43 | −108.7 | 1.42 | −170.5 |
| Formate | 1.43 | −107.2 | 1.42 | −172.5 |
| Acetate | 1.43 | −104.7 | 1.42 | −170.6 |
| Tartrate | 1.43 | −118.3 | 1.42 | −183.1 |
| Benzoate | 1.43 | −118.6 | — | — |
| Palmitate | 1.43 | −112.5 | 1.42 | −174.1 |
| Stearate | 1.43 | −112.1 | 1.42 | −174.3 |

TABLE IV.

| Compounds | $p_1$ | $p_2$ | $\chi_m$ cal. | $\chi_m$ obs. | $\chi_{Hg^{++}}$ |
|---|---|---|---|---|---|
| Chloride | 0.510 | 23.00 | 85.78 | 82.21 | 36.21 |
| Bromide | 0.500 | 33.00 | 105.00 | 105.10 | 39.10 |
| Iodide | 0.550 | 44.00 | — | — | 45.20 |
| Oxide | 0.550 | 6.00 | 48.90 | 50.76 | 44.76 |
| Sulfate | 0.520 | 38.00 | 78.56 | 73.70 | 35.70 |
| Oxalate | 0.420 | 36.00 | 68.76 | 68.63 | 32.63 |
| Formate | 0.430 | 19.50 | 72.54 | 73.00 | 34.00 |
| Acetate | 0.490 | 29.50 | 97.22 | 98.37 | 39.37 |
| Tartrate | 0.530 | 60.00 | 101.34 | 104.70 | 44.70 |
| Benzoate | 0.540 | 68.10 | 178.83 | 175.90 | 39.70 |
| Palmitate | 0.600 | 185.00 | 416.80 | 410.90 | 40.90 |
| Stearate | 0.550 | 208.50 | 459.90 | 457.10 | 40.10 |

For the purpose of comparison, the mean values obtained by the three methods described above are given in columns 2, 3, and 4, respectively, of Table V along with the theoretically calculated values for the mercuric and mercurous ions. The following conclusions can be drawn from Tables V(a) and V(b):

### (a) Mercuric Salts

(i) The value of the mercuric ion obtained by the statistical method from salts of inorganic acids is less

[5] Bhatnagar, Nevgi, and Ohri, Proc. Ind. Acad. Sci. 9A, 86 (1939).

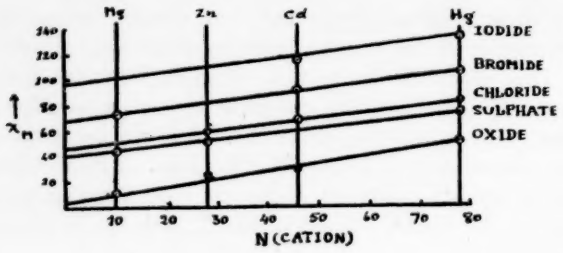


FIG. 5.

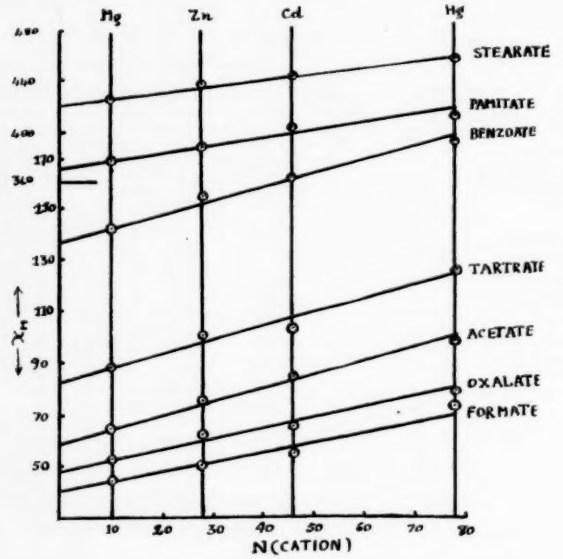


FIG. 6.

than that obtained from salts of organic acids. This is in conformity with the results obtained by Prasad and co-workers[1] for other elements of the second group. The graphical method, however, does not give results of this nature.

(ii) The theoretical values are higher than the experimental values obtained by the authors. The value obtained in the manner suggested by Bhatnagar, Nevgi, and Ohri is higher than the statistical values obtained for salts of inorganic acids but is lower for salts of organic acids.

(iii) The divergence in the values of the susceptibility of the mercuric ion deduced from inorganic salts by the statistical and graphical methods is quite small and hence a mean of the two values can be taken. This comes out to be (38.56) and can serve well as the value of the susceptibility of $Hg^{+2}$ ions for all approximate calculations.

### (b) Mercurous Salts

(i) The value of the susceptibility of the mercurous ion obtained from salts of inorganic acids by the statistical method is lower than that obtained similarly from salts of organic acids [cf. (a) (i) above].

(ii) The value obtained in the manner suggested by Bhatnagar, Nevgi, and Ohri is higher than the value obtained by the statistical method for salts of inorganic acids but is less than that obtained by the statistical method for salts of organic acids.

(iii) The susceptibility values for mercurous ion are in general higher than that of the mercuric ion. This is probably due to the fact that in the mercurous ion two Hg atoms are combined together with common electrons, on account of which the electronic orbits are likely to have greater radii as suggested by Ehrenfest's hypothesis and hence brings about an increase in susceptibility.

### (c) Ionic Radius

The ionic radii of mercuric and mercurous ions were calculated from the susceptibilities of these ions deduced from inorganic and organic salts by the statistical and the graphical methods, from the relation—

$$(\Sigma \bar{r}_e^2)^{\frac{1}{2}} : (\Sigma \bar{r}_t^2)^{\frac{1}{2}} = \bar{r}_e' : \bar{r}_t',$$

where

$\bar{r}_t'$ = the theoretical value of the radius;
$\bar{r}_e'$ = the experimental value of the radius (required);
$\Sigma \bar{r}_e^2$ = the mean square radius obtained from experimental ionic magnetic susceptibility;
$\Sigma \bar{r}_t^2$ = the theoretical mean square radius.

The calculated values of the radii are given in Table VI, together with the values obtained by other methods.


### SUMMARY

Magnetic susceptibilities of a number of pure mercuric and mercurous salts of inorganic and organic acids have been measured by the modified form of a Gouy's balance. Values for the ionic susceptibilities of mercuric and mercurous ions have been deduced from the molecular susceptibilities of the salts on the additivity basis by subtracting all the known values of the susceptibilities of anions reported in literature and finding an arithmetic mean of the values thus obtained (1) from salts of inorganic acids and (2) from those of organic acids, separately. It has been found that the mean values obtained for the mercuric and mercurous ions from


TABLE V(a) (mercuric). Values of $\chi_{Hg^{++}}$.

| Ion | Statistical method (Authors) (i) | Bhatnagar's method (ii) | Graphical method (Authors) (iii) | Theoretical (Slater) | Theoretical (Angus) |
|---|---|---|---|---|---|
| $Hg^{++}$ Inorganic | 36.92 | 44.03 | 40.19 | 47.77 | 47.57 |
| $Hg^{++}$ Organic | 37.21 | 35.20 | 38.77 | — | — |

TABLE V(b) (mercurous).

| Ion | $\chi_{Hg_2^{++}}$ Statistical method (Authors) | Bhatnagar's method |
|---|---|---|
| $Hg_2^{++}$ Inorganic | 37.99×2 | 42.70×2 |
| $Hg_2^{++}$ Organic | 41.97×2 | 41.05×2 |

salts of inorganic acids are numerically higher than those obtained from salts of organic acids but the difference in the values obtained for the mercuric ion from the two types of salts is not statistically significant. The susceptibility of mercurous ion obtained from both the salts of inorganic and organic acids is higher than that for the mercuric ion.

The graph for $\chi_m$ against $N$ (the number of electrons in the molecule) for the mercuric and mercurous salts is definitely non-linear, if all the salts are taken into consideration. This shows that the Ikenmeyer's relation does not hold true. The pattern obtained by plotting $\chi_m$ of all mercuric salts against $N$ is similar to the pattern for the corresponding salts of Mg, Zn, and Cd showing, thereby, a family relationship of Mg, Zn, Cd, and Hg.

A linear relation has been shown to exist between the molecular susceptibilities of salts of Mg, Zn, Cd, and Hg (*ic*) containing the same anion and the number of electrons contained in the cations. The significance of this relation has been discussed and values for the susceptibility of mercuric ion from salts of inorganic and organic acids have been deduced from this relation and have been compared with the values obtained by statistical method.

TABLE VI.

| Ion | Radius | Authors | | Source |
|---|---|---|---|---|
| $Hg^{++}$ | 1.65 | Author | $Hg^{++}$ | from inorganic salts of $Hg^{++}$ (statistical method) |
| | 1.72 | Author | $Hg^{++}$ | from inorganic salts of $Hg^{++}$ (graphical method) |
| | 1.65 | Author | $Hg^{++}$ | from organic salts of $Hg^{++}$ (statistical method) |
| | 1.69 | Author | $Hg^{++}$ | from organic salts of $Hg^{++}$ (graphical method) |
| | 1.12 | Goldschmidt | $Hg^{++}$ | from x-ray data |
| | 0.66 | Wyckoff | $Hg^{++}$ | from x-ray data |
| | 1.10 | Pauling | $Hg^{++}$ | from wave-mechanical concepts |
| | 1.67 | Author | $Hg_2^{++}$ | from inorganic salts of $Hg_2^{++}$ (statistical method) |
| | 1.75 | Author | $Hg_2^{++}$ | from organic salts of $Hg_2^{++}$ (statistical method) |
| | 0.72 | Wyckoff | $Hg_2^{++}$ | from x-ray data |

Ionic radii for the mercuric and mercurous ions have been calculated from the values of the susceptibilities of these ions in combination with inorganic and organic anions.

One of the authors (S.S.D.) acknowledges the benefit of a very helpful discussion with Dr. W. K. Wilmarth of the University of Southern California.

THE JOURNAL OF CHEMICAL PHYSICS VOLUME 17, NUMBER 9 SEPTEMBER, 1949

# The Asymmetric Rotor. VII. Extension of the Calculation of Energy Levels

R. M. HAINER*
*Arthur D. Little, Inc., Cambridge, Massachusetts*

PAUL C. CROSS**
*Brown University, Providence, Rhode Island*

AND

GILBERT W. KING
*Arthur D. Little, Inc., and Research Laboratory of Electronics, Massachusetts Institute of Technology, Cambridge, Massachusetts*

(Received March 1, 1949)

Various methods of computing the energy levels of the asymmetric rotor are reviewed for values of high angular momentum which are required in the interpretation of infra-red and micro-wave spectra. A table of values of $J=11$ and 12 is given and over the whole range of asymmetry $-1\leqslant\kappa\leqslant 1$. Methods of using the Correspondence Principle, Mathieu functions, harmonic oscillator matrices, and power series expansions are discussed, and this survey indicates there is always a region of some degree of asymmetry where the exact value has to be obtained from the rigorous matrix-mechanical formulation. Methods of obtaining energy values for small intervals in $\kappa$ from existing tables are also discussed.

## THE PROBLEM OF EXTENDING THE ENERGY-LEVEL TABLES

IN spite of a voluminous literature, the energy levels of the rigid asymmetric rotor remain of considerable interest in the analysis of spectra of polyatomic molecules. The energy levels are difficult to calculate and, to warrant further effort, it is desirable to know exactly what uses would be made of them. The actual levels of a molecule can be simply calculated from those of a rotor with reciprocal moments of inertia $-1$, $\kappa$, 1, where $-1\leqslant\kappa\leqslant 1$ is a parameter of asymmetry. The exact values obtained by the New Quantum Theory have been[1] called $E(\kappa)_{J,K_{-1},K_1}$: they are characterized by the number $J$, quantizing the total angular momentum, and by a bipartite index $K_{-1}$, $K_1$ giving the true internal quantum numbers in the limiting cases of prolate ($\kappa=-1$) and oblate ($\kappa=1$) symmetry. In this paper we shall find it more convenient to refer to energy ratios $\eta_J(\kappa)=E(\kappa)/J(J+1)$ and to quantum-number ratios $\lambda=K/[J(J+1)]^{\frac{1}{2}}$, introduced by a study of high $J$ values.[2]

## RANGE OF VALUES

An advantage of the quantities $\eta$ and $\lambda$ is that like $\kappa$ they are bounded: $\lambda$ varies from 0 to 1 and $\eta$ varies from $-1$ to $+1$. A study of the convergence at high $J$ has brought to light the fact that at all $J$ the symmetry of $\eta(\kappa,\lambda)$ should be considered to be not about the value $\kappa=0$ (which is the most convenient in presenting tables) but around the line $\eta=\kappa$ which in the limit is $\pm\cos\lambda\pi$. In the following we discuss the properties $\eta(\kappa,\lambda)$ only in the triangular region of $-1\leqslant\kappa\leqslant 1$ and $0<\lambda<1$, $\eta>\kappa$ (see Fig. 2 and reference 2, Figs. 1 and 2). Values for the other half are obtained by the relation

$$\eta(\kappa,\lambda)=-\eta(-\kappa,1-\lambda). \tag{1}$$

The quantity $\eta(\kappa,\lambda)$ has an advantage over $E(\kappa)$ in that it can be considered, for purposes of many discussions, independent of $J$, and in fact converges to a calculable limit, $\eta_\infty$, at infinite $J$. For these discussions, each block of our tables of $E_{K_{-1},K_1}{}^J(\kappa)$ should be divided by $J(J+1)$ and $K_{-1}$ by $[J(J+1)]^{\frac{1}{2}}$ to give $\lambda$ decreasing down the table. At some point, for each $\kappa$, we reach the condition $\eta=\kappa$, so that entries below that can be considered as values of positive $\kappa$ and $\lambda=K_1/[J(J+1)]^{\frac{1}{2}}$. The absolute value of the $K$'s is implied throughout this paper.

## SIGNIFICANT FIGURES

The number of significant figures in $\kappa$ probably need be no more than three, since the *rigid* rotor is only an approximation. The quantum number ratio $\lambda$ is always known precisely.

The positions of spectral lines will be known to a certain number of significant figures in wave numbers, depending on the experimental technique. In microwave spectra this may be of the order of six. Hence, if the rigid rotor is applicable or used as a first approximation, the energy levels should be calculable to one more place. This means $E(\kappa)$ should be known to $7+\log_{10} a$, where $a$ is $h/8\pi^2c$, or $27.9865\times10^{-40}$, divided by the least moment of inertia in units of $10^{-40}$ g cm$^2$. Finally $\eta$ requires in addition $\log_{10} J(J+1)$ more significant figures, i.e., needs to be determined with higher and higher accuracy as $J$ increases.

* This paper in part is based on a portion of a thesis submitted in June 1947 by R. M. Hainer in partial fulfillment of the requirements for the degree of Doctor of Philosophy at Brown University.

** Present address, Chemistry Department, University of Washington, Seattle, Washington.

[1] King, Hainer, Cross, J. Chem. Phys. **11**, 27 (1943).

[2] G. W. King, J. Chem. Phys. **15**, 820 (1947). A valuable discussion of the tables in this paper has been given by A. Fletcher, Math. Tables and other Aids to Computation **3**, 27 (1948).

### Extension of Tables to Higher $J$ and Smaller Intervals in $\kappa$

For molecules with small moments of inertia (such as the water-type molecules) the infra-red spectra involve only levels up to about $J=12$, because of Boltzmann factors. A few of higher $J$ are sometimes required, but can be obtained accurately by extrapolation. For this application the original table of $E(\kappa)$ published by us,[1] going to $J=10$ is not quite adequate, and in this paper we supply values of $E(\kappa)$ for $J=11$ and 12 (see Appendix I). The fact that these tables apply to *rigid* rotors is not a serious handicap in analysis of infra-red absorption spectra, since the principal lines arise from levels of low $K_{-1}$ which can be well fitted by rigid-rotor values.[3] This also applies, by and large, to microwave spectra.[4] In the emission spectra of these molecules high $K_{-1}$ levels are involved, which are subject to substantial centrifugal distortion, so the tables are inadequate for direct application, but remain a basis for further elaboration of the theory.

Other simple molecules such as $NO_2$, $SO_2$, $O_3$, etc., have well populated levels of higher $J$'s, whose energies are necessary to interpret their spectra. Microwave spectra, likewise, may require a knowledge of the energies to values of $J=20$ or 40 and an accuracy of eight decimal places.

The original table, and the one given here for $J=11$ and 12, were prepared for intervals of 0.1 in the asymmetry parameter $\kappa$, which is adequate for infra-red and possibly visible or ultraviolet spectra. The high precision of microwave measurements demands the calculation of the energies to finer intervals of $\kappa$, probably to 0.001. This can be achieved by the explicit formulae for the energies for most levels up to $J=4$. In Appendix II we extend this procedure by giving the explicit trigonometric formulae for the energies up to some levels of $J=7$.

In general, however, the problem is to obtain energy levels of high $J$ (say to 40) and intervals of $\kappa$ perhaps of 0.001. An exact determination of these $10^6$ energy levels by the New Quantum Theory could be embarked upon by modern computing methods. The results would consist of a bulky table, of which as usual most of the entries would never be used at all. It would be preferable to obtain the levels by analytical methods as far as possible.

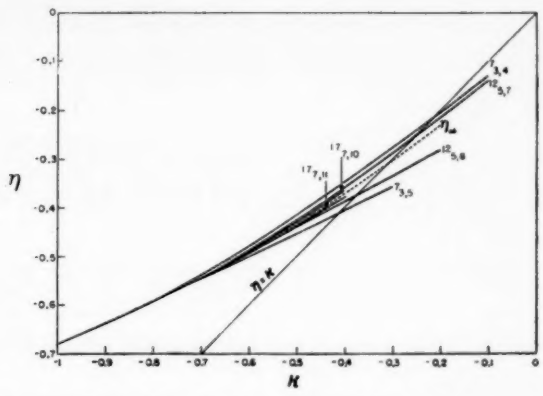


FIG. 1. Illustration of convergence of levels with same $K_{-1}$ value to the limit given by the Correspondence Principle; and of the separation of these pairs at the boundary $\eta=\kappa$.

We have already shown[2] that according to the Correspondence Principle levels of high $J$ converge to values (say $\eta_\infty$) obtained from the inversion of the complete elliptic integral of the third kind, except in a region (ultimately infinitely narrow) around a line of singularities, at $\eta=\kappa$. In the present paper, we describe how closely the levels from the Correspondence Principle agree with the New-Quantum-Theory value over the whole range of internal quantum number $(K_{-1}, K_1)$ and asymmetry $(\kappa)$.

It has also been shown[5] that the energy levels can be obtained from the characteristic values of the Mathieu functions. But here again, it is necessary to know the accuracy of this approximation which (as in the case of the elliptic functions) varies enormously with $K_{-1}$ (or $K_1$) and $\kappa$. The same applies to a new method[5a] using harmonic-oscillator functions.

Finally, it is desirable to know the errors involved in interpolating for $\kappa$ throughout the whole range in each of the methods used for determining the energy levels.

The results of this survey indicate that the levels can be obtained for any value of $J$, $K$, and $\kappa$ to various degrees of approximation, of error stated in this paper. In many cases, namely those lying in a relatively small region around $\eta\sim\kappa$, the error will be too large for the application. The only recourse will be successive substitution of the estimated value in the continued fraction of the New Quantum Theory.[1] Until some new analytical approach is discovered (such as with Lamé functions) it would be desirable to make a table of the individual levels in the region where the error is greater than one part in $10^6$ by punched-card procedures.

To calculate an energy level, one first sees if any of the approximations (elliptic integrals, Mathieu functions, harmonic-oscillator matrices, or various power

[3] For example see the well-known analyses of $H_2O$, R. Mecke et al., Z. Physik **81**, 313, 445, 465 (1933); of $D_2O$, Fuson, Randall, and Dennison, Phys. Rev. **56**, 982 (1939); of HDO, L. Herzberg, Z. Physik **107**, 549 (1937); and of $H_2S$, P. C. Cross, Phys. Rev. **47**, 7 (1935), R. M. Hainer and G. W. King, J. Chem. Phys. **15**, 89 (1947). Deviations from the levels of the rigid rotor have been discussed by H. H. Nielsen, Phys. Rev. **59**, 565 (1941), **62**, 422 (1942), and by F. P. Dickey and H. H. Nielsen, Phys. Rev. **73**, 1164 (1948).

[4] As in HDO, King, Hainer and Cross, Phys. Rev. **71**, 433 (1947) and M. W. P. Strandberg, private communication; and in ethylene oxide, Shulman, Daily and Townes, Phys. Rev. **74**, 846 (1948). Dakin, Good, and Coles, Phys. Rev. **71**, 640 (1947) have shown that centrifugal distortion is negligible in the symmetric rotor COS where only valence bonds would be stretched. S. Golden, Ph.D. Thesis, Harvard University, 1948, has shown the rigid rotor is an excellent approximation in heavy bent molecules such as $SO_2$.

[5] S. Golden, J. Chem. Phys. **16**, 78 (1948).

[5a] S. Golden and J. K. Bragg, J. Chem. Phys. **17**, 439 (1949).

TABLE I. $J=12$.

| $K_{-1}$, $K_1$ | | $\lambda$ | $\kappa=-0.9$ | | | | $\kappa=-0.5$ | | | | $\kappa=0$ | |
|---|---|---|---|---|---|---|---|---|---|---|---|---|
| | | | $\eta J$ | $\eta J-\eta_\infty$ | $\eta J-\eta M$ | $\eta J-\eta H$ | $\eta J$ | $\eta J-\eta_\infty$ | $\eta J-\eta M^*$ | $\eta J-\eta H$ | $\eta J$ | $\eta J-\eta_\infty$ | $\eta J-\eta H$ |
| 12 | 0 | .960 76892 | .850 05154 | .000 001 | −.000 121* | .000 000 | .866 82814 | .000 035 | −.003 374 | .000 000 | .891 51532 | .000 169 | .000 000 |
| 12 | 1 | .960 76892 | .850 05154 | .000 001 | −.000 121* | .000 000 | .866 82814 | .000 035 | −.003 374 | .000 000 | .891 51532 | .000 169 | .000 000 |
| 11 | 1 | .880 70485 | .562 65596 | .000 002 | −.000 050* | .000 000 | .611 73872 | .000 048 | −.001 378 | .000 000 | .684 34321 | .000 237 | .000 001 |
| 11 | 2 | .880 70485 | .562 65596 | .000 002 | −.000 050* | .000 000 | .611 73872 | .000 048 | −.001 378 | .000 000 | .684 34308 | .000 237 | .000 001 |
| 10 | 2 | .800 64077 | .300 26494 | .000 004 | .000 016* | .000 000 | .379 21340 | .000 106 | .000 455 | .000 000 | .497 05660 | .000 542 | .000 004 |
| 10 | 3 | .800 64077 | .300 26494 | .000 004 | .000 016* | .000 000 | .379 21340 | .000 106 | .000 455 | .000 000 | .497 05096 | .000 536 | −.000 001 |
| 9 | 3 | .720 57669 | .062 88346 | .000 006 | .000 075* | .000 000 | .169 39878 | .000 144 | .002 095 | .000 002 | .330 52603 | .000 847 | .000 154 |
| 9 | 4 | .720 57669 | .062 88346 | .000 006 | .000 075* | .000 000 | .169 39872 | .000 144 | .002 095 | .000 002 | .330 37910 | .000 700 | .000 007 |
| 8 | 4 | .640 51262 | −.149 47981 | .000 006 | .000 128* | .000 000 | −.017 45109 | .000 210 | .003 563 | .000 014 | .187 23846 | .002 414 | .001 585 |
| 8 | 5 | .640 51262 | −.149 47981 | .000 006 | .000 128* | .000 000 | −.017 45462 | .000 206 | .003 570 | .000 010 | .185 05872 | .000 234 | −.000 594 |
| 7 | 5 | .560 44854 | −.336 80942 | .000 012 | .000 176* | .000 000 | −.180 82000 | .000 394 | .004 796 | .000 107 | .075 89628 | .010 712 | .010 504 |
| 7 | 6 | .560 44854 | −.336 80942 | .000 012 | .000 176* | .000 000 | −.180 91295 | .000 301 | .004 893 | .000 014 | .058 90282 | −.006 282 | −.006 489 |
| 6 | 6 | .480 38446 | −.499 07551 | .000 020 | .000 218* | .000 000 | −.319 06192 | .001 454 | .005 493 | .001 056 | 0 | .000 000§ | .025 170 |
| 6 | 7 | .480 38446 | −.499 07558 | .000 020 | −.000 110** | .000 000 | −.320 54955 | −.000 034 | .006 253 | −.000 432 | | | |
| 5 | 7 | .400 32038 | −.636 21064 | .000 072 | −.000 076** | .000 003 | −.425 45474 | .009 075 | .005 215 | .007 659 | | | |
| 5 | 8 | .400 32038 | −.636 21474 | .000 067 | −.000 076** | −.000 001 | −.438 32917 | −.003 799 | .008 144 | −.005 216 | Negative of above values, interchanging | | |
| 4 | 8 | .320 25631 | −.747 97647 | .000 226 | −.000 047** | .000 084 | *−.495 64577* | *−.015 796* | .006 239 | *.019 259* | $K_1$ and $K_{-1}$. | | |
| 4 | 9 | .320 25631 | −.748 12462 | .000 078 | .000 000 | −.000 065 | −.544 22449 | .005 153 | .010 433 | .007 285 | § Special case. | | |
| 3 | 9 | .240 19223 | −.832 65679 | .001 817 | .000 000 | .001 419 | −.560 94705 | −.011 570 | .009 600 | −.009 437 | | | |
| 3 | 10 | .240 19223 | −.835 38417 | −.000 910 | .000 000 | −.001 309 | −.654 59942 | −.001 046 | .011 398 | .000 752 | | | |
| 2 | 10 | .160 12815 | −.885 *12090* | *−.006 997* | .000 000 | *.006 200* | −.656 58481 | −.003 032 | .011 382 | −.001 233 | | | |
| 2 | 11 | .160 12815 | −.903 63647 | .007 447 | .000 000 | .010 068 | −.780 47955 | −.000 696 | .009 121 | .000 033 | | | |
| 1 | 11 | .080 06408 | −.919 86256 | −.008 779 | .000 000 | −.006 158 | −.780 58237 | −.000 798 | .009 134 | −.000 070 | | | |
| 1 | 12 | .080 06408 | −.967 13109 | −.000 604 | .000 000 | .000 759 | −.923 96256 | −.000 501 | .002 700 | .000 000 | | | |
| 0 | 12 | 0 | −.968 66378 | −.002 137 | .000 000 | −.000 773 | −.923 96462 | −.000 503 | .002 701 | −.000 002 | | | |

Differences at $J=12$ between exact (New Quantum Theory) values of the energy $\eta J(\kappa, \lambda)$ and the approximation by the Correspondence Principle, $\eta_\infty$, and by Mathieu functions, $\eta M$, and by harmonic-oscillator functions, $\eta H$.

The limited range of tables does not permit first- and second-order correction to $\eta M$ in levels marked with an asterisk, nor second-order correction in levels marked with two asterisks.

The exact energy levels are known to seven decimals. Both $\eta M$ and $\eta H$ can be calculated to more decimals. Entries 0.000 000 bound the regions where this would be profitable. (Estimates of $\eta_\infty$ are limited to six decimals by Heuman's table of the complete elliptic integral of the third kind.)

The *italics* mark the boundary $\eta=\kappa$. For $\eta J$, as calculated by the New Quantum Theory, and for $\eta M$, this is immaterial. For $\eta_\infty$ it is essential, and values below the line are calculated for $\kappa$ of opposite sign, and $\lambda$ given by $K_1$ (not $K_{-1}$ as above the line), i.e., by Eq. 1. The formulae for $\eta H$ likewise should not be used for levels below the diagonal, when using $K_{-1}$. The values in the table below the horizontal line were in fact calculated with $K_1$ and opposite sign of $\kappa$.

series) will give the result to sufficient accuracy, by means of the figures and tables described below. If none do, the continued-fraction method will ultimately have to be used. Now repeated substitution in the continued-fraction method, if written out algebraically, would be extremely complicated. However, as a computing scheme it is quite straightforward, and, as a matter of fact, competes favorably with the other methods, although the latter may have more elegant algebraic expression. Thus if the continued fraction method is to be used at all, it might as well be used throughout, since the approximation methods as a rule involve a computing schedule more complicated than two or three substitutions in the continued fraction (assuming it has to be set up anyway). The only exception is the method using the Correspondence Principle, for here the arithmetic needed for this approximation is less than the equivalent substitution in the continued fraction.

## CONVERGENCE OF $\eta_J$ AT HIGH J

Of the various methods approximating $\eta$, the simplest one arithmetically is by means of the table deduced from the Correspondence Principle.[2] This treatment is also the only one surveying the whole range of $\kappa$ and $\lambda$, and forms a basis for comparison of the various methods.

In reference 2, Fig. 2, the relationship between the New-Quantum-Theory and Correspondence-Principle values ($\eta_J$ and $\eta_\infty$) were plotted for $J=3$ to show the geometrical relationships. At higher $J$'s where the Correspondence Principle can be expected to be of real value the same general relationship holds, but of course there are more (namely $2J+1$) levels in the $\eta$, $\kappa$ diagram and the differences $\eta_J-\eta_\infty$ are much smaller. As an example, the convergence of $\eta_J$ to $\eta_\infty$ is indicated in Fig. 1 for the levels $7_{3,4-5}$, $12_{5,7-8}$, and $17_{7,10-11}$. For each of these levels $\lambda$ is very close to 0.4, for which value $\eta_\infty$ can be obtained directly from Table I in reference 3. It is seen that $\eta_\infty$ is a good approximation in some places, yet always becomes bad at the diagonal $\eta=\kappa$.

Successive levels (for a given J) cut the diagonal $\eta=\kappa$ at approximately equal intervals. This cannot be shown very easily in Fig. 1, but is shown in Fig. 2 of reference 2. Thus the worst error (at the boundary $\eta=\kappa$) is in fact of the *order* of the splitting between the two levels with same $K_{-1}$ (or $K_1$ when approaching in the region $\eta<\kappa$).

The differences $\eta_J-\eta_\infty$ are given numerically in Table I for all the $J=12$ levels for representative values of $\kappa$. The values are presented for all levels at $\kappa=-0.9$, $-0.5$, and 0. Actually $\eta_\infty$ of low $K_{-1}$, where $\eta<\kappa$, have to be calculated as $-\eta_\infty$ for the $\lambda$ obtained from $K_1$, at values $\kappa=+0.9$ and $+0.5$ respectively—hence the table really covers the whole range of $\kappa$. At $\kappa=0$ the levels are symmetrically placed around $\eta=0$.

Our original table[1] of $E(\kappa)$ is composed of blocks, one for each $J$. The numbers in each block can be divided by $J(J+1)$, so that each block reduces to a $\lambda$, $\kappa$ diagram such as Fig. 2, where the results of calculations $\eta_J-\eta_\infty$ such as those given in Table I are indicated schematically. The approximation $\eta_\infty$ is good in the region $A$, considerably worse in a region $B$, bad in $C$, and very bad in $D$ and $E$.

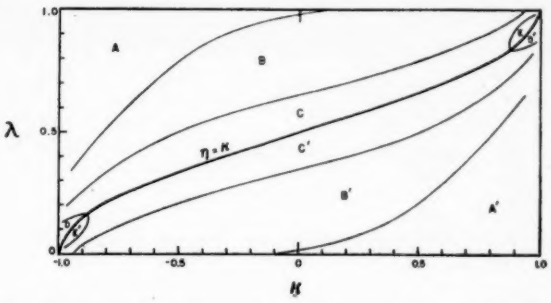


FIG. 2. Sketch of the regions of error expected in approximating $\eta$; and also in differencing $\eta$.

## CHARACTERISTIC VALUES OF MATHIEU FUNCTIONS

Table I also gives $\eta_J-\eta_M$ where $\eta_M$ is the approximation made with Mathieu functions.[6] This error is very small at low $K$ values, in region $D$ of Fig. 2, just where $\eta_J-\eta_\infty$ is worst. Hence $\eta_M$ complements $\eta_\infty$ very conveniently. Elsewhere in the diagram it is not significantly better than $\eta_\infty$ to warrant the additional computation. At $\kappa=0$ it cannot be made at all. When more extensive tables of the Mathieu functions are available, the range of applicability will be larger.

## HARMONIC OSCILLATOR FUNCTIONS

To complement the last method Golden and Bragg[5a] have developed another scheme which gives excellent values at high $K$'s. We have calculated their approximation, $\eta_H$, and give $\eta_J-\eta_H$ in Table I. The range of application is shown graphically in Fig. 2 as region $A$.

## FIRST-ORDER CORRECTIONS

The discrepancy in the "zero'th order" approximation by analytical functions, shown qualitatively in Fig. 2 and quantitatively for certain regions in Table I, can be systematized and used as a first-order correction to $\eta$. In some cases this will give a sufficiently accurate approximation to $\eta_J$, but in general $\eta_J$ will have to be found by the exact procedure of the New Quantum Theory. The first-order approximation saves a number of successive substitutions in the method with continued fractions and for this reason a detailed discussion of the use of $\eta_\infty$ follows. Similar studies of $\eta_M$ and $\eta_H$ could be made.

The corrections to $\eta_\infty$ can be expressed graphically as $\eta_J-\eta_\infty$ for various values of $\lambda$ and $\kappa$ (both in inter-

[6] A comparison of $\eta_J$ and $\eta_M$ for some levels of $J=10$ and $\kappa=-0.8$ and $-0.9$ can be made from Table V of reference 5. Column 3, line 2 of this table should read 105.67708.

TABLE II.

| $K_{-1}$ \ $\kappa$ | −0.9 | −0.8 | −0.7 | −0.6 | −0.5 | −0.4 | −0.3 | −0.2 | −0.1 |
|---|---|---|---|---|---|---|---|---|---|
| 12 | | | | | | | | | |
| | | | | | | | | | .000 0001 |
| 11 | | | | | | | | | .000 0000 |
| | | | | | | | | | — |
| | | | | | | | .000 0001 | .000 0003 | .000 0015 |
| 10 | | | | | | | .000 0001 | .000 0003 | .000 0013 |
| | | | | | | | *1.0* | *1.0* | *1.2* |
| | | | | | .000 0001 | .000 0005 | .000 0029 | .000 0120 | .000 0443 |
| 9 | | | | | .000 0001 | .000 0005 | .000 0029 | .000 0122 | .000 0455 |
| | | | | | *1.0* | *1.0* | *1.0* | *0.985* | *0.974* |
| | | | .000 0001 | .000 0005 | .000 0035 | .000 0184 | .000 0758 | .000 2635 | .000 8019 |
| 8 | | | .000 0000 | .000 0005 | .000 0037 | .000 0195 | .000 0825 | .000 2978 | .000 9543 |
| | | | — | *1.0* | *0.95* | *0.944* | *0.919* | *0.884* | *0.840* |
| | | .000 0001 | .000 0020 | .000 0171 | .000 0929 | .000 3769 | .001 2359 | .003 4274 | .008 2003 |
| 7 | | .000 0001 | .000 0020 | .000 0180 | .000 1016 | .000 4333 | .001 5246 | .004 6697 | .012 8849 |
| | | *1.0* | *1.0* | *0.950* | *0.914* | *0.870* | *0.811* | *0.734* | *0.636* |
| | .000 0001 | .000 0047 | .000 0599 | .000 3667 | .001 4876 | .004 5668 | .011 2437 | .022 8296 | |
| 6 | .000 0001 | .000 0049 | .000 0635 | .000 4092 | .001 7969 | .006 2023 | .018 1577 | .047 1880 | |
| | *1.0* | *0.96* | *0.943* | *0.896* | *0.828* | *0.736* | *0.619* | *0.484* | |
| | .000 0041 | .000 1401 | .001 1010 | .004 5810 | .012 8744 | .027 1476 | | | |
| 5 | .000 0041 | .000 1471 | .001 2431 | .005 8451 | .019 9654 | .055 7881 | | | |
| | *1.0* | *0.952* | *0.886* | *0.784* | *0.645* | *0.487* | | | |
| | .000 1481 | .002 3343 | .010 5647 | .026 7459 | | | | | |
| 4 | .000 1521 | .002 6311 | .014 4295 | .049 5113 | | | | | |
| | *0.974* | *0.887* | *0.732* | *0.540* | | | | | |
| | .002 7274 | .017 3794 | | | | | | | |
| 3 | .002 9663 | .024 9957 | | | | | | | |
| | *0.919* | *0.695* | | | | | | | |

vals of 0.1), of which an example is given in Fig. 3. It is seen that the magnitude of $\eta_J-\eta_\infty$ for any $\lambda$ decreases with $\kappa$. For any $\kappa$, it decreases as $\lambda$ increases. It is important to note that $\eta_\infty$ does not always lie between the two exact levels which converge to it. This is shown more clearly when $\eta_J-\eta_\infty$ for various $\kappa$'s and a given $J$ is plotted against $\lambda$. Fig. 4 gives these curves for $J=12$. As $J$ increases, the curves for a given $\kappa$ retain their shape quite closely, but get pushed to lower $\lambda$'s, as indicated by the three $\lambda$ scales on the figure. Thus Fig. 4 gives roughly the error $\eta_J-\eta_\infty$ for all $J$'s as far as we have investigated them. One could attempt to fit these curves analytically, to extrapolate to high $J$'s, but it is unlikely that this can be done with any elementary functions, for we must remember that $\eta_J$ are eigenvalues of Lamé functions, and probably only expressible in terms of theta functions. The curves in Fig. 3 approach the origin much faster than exponentially. The most reliable study of them is empirical. Every time a new level is computed (say at $J=20$) its value can be used to improve the graphs for subsequent use. If $\eta_J-\eta_\infty$ is plotted as a surface in three dimensions against $\lambda$ and $J$, Fig. 3 is the projection of lines of constant $\kappa$ on the $(\eta_J-\eta_\infty)$, $J$ axes; Fig. 4 is the projection on the $(\eta_J-\eta_\infty)$, $\lambda$ axes.

In Fig. 3 the outermost curve drawn (for $\lambda=0.4$) is for $\kappa=-0.4$, since at $\kappa=-0.3$ we would be beyond the boundary $\eta=\kappa$. Actually, the maximum error occurs when $\eta=\kappa=-\cos\lambda\pi$($\lambda$ referring to $K_{-1}$), in this case for $\kappa=-\cos 0.4\pi=-0.31$. The curve of errors for this value of $\kappa$ would lie considerably outside the last drawn, $\kappa=-0.4$.

In Fig. 4 the curves rise to an envelope somewhat outside the scope of the diagram, giving maximum error $\eta_J-\eta_\infty$ possible, namely the separation of levels on the diagonal $\eta=\kappa$, mentioned previously. This envelope shrinks proportionally with $J$ as $J$ increases, since the number of levels cutting the line $-1<\eta=\kappa<1$ increases linearly with $J$, as $2J+1$.

These plots show then that the Correspondence Principle gives an approximation in error at most by an amount of the order of magnitude but, in value, less than the separation of the unpaired levels. Since in the New Quantum Theory only every fourth level belongs to any one submatrix for which roots have to be found, the approximation $\eta_\infty$ already permits convergence to the correct value, if the method of Eq. (40)

TABLE II. (*Continued*)

| 0 | 0.1 | 0.2 | 0.3 | 0.4 | 0.5 | 0.6 | 0.7 | 0.8 | 0.9 |
|---|---|---|---|---|---|---|---|---|---|
| | | .000 0001<br>.000 0000<br>— | .000 0001<br>.000 0001<br>*1.0* | .000 0005<br>.000 0002<br>*2.5* | .000 0021<br>.000 0008<br>*2.6* | .000 0092<br>.000 0027<br>*3.4* | .000 0437<br>.000 0089<br>*4.91* | .000 2324<br>.000 0288<br>*8.069* | .001 5327<br>.000 0918<br>*16.696* |
| .000 0001<br>.000 0001<br>*1.0* | .000 0004<br>.000 0004<br>*1.0* | .000 0021<br>.000 0015<br>*1.4* | .000 0077<br>.000 0051<br>*1.5* | .000 0283<br>.000 0168<br>*1.68* | .000 1028<br>.000 0532<br>*1.93* | .000 3722<br>.000 1626<br>*2.289* | .001 3599<br>.000 4848<br>*2.805* | .004 9592<br>.001 4180<br>*3.497* | .016 2261<br>.004 0927<br>*3.965* |
| .000 0056<br>.000 0052<br>*1.1* | .000 0206<br>.000 0182<br>*1.13* | .000 0695<br>.000 0597<br>*1.16* | .000 2223<br>.000 1843<br>*1.206* | .000 6789<br>.000 5430<br>*1.250* | .001 9854<br>.001 5406<br>*1.289* | .005 4919<br>.004 2417<br>*1.295* | .013 7678<br>.011 4073<br>*1.207* | | |
| .000 1469<br>.000 1525<br>*0.963* | .000 4453<br>.000 4717<br>*0.944* | .001 2495<br>.001 3666<br>*0.914* | .003 2541<br>.003 7571<br>*0.866* | .007 7921<br>.009 9002<br>*0.787* | .016 7226<br>.025 2103<br>*0.663* | | | | |
| .002 1797<br>.002 7888<br>*0.782* | .005 3321<br>.007 5792<br>*0.704* | .011 6774<br>.019 4362<br>*0.601* | .022 5826<br>.047 5629<br>*0.475* | | | | | | |
| .016 9935<br>.032 7964<br>*0.518* | .030 5382<br>.078 3276<br>*0.390* | | | | | | | | |

Example of splitting of levels, for $J=12$, at $\kappa=-0.9(0.1)+0.9$ for each $K_{-1}$. For each value of $K_{-1}$ and $\kappa$ there are three numbers. The first is the exact splitting $\Delta\eta_J$ obtained from the individual levels as calculated by the New Quantum Theory (Appendix I). The second entry is that calculated by the Wang splitting formula, $\Delta\eta$. The third entry, in italics, is the ratio $\Delta\eta_J/\Delta\eta$. There are no entries in the upper left-hand corner, because they are less than $10^{-7}$, the accuracy to which $\eta_J$ were calculated. There are no entries on the lower right-hand corner since this is below the diagonal $\eta=\kappa$. Levels here pair on $K_1$, and their splitting is obtained by symmetry, using a value of $K_{-1}=K_1$, but with $\kappa$ of opposite sign.

of reference 1 is adhered to. The use of additional corrections by Fig. 3 speeds up the convergence.

The only difficulty in preparing these plots was to get the difference for the definite value of $\lambda=0.1\times n$, $n$ being an integer. This of course never obtains for any real level, since $\lambda$ is irrational. It is possible to take $\eta_J$ for a real level (and hence a given $\lambda$) and "correct" it to give an $\eta_J$ that a quantized level of that value of $J$ would have had if $n$ had been integral. To do this we made use of the fact that $\Delta\eta_J/\Delta\lambda$ (between quantized levels, of integral $K$'s) is well approximated by $\partial\eta_\infty/\partial\lambda$, computed at the average value $\lambda$ for the two levels in question from the first and second derivatives in Table I, reference 2. This comparison was made for several levels, and showed that $(\partial\eta_\infty/\partial\lambda)$ at the average $\lambda$ can be used for graphical results, provided care is taken near the boundary. To summarize, the curves in Figs. 3 and 4 were obtained by taking $\eta_J$'s for those levels of $J\leqslant 12$ for which $\lambda/0.1$ is approximately an integer; and correcting them to make $\lambda/0.1$ an integer by the known values of $\partial\eta_\infty/\partial\lambda$. These tables therefore can be used as second approximations to $\eta_J$.

## SPLITTING OF PAIRED LEVELS

Figures 3 and 4 also indicate a further technique in calculating levels of high $J$. For a given value of $\lambda$ there are two New-Quantum-Theory levels shown in the Figures (generally above and below the line $\eta_J-\eta_\infty=0$). These are called paired levels because they converge to the same doubly degenerate level of the symmetric rotor in the limit $\kappa=-1$. (The other case $\kappa=+1$ is obtained by symmetry around $\eta=\kappa$.) Figs. 3 and 4 show that, where the splitting is large, it is of the order of the error $\eta_J-\eta_\infty$. For levels of high $J$, or high $\lambda$, where the two curves lie on the upper side of the line $\eta_J-\eta_\infty=0$, the splitting gets very much smaller than $\eta_J-\eta_\infty$. Now Wang[7] has calculated the splitting of the symmetric-rotor levels characteristic of the New Quantum Theory

[7] S. C. Wang, Phys. Rev. **34**, 243 (1929).

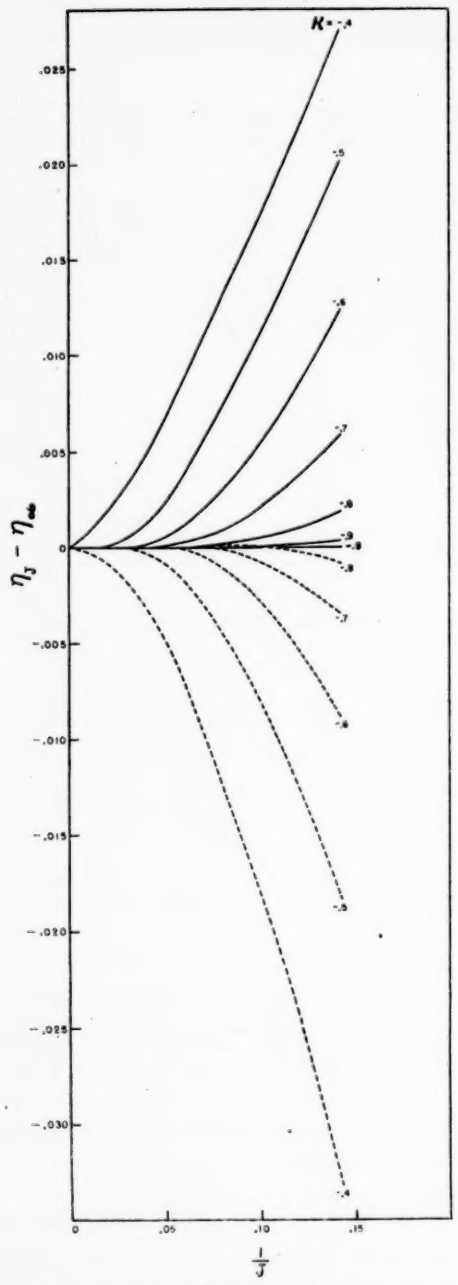


FIG. 3. Convergence of actual levels ($\lambda=0.4$) to $\eta_\infty$, as $J$ increases, for various values of $\kappa$.

to a first approximation by high order perturbation theory. For the region $\eta>\kappa$, where $\kappa$ approaches $-1$, his formula can be written

$$|\Delta\eta| = A(\kappa, K)B(J, K). \tag{2}$$

The first factor is independent of $J$,

$$A(\kappa, K)=16(\beta/8)^K/(1-\beta), \tag{3}$$

$\beta$ being Wang's parameter of asymmetry $(\kappa+1)(\kappa-3)$; the second is independent of $\kappa$,

$$B(J, K)=\binom{J+K}{K}\binom{J}{K}\lambda^2 \tag{4}$$

Table II gives the actual and calculated splitting, and their ratio, for $J=12$ over the whole range of $K$ and $\kappa$. We see that where the splitting is large, $\Delta\eta\sim\eta_J-\eta_\infty$, and that the Wang formula is not particularly good, so that the first-order corrections are obtained most easily from Fig. 3 or 4, and no use can be made of Eq. (2). On the other hand, soon after $\eta_J-\eta_\infty$ is positive for both levels, the Wang formula can be used with advantage. One level is calculated by $\eta_\infty$, the corrections added from Fig. 3 or 4, and an accurate value of $\eta_J$ obtained from the continued-fraction method. To get the other level

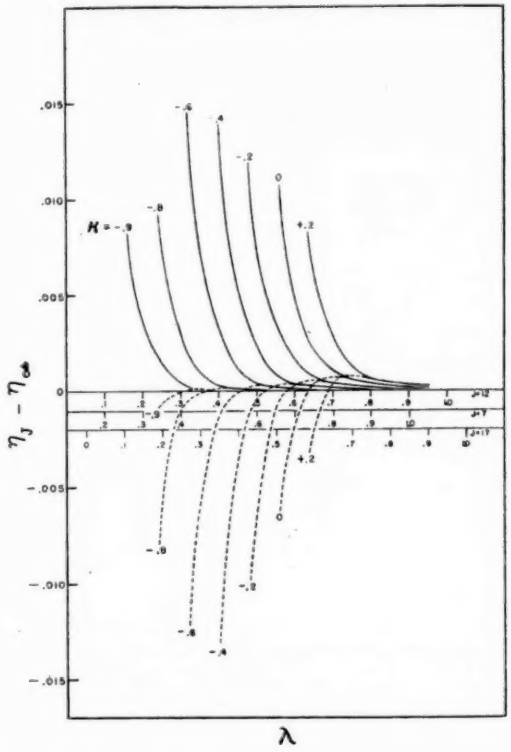


FIG. 4. The error of the Correspondence-Principle approximation $\eta_J-\eta_\infty$ as a function of $\lambda$ and $\kappa$. The curves as drawn are for $J=12$. Curves for $J=7$ and 17 are approximately the same, but shifted to higher and lower $\lambda$ values, respectively, as shown by the additional abscissa scales.

of the pair, the $\Delta\eta$ is calculated to $K$'th order approximation by (2) and added to it with appropriate sign. The resulting value can then be tested in its continued fraction.

To facilitate these calculations, tables of $A(\kappa, K)$ and $B(J, K)$, $-1<\kappa<1$, $12\leqslant J\leqslant 20$, and $K\leqslant J$ are given in Appendices III and IV, from which $\Delta\eta$ can be obtained by multiplication.

## POWER SERIES

Power series expansions in terms of a parameter of asymmetry have been suggested[8] as means of calculating the energy levels. A typical one given in reference

[8] See reference 1, Appendices II and III; also abstracts by E. E. Witmer, Phys. Rev. 74 1247, 1250 (1948).

1 can be considered as perturbation of the prolate symmetric rotor ($\kappa=-1$) by an expansion in powers of $\delta=(\kappa-1)/2$. This expansion gives excellent values at high $\lambda$'s for quite large values of $\delta$; but the series are worthless even for very small $\delta$'s when $\lambda$(i.e., $K_{-1}$) is small, i.e., even for very small deviations from the symmetric-rotor moments.[9] The reason for this is that the boundary $\eta=\kappa$ is a diagonal in the $\eta$, $\kappa$ plane and hence close to $\delta=0$ ($\kappa=-1$) at low $\lambda$, in fact is at $\delta=0$ when $\lambda=0$. In the limit of infinite $J$ there is a singularity at $\eta=\kappa$, and at any finite $J$ an energy level follows a rapidly changing path as it approaches and crosses this boundary. This is made apparent by the very large coefficients in power series expansions at low $\lambda$ (reference 1, Appendix III). It is important to note that whatever $\lambda$ is, sooner or later high valued coefficients occur, which contribute strongly to the transition across the boundary.

Figures 3 and 4 reveal graphically another point in connection with power series expansion. Paired levels have the same expansion in $\delta$, or in Wang's parameter $\beta=\delta/(2-\delta)$, up to $K$'th order. The splitting is caused by different coefficients of the $K$'th and subsequent orders. Where Wang's formula is good, the power series is good, in the region of coalescence above the line $\eta_J-\eta_\infty=0$ in Fig. 4. But as we have already pointed out (Fig. 1), there is always some value of $\kappa$ (hence of $\delta$ or $\beta$), namely at $\eta=\kappa$, where the splitting becomes relatively enormous, of the order of magnitude of the separation of non-paired levels. Thus the power series can never be satisfactory over the whole range of $\kappa$, and again Fig. 2 can be used to illustrate the regions of convergence. As with $\eta_\infty$, there is a region, $C$, $D$, or $E$, around $\eta=\kappa$ where it will not give close values. It is interesting to note that convergence is poor in region $D$ because $\lambda$ is small, and poor in region $E$ because $\beta$ (or $\delta$) is large.

The coefficients of the power series are of course closely related to the finite differences of the $E(\kappa)$ table which is discussed in the next section. Very large differences occur as a level crosses the line $\eta=\kappa$.

## INTERPOLATION FOR $\kappa$

In the application of the reduced energies to the analysis of a rotational spectrum, values are normally required for a $\kappa$ other than those tabulated. For levels of low $J$ there are explicit solutions from which the energy can be found for any value of $\kappa$. These were given in Table XII of reference 1. In Appendix II formulas for the energy levels arising from cubic equations are given, and carry the explicit method up to $J=7$.

For higher $J$'s it is desirable to investigate the accuracy obtainable by interpolation. Lagrangian formulae are the most convenient, and the maximum error can be calculated in terms of differences in $\eta_J$ with respect to $\kappa$, viz., for an $n$-point interpolation for a fraction of an interval $p$ the remainder is

$$R_n=\Pi_k(p-k)\Delta^{(n)}/n!, \quad \begin{matrix} 2k=2-n \text{ to } n, & n \text{ even} \\ =1-n \text{ to } n, & n \text{ odd.}\end{matrix}$$

The maximum error obtains for $p\cong 1/2$. It remains to investigate $\Delta^{(n)}\eta$ over the whole range of $\kappa$ and $\lambda$.

For the above purpose it would also be adequate to investigate $n$'th differentials $(\partial^n\eta/\partial^n\kappa)_\lambda$. These could be obtained in complete detail from the partial derivatives of the secular equations $p(\kappa, \eta)$ of reference 1. This is only practical for detailed study of a few particular levels. We shall have to be content with a more general, and hence less specific, survey, based on the $n$'th order differences themselves. These vary greatly over the range of $\kappa$ for a given level, and also vary discontinuously from one level to the next. As an illustration the first differences of the six discrete levels and the doubly degenerate $\eta_\infty$ shown in Fig. 1 (with the same $\lambda$'s) are plotted in Fig. 5. We note, as is true for higher differences, they all converge to the same value at $\kappa=-1$, and are the same as that given by the power series of perturbation theory, Appendix III in reference 1. We

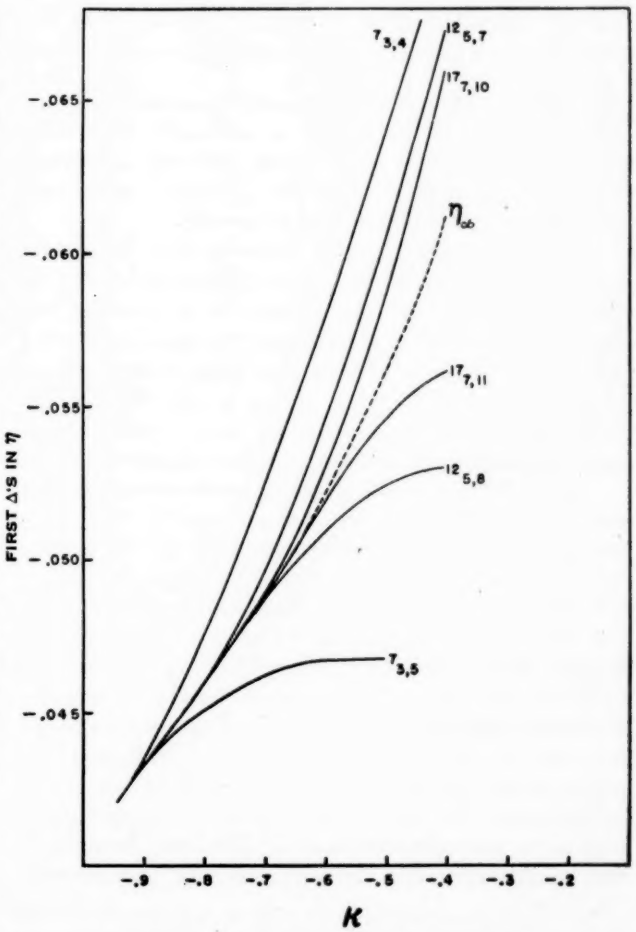


FIG. 5. First-order differences with respect to $\kappa$ of various levels with $\lambda=0$ 4.

[9] For some comparisons see reference 5, Table V, column 4.

TABLE III. The approximate maximum error over the $E(\kappa)$ pattern for several $J$'s from a 2-point Lagrangean interpolation. Areas $A$, $B$, $C$, $D$, and $E$ refer to the arbitrarily chosen geometric pattern of Fig. 2. The parity of $J+K_{-1}+K_1$ is the same as that of $\gamma$.

| | $J$ Value | Error in $E(\kappa)$ Areas | | | |
|---|---|---|---|---|---|
| | | $A$ | $B$ | $C$ | $D$ & $E$ |
| $\gamma$ even | 6 | .005 | .01 | .03 | .05 |
| | 9 | .03 | .05 | .1 | .17 |
| | 12 | .03 | .08 | .25 | .35 |
| $\gamma$ odd | 6 | .005 | .007 | .01 | .02 |
| | 9 | .01 | .02 | .04 | .05 |
| | 12 | .01 | .03 | .1 | .12 |

TABLE IV. The approximate maximum error over the $E(\kappa)$ pattern for several $J$'s from a 4-point Lagrangean interpolation. Areas $A$, $B$, $C$, $D$ and $E$ refer to the arbitrarily chosen geometric pattern of Fig. 2.

| | $J$ Value | Error in $E(\kappa)$ Areas | | | |
|---|---|---|---|---|---|
| | | $A$ | $B$ | $C$ | $D$ & $E$ |
| $\gamma$ even | 6 | .00007 | .0003 | .0007 | .001 |
| | 9 | .0001 | .0005 | .002 | .01 |
| | 12 | .0001 | .001 | .004 | .04 |
| $\gamma$ odd | 6 | .00001 | .00003 | .00004 | .00004 |
| | 9 | .00005 | .0002 | .0003 | .001 |
| | 12 | .00006 | .0004 | .001 | .006 |

also note the two main characteristics: rapid changes in $\Delta^{(n)}$, i.e., high values of $\Delta^{(n)}$, $n$ arbitrarily high, near the boundary $\eta=\kappa$, and entirely different characteristics in magnitude of the $\Delta^{(n)}$'s for neighboring levels, although the variation with $J$ is smooth.

The high values of $\Delta^{(n)}$ in crossing over the region is of course closely related to the singularity shown by the elliptical integral in the limit $J=\infty$ and the fact that a given $\eta_J(\lambda_{-1}, \lambda_1)$ changes its association with $\eta_\infty(\lambda_{-1})$ to $-\eta_\infty(\lambda_1)$, the latter not being a continuation of $\eta(\lambda_{-1})$ since $\lambda_1 \neq 1-\lambda_{-1}$ except in the limit. These large differences are reflected in large coefficients of power series expansions in parameters of asymmetry.

The variations of $\Delta^{(n)}$ with respect to $\kappa$ are however rationalized when the levels are grouped by their symmetry species, i.e., by their origin in the same submatrix of the Hamiltonian. Here continuous changes of $\Delta^{(n)}$ are found. Paired levels show distinct differences in the magnitude of their $\Delta^{(n)}$'s. This can be understood as follows. When levels pair it is most convenient to consider the type of representation of the Hamiltonian in which off diagonal elements are small, namely Type III for $\kappa$ near $+1$ and Type I for $\kappa$ near $-1$. In these types paired levels arise from either the two $E$ or the two $O$ submatrices. The two numbers of $E$ (or $O$) pairs differ only in the first row and column.[10] The levels from a pair will be approximately the same, differing only because of the effect of the first row and column. In fact the Wang splitting formula gives the principal term in the difference. However, the effect of the first row and column is asymmetrical, depressing the smaller roots more than it raises the larger roots. This also makes the Wang splitting asymmetrical around the limiting case $\eta_\infty$, and its effect can be seen in the higher differences, as shown in Fig. 5.

Now since $E$ and $O$ matrices give the same Wang splitting formula, the upper levels of pairs (one for the $+$ and the other for the $-$) behave the same way, as do the lower of the pairs. Tracing this through (in any particular case, say III$^r$), levels of species ee and oo behave alike as do eo and oe, but each pair is distinct. Since the ee or oo levels are the higher of a pair when $J$ is even, and eo or oe are for $J$ odd, we find the levels belong to two classes as far as the effect of splitting in the energy and the differences are concerned, depending on $J+K_{-1}+K_1$ being even or odd.

We are thus led to the same diagram (Fig. 2) as that derived in discussing the difference $\eta_J-\eta_\infty$, in which regions of orders of magnitude of $\Delta^{(n)}$ and hence of the accuracy of interpolation obtain. In the region $A$ good interpolation is possible, in $B$ it is worse, while in $C$, and in particular, $D$ and $E$, interpolation can be bad and of the order of magnitude of the separation of levels. The magnitude of the error in any region is different for $J+K_{-1}+K_1$ even or odd. The maximum errors of interpolation are given numerically for $J=6$, 9, and 12 and each parity of $J+K_{-1}+K_1$ in each of the four regions of Fig. 2; in Table III for linear interpolations; and in Table IV for four-point interpolations.


## ACKNOWLEDGMENTS

The authors wish to acknowledge the work of Messrs. David Hedberg, Paul M. Gross, Jr., Robert E. Hoffman, and Miss L. Joanne Edson for aid in the calculations reported here.


## Errata: The Asymmetric Rotor.

### Parts I and VI.


GILBERT W. KING, *Arthur D. Little, Inc., Cambridge, Massachusetts*
R. M. HAINER, AND PAUL C. CROSS, *Brown University, Providence, Rhode Island*


[J. Chem. Phys. **11**, 27 (1943) and **15**, 820 (1947)]

WE wish to correct a few numerical errors in reference 1.

Appendix I:

| $JK_{-1},K_1$ | $\kappa$ | Now Reads $E(\kappa)$ | Should Read $E(\kappa)$ |
|---|---|---|---|
| $3_{3,0}$ | $-0.5$ | 6.82496 | 6.82456 |
| $3_{1,2}$ | $-0.5$ | $-5.82496$ | $-5.82456$ |
| $5_{1,4}$ | $-0.6$ | $-19.76369$ | $-19.76378$ |

Appendix III:

| | $\delta°$ | |
|---|---|---|
| $11_{10,1-2}$ | 74 | 68 |
| $11_{9,2-3}$ | 32 | 30 |

In reference 2, the middle expression to Eq. (5) lacks a cyclic integral sign. In Eq. (8) the integrand lacks a square root sign. The last term, $F_0$, in Eq. (35) is $F_0(\alpha)$.

[10] $E^-$ is considered here to be $E^+$ with the first row and column made zero. The letters $E$ and $O$ refer to the parity of $K$ in the symmetric-rotor functions used as a basis; and $+$ and $-$ refer to the sign with which the two functions of the same $K$ are combined.

## APPENDIX I. EXTENSION OF RIGID ROTOR ENERGY LEVEL PATTERNS, $E(\kappa)$, TO $J=11$ AND 12

The asymmetry parameter $\kappa=(2b-a-c)/(a-c)$, where $a$, $b$, $c$, equal $\hbar^2/2I_a$, $\hbar^2/2I_b$, $\hbar^2/2I_c$, respectively, and where the condition $I_a \leqslant I_b \leqslant I_c$ is applied in assigning the moments of inertia.

Energy level patterns for $0 \leqslant \kappa \leqslant 1$ may be readily obtained from the table by the use of the relation

$$E_\tau^J(\kappa) = -E_{-\tau}^J(-\kappa).$$

Rotational energy levels are given by

$$E_\tau^J(a, b, c) = [(a+c)/2]J(J+1) + [(a-c)/2]E_\tau^J(\kappa).$$

Symmetries are included in terms of the $JK_{-1}K_1$ notation.

| $JK_{-1}, K_1$ | $\delta$ 0.0 $\kappa$ −1.0 | 0.05 −0.9 | 0.1 −0.8 | 0.15 −0.7 | 0.2 −0.6 | 0.25 −0.5 | 0.3 −0.4 | 0.35 −0.3 | 0.4 −0.2 | 0.45 −0.1 | 0.5 0.0 | $\delta$ $\kappa$ / $J\tau$ |
|---|---|---|---|---|---|---|---|---|---|---|---|---|
| $11_{11,0}$ | 110 | 110.55741 | 111.13042 | 111.72035 | 112.32873 | 112.95732 | 113.60817 | 114.28371 | 114.98687 | 115.72118 | 116.49101 | $11_{11}$ |
| $11_{11,1}$ | 110 | 110.55741 | 111.13042 | 111.72035 | 112.32873 | 112.95732 | 113.60817 | 114.28371 | 114.98687 | 115.72118 | 116.49101 | $11_{10}$ |
| $11_{10,1}$ | 68 | 69.62244 | 71.29217 | 73.01320 | 74.79013 | 76.62830 | 78.53398 | 80.51457 | 82.57895 | 84.73792 | 87.00484 | $11_9$ |
| $11_{10,2}$ | 68 | 69.62244 | 71.29217 | 73.01320 | 74.79013 | 76.62830 | 78.53398 | 80.51457 | 82.57895 | 84.73790 | 87.00476 | $11_8$ |
| $11_{9,2}$ | 30 | 32.58828 | 35.25722 | 38.01369 | 40.86557 | 43.82203 | 46.89387 | 50.09389 | 53.43757 | 56.94391 | 60.63695 | $11_7$ |
| $11_{9,3}$ | 30 | 32.58828 | 35.25722 | 38.01369 | 40.86557 | 43.82203 | 46.89386 | 50.09383 | 53.43728 | 56.94285 | 60.63335 | $11_6$ |
| $11_{8,3}$ | −4 | −0.54413 | 3.02952 | 6.73101 | 10.57202 | 14.56622 | 18.72994 | 23.08308 | 27.65082 | 32.46668 | 37.57816 | $11_5$ |
| $11_{8,4}$ | −4 | −0.54413 | 3.02952 | 6.73101 | 10.57200 | 14.56612 | 18.72935 | 23.08058 | 27.64194 | 32.43881 | 37.49896 | $11_4$ |
| $11_{7,4}$ | −34 | −29.77306 | −25.38384 | −20.81819 | −16.05925 | −11.08615 | −5.87160 | −0.37697 | 5.45566 | 11.71501 | 18.52846 | $11_3$ |
| $11_{7,5}$ | −34 | −29.77306 | −25.38384 | −20.81827 | −16.05996 | −11.09013 | −5.88800 | −0.43240 | 5.29497 | 11.30427 | 17.59094 | $11_2$ |
| $11_{6,5}$ | −60 | −55.09517 | −49.96884 | −44.59948 | −38.95660 | −32.99222 | −26.62837 | −19.74690 | −12.20554 | −3.91237 | 5.07342 | $11_1$ |
| $11_{6,6}$ | −60 | −55.09517 | −49.96909 | −44.60266 | −38.97639 | −33.07488 | −26.89374 | −20.44706 | −13.77235 | −6.93039 | 0.00000 | $11_0$ |
| $11_{5,6}$ | −82 | −76.50325 | −70.69043 | −64.50488 | −57.83704 | −50.52275 | −42.41746 | −33.54235 | −24.13221 | −14.52682 | −5.07342 | $11_{-1}$ |
| $11_{5,7}$ | −82 | −76.50333 | −70.69956 | −64.57838 | −58.15601 | −51.48395 | −44.64497 | −37.73949 | −30.87020 | −24.12952 | −17.59094 | $11_{-2}$ |
| $11_{4,7}$ | −100 | −93.97251 | −87.38351 | −79.97747 | −71.57973 | −62.37910 | −52.82106 | −43.35259 | −34.34210 | −26.04216 | −18.52846 | $11_{-3}$ |
| $11_{4,8}$ | −100 | −93.98416 | −87.57242 | −80.88745 | −74.09626 | −67.35804 | −60.79826 | −54.50178 | −48.51452 | −42.85004 | −37.49896 | $11_{-4}$ |
| $11_{3,8}$ | −114 | −107.32617 | −99.22088 | −89.98920 | −80.49073 | −71.37141 | −63.02979 | −55.60829 | −49.01277 | −43.05668 | −37.57816 | $11_{-5}$ |
| $11_{3,9}$ | −114 | −107.58790 | −101.02059 | −94.65135 | −88.64681 | −83.06597 | −77.90522 | −73.12851 | −68.68815 | −64.53694 | −60.63335 | $11_{-6}$ |
| $11_{2,9}$ | −124 | −115.80441 | −106.42498 | −97.66776 | −90.09101 | −83.68305 | −78.15043 | −73.22096 | −68.72135 | −64.54822 | −60.63695 | $11_{-7}$ |
| $11_{2,10}$ | −124 | −117.99898 | −112.78018 | −108.25410 | −104.28948 | −100.76150 | −97.57133 | −94.64631 | −91.93402 | −89.39628 | −87.00476 | $11_{-8}$ |
| $11_{1,10}$ | −130 | −120.94321 | −113.89249 | −108.62177 | −104.40728 | −100.79904 | −97.58319 | −94.64999 | −91.93512 | −89.39660 | −87.00484 | $11_{-9}$ |
| $11_{1,11}$ | −130 | −127.28140 | −125.28365 | −123.68604 | −122.33152 | −121.13930 | −120.06384 | −119.07714 | −118.16077 | −117.30184 | −116.49101 | $11_{-10}$ |
| $11_{0,11}$ | −132 | −127.60622 | −125.34436 | −123.69950 | −122.33481 | −121.14015 | −120.06406 | −119.07720 | −118.16078 | −117.30185 | −116.49101 | $11_{-11}$ |
| $12_{12,0}$ | 132 | 132.60804 | 133.23304 | 133.87642 | 134.53983 | 135.22519 | 135.93472 | 136.67109 | 137.43744 | 138.23763 | 139.07639 | $12_{12}$ |
| $12_{12,1}$ | 132 | 132.60804 | 133.23304 | 133.87642 | 134.53983 | 135.22519 | 135.93472 | 136.67109 | 137.43744 | 138.23763 | 139.07639 | $12_{11}$ |
| $12_{11,1}$ | 86 | 87.77433 | 89.59994 | 91.48116 | 93.42300 | 95.43124 | 97.51266 | 99.67528 | 101.92873 | 104.28467 | 106.75754 | $12_{10}$ |
| $12_{11,2}$ | 86 | 87.77433 | 89.59994 | 91.48116 | 93.42300 | 95.43124 | 97.51266 | 99.67528 | 101.92873 | 104.28466 | 106.75752 | $12_9$ |
| $12_{10,2}$ | 44 | 46.84133 | 49.76974 | 52.79264 | 55.91853 | 59.15729 | 62.52052 | 66.02198 | 69.67821 | 73.50943 | 77.54083 | $12_8$ |
| $12_{10,3}$ | 44 | 46.84133 | 49.76974 | 52.79264 | 55.91853 | 59.15729 | 62.52052 | 66.02197 | 69.67816 | 73.50920 | 77.53995 | $12_7$ |
| $12_{9,3}$ | 6 | 9.80982 | 13.74573 | 17.81847 | 22.04046 | 26.42621 | 30.99284 | 35.76089 | 40.75549 | 46.00848 | 51.56206 | $12_6$ |
| $12_{9,4}$ | 6 | 9.80982 | 13.74573 | 17.81847 | 22.04046 | 26.42620 | 30.99276 | 35.76044 | 40.75362 | 46.00157 | 51.53914 | $12_5$ |
| $12_{8,4}$ | −28 | −23.31885 | −18.46658 | −13.42845 | −8.18721 | −2.72237 | 2.99115 | 8.98537 | 15.30406 | 22.01179 | 29.20920 | $12_4$ |
| $12_{8,5}$ | −28 | −23.31885 | −18.46658 | −13.42846 | −8.18729 | −2.72292 | 2.98828 | 8.97354 | 15.26295 | 21.88669 | 28.86916 | $12_3$ |
| $12_{7,5}$ | −58 | −52.54227 | −46.85722 | −40.92453 | −34.71915 | −28.20792 | −21.34247 | −14.04652 | −6.19852 | 2.37386 | 11.83982 | $12_2$ |
| $12_{7,6}$ | −58 | −52.54227 | −46.85724 | −40.92484 | −34.72181 | −28.22242 | −21.40126 | −14.23932 | −6.73320 | 1.09462 | 9.18884 | $12_1$ |
| $12_{6,6}$ | −84 | −77.85578 | −71.40626 | −64.61849 | −57.43904 | −49.77366 | −41.46701 | −32.32446 | −22.23803 | −11.34297 | 0.00000 | $12_0$ |
| $12_{6,7}$ | −84 | −77.85579 | −71.40700 | −64.62784 | −57.49624 | −50.00573 | −42.17943 | −34.07848 | −25.79945 | −17.46142 | −9.18884 | $12_{-1}$ |
| $12_{5,7}$ | −106 | −99.24886 | −92.05990 | −84.32677 | −75.84376 | −66.37094 | −55.87896 | −44.69269 | −33.31136 | −22.22538 | −11.83982 | $12_{-2}$ |
| $12_{5,8}$ | −106 | −99.24950 | −92.08176 | −84.49852 | −76.55839 | −68.37935 | −60.11399 | −51.91698 | −43.92037 | −36.21961 | −28.86916 | $12_{-3}$ |
| $12_{4,8}$ | −124 | −116.68433 | −108.54615 | −99.19126 | −88.59068 | −77.32074 | −66.08323 | −55.43986 | −45.74204 | −37.05142 | −29.20920 | $12_{-4}$ |
| $12_{4,9}$ | −124 | −116.70744 | −108.91030 | −100.83935 | −92.76304 | −84.89902 | −77.38842 | −70.30021 | −63.64716 | −57.40662 | −51.53914 | $12_{-5}$ |
| $12_{3,9}$ | −138 | −129.89446 | −119.83602 | −108.66278 | −97.63069 | −87.50774 | −78.60398 | −70.80785 | −63.84208 | −57.47608 | −51.56206 | $12_{-6}$ |
| $12_{3,10}$ | −138 | −130.31993 | −122.54720 | −115.16409 | −108.34710 | −102.11751 | −96.42279 | −91.18633 | −86.33359 | −81.80156 | −77.53995 | $12_{-7}$ |
| $12_{2,10}$ | −148 | −138.07886 | −127.08806 | −117.31187 | −109.20383 | −102.42723 | −96.52870 | −91.22101 | −86.34443 | −81.80478 | −77.54083 | $12_{-8}$ |
| $12_{2,11}$ | −148 | −140.96729 | −135.01890 | −129.97341 | −125.61179 | −121.75481 | −118.27567 | −115.08791 | −112.13194 | −109.36548 | −106.75752 | $12_{-9}$ |
| $12_{1,11}$ | −154 | −143.49856 | −135.79253 | −130.18555 | −125.66986 | −121.77085 | −118.28009 | −115.08911 | −112.13226 | −109.36555 | −106.75754 | $12_{-10}$ |
| $12_{1,12}$ | −154 | −150.87245 | −148.65947 | −146.91218 | −145.43616 | −144.13816 | −142.96738 | −141.89309 | −140.89519 | −139.95968 | −139.07639 | $12_{-11}$ |
| $12_{0,12}$ | −156 | −151.11155 | −148.69573 | −146.91899 | −145.43760 | −144.13848 | −142.96745 | −141.89311 | −140.89521 | −139.95968 | −139.07639 | $12_{-12}$ |

## APPENDIX II. EXPRESSIONS FOR ENERGY LEVELS, $EK_{-1}{}^JK_1(\kappa)$, WHICH ARE ROOTS OF CUBIC SECULAR EQUATIONS

$$EK_{-1}{}^JK_1(\kappa) = x - p(\kappa)$$
$$x = \mp 8/3a(\kappa)^{\frac{1}{2}} \cos(\phi/3 + 120°n)$$
$$\cos\phi = |b(\kappa)|\,a(\kappa)^{-\frac{3}{2}}$$

The upper sign is used in the equation for $x$ if $b(\kappa)$ is negative, the lower if it is positive. Three roots are obtained for $n=0$, 1, and 2. The levels are identified by the indices $K_{-1}$ and $K_1$ which are obtained in two steps. Their parity is defined by the submatrix giving the secular equations, and is given in column 2. The numerical assignment is made by noting the three roots of any one secular equation can be arranged in magnitude in the same order as their $K_{-1}$ values, which are all different.

| $J$ | $K_{-1}K_1$ | $b(\kappa)$ | $a(\kappa)$ | $p(\kappa)$ |
|---|---|---|---|---|
| 4 | ee | $35\kappa(\kappa^2-9)$ | $13(\kappa^2+3)$ | $-20\kappa/3$ |
| 5 | oo | $-5\kappa(7\kappa^2-135)$ | $13\kappa^2+99$ | $-20\kappa/3$ |
| 5 | oe | $-5(16\kappa^3 \pm 9\kappa^2 - 108\kappa \pm 27)$ | $2(14\kappa^2 \mp 15\kappa + 27)$ | $-(35\kappa \pm 15)/3$ |
| | eo | ditto, lower sign | | |
| 6 | oo | $\kappa(143\kappa^2-783)$ | $7(7\kappa^2+9)$ | $-56\kappa/3$ |
| 6 | oe | $80\kappa^3 \mp 63\kappa^2 - 972\kappa \mp 189$ | $14(2\kappa^2 \pm 3\kappa + 9)$ | $-(35\kappa \mp 21)/3$, |
| | eo | ditto, lower sign | | |
| 7 | ee | $143\kappa(\kappa^2-9)$ | $49(\kappa^2+3)$ | $-56\kappa/3$ |

## APPENDIX III. COEFFICIENT $A(\kappa, K)$ OF THE WANG SPLITTING FORMULA

The coefficient of Eq. (2) dependent only on $\kappa$ and $K$ is

$$A(\kappa, K) = 16(\beta/8)^K/1-\beta,$$

which is evaluated for $\kappa=-0.9(0.1)+0.9$ and $K=3(1)20$; with the following restriction. The $K$ corresponds to that at $\kappa=-1$, i.e., is $K_{-1}$. Entries for the upper right-hand triangle are omitted since for the $J=12(1)20$, the corresponding $\lambda$ is such that $\eta<\kappa$, and the

pairing is on $K_1$, in which case the splitting is obtained by symmetry, using $K_{-1}$ and $\kappa$ of opposite sign. Entries in the lower left triangle are omitted because they are so small that even for $J=20$, $\Delta\eta<10^{-8}$.

The subscript after the decimal preceding the normal figures indicates the number of zeros preceding the first non-zero digit, e.g., for $\kappa=-0.5$, $K=7$, the entry is $.{}_{11}810\ 60978$, meaning $A(-0.5, 7)=0.81060978\times10^{-11}$.

| $K$ \ $\kappa$ | −0.9 | −0.8 | −0.7 | −0.6 | −0.5 | −0.4 | −0.3 | −0.2 | −0.1 |
|---|---|---|---|---|---|---|---|---|---|
| 3 | $.{}_{06}513\ 64234$ | $.{}_{08}432\ 82548$ | | | | | | | |
| 4 | $.{}_{08}164\ 62895$ | $.{}_{07}284\ 75361$ | $.{}_{06}156\ 16363$ | $.{}_{06}535\ 83676$ | | | | | |
| 5 | $.{}_{11}527\ 65691$ | $.{}_{09}187\ 33789$ | $.{}_{08}158\ 27395$ | $.{}_{08}744\ 21774$ | $.{}_{07}254\ 20723$ | $.{}_{07}710\ 31443$ | | | |
| 6 | $.{}_{13}169\ 12080$ | $.{}_{11}123\ 24862$ | $.{}_{10}160\ 41278$ | $.{}_{09}103\ 36357$ | $.{}_{09}453\ 94149$ | $.{}_{08}156\ 68701$ | $.{}_{08}458\ 71042$ | $.{}_{07}119\ 20929$ | |
| 7 | $.{}_{16}542\ 05384$ | $.{}_{14}810\ 84619$ | $.{}_{12}162\ 58052$ | $.{}_{11}143\ 56052$ | $.{}_{11}810\ 60978$ | $.{}_{10}345\ 63311$ | $.{}_{09}121\ 62777$ | $.{}_{09}372\ 52903$ | $.{}_{08}102\ 79157$ |
| 8 | $.{}_{18}173\ 73521$ | $.{}_{16}533\ 45143$ | $.{}_{14}164\ 77756$ | $.{}_{13}199\ 38961$ | $.{}_{12}144\ 75175$ | $.{}_{12}762\ 42595$ | $.{}_{11}322\ 49786$ | $.{}_{10}116\ 41532$ | $.{}_{10}373\ 03390$ |
| 9 | | $.{}_{18}350\ 95489$ | $.{}_{16}167\ 00428$ | $.{}_{15}276\ 93001$ | $.{}_{14}258\ 48527$ | $.{}_{13}168\ 18219$ | $.{}_{13}855\ 10797$ | $.{}_{13}363\ 79788$ | $.{}_{11}135\ 37521$ |
| 10 | | | $.{}_{18}169\ 26110$ | $.{}_{17}384\ 62502$ | $.{}_{16}461\ 58083$ | $.{}_{15}370\ 99015$ | $.{}_{14}226\ 73317$ | $.{}_{13}113\ 68684$ | $.{}_{13}491\ 28099$ |
| 11 | | | | $.{}_{19}534\ 20140$ | $.{}_{18}824\ 25149$ | $.{}_{17}818\ 36062$ | $.{}_{16}601\ 18642$ | $.{}_{15}355\ 27137$ | $.{}_{14}178\ 28747$ |
| 12 | | | | | $.{}_{19}147\ 18777$ | $.{}_{18}180\ 52072$ | $.{}_{17}159\ 40549$ | $.{}_{16}111\ 02230$ | $.{}_{16}647\ 01095$ |
| 13 | | | | | | $.{}_{20}398\ 20748$ | $.{}_{19}422\ 66609$ | $.{}_{18}346\ 94470$ | $.{}_{17}234\ 80236$ |
| 14 | | | | | | $.{}_{22}878\ 39889$ | $.{}_{20}112\ 07055$ | $.{}_{19}108\ 42022$ | $.{}_{19}852\ 10532$ |
| 15 | | | | | | | | | $.{}_{20}309\ 23178$ |
| 16 | | | | | | | | | |
| 17 | | | | | | | | | |
| 18 | | | | | | | | | |
| 19 | | | | | | | | | |
| 20 | | | | | | | | | |

| $K$ \ $\kappa$ | 0 | 0.1 | 0.2 | 0.3 | 0.4 | 0.5 | 0.6 | 0.7 | 0.8 | 0.9 |
|---|---|---|---|---|---|---|---|---|---|---|
| | $.{}_{08}261\ 63905$ | $.{}_{08}624\ 87176$ | | | | | | | | |
| | $.{}_{09}109\ 01627$ | $.{}_{09}296\ 27539$ | $.{}_{09}759\ 77298$ | $.{}_{08}185\ 92619$ | | | | | | |
| | $.{}_{11}454\ 23446$ | $.{}_{10}140\ 47541$ | $.{}_{10}407\ 02124$ | $.{}_{09}111\ 90001$ | $.{}_{09}294\ 85986$ | $.{}_{09}750\ 84686$ | | | | |
| | $.{}_{12}189\ 26436$ | $.{}_{12}666\ 04719$ | $.{}_{11}218\ 04709$ | $.{}_{11}673\ 47234$ | $.{}_{10}198\ 46337$ | $.{}_{10}563\ 13515$ | $.{}_{09}155\ 04536$ | $.{}_{09}416\ 96424$ | | |
| | $.{}_{14}788\ 60148$ | $.{}_{13}315\ 79822$ | $.{}_{12}116\ 81094$ | $.{}_{13}405\ 33057$ | $.{}_{11}133\ 58110$ | $.{}_{11}422\ 35136$ | $.{}_{10}129\ 20447$ | $.{}_{10}385\ 23869$ | $.{}_{09}112\ 67845$ | $.{}_{09}325\ 21218$ |
| | $.{}_{15}328\ 58396$ | $.{}_{14}149\ 73192$ | $.{}_{14}625\ 77291$ | $.{}_{13}243\ 94896$ | $.{}_{13}899\ 10360$ | $.{}_{13}316\ 76352$ | $.{}_{11}107\ 67039$ | $.{}_{11}355\ 92706$ | $.{}_{10}115\ 23933$ | $.{}_{10}367\ 79948$ |
| | $.{}_{16}136\ 90998$ | $.{}_{16}709\ 93580$ | $.{}_{15}335\ 23548$ | $.{}_{14}146\ 82113$ | $.{}_{14}605\ 16589$ | $.{}_{13}237\ 57264$ | $.{}_{12}897\ 25326$ | $.{}_{12}328\ 84565$ | $.{}_{11}117\ 85841$ | $.{}_{11}415\ 96370$ |
| | $.{}_{18}570\ 45825$ | $.{}_{17}336\ 60750$ | $.{}_{16}179\ 59044$ | $.{}_{16}883\ 64572$ | $.{}_{15}407\ 32319$ | $.{}_{14}178\ 17948$ | $.{}_{14}747\ 71104$ | $.{}_{13}303\ 82479$ | $.{}_{12}120\ 53701$ | $.{}_{12}470\ 43515$ |
| | $.{}_{19}237\ 69094$ | $.{}_{18}159\ 59839$ | $.{}_{18}962\ 09165$ | $.{}_{17}531\ 82379$ | $.{}_{16}274\ 15984$ | $.{}_{15}133\ 63461$ | $.{}_{15}623\ 09253$ | $.{}_{14}280\ 70768$ | $.{}_{13}123\ 27648$ | $.{}_{13}532\ 03973$ |
| | $.{}_{21}990\ 37893$ | $.{}_{20}756\ 71650$ | $.{}_{19}515\ 40623$ | $.{}_{18}320\ 07914$ | $.{}_{17}184\ 53067$ | $.{}_{16}100\ 22596$ | $.{}_{16}519\ 24379$ | $.{}_{15}259\ 34949$ | $.{}_{14}126\ 07822$ | $.{}_{14}601\ 71161$ |
| | 17 | | $.{}_{20}276\ 11048$ | $.{}_{19}192\ 64022$ | $.{}_{18}124\ 20333$ | $.{}_{16}751\ 69465$ | $.{}_{17}432\ 70315$ | $.{}_{16}239\ 61638$ | $.{}_{15}128\ 94364$ | $.{}_{15}680\ 50719$ |
| | | | 18 | | $.{}_{20}835\ 98396$ | $.{}_{19}563\ 77103$ | $.{}_{18}360\ 58595$ | $.{}_{17}221\ 38469$ | $.{}_{16}131\ 87417$ | $.{}_{16}769\ 62124$ |
| | | | | | 19 | | $.{}_{19}300\ 48828$ | $.{}_{18}204\ 54020$ | $.{}_{17}134\ 87131$ | $.{}_{17}870\ 40492$ |
| | | | | | | | 20 | $.{}_{19}188\ 97737$ | $.{}_{18}137\ 93656$ | $.{}_{18}984\ 38652$ |

## APPENDIX IV. COEFFICIENT $B(J, K)$ OF THE WANG SPLITTING FORMULA

The coefficient of Eq. (2) dependent only on $J$ and $K$ is

$$B(J,K)=\binom{J+K}{K}\binom{J}{K}K^2/J(J+1),$$

which is evaluated for $J=12(1)20$, $K\leqslant J$. Values for $K=0$, 1, and 2 are omitted since the paired levels with the corresponding $\lambda=K/[J(J+1)]^{\frac{1}{2}}$ do not exist at these $J$'s except for $\kappa<-0.9$, i.e., within the first interval of the table of $A(\kappa, K)$. In any case the splitting is so large at $\lambda\sim0$, $\kappa\sim-1$ that the Wang formula does not apply in general.

Note that the subscript on the right of the entries is the power of ten by which the eight-digit main entry is to be multiplied, e.g., for $J=17$, $K=7$, the table reads $107{,}78448_2$, meaning $B(17, 7)=10778{,}44800$.

| $K$ \ $J$ | 12 | 13 | 14 | 15 | 16 | 17 | 18 | 19 | 20 |
|---|---|---|---|---|---|---|---|---|---|
| 3 | 5775 | 7920 | 10608 | 13923 | 17955 | 22800 | 28560 | 35343 | 43263 |
| 4 | 92400 | 1 49600 | 2 33376 | 3 52716 | 5 18700 | 7 44800 | 10 47200 | 14 45136 | 19 61256 |
| 5 | 7 85400 | 15 14700 | 27 71340 | 48 49845 | 81 69525 | 133 13300 | 210 74900 | 325 15560 | 490 31400 |
| 6 | 39 58416 | 92 09376 | 199 53648 | 407 38698 | 790 81001 | $146\ 97884_1$ | $263\ 01475_1$ | 455 21784$_1$ | $764\ 88984_1$ |
| 7 | 125 34984 | 358 14240 | 931 17023 | $224\ 06283_1$ | $505\ 23974_1$ | $107\ 78448_2$ | $219\ 17896_2$ | 427 39897$_2$ | $803\ 13436_2$ |
| 8 | 255 81600 | 920 93760 | $292\ 65350_1$ | $841\ 37884_1$ | $222\ 71793_2$ | $549\ 92080_2$ | $127\ 92894_3$ | 282 60667$_3$ | $596\ 61407_3$ |
| 9 | 335 75850 | 158 28615$_1$ | $631\ 03413_1$ | $220\ 86194_2$ | $695\ 99352_2$ | $201\ 06479_3$ | $539\ 70024_3$ | 136 00446$_4$ | $324\ 40889_4$ |
| 10 | 273 58100 | 179 78180$_1$ | $934\ 86539_1$ | $409\ 00360_2$ | $156\ 38373_3$ | $536\ 17278_3$ | $167\ 90674_4$ | 486 92954$_4$ | $132\ 16659_5$ |
| 11 | 125 84726 | 129 44289$_1$ | $934\ 86537_1$ | $531\ 70466_2$ | $253\ 34164_3$ | $105\ 08987_4$ | $389\ 54365_4$ | 131 47098$_5$ | $409\ 71643_5$ |
| 12 | 24 96144 | 534 88800 | $602\ 64048_1$ | $474\ 57938_2$ | $293\ 12255_3$ | $151\ 12097_4$ | $676\ 06745_4$ | 269 46118$_5$ | $975\ 19281_5$ |
| 13 | | 96 57700 | $225\ 99018_1$ | $276\ 83797_2$ | $236\ 12650_3$ | $157\ 41767_4$ | $873\ 25379_4$ | 419 16183$_5$ | $178\ 78535_6$ |
| 14 | | | 374 42160 | $950\ 09481_1$ | $125\ 74784_2$ | $115\ 50172_4$ | $826\ 74915_4$ | 491 08900$_5$ | $251\ 78056_6$ |
| 15 | | | | 145 42268$_1$ | $397\ 77378_2$ | $565\ 72272_3$ | $556\ 79026_4$ | 425 94454$_5$ | $269\ 76488_6$ |
| 16 | | | | | $565\ 72272_1$ | $165\ 94533_3$ | $252\ 41158_4$ | 265 03261$_5$ | $215\ 81190_6$ |
| 17 | | | | | | $220\ 39614_2$ | $690\ 18792_3$ | 111 81044$_6$ | $124\ 76625_6$ |
| 18 | | | | | | | $859\ 74966_2$ | 286 29664$_6$ | $492\ 15755_6$ |
| 19 | | | | | | | | 335 78001$_3$ | $118\ 48237_6$ |
| 20 | | | | | | | | | $131\ 28241_6$ |

# Letters to the Editor

*THIS section will accept reports of new work, provided these are terse and contain few figures, and especially few half-tone cuts. The Editorial Board will not hold itself responsible for opinions expressed by the correspondents. Contributions to this section should not exceed 600 words in length and must reach the office of the Managing Editor not later than the 15th of the month preceding that of the issue in which the letter is to appear. No proof will be sent to the authors. The usual publication charge ($4.00 per page) will not be made and no reprints will be furnished free.*

## On Grüneisen's Constant for Metals

A. KÓNYA
*Physical Institute of the University for Technical Sciences, Budapest, Hungary*
June 14, 1949

GRÜNEISEN'S constant $\gamma=\alpha V/\kappa C_v$ can also be found—as Slater has pointed out—from the compressibility $\kappa$ and change of compressibility with volume $d\kappa/dV$ by the relation[1]

$$\gamma=-1/6+1/2\cdot d(\ln\kappa)/d(\ln V)=-1/6+1/2\cdot V/\kappa\cdot d\kappa/dV. \quad (1)$$

The theory of metals as developed by Gombás[2] makes it possible to determine this important metallic constant in a purely theoretical way. According to this theory the energy per atom in metals can be written as a polynom of fourth degree in $1/R$

$$U=A_0+A_1/R+A_2/R^2+A_3/R^3+A_4/R^4,$$

where $R$ is the radius of the unit sphere containing one atom. The $A_i-s$ are constants characteristic for the metal and independent of $R$. The values of these constants are determined by the theory without the use of any empirical parameter.

It is well known that the pressure can be calculated as $P=-dU/dV=-1/4\pi R^2\cdot dU/dR$, by means of which we get

$$\kappa=-1/V\cdot dV/dP=1/V\cdot 1/(d^2U/dV^2)$$
$$=12\pi R/(d^2U/dR^2-2/R\cdot dU/dR)$$

and

$$d\kappa/dV=-3/R^2\cdot(Rd^3U/dR^3-3\cdot d^2U/dR^2+4/R\cdot dU/dR)/$$
$$(d^2U/dR^2-2/R\cdot dU/dR)^2.$$

When we use for $V$, $\kappa$ and $d\kappa/dV$ their values at the equilibrium configuration $R=R_0$ obtained theoretically from the equation

$$(dU/dR)_{R=R_0}=-(A_1R_0^3+2A_2R_0^2+3A^3R_0+4A_4)/R_0^5=0, \quad (2)$$

$\gamma$ is given by the following formula

$$\gamma=1/3-R_0/6\cdot(d^3U/dR^3)_{R=R_0}/(d^2U/dR^2)_{R=R_0}$$
$$=1/3+1/2\cdot(A_1R_0^3+4A_2R_0^2+10A_3R_0+20A_4)/$$
$$(A_1R_0^3+3A_2R_0^2+6A_3R_0+10A_4).$$

TABLE I.

| | Calculated from (3) | Calc. with exp. data by Grüneisen | Calc. with exp. data of Bridgman from (1) | Obtained semi-empirically by Slater*** |
|---|---|---|---|---|
| Na | 1.552 | 1.25 | 1.83* | 1.58 |
| K | 1.560 | 1.34 | 2.55* | 1.53 |
| Rb | 1.567 | 1.48 | | 1.48 |
| Cs | 1.570 | 1.29 | | 1.48 |
| Mg | 1.521 | | 1.62* | 2.15 |
| Ca | 1.529 | | 1.28** | 1.98 |
| Sr | 1.536 | | 0.83** | |
| Ba | 1.539 | | 0.58** | |

* J. C. Slater. See reference 1, p. 451.
** F. Birch, Phys. Rev. 71, 809 (1947).
*** J. C. Slater. See reference 1, p. 454.

Taking into account (2), finally we get

$$\gamma=4/3+1/2\cdot(A_3R_0+4A_4)/(A_2R_0^2+3A_3R_0+6A_4).$$

The results obtained from (3) together with values for $\gamma$ calculated otherwise are summarized in Table I.

As the table shows, the theoretical values are in a good accordance with the results obtained from experimental data or semi-empirically, especially for the alkaline metals. The agreement for the alkaline-earth-metals is not as good as for the alkalies. This is because the fundamental assumptions of the theory of Gombás are less adapted for these metals than for the alkalies.

[1] For a full discussion of this relation see for instance J. C. Slater, *Introduction to Chemical Physics* (McGraw-Hill Book Company, Inc., New York, 1939), pp. 217 and 238.
[2] P. Gombás, Nature 157, 668 (1946); Hungarica Acta Physica Vol. I. fasc. 2. (1947); *Die statistische Theorie des Atoms und ihre Anwendungen* (Verlag Julius Springer, Berlin, 1948).

## On the Theory of Burning Velocities in Gas Mixtures

N. MANSON
*Station Nationale Claude Bonnier (Institut Francais du Petrole), Bellevue (S. & O.) France*
July 11, 1949

IN a recent paper, Badin, Stuart, and Pease[1] have compared the burning velocity ratios measured and calculated by them, for the stoichiometric mixtures of butadiene-1,3 with normal air and with "helium air" (He—79 percent, $O_2$—21 percent).

Some of their conclusions are: (1) that in the calculations, the somewhat greater diffusibility of the H-atoms in the helium air than in the normal air must be taken into account; (2) higher burning velocities at pressures below 1 atmos. are due to the increase of the diffusion coefficient of the H-atoms with decreasing pressure.

A different interpretation may be obtained by the use of the theory in which the flame is treated as a shock and combustion wave with a small pressure drop (Jouguet[2]). This pressure drop $\Delta p$ is determined, not by the diffusion of the hydrogen atoms into the unburned gauges, but by a more dynamic phenomenon: the projection of the H-atoms into the unburned gases.[3] According to that theory, the burning velocity is given by:

$$V=[\mu\cdot\Delta p/\rho_u\cdot(1-\mu)]^{\frac{1}{2}}, \quad (1)$$

where $\mu=\rho_b/\rho_u$ is the ratio of the specific masses of the burned ($\rho_b$) and the unburned ($\rho_u$) gases. Since $\Delta p=T_u\cdot p_H/2T_b$ ($T_b$ and $T_u$ being the temperatures of these gases, and $p_H$ the partial pressure of the H-atoms in the burned gases) the substitution of $N_2$ by He in the mixture not only increases $T_b$ and $p_H$ but also decreases $\rho_u$ ($\mu/(1-\mu)$ varying slightly). The same may be said for the influence of the pressure $p$, $\rho_u$ decreasing with $p$. These statements are more precisely expressed by the results of calculations summarized in Tables I and II.[4] They are also substantiated by a

TABLE I. Burning velocities of stoichiometric mixtures of butadiene-1,3 with normal air and helium air.

| Mixture with | Total pressure $p$ atmos. | Flame temp. (calc.)[a] $T$ °K | Partial pressure of H-atoms[a] $p_H$ atmos. | Specific mass of fresh gases $\rho_u$ Kg/m³ | $\frac{\mu}{1-\mu}$ | Pressure drop $\Delta p$ mm $H_2O$ | Burning velocity $V$ cm/sec, Calc. | Obs.[a] |
|---|---|---|---|---|---|---|---|---|
| Normal air | 1 | 2 380° | 8.8 $10^{-4}$ | 1.21 | 0.137 | 0.57 | 79 | 43 |
| | 0.5 | 2 350° | 5.7 $10^{-4}$ | 0.60 | 0.139 | 0.37 | 92 | 53 |
| Helium air | 1 | 2 660° | 4.3 $10^{-3}$ | 0.47 | 0.117 | 2.48 | 246 | 143 |
| | 0.5 | 2 600° | 2.64 $10^{-3}$ | 0.23 | 0.120 | 1.56 | 282 | 179 |

[a] See reference 1.

TABLE II. Burning velocity ratios of butadiene-1,3 with normal air and helium air mixtures.

| Total pressure | ratio: $r=(V)_H/(V)_A$ Obs.[a] | Calc.[a] | Calc. | Mixture | ratio: $(V)p=1/(V)p=0.5$ Obs.[a] | Calc.[a] | Calc. |
|---|---|---|---|---|---|---|---|
| 1 atmos. | 3.3 | 3.2 | 3.1 | *n* air | 0.81 | 0.88 | 0.86 |
| 0.5 | 3.4 | 3.1 | 3.1 | He air | 0.80 | 0.90 | 0.87 |

[a] See reference 1.

TABLE III. Burning velocity ratios of flames in $CO$-$O_2$-He and $CO$-$O_2$-A mixture with $H_2O$ (mole fraction: 0.0269).

| Mole fraction of inert gas | $[CO]/[O_2]$ =0.503 | | Ratio: $r=(V)_{He}/(V)_A$ =1.083 | | =1.234 | | =2.698 | |
|---|---|---|---|---|---|---|---|---|
| | Obs.[a] | Calc.[b] | Obs.[a] | Calc.[b] | Obs.[a] | Calc.[b] | Obs.[a] | Calc.[b] |
| 0.10 | 1.05 | 1.07 | 1.09 | 1.07 | 1.05 | 1.07 | 1.03 | 1.07 |
| 0.15 | 1.09 | 1.12 | 1.12 | 1.10 | 1.09 | 1.10 | 1.06 | 1.10 |
| 0.20 | 1.13 | 1.15 | 1.19 | 1.14 | 1.13 | 1.14 | 1.08 | 1.14 |
| 0.25 | — | — | 1.25 | 1.18 | 1.16 | 1.18 | — | — |

[a] See reference 4.
[b] Formula (2).

study of the ratios of burning velocities in mixtures of $CO$-$O_2$-$H_2O$ with helium or argon as investigated by Fiok and Roeder[5] by means of the soap bubble method. It is then found that (Table III)

$$r=\frac{V \text{ in mixture with He}}{V \text{ in mixture with A}}=\left[\frac{\rho_u \text{ of the mixture with A}}{\rho_u \text{ of the mixture with He}}\right]^{\frac{1}{2}}. \quad (2)$$

These remarks as well as others show that at present the theory of shock and combustion waves supplemented by the hypothesis of the projection of the hydrogen atoms (which explains the pressure drop in the combustion zone) yields a rather complete interpretation of the influence of various factors on the burning velocities in gas mixtures.

[1] Badin, Stuart, and Pease, J. Chem. Phys. **17**, 324 (1949).
[2] E. Jouguet, *La Mécanique des Explosifs* (Ed. Doin, Paris, 1947).
[3] N. Manson, Comptes Rendus 226, 230 (1948); Revue de l'Institut Francais du Petrole **4**, No. 7, 9 (1949).
[4] In the comparison of values of $V$ calculated by means of Eq. (1) and measured by the burner method, one must not forget that the latter method yields (as B. Lewis and G. von Elbe, J. Chem. Phys. **11**, 75 (1943) and others have shown) a certain average velocity along the flame cone and not the velocity actually defined in theory.
[5] E. F. Fiok and Ch. Roeder, N.A.C.A. Report No. 553.

## Infra-Red Absorption Spectra at Low Temperatures

A. WALSH AND J. B. WILLIS
*Division of Industrial Chemistry, Commonwealth Scientific and Industrial Research Organization, Melbourne, Australia*
July 18, 1949

THE temperature dependence of infra-red absorption bands has been studied by Avery and Ellis,[1] who state that for several aliphatic hydrocarbons there is a distinct sharpening of the bands in going from room temperature to −195°C. They interpret their results on the basis of Bjerrum's formula, according to which the separation of the maxima of the $P$ and $R$ branches of an absorption band is proportional to $T_{abs}^{\frac{1}{2}}$. This formula obviously only applies to gases, and would not be expected to hold for liquids and solids, whose spectra do not normally exhibit rotational structure. All the compounds studied by Avery and Ellis were either liquid or solid at −195°C, and it is surprising to find that Bjerrum's formula is even approximately true. For low boiling gases, such as ethane, appreciable narrowing of the bands will occur before the gas liquefies, and thus we might expect the low temperature spectrum of the liquid to have narrower bands than the gas at room temperature, quite apart from any changes accompanying liquefaction. In the case of 2,2-dimethylbutane, which boils at 50°C, it is difficult on this basis to see why the bands of the liquid spectrum at −195°C should be much narrower than those in the vapor at room temperature. It is even more surprising that the narrowing actually observed by Avery and Ellis is in good agreement with the Bjerrum formula. In our opinion this agreement is entirely fortuitous, since comparison with spectrogram No. 245 issued by the American Petroleum Institute shows that the absorption bands in the spectrum of *liquid* 2,2-dimethylbutane at room temperature have the same width as those in the low temperature spectrum given by Avery and Ellis. The band-narrowing attributed by these authors to the temperature effect is thus seen to be entirely due to the change of state.

We have recently obtained the infra-red spectra of several solids at room temperature and at −180°C, and find no systematic change of band-width with temperature. In general there is little or no narrowing of the bands with decreasing temperature, though minor changes in the spectrum do sometimes occur, due perhaps to changes in crystal structure or to λ-point transitions. In the case of a mixture of higher paraffins (Nujol), there is practically no change in going from the liquid at room temperature to the solid at −180°C.

In a later paper[2] Avery and Morrison imply that the Bjerrum formula holds quite generally, irrespective of the state of the sample, and suggest that further narrowing of absorption bands may be obtained by using liquid hydrogen or helium as cooling agents. In view of our results we consider this to be unlikely, since most compounds are solid at −195°C, and we do not consider that any further decrease in temperature will result in appreciable narrowing of the absorption bands.

A full report of our investigations will be published subsequently.

[1] W. H. Avery and C. F. Ellis, J. Chem. Phys. **10**, 10 (1942).
[2] W. H. Avery and J. R. Morrison, J. App. Phys. **18**, 960 (1947).

## Infra-Red and Raman Spectra of Hexachloroethane

S. MIZUSHIMA, Y. MORINO, T. SIMANOUTI, AND K. KURATANI
*Chemical Institute, Faculty of Science, Tokyo University, Tokyo, Japan*
July 7, 1949

AS a part of a series of researches on intra-molecular rotation we studied the Raman spectrum of hexachloroethane.[1] This was also studied by Hamilton and Cleveland in various solutions.[2] Recently, one of us has calculated the normal vibrations of ethane-like molecules in the staggered form **D3d** by use of the Urey-Bradley field.[3] However, it is evident from the symmetry of the molecule that the normal frequencies of this form are coincident with those of the eclipsed form **D3h**, so far as the interaction between the chlorine atoms attached to different movable parts of the molecule is neglected. Therefore, for the discrimination between these two molecular forms we have to refer to the selection rule: in other words, we must observe not only the Raman effect but also the **infra-red** absorption.

TABLE I. Infra-red and Raman spectra of hexachloroethane.

| Infra-red spectrum* Wave number ($cm^{-1}$) | Intensity | Raman spectrum Wave number ($cm^{-1}$) | Intensity |
|---|---|---|---|
| | | 140 | 1 broad |
| 675 | Medium | 169 | 2 broad |
| | | 224 | 6 |
| 769 | Strong | 341 | 5 |
| | | 432 | 10 |
| 1008 | Weak | 853 | 2 |
| | | 974 | 1 |

* The spectrum observed in $CCl_4$ solution was essentially the same as that in the solid state.

TABLE II. The comparison of the observed and the calculated fundamental frequencies of hexachloroethane.

| Type | Calculated* ($cm^{-1}$) | Raman observed | Type | Calculated* ($cm^{-1}$) | Infra-red observed |
|---|---|---|---|---|---|
| | 198 | 169 | | | |
| | | | | 382 | — |
| $A_{1g}$ | 432 | 432 | $A_{2u}$ | | |
| | | | | 729 | 675 |
| | 1008 | 974 | | | |
| | 218 | 224 | | 134 | — |
| $E_g$ | 322 | 341 | $E_u$ | 278 | — |
| | 889 | 853 | | 744 | 769 |

* For the form of the potential function and the values of the force constants see reference 3.

The absorption spectra (8–16$\mu$) were observed in the solid state and in carbon tetrachloride solution. The experimental technique and the apparatus used were essentially the same as described in our previous paper.[4] The result is shown in Table I. The band observed at 1008 $cm^{-1}$ is very weak and might be assigned to one of the combination tones.

The Raman spectra were remeasured in the solid state. In Table I the result is shown, which is in good agreement with that obtained by Hamilton and Cleveland.[2] The existence of a line at 169 $cm^{-1}$ reported by them was confirmed. It seems that there was found a line at 140 $cm^{-1}$ by Hg$-e$ excitation, but we are not sure if this is really a Raman line, because there is a weak mercury line practically at the same position. We can assign the line at 169 $cm^{-1}$ to a deformation vibration of the molecule and that at 140 $cm^{-1}$ to the lattice vibration, because the latter was not observed by Hamilton and Cleveland in the spectra of solutions.

The two infra-red active vibrations expected for the staggered form were detected by the present experiment (see Table II). The other three frequencies also active in the infra-red lie out of the observable region of our apparatus. If the molecular form were the eclipsed one, the frequency 769 $cm^{-1}$ of **Eu** observed in the infra-red spectra should also appear in the Raman effect. However, no Raman line was detected in this frequency region. We can, therefore, conclude in conformity with our previous result that the stable configuration of hexachloroethane is the staggered form **D3d**. This conclusion had been established by our electron diffraction investigation.[5]

The calculated frequencies of the Raman active vibrations are in good agreement with the observed values (see Table II). This agreement shows that the Urey-Bradley field is an adequate potential function for the treatment of the normal vibration of such a molecule.

[1] S. Mizushima and Y. Morino, Sci. Papers Inst. Phys. Chem. Research (Tokyo) **29**, 188 (1936).
[2] D. T. Hamilton and F. F. Cleveland, J. Chem. Phys. **12**, 249 (1944).
[3] T. Simanouti, J. Chem. Phys. **17**, 734 (1949).
[4] Simanouti, Turuta, and Mizushima, Sci. Papers Inst. Phys. Chem. Research (Tokyo) **42**, 51 (1946).
[5] Y. Morino and M. Iwasaki, J. Chem. Phys. **17**, 216 (1949).

## Viscoelastic and Photoelastic Properties of Polystyrene above Its Softening Temperature

LAWRENCE E. NIELSEN AND ROLF BUCHDAHL
*Research Department, Plastics Division, Monsanto Chemical Company, Springfield, Massachusetts*

July 21, 1949

IN a study of creep, recovery after creep, stress relaxation, and optical anisotropy of polystyrene films above their softening temperature, we have obtained certain results which appear to be of significance in obtaining a better understanding of the mechanism of viscoelastic deformations and of the molecular structure, not only of polystyrene, but also of so-called linear and amorphous linear high polymers in general.

TABLE I. Creep of polystyrene at 110°C.

| Time (sec.) | Elongation % | Birefringence A/mil | Stress lb./in.$^2$ | Birefringence stress |
|---|---|---|---|---|
| 0 | 0 | 0 | 24.4 | — |
| 40 | 22.1 | −217 | 29.8 | −7.28 |
| 75 | 33.3 | −289 | 32.5 | −8.90 |
| 130 | 46.5 | −324 | 35.7 | −9.08 |
| 190 | 57.2 | −359 | 38.3 | −9.38 |
| 275 | 69.3 | −373 | 41.3 | −9.02 |
| 375 | 83.9 | −413 | 44.9 | −9.22 |
| 480 | 99.5 | −448 | 48.7 | −9.22 |
| 590 | 116.4 | −485 | 52.8 | −9.18 |
| 700 | 132 | −513 | 56.6 | −9.08 |
| 820 | 154 | −556 | 62.0 | −8.97 |
| 940 | 173 | −605 | 66.6 | −9.08 |
| 1060 | 193 | −634 | 71.5 | −8.88 |

Table I gives the strain and birefringence (A/mil) as a function of time at 110°C, when a constant weight is applied to a film* made from unfractionated polystyrene ($(\eta)=1.13$). As the cross section changes during the run, the stress per unit area varies also, and column 4 of Table I gives the actual values of stress calculated from the elongation using a Poisson's ratio of 0.5. Column 5 shows the ratio of the birefringence to stress which is constant except for the initial part of the run. It can also be seen that the ratio of birefringence to strain changes continuously. Similar experiments at other temperatures and with films made from fractionated polystyrene ($(\eta)=1.56(\eta)\doteq0.59$) and a film consisting of a mixture of fractionated polystyrene and a low molecular weight compound showed that this ratio is not only independent of stress, strain, and time but also does not depend on molecular weight within the investigated range and depends only very slightly on temperature.

Table II shows the stress and birefringence relaxation of a polystyrene film. Again the ratio of birefringence to stress is essentially independent of time and is the same as obtained from the "creep" experiment given in Table I. The significant feature of this experiment is the fact that this stretched film recovered almost completely when the external force was removed at any time during the relaxation process of stress and birefringence.

Finally, it was found that repeated stress and birefringence relaxation runs (cycling) on the same film had an effect on the shape and magnitude of the stress and birefringence relaxation curves; cycling always decreases the magnitude of the stress and leads to a more rapid initial stress decay. Similarly, it was found that repeated creep runs (in shear) did not yield identical curves but frequently gave higher initial compliances on consecutive runs.

In an attempt to find at least a qualitative interpretation of these results, we have come to the conclusion that the usual assumptions made to explain the viscoelastic behavior of linear high polymers[1]—retarded elastic deformation and viscous flow—are not sufficient but that it becomes necessary to assume the existence of a semipermanent network structure.** This structure

TABLE II. Stress and birefringence relaxation in polystyrene at 110°C (elongation = 95 percent).

| Time (sec.) | Birefringence A/mil | Stress lb./in.$^2$ | Birefringence stress |
|---|---|---|---|
| 0 | — | — | — |
| 45 | −738 | >75 | — |
| 90 | −573 | 62.5 | −9.17 |
| 135 | −516 | 56.0 | −9.22 |
| 170 | −476 | 50.8 | −9.36 |
| 245 | −426 | 46.8 | −9.10 |
| 300 | −410 | 44.3 | −9.25 |
| 400 | −369 | 40.2 | −9.17 |
| 475 | −361 | 39.1 | −9.24 |
| 600 | −343 | 36.5 | −9.40 |
| 730 | −311 | 33.9 | −9.18 |
| 900 | −295 | 33.9 | −8.72 |
| 950 | −287 | 32.6 | −8.80 |

is most likely brought about by the intertwining of at least two or more chain segments belonging to the same or to different chain molecules and it is obvious that temperature and external forces have a pronounced effect on the average lifetime of these net points which are much less stable than the net points due to chemical crosslinking. Without the assumption of a semipermanent network, it does not seem possible to account for the fact (a) that the birefringence stress ratio remains constant and the deformation is almost completely recoverable at the same time, (b) that the birefringence and the stress can relax by a factor 2 to 3 without destroying the ability of the material to recover to its original length, (c) that "cycling" has an effect on the stress and birefringence relaxation and the initial creep compliance, and (d) that polystyrene exhibits anomalous flow characteristics[2] at temperatures much above its softening temperature. More experimental data and a more thorough discussion of some of the results given above, such as the initial change of the birefringence-stress ratio with time, the relationship of birefringence to orientation, etc., will be published in the near future.

* All films were prepared following a technique previously described; see Abstracts in Proceedings of the American Physical Society Meeting at New York, Phys. Rev. 75, 1279 (1949).

[1] T. Alfrey, Jr., *Mechanical Behavior of High Polymers* (Interscience Publishers, Inc., New York, 1948), pp. 93–228.

** Recently one of the authors suggested such a network structure on the basis of flow measurements on polystyrene at high temperature. (See J. Colloid Sci.)

[2] R. Buchdahl, J. Colloid Sci. 3, 87 (1948).

## On the Detection and Determination of Redundant Vibrational Coordinates*

C. E. Sun,** Robert G. Parr,*** and Bryce L. Crawford, Jr.
*School of Chemistry, University of Minnesota, Minneapolis, Minnesota*
July 5, 1949

In using valence-force coordinates (*VFC*) in a normal-coordinate treatment, one not infrequently finds it convenient, for symmetry reasons, to consider a redundant set; i.e., a set of coordinates which are not all independent. The neatest example is the set of six HCH angle deformations, $\Delta\alpha_{ij}$, in $CH_4$; these are of course connected by the *redundancy condition*

$$\sum_{i>j} \Delta\alpha_{ij}=0. \tag{1}$$

Wilson[1] has discussed such redundant coordinates, the possible ways of treating them, and the consequent restrictions on the potential energy.

While one usually knows or easily finds out that a set of coordinates is redundant, it is not always so easy to find the redundancy condition analogous to (1).[2] The purpose of this note is to present a convenient way to do this, using Wilson's $G$ matrix technique.[1] In our practice we need to find this redundancy, for we prefer to transform from our initial *VFC* to a set of symmetry coordinates *one of which is precisely the redundancy;* both the $F$ and $G$ matrices are so transformed. Then the $G$ matrix has a row and column of zeros,[1] which may be neglected together with the corresponding row and column of the $F$ matrix.

If the redundancy condition is initially not known, we may still set up symmetry coordinates, found from the *VFC* by elementary group theory.[3] Moreover, the symmetry species containing the redundancy is easily found, either by noting which species has an extra coordinate, or (in case a needed coordinate has been inadvertently neglected and a redundant one unwittingly included) by observing that the $G$ matrix factor for this species has a zero determinant.

Let $S_k$ be the symmetry coordinates in which a redundancy lurks, so that $|G|=0$, where $G$ is the inverse kinetic-energy matrix for the $S_k$. We seek to transform to the coordinates $\bar{S}_n$ such that $\bar{S}_1$ is the redundancy condition: $\bar{S}_1=0$. Let the transformation be orthogonal, so that

$$\bar{S}_n=\Sigma_k L_{nk}S_k, \tag{2}$$
$$\Sigma_n L_{nk}L_{nj}=\delta_{kj}. \tag{3}$$

Now if $\bar{G}$ is the inverse kinetic-energy matrix for the $\bar{S}_n$, $\bar{G}$ and $G$ are related:

$$\bar{G}_{nm}=\Sigma_{jk} L_{nk}G_{kj}L_{mj}. \tag{4}$$

Moreover, since $\bar{S}_1$ is the redundancy,

$$\bar{G}_{1n}=\bar{G}_{n1}=0, \quad \text{all } n. \tag{5}$$

Hence, taking $m=1$ in (4), multiplying through by $L_{ni}$, summing on $n$ and using (3), we find

$$\Sigma_j G_{ij}L_{1j}=0. \tag{6}$$

This tells us, then, how to find our redundancy condition $\bar{S}_1=\Sigma_j L_{1j}S_j=0$; if we regard our original $G$ as the matrix of coefficients of a set of homogeneous linear equations, the transformation coefficients $L_{1j}$ are just the "unknowns" whose ratios are determined. (Normalization completes the determination of the $L_{1j}$.) The remaining coefficients $L_{nk}(n\neq 1)$ may be written down as usual to make $L$ orthogonal,[4] and the resulting $L$ used to transform both $F$ and $G$.

If a species contains, say, $s$ redundancies among $n$ coordinates ($s>1$), then the $G$ matrix factor will be of order $n$ but of rank $(n-s)$. The usual algebraic procedures[5] for treating linear homogeneous equations will then give us the $s$ sets of redundancy coefficients $L_{1j}, L_{2j}, \cdots, L_{sj}$.

* The studies here reported form part of a research program which is facilitated by support from the Navy Department, ONR, through contract N5ori-212, T.O. II, with the University of Minnesota.

** At Minnesota on leave from National University of Peking, China, 1947–48.

*** Present address: Department of Chemistry, Carnegie Institute of Technology, Pittsburgh, Pennsylvania.

[1] E. Bright Wilson, Jr., J. Chem. Phys. 9, 76 (1941).

[2] The reader complacent about geometry may write down the redundancy conditions among the six C-C distances and six C-C-C angles in cyclohexane.

[3] E. P. Wigner, *Gruppentheorie* (Edwards Brothers, Inc., Ann Arbor, Michigan, 1944); p. 123.

[4] *Inter alia*, reference 3, p. 31.

[5] Bocher, *Higher Algebra* (The Macmillan Company, New York, 1907); Chapter IV.

## The Methylene Radical

George H. Duffey
*Chemistry Department, South Dakota State College, Brookings, South Dakota*
July 28, 1949

In a recent Letter to the Editor Laidler and Casey[1] discuss the methylene radical, $CH_2$. They state that since the bond angle in the lowest state is about 140°, this state cannot be a triplet state. However, one may use hybrid orbitals for the two unshared electrons as well as for the two shared electron pairs.

Thus one may use the $sp^3$ hybrid orbitals[2] appropriate to $AB_2C_2$ for the covalent triplet structure. If Pauling's criterion[3] of strength is employed and if the interaction energy[4] of a shared electron pair equals that of an unshared electron, one would expect the tetrahedral structure (the structure with the H-C-H angle equal to 109° 28′) to be the most stable of the triplet structures.

The covalent singlet structure may be discussed as follows. Set up the functions appropriate to $AB_2C$, where A is the central atom, assuming the bonds lie in a plane. Thus

$$\psi_1=a_1s+b_1p_x, \tag{1}$$
$$\psi_2=a_2s-b_2p_x+c_2p_y, \tag{2}$$
$$\psi_3=a_3s-b_3p_x-c_3p_y. \tag{3}$$

Here $\psi_1$ describes the orbital occupied by the unshared electron pair, and $\psi_2$ and $\psi_3$ describe the orbitals used in forming the bonds.

The orthogonality and normalization conditions together with the equation $a_2=a_3$ yield

$$c_2=c_3=\frac{1}{\sqrt{2}}, \tag{4}$$

$$b_2=b_3=(\tfrac{1}{2}-a_2^2)^{\frac{1}{2}}. \tag{5}$$

The constants $a_1$ and $b_1$ can be expressed in terms of $a_2$ also. The functions $\psi_2$ and $\psi_3$ depend on the parameter $a_2$. They are strongest when the angle between their maxima, $\theta$, equals the tetrahedral angle and their strength, $S$, equals that of tetrahedral bonds. This singlet structure does not require the promotion of an $s$ electron since it requires no contribution from $p_z$. Hence it should be more stable than the triplet structure. The conclusion is supported by the experimental work cited by Laidler and Casey.[1]

If we assume $\theta$ equals 140° in the singlet structure, we find that $a_2$ equals 0.659 and $S$ equals 1.962. Now $S$ equals 2.000 when $\theta$ equals 109° 28′. The 140° structure might be stabilized by the ionic character of the bonds. An alternative explanation is that Pauling's criterion of strength underestimates somewhat the contribution from the $s$ orbital to the stability of the bonds.[5]

[1] K. J. Laidler and E. J. Casey, J. Chem. Phys. **17**, 213 (1949).
[2] G. H. Duffey, J. Chem. Phys. **14**, 342 (1946).
[3] L. Pauling, *The Nature of the Chemical Bond* (Cornell University Press, Ithaca, 1940).
[4] See H. Kuhn, J. Chem. Phys. **16**, 727 (1948).
[5] See R. S. Mulliken *et al.*, J. Chem. Phys. **17**, 510 (1949). The author has received a private communication (1949) from A. Maccoll of University College, London regarding the same subject.

## Near-Equilibrium Criteria for Complex Chemical Reactions during Flow through a Nozzle*

S. S. PENNER
*Jet Propulsion Laboratory, California Institute of Technology, Pasadena, California*
June 29, 1949

CALCULATIONS of the effect of vibrational and chemical lags on the exhaust velocity of the combustion products formed in conventional rocket motors have been restricted previously[1] to a consideration of individual processes without the introduction of corrections for the interdependence of the chemical reactions or of the vibrational distributions. The approach to chemical equilibrium for a number of interdependent chemical reactions can be handled, at least in principle, by a straightforward generalization of the techniques described previously. Calculations on complex systems require the solution of a number of simultaneous linear and non-linear equations.

*Non-linear relations between the temperature lags in complex systems.* Consider a system of chemical reactions of $n-1$ individual steps leading to the over-all reaction shown in the $n$'th step, as follows:

$$\alpha_j+\beta_j+\cdots\rightleftarrows\gamma_j+\delta_j+\cdots, \quad j=1, 2, \cdots, n.$$

The statement that step $n$ is the sum of steps 1 to $n-1$ means that

$$\alpha_n+\beta_n+\cdots=\sum_{i=1}^{n-1}\alpha_i+\sum_{i=1}^{n-1}\beta_i+\cdots;$$

$$\gamma_n+\delta_n+\cdots=\sum_{i=1}^{n-1}\gamma_i+\sum_{i=1}^{n-1}\delta_i+\cdots.$$

Furthermore, if $K_j^0$ ($j=1, 2, \cdots, n$) denotes the equilibrium constant for the $j$'th step, then

$$K_n^0=\prod_{i=1}^{n-1}K_i^0.$$

During the adiabatic expansion through a nozzle thermodynamic equilibrium is not maintained with respect to the $n$ chemical reactions described above. Each of the $n$ reactions, considered individually, suffers a temperature lag which is designated as $T_j-T$ and defined by the relation

$$K_j=\frac{\Pi\text{-molecular concentrations of the species formed in step } j}{\Pi\text{-molecular concentrations of the species reacting in step } j}$$

where $K_j$ is the equilibrium constant for the $j$'th step not at the true temperature $T$, but at a temperature $T_j$ which differs from $T$. If the temperature lag $T_j-T$ is sufficiently small, then it is said that step $j$ is in near-equilibrium. From the definition of $K_j$ it is evident that

$$K_n=\prod_{i=1}^{n-1}K_i. \tag{2}$$

The quantities $K_j$ may be expressed[1] in terms of the quantities $K_j^0$ by making use of a Taylor series; if $T_j-T$ is sufficiently small, all but the first two terms of the Taylor series may be neglected. Therefore

$$K_j=K_j^0+K_j^0\frac{d\ln K_j^0}{dT}(T_j-T). \tag{3}$$

Replacing $K_j$ in Eq. (2) by its value from Eq. (3) it can readily be shown that

$$T_n-T=\sum_{i=1}^{n-1}\frac{d\ln K_i^0/dT}{d\ln K_n^0/dT}(T_i-T)+\sum_{i<m=2}^{m=n-1}\frac{d\ln K_i^0/dT}{d\ln K_n^0/dT}\cdot(d\ln K_m^0/dT)(T_i-T)(T_m-T)+\cdots+\prod_{i=1}^{n-1}\frac{d\ln K_i^0/dT}{d\ln K_n^0/dT}(T_i-T). \tag{4}$$

Equation (4) is the desired result, since it gives an analytic expression for the temperature lag $T_n-T$ in terms of the temperature lags of the individual $n-1$ steps provided near-equilibrium is maintained with respect to each of the $n$ individual reactions.

*Linear relations between the temperature lags in complex systems.* The linear relations between the temperature lags in complex systems involve the individual rate constants for each of the steps of a complex chemical reaction. It is possible to write one equation which is linear in the terms $T_j-T$ for each of the steps of a complex reaction. The number of independent linear equations is equal to the number of chemical reactions which cannot be constructed by simple additions or subtractions involving other chemical reactions which are known to be independent in this sense.

The linear equations can be obtained by following the procedure outlined previously[1] taking care, however, to allow for the simultaneous participation of a given reactant in several alternative reaction paths. A representative result obtained from Eq. (5) for the set of reactions

$$2H+M\rightleftarrows H_2+M \tag{5}$$
$$H_2+F\rightleftarrows HF+H \tag{6}$$
$$2F+M\rightleftarrows F_2+M \tag{7}$$
$$H+F_2\rightleftarrows HF+F \tag{8}$$
$$H+F+M\rightleftarrows HF+M \tag{9}$$
$$H_2+F_2\rightleftarrows 2HF \tag{10}$$

is

$$\begin{aligned}&[\Delta H_5-\gamma RT(\gamma-1)^{-1}](-dT/dt)\\&=kf_5(M)(\Delta H_5-RT)[1/K_5+2(H)](T_5-T)\\&\quad-kf_6(F)(\Delta H_6)[1+2(H_2)/(H)](T_6-T)\\&\quad+2kf_8(F_2)(\Delta H_8)(T_8-T)+2kf_9(F)(M)\\&\qquad\times[\Delta H_9-RT](T_9-T)-kf_{10}(F_2)(\Delta H_{10})(T_{10}-T)\end{aligned} \tag{11}$$

where the contributions to the concentration changes resulting from the change of state during adiabatic expansion have been taken into account. Equations similar to Eq. (11) can be derived readily from Eqs. (6) to (10). However, of the six linear equations involving the temperature lags $T_5-T$ to $T_{10}-T$ only three are independent. This must be true, since it is possible, for example, to derive Eqs. (6), (8), and (10) from Eqs. (5), (7), and (9). A sufficient number of relations between the temperature lags

can then be obtained by making use of an adequate number of non-linear equations.

*Application to propellant systems.* As soon as attempts are made to utilize the general formulas between the temperature lags, difficulties are encountered because of the lack of adequate data for the reaction rate constants. The six simultaneous relations determined from Eqs. (5) to (10) do not necessarily lead to meaningful results unless some of the rate constants $k_{f5}$ to $k_{f10}$ are known with considerable accuracy. This conclusion follows immediately from the well-known loss of significant digits which may be encountered during the inversion of matrices.[2]

Limited application of the techniques discussed here is of interest, and has been made for the set of reactions given in Eqs. (5) to (10). For example, it is found that the temperature lag $(T_{10}-T)$ is of the same order of magnitude as the temperature lags $(T_6-T)$ and $(T_8-T)$ even if the direct reaction between $H_2$ and $F_2$ occurs relatively slowly. Similarly, the simultaneous occurrence of reactions (6) and (8) does not produce temperature lags significantly different from those determined on the assumption that these reactions occur independently. Finally, by applying the usual intuitive rules of chemical kinetics to complex systems, the qualitative conclusion may be drawn that near-equilibrium will obtain for a complex set of reaction if some of the possible reactions occur with sufficient speed to maintain nearly complete thermodynamic equilibrium, and these fast reactions are sufficient in number to allow all of the necessary atomic and molecular concentration changes.

In conclusion, the author takes pleasure in expressing his appreciation to Mr. J. Lorell for helpful discussion of various sections of this report.

* This paper presents the results of one phase of research carried out at the Jet Propulsion Laboratory, California Institute of Technology, under U. S. Army Ordnance Department Contract No. W-04-200-ORD-1482.

[1] S. S. Penner, J. Am. Chem. Soc. **71**, 788 (1949). See also J. Franklin Inst. **245**, 421 (1948); J. Chem. Phys. **17**, 56 (1949); J. App. Phys. **20**, 445 (1949).

[2] J. von Neumann and H. H. Goldstein, Bull. Am. Math. Soc. **53**, 1021 (1947). The physical reason for the loss of significant figures is associated with the fact that several of the rate-determining reaction rates are of similar magnitude.

## The Deslandres-D'Azambuja Band System of the $C_2$ Molecule in the Ethylene-Oxygen Flame*

GEORGE A. HORNBECK AND ROBERT C. HERMAN
*Applied Physics Laboratory, The Johns Hopkins University, Silver Spring, Maryland*

July 21, 1949

THE Deslandres-D'Azambuja band system of the $C_2$ molecule has heretofore been obtained in both condensed and uncondensed discharges. These bands were analyzed by Dieke and Lochte-Holtgreven[1] and Kopfermann and Schweitzer.[2] Most recently, Herzberg and Sutton[3] analyzed a number of new bands of the $C_2$ molecule, which were found to be tail bands of the Deslandres-D'Azambuja system.

Investigators of hydrocarbon flame spectra have reported the Swan ($^3\Pi_g-{}^3\Pi_u$) and Mulliken ($^1\Sigma_u^+-{}^1\Sigma_g^+$) band systems of the $C_2$ molecule.[4] The purpose of this note is to report the appearance of the Deslandres-D'Azambuja bands ($^1\Pi_g-{}^1\Pi_u$) as a prominent feature of both the ethylene-oxygen and methane-oxygen flames.

The fuel and oxygen were premixed and burned off a grid orifice at a pressure of about 50 mm. In each case the fuel-oxygen ratio was stoichiometric. Under these conditions an intense blue flat reaction zone was obtained. Spectrograms were obtained in the second order of a 2-meter Baird grating spectrograph (4A/mm) in the region ~3100A to ~4100A.

All the Deslandres-D'Azambuja bands listed by Herzberg and Sutton[3] have been identified in the case of the ethylene-oxygen flame except the (5,3) and (4,2) bands. The former is obscured by the (0,1) band of OH and the latter is headless. While band heads were not measured for the methane-oxygen flame spectra direct comparison reveals the presence of most of these bands. In Fig. 1 is a densitometer tracing of a sequence of Deslandres-D'Azambuja bands.

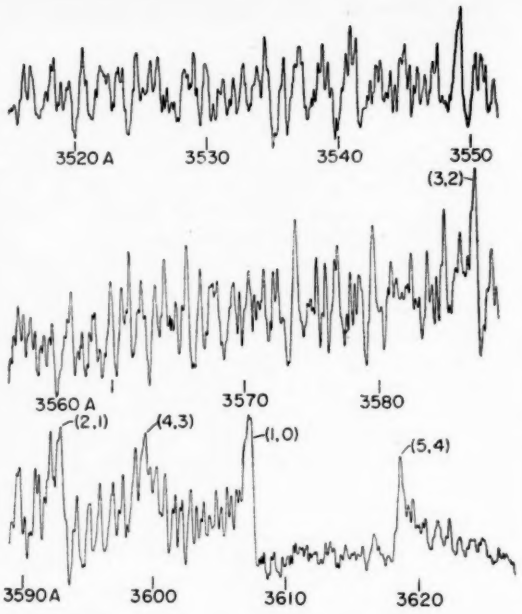


FIG. 1. Densitometer tracing of a sequence of Deslandres-D'Azambuja bands of the $C_2$ molecule.

We wish to express our appreciation to Dr. G. Herzberg, National Research Council, Canada, for his interest and invaluable discussion. We thank Helen S. Hopfield for her aid in making the plate measurements.

* The work described in this paper was supported by the Bureau of Ordnance, U. S. Navy, under Contract NOrd-7386.

[1] G. H. Dieke and W. W. Lochte-Holtgreven, Zeits. f. Physik **62**, 767 (1930).

[2] H. Kopfermann and H. Schweitzer, Zeits. f. Physik **61**, 87 (1930).

[3] G. Herzberg and R. B. Sutton, Can. J. Research **18**, 74 (1940).

[4] A. G. Gaydon, *Spectroscopy and Combustion Theory* (Chapman and Hall, Ltd., London, 1948).

## Erratum: The Quantum Mechanics of Chemical Kinetics of Homogeneous Gas Phase Reactions. II. Approximations for Displacement Reaction between an Atom and a Diatomic Molecule

[J. Chem. Phys. **17**, 630 (1949)]

S. GOLDEN AND A. M. PEISER
*Hydrocarbon Research, Inc., New York, New York*

THE designation of ortho and para states for the upper curve of Fig. 3 (labeled $n=1$) should be interchanged. Ortho states are all those having odd rotational quantum numbers, while para states have even rotational quantum numbers.

This means that approximately 40 percent of the contribution to the rate comes from hydrogen molecules in the first excited vibrational states having rotational quantum number $K=3$, instead of $K=4$ as stated in the text. Hydrogen molecules having rotational quantum numbers 2, 3, 4 make up approximately 60 percent of the rate, instead of 75 percent as stated in the text. All other conclusions are not affected.

## Infra-Red Evidence for Free Rotation in the Solid State

L. F. H. Bovey and G. B. B. M. Sutherland*
*Laboratory of Colloid Science, Cambridge, England*
July 28, 1949

THE exact nature of what happens at phase transitions in many crystals and in particular whether certain λ-points are to be associated with the onset of free rotation of either the entire molecule or of certain molecular groups in the crystal is a problem which has been studied from time to time by the methods of infra-red spectroscopy. In two separate publications[1,2] it has been stated that rotational fine structure has been observed in the infra-red spectra of crystalline materials (HCl and ammonium halides) and this evidence has been quoted as proof of the existence of free rotation in these cases. In the case of solid HCl, subsequent workers[3] failed entirely to confirm the presence of rotational fine structure and produced strong evidence that the so-called fine structure was spurious and due to water vapor. In the case of the ammonium halides subsequent workers[4] have also failed to confirm the rotational fine structure, which again appears to arise from spurious water vapor fine structure superimposed on a structureless band.

We wish to report briefly that we have been engaged periodically for some years on a careful study of the infra-red absorption spectra of the ammonium halides over a wide range of temperature (−150°C to 20°C). In agreement with Wagner and Hornig[4] we have found no sign whatever of rotational fine structure, although we have examined the bands given in the following table of ammonium fluoride, chloride, and bromide under very high resolving power using either a grating or a prism spectrometer of high dispersive power, both with continuous recording of spectra (see Table I).

Table I.*

| Band | Equivalent slit width | $NH_4F$ 20°C | $NH_4F$ −150°C | $NH_4Cl$ 20°C | $NH_4Cl$ −150°C | $NH_4Br$ 20°C | $NH_4Br$ −150°C |
|---|---|---|---|---|---|---|---|
| 7μ | 3 ohm$^{-1}$ | 1482 | 1492 | 1398<br>1435 | 1400 | 1375<br>1425 | 1405<br>1435 |
| 5.5μ | 4 ohm$^{-1}$ | | | 1762 | 1818 | 1695 | 1705 |
| 5.0μ | 5 ohm$^{-1}$ | 2050 | 2050<br>(2150) | 2010 | 2035<br>2070<br>2175 | 1950 | 1956 |
| 4.0μ | 5 ohm$^{-1}$ | 2298 | 2300 | | (2460)<br>(2690) | | |
| 3.2μ | 5 ohm$^{-1}$ | | | 2835<br>2990<br>3115 | 2835<br>3050<br>3095<br>3116<br>3134 | 2800<br>3065<br>3170 | 2800<br>3025<br>3075<br>3205 |

* Frequencies in brackets correspond to absorption of very low intensity and narrow width.

The table gives results obtained with the prism instrument but the spectra obtained by Mr. D. E. Blackwell with gratings with equivalent slit width in the 5μ region of 1 ohm$^{-1}$ show no sign of the fine structure reported by Beck[2] as having a mean speacing of 15 ohm$^{-1}$ work with a double beam instrument (which automatically corrects for atmospheric absorption) confirms these conclusions.

Work in progress on the 3.2μ band of fluoride shows it to be similar to that of the other halides while preliminary results on ammonium iodide indicate that although the 7μ and 3.2μ bands are again present, the absorption in other regions is either absent or very much weaker than in the remaining halide salts.

It is interesting that although the infra-red spectra of all four compounds show considerable changes with temperature (similar in general character to those reported by Wagner and Hornig[4]) no sharp change appears to take place in the spectrum at the transition temperature. We should add, however, that only a certain number of the bands in the above table have been investigated in the neighborhood of the transition point. We would also remark a difference in the 5.5μ band of ammonium chloride at low temperatures (−150°C) in comparing our spectra with those of Wagner and Hornig.[4] Our results are illustrated in Fig. 1, where it will be observed that at the lowest temperature we have reached, the band is still single and, moreover, has its maximum intensity at 1818 ohm$^{-1}$, this being the frequency quoted for the weaker component by these workers.

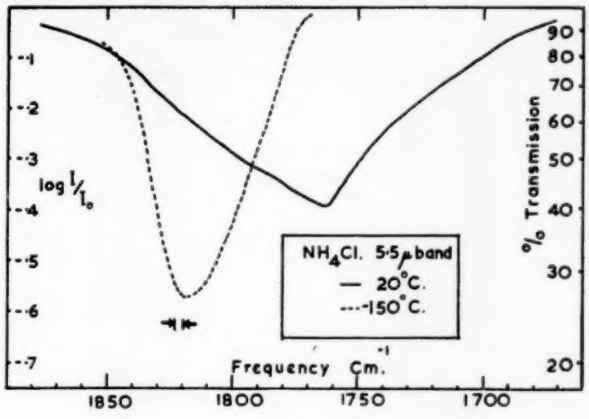


Fig. 1.

A full description of our experiments together with a discussion of the results will be published in due course. The main purpose of this note was to re-affirm the absence of rotational fine structure in the infra-red spectra of the ammonium halides.

* Now at Physics Department, University of Michigan, Ann Arbor, Michigan.
[1] P. E. Shearin, Phys. Rev. **48**, 299 (1935).
[2] C. Beck, J. Chem. Phys. **12**, 71 (1944).
[3] Lee, Sutherland, and Wu, Proc. Roy. Soc. 176A, 484 (1940).
[4] E. L. Wagner and D. F. Hornig, J. Chem. Phys. **17**, 105 (1949).

## "Vapor Snakes" in Cyclohexane

M. K. Phibbs and H. I. Schiff
*Division of Chemistry, National Research Council of Canada, Ottawa, Canada*
July 5, 1949

IF a glass ampule of thoroughly degassed, pure cyclohexane is immersed in a dry ice-acetone mixture for a few seconds, a striking phenomenon occurs, which, to our knowledge, has not been previously reported. The surface of the liquid first solidifies to a rigid, microcrystalline crust, while a thin sheath of glassy solid forms next to the walls of the ampule—the rest of the cyclohexane remaining liquid. A small vapor bubble next appears directly below the crust, from which a small tubule of vapor grows and extends rapidly into the supercooled liquid—much like a long, thin snake, about 1 mm in diameter. The tip of the "snake" travels at a rate of about 3 cm per second throughout the liquid, changing direction upon meeting an obstacle and leaving an interwoven trail, until all the available space is filled. Visible crystallization occurs around the wall of the "snake" about 1 cm behind the tip and spreads slowly outward to the glassy sheath into which the "snake" is unable to penetrate. Although the sequence of pictures (paper negatives from a movie strip) in Fig. 1 show the type of path followed by the "snake" they do not give its true appearance,—the vapor tubule is definitely hollow over its entire length. This behavior seems extremely sensitive to slight traces of air, the introduction of a very small air bubble

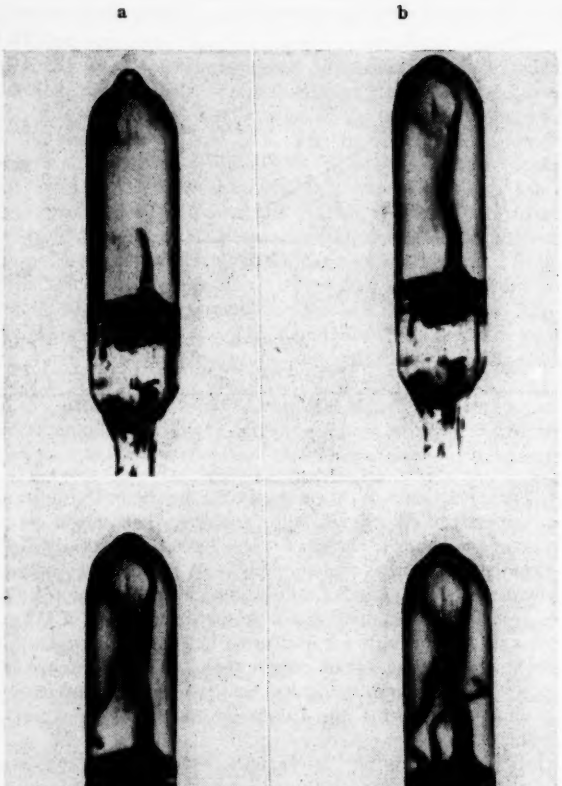


FIG. 1.

being sufficient to cause spontaneous crystallization through the liquid, and completely obliterates the effect.

This unusual phenomenon can probably be attributed to the high vapor pressure of cyclohexane at its melting point (*ca.* 35 mm at 6.4°C) along with the observed fact that crystallization tends to take place only at a liquid-vapor interface in the absence of dissolved gas. The latter is supported by the fact that gradual cooling from the bottom produced only a clear, glassy solid. Furthermore, when the sample was confined in a sealed tube over mercury and subjected to a hydrostatic head of more than 4 cm of Hg (so that no vapor could be formed) again only a glassy solid was produced. When the sample is cooled crystallization therefore occurs at the surface. Due to contraction a vapor bubble forms below the crust; as crystals form around this bubble, heat of fusion is liberated which causes further vaporization. The increase in pressure forces the vapor into a tubule which is propagated through the supercooled liquid by this repeating cycle of crystallization and vaporization. Since the "snake" travels rapidly through the viscous liquid, is not curved upwards by buoyant forces, and is sharply reflected from obstacles at all but grazing angles, there seems to be no doubt that it is propelled by a considerable force. This lends support to a vapor mechanism since the pressure is probably highest at the tip which would therefore move by a sort of jet-propulsion.

It is well known that organic molecules possessing considerable structural symmetry have abnormally high melting points and correspondingly high vapor pressures at their melting points. Since cyclohexane is such a compound, it was natural to look for the same phenomenon in other symmetrical compounds. Neopentane showed the effect, but either due to its higher vapor pressure and/or its higher latent heat, so much vapor was produced that the surface crust was frequently blown off before the "snake" had progressed any distance. Benzene and tertiary butyl alcohol were also tried with some success but the "snake" moved much slower in both liquids and crystallization and was not confined solely to the vapor-liquid interface. On the other hand, straight chain hydrocarbons such as decane froze only by crystallization whereas asymmetric compounds such as 3-methyl pentane formed glasses only.

It can safely be concluded that while the vapor "snake" phenomenon is most impressive in the case of cyclohexane it can be produced in other symmetrical compounds which possess high vapor pressures at their melting points.

## Repulsive Interaction Potentials at Small Interaction Distances: He-He and H-$H_2$ Systems

I. AMDUR
*Department of Chemistry, Massachusetts Institute of Technology, Cambridge, Massachusetts*

July 25, 1949

THE total collision cross sections of high velocity helium atoms scattered in helium gas and of high velocity hydrogen atoms scattered in hydrogen gas have been measured as functions of velocity for the purpose of evaluating intermolecular repulsive potentials as functions of interaction distances.[1,2] For the He-He system the deduced potential function was

$$V(r)=11.3\exp(-4.63r^{\frac{1}{2}})\times10^{-10}\text{ erg}\quad(r\text{ in A}) \tag{1}$$

for values of $r$ in the range 0.55–1.05A, while for the H-$H_2$ system the function was

$$V(r)=[0.846\exp(-24.9r^2)+0.211\exp(-2.40r^2)]\times10^{-10}\text{ erg} \tag{2}$$

for values of $r$ in the range 0.28–0.70A. In the latter case, both the hydrogen atom and the hydrogen molecule were treated as mass points.

The evaluation of the above potential functions required, in principle, knowledge of the average angular deflection experienced by a beam particle of given velocity which is scattered beyond the detector, since the scattering of the beam does not occur at a point but along a relatively long path (about 8 cm). The usual assumption was made, that the average angular deflection for beam axis scattering was the same as the average angular aperture of the detecting system which was computed by averaging linearly, with respect to distance along the beam axis, all half-angles subtended by the detector. The use of such an average aperture to represent the average angular deflection of a single beam particle cannot be correct in general, since it assumes that all scattering angles are equally probable, whereas, for systems with relative initial velocities as high as those under discussion, the intensity of small angle scattering is known to be very much greater than that of large angle scattering.

A procedure which takes into account the variation of scattered intensity with angle has been proposed by Simons, Fontana, Muschlitz, and Jackson,[3] and by Simons, Muschlitz, and Unger.[4] Their method consists, in effect, of integrating the collision cross section along the entire scattering path under the assumptions that the scattering is classical, and that the interaction potential between a beam particle and a scattering particle is of the form $V(r)=K/r^n$. Kells[5] has analyzed the original assumptions and approximations and, by introducing self-consistent small angle approximations, has obtained an analytical development which eliminates tedious graphical integrations and which is accurate to

better than one percent over a wide range of the parameters and variables involved (detector geometry, particle masses, and exponent in the interaction potential). Application of Kells' method to the experimental results for He scattered in He yields the following potential, valid in the range 0.52–1.02A,

$$V(r)=4.62\times10^{-12}/r^{1.79}\text{ erg} \quad (3)$$

which is equivalent, within about 3 percent, to

$$V(r)=3.14\exp(-4.21r)\times10^{-10}\text{ erg}. \quad (4)$$

At a given value of $r$, the potential calculated from Eq. (4) is about 0.4 that given by Eq. (1) showing that the *effective* relative angular aperture, weighted according to the intensity of scattering along the path from the beam source to the detector, is about 1.8° as compared with 4.5°, the geometric average relative angular aperture.

It is interesting to compare the results contained in Eqs. (3) and (4) with other information on the interaction potential between two helium atoms at small distances of separation. Slater[6] has calculated the repulsive potential between two helium atoms at distances greater than 1A by considering first-order exchange forces, and represented his results by

$$V(r)=7.70\exp(-4.60r)\times10^{-10}\text{ erg}. \quad (5)$$

Margenau[7] considered second-order exchange forces and showed that Slater's equation gives values which are too large. If the form of Margenau's correction term is assumed to be valid at small interaction distances as well as near the minimum, where his calculations were made, the corrected potential energy function for distances greater than 1A may be written

$$V(r)=[7.70\exp(-4.60r)-5.60\exp(-5.33r)]\times10^{-10}\text{ erg}. \quad (6)$$

Equations (3) and (4) predict $V(r)$ values at 0.52A which are less than half those given by Eq. (6), but, significantly, as the interaction distance increases, the discrepancy decreases until the curves merge quite smoothly at about 1A. It would thus appear that the interaction potential determined from scattering experiments confirms the theoretical calculations of Slater and Margenau near the point of common validity, 1A. It is therefore proposed that the following relation be used for the repulsive potential at *all distances* greater than 0.52A

$$V(r)=[7.70\exp(-4.60r)-5.60\exp(-5.33r)-0.68\exp(-4.50r^2)]\times10^{-10}\text{ erg}. \quad (7)$$

In the range 0.52–0.102A, Eq. (7) agrees with Eqs. (3) and (4) within about 4.5 percent. By the time the interaction distance has increased to 1.5A, the correction term, $0.68\exp(-4.60r^2)\times10^{-10}$, contributes less than 1 percent to $V(r)$.

In the case of high speed hydrogen atoms scattered in room temperature hydrogen molecules, it was not possible to fit the experimental results with a single potential function of the form $V(r)=K/r^n$. The use of several potential laws of the above form, each covering a portion of the experimental results, as suggested by Simons, Fontana, Muschlitz, and Jackson, was rejected since this procedure results in two different values of $V(r)$ at every value of $r$ which is common to two potential laws. Accordingly, the following method was used. An analytical expression was fitted to the experimental total collision cross sections, $S$, as functions of the relative initial kinetic energy of the scattering system, $\frac{1}{2}\mu v^2$. From calculated values of $d\ln S/d\ln(\mu v^2)$ at each experimental value of $\frac{1}{2}\mu v^2$, it is possible to determine the exponent, $n$, appropriate to the particular value of $K/r^n$ which is valid at any chosen value of $\frac{1}{2}\mu v^2$. The corresponding value of $K$ is then computed from the absolute magnitude of $S$ as given by the original analytical expression. Thus, for $q$ sets of experimental values of $S$ and $\frac{1}{2}\mu v^2$, $q$ numerical values of $V(r)$ are obtained, each computed from the general relation $V(r)=K/r^n$ using $q$ sets of $K$ and $n$. These numerical values of $V(r)$ are then represented by a suitable analytical function. The final result for the interaction potential between a hydrogen atom and a hydrogen molecule, both considered as mass points, is

$$V(r)=[0.567\exp(-24.9r^2)+0.215r\exp(-2.40r^2)]\times10^{-10}\text{ ergs} \quad (8)$$

for separation distances in the range 0.27–0.68A.

At a given value of $r$, the potential calculated from Eq. (8) is 0.41 to 0.695 that given by Eq. (2), showing that, in this case, the *effective* relative angular aperture varies from 1.38° to 2.34° as compared with 3.37°, the geometric average relative angular aperture.

[1] I. Amdur and H. Pearlman, J. Chem. Phys. 8, 7 (1940); 9, 503 (1941).
[2] I. Amdur, J. Chem. Phys. 11, 157 (1943).
[3] Simons, Fontana, Muschlitz, and Jackson, J. Chem. Phys. 11, 307 (1943).
[4] Simons, Muschlitz, and Unger, J. Chem. Phys. 11, 322 (1943).
[5] M. C. Kells, J. Chem. Phys. 16, 1174 (1948).
[6] J. C. Slater, Phys. Rev. 32, 349 (1928).
[7] H. Margenau, Phys. Rev. 56, 1000 (1939).

## Ultraviolet Absorption of Fluorinated Aromatic Hydrocarbons

C. H. Miller and H. W. Thompson
*The Physical Chemistry Laboratory, Oxford University, England*
July 26, 1949

As part of a program of work on the spectra of fluorinated hydrocarbons, we have recently measured the ultraviolet spectra of some fluorinated toluenes. The detailed results of a vibrational analysis of the ultraviolet band systems of the vapors will shortly be published elsewhere.[1] In the course of this work, sharp differences were noted in the extinction coefficients for the different compounds. These have now been measured for solution in *n*-heptane, using a photoelectrically recording instrument built in this laboratory and about equal in optical performance to a Hilger medium quartz spectrograph. The absorption curves are shown in Figs. 1 and 2. The corresponding curves for benzene and toluene were also measured, both for comparison with the fluorinated toluenes, and as a check on the performance of the instrument now used. In these two cases the curves obtained

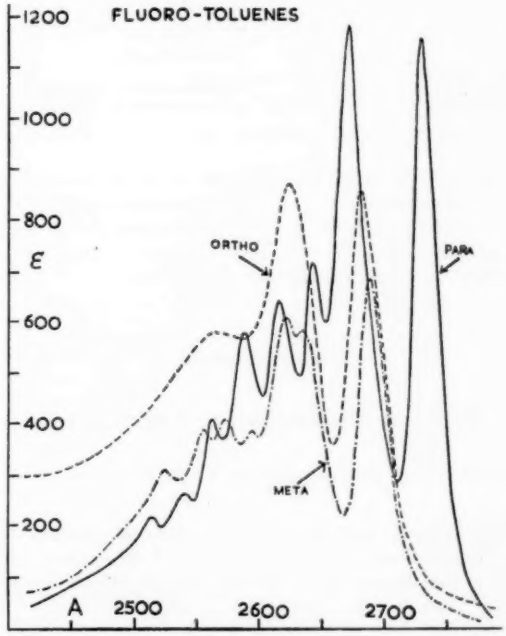


Fig. 1.

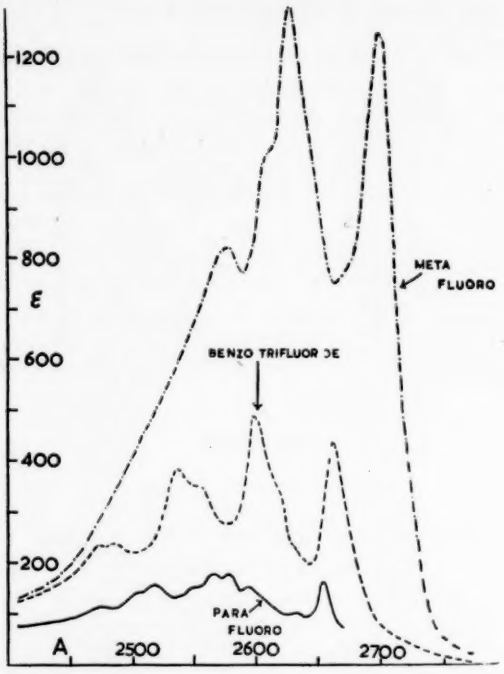


FIG. 2.

agreed closely with those given in A.P.I. reference curves (Serial Nos. 11 and 12).

Two points of interest may be noted. First, along the series *ortho*-fluorotoluene, *meta*-fluorotoluene, *para*-fluorotoluene, the onset of absorption as indicated by the intense band of longest wave-length, moves towards longer wave-lengths. With the substituted benzotrifluorides, however, the *para*-derivative is anomalous in having its first band at shorter wave-lengths than *meta*-fluorobenzotrifluoride or benzotrifluoride itself.

This anomaly is further brought out by the extinction coefficient for the bands involved. The values (liters/gmoles/cm/$\log_{10}$ units) are given in Table I, in which the remarkable fall in

TABLE I. Values of $\epsilon$ for long wave-length band.

| | | | |
|---|---|---|---|
| Toluene | 240 | Benzotrifluoride | 440 |
| *o*-fluorotoluene | 860 | | |
| *m*-fluorotoluene | 690 | *m*-fluorobenzotrifluoride | 1250 |
| *p*-fluorotoluene | 1160 | *p*-fluorobenzotrifluoride | 168 |

the case of *para*-fluorobenzotrifluoride is to be contrasted with the high value in *para*-fluorotoluene. The results indicate that the electronic influences introduced by the presence of $-CF_3$ and $-F$ groups, both separately and together, may be considerable, and suggests a topic for theoretical consideration.

[1] W. T. Cave and H. W. Thompson, in press.

## Reaction Mechanism in Ionic Systems

BAL KRISHNA
*Department of Chemistry, Allahabad University, Allahabad, India*
July 5, 1949

THE velocity and mechanism of chemical reaction between charged ions, are, to a great extent dependent upon the nature of the charges of the reacting species. Where the reaction occurs between oppositely charged ions, the process is likely to be helped by the Coulombic attraction present between the reacting ions, while in case of similarly charged ions, the process has to be slow, adopt a different mechanism, and take the aid of a catalyst in order to overcome the resistance of the reaction present in the form of Coulombic repulsion. Incidentally, it may be pointed out that a detailed study of the reactions between similarly charged ions is likely to be of great value in understanding the exact role of a catalyst, and an exact physical significance of such terms as "collision complexes," "energy of activation" and "potential barriers" in any particular instance.

Moreover as pointed out by Bronsted[1] a change in the electrical properties of the medium in such cases greatly affects the reaction velocity. An increase of ionic strength in case of a reaction between similarly charged ions leads to an enhancement in the value of the specific reaction rate, while in case of oppositely charged ions, the value of specific reaction rate decreases with an increase in the ionic strength of the medium. These two effects are expressed by the following equation for a bimolecular reaction:

$$\log K = \log Ko + Z_A Z_B(\mu)^{\frac{1}{2}} \quad (1)$$

where $Z$ represents the charge of the ions, $\mu$ the ionic strength, $K$ the specific reaction rate, and $Ko$ is defined by the following equation:

$$K = Ko(f_A f_B / f_x) \quad (2)$$

where $f_A$ and $f_B$ are activity coefficients the ions $A$ and $B$ respectively, and $f_x$ the activity coefficient of the "collision complex." Bronsted has deduced these equations semi-thermodynamically and they are of great help in elucidating the mechanism of ionic reactions.

The study of the reaction between ferric ion and the stannous ion affords an interesting example from this point of view. The over-all ionic reaction can be represented as follows:

$$2Fe^{+++} + Sn^{++} \rightarrow 2Fe^{++} + Sn^{++++}.$$

The reaction was first studied by Noyes[3] who found that the reaction is termolecular in absence of hydrochloric acid, and bimolecular in presence of it. Weiss[4] points out that the experimental results obtained by Noyes, can be well explained if one assumes that the reaction proceeds in the following way:

$$\text{(a)} \quad SnCl_2 + 2Cl^- \rightleftharpoons SnCl_4^{--},$$
$$\text{(b)} \quad SnCl_4^{--} + Fe^{+++} \rightleftharpoons SnCl_4^{-} + Fe^{++},$$
$$\text{(c)} \quad SnCl_4^{-} + Fe^{+++} \rightarrow SnCl_4 + Fe^{++}.$$

It is obvious that the electron transfer occurs between oppositely charged ions. But apart from theoretical considerations,[2] there has come no evidence that the rate determining process occurs between two oppositely charged ions.

In order to understand that exact mechanism of the reaction between ferric ion and stannous ion, the present author has studied the kinetics of this reaction in detail at the temperature of melting ice. It has been found that the increase in ionic strength of the medium produces a retardation in reaction velocity in all cases except where the ionic strength is increased by adding nitric acid, or hydrochloric acid, or other chlorides. Chloride ion as was already known produces a powerful accelerating effect.

Assuming the validity of Bronsted's equation, we are forced to conclude that the rate determining process occurs between oppositely charged ions. My experiment therefore provides one of the ways in which the intermediate links of the reaction in ionic media can be traced, and a new utility of Bronsted's equation.

[1] Bronsted, Chem. Rev. **5**, 231 (1928).
[2] Hinshelwood, J. Chem. Soc., p. 694 (1947).
[3] Noyes, Zeits. f. physik. Chemie **16**, 576 (1895).
[4] Weiss, J. Chem. Soc., p. 309 (1944)